Electron Transfer and Proton Pumping Pathways in Cytochrome aa_3

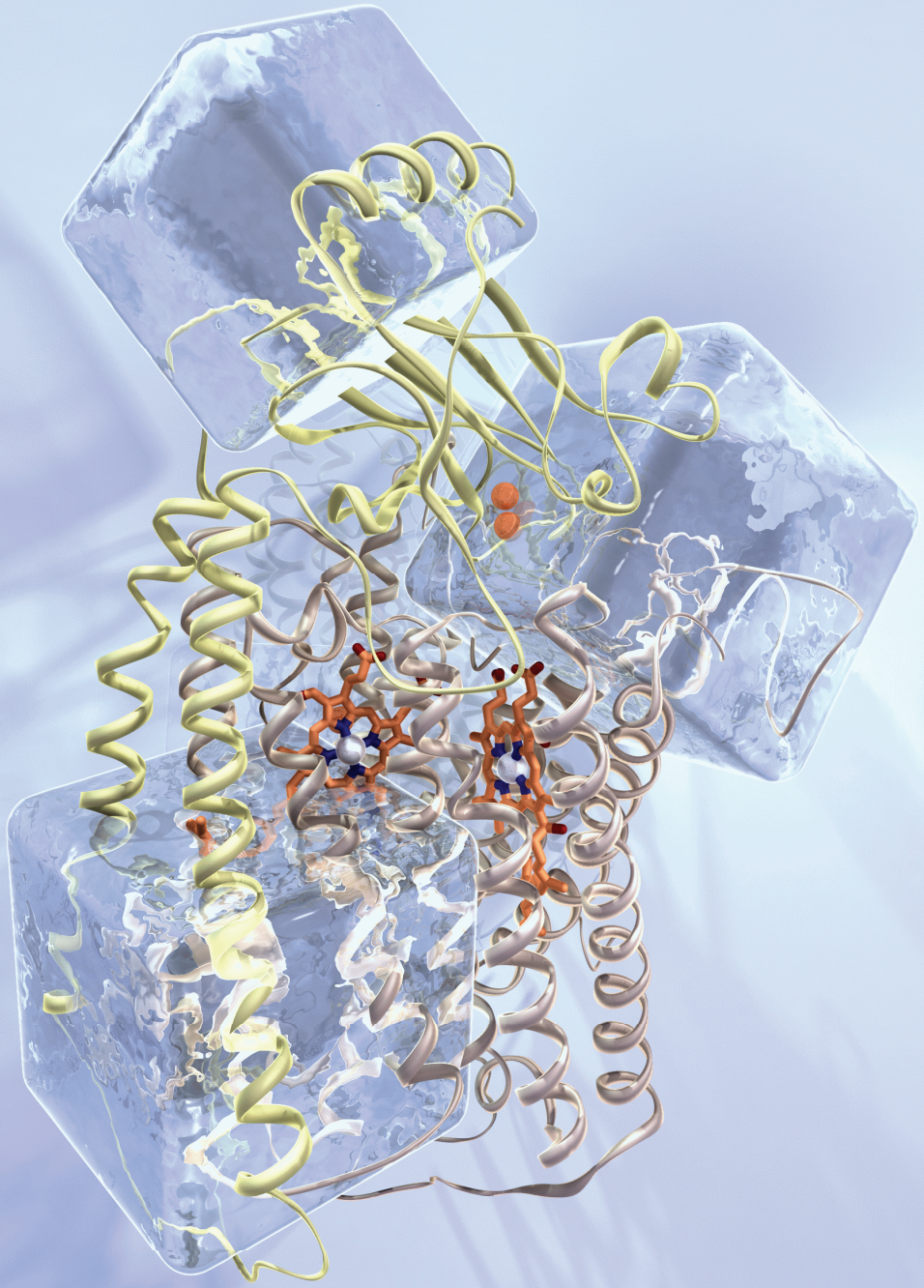

Frank Wiertz

Electron transfer and proton pumping pathways in cytochrome aa_3

PROEFSCHRIFT

Ter verkrijging van de graad van doctor
aan de Technische Universiteit Delft,
op gezag van de Rector Magnificus Prof.dr.ir. J.T. Fokkema,
voorzitter van het College voor Promoties,
in het openbaar te verdedigen op maandag 17 november 2008 om 15.00 uur

door

Frank Gerard Marie WIERTZ

ingenieur in de bioprocestechnologie
geboren te Heerlen

Dit Proefschrift is goedgekeurd door de promotor:

Prof.dr. S. De Vries

Samenstelling promotie comissie:

Rector Magnificus	Voorzitter
Prof.dr. S. de Vries	Technische Universiteit Delft, promotor
Prof.dr. W.R. Hagen	Technische Universiteit Delft
Prof.dr. B. Ludwig	Johan-Wolfgang Goethe Universität Frankfurt
Prof.dr. T.J. Aartsma	Universiteit Leiden
Prof.dr. C. Dekker	Technische Universiteit Delft
Prof.dr. R. Wever	Universiteit van Amsterdam
Dr.ir. H.A. Heering	Universiteit Leiden, Adviseur

The studies presented in this thesis were performed at the Department of Biotechnology, Delft University of Technology.
The research was supported by the Stichting voor Fundamenteel Onderzoek der Materie (FOM) grant D-26.

The cover design is an artist impression of freeze-hyperquenched cytochrome aa_3 by W.J.W. Tepper (Armand)

ISBN: 978-90-9023560-8

Man muss die Welt nicht verstehen
Man muss sich nur darin zurecht finden
Albert Einstein

Contents

Chapter 1

Introduction

Cells need energy for growth, maintenance of cellular components, movement and transport of nutrients and macromolecules. The energy necessary for these processes is generated by catabolic processes like fermentation or respiration. Catabolism comprises the breakdown of nutrients such as (poly) saccharides, fatty acids and peptides. Anabolism on the contrary, refers to processes in which the cell builds up cell material for maintenance, growth and division. The energy and products produced by catabolism are used in anabolic processes except the 'waste' products' which are excreted. Metabolism represents the total of anabolic and catabolic processes (Figure 1) [1].

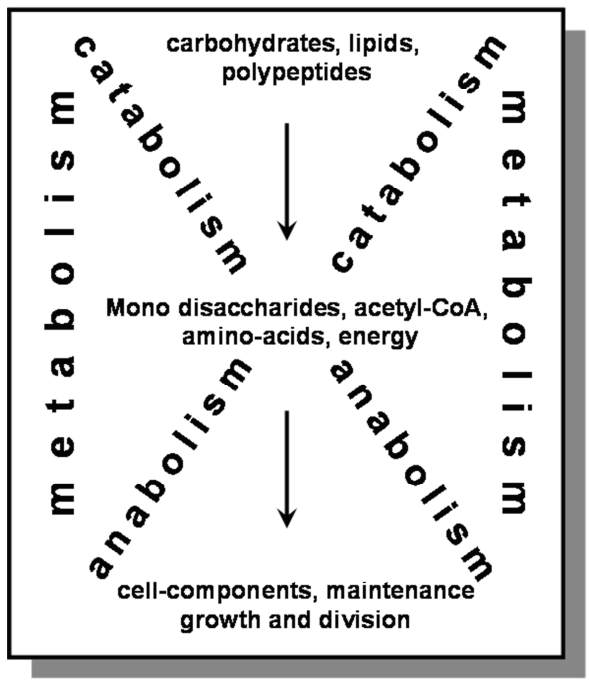

Figure 1 Schematic drawing of the relation between catabolic and anabolic processes. For further explanation see the text.

The energy produced during catabolism must be made available in such a way that it can be produced where needed or transported to parts of the cell where needed. In general the energy liberated during catabolism is

either stored as ATP or in an electrochemical gradient in the form of protons (mostly) or sodium ions. ATP is an energy rich compound that can be used in many different metabolic reactions that require energy.
ATP is formed by phosphorylation of ADP (ADP + $P_i \rightarrow$ ATP) and produced, in general, in the following two processes:

1) Substrate phosphorylation: the production of ATP is directly coupled to formation of an energy-rich phosphorylated intermediate. During fermentation this is the exclusive source of ATP production.

2) Oxidative phosphorylation or respiration: ATP production via the membrane bound F_oF_1-ATP-synthase by means of a proton electrochemical gradient. This process optimally utilizes the energy stored in molecules for building a proton electrochemical gradient and ATP production.

In respiration, nutrients are completely oxidized to CO_2 and H_2O, in contrast to fermentation. Therefore much more ATP is formed per nutrient molecule in respiration than in fermentation and much more cell mass is obtained. ATP is often referred to as "the main currency of life". This is incorrect. Both the proton electrochemical gradient and ATP are the currencies of life. They are interchangeable when and where needed and function in the cell on equal levels of importance. The proton electrochemical gradient can be seen as the electric network which is fixed to the membrane and the ATP as a chargeable battery, being charged by the network and transportable. If necessary the battery can be uncharged back into the network if "extra" energy would be needed there.

The chemiosmotic theory

In 1953 Slater postulated that ATP production in oxidative phosphorylation occurred solely via direct phosphorylation by a mechanism inspired by and similar to substrate phosphorylation [2]. He postulated his theory on basis of the research of several groups that provided experimental evidence for ATP production during the oxidative respiration [3-7]. Slater postulated the formation of so called "energy-rich" intermediates, which were used by an ATP-synthase for the formation of ATP. The energy-rich

intermediates have never been found in spite of intensive research for two decades.

In 1961 Peter Mitchell put forward the chemiosmotic theory, which he refined later and which consists of the following four postulates [8-11]:

1) The ATP-synthase, which is located in a chemiosmotic membrane, is a reversible protonmotive ATP-ase with a characteristic H^+/P_i stoichiometry.

2) The respiratory and photoredox chains are located in the chemiosmotic membrane, building up the proton gradient in the opposite direction of the ATP-synthase.

3) There are proton-linked solute porter systems for osmotic stabilization and metabolite transport.

4) The various complexes are all "plugged through" a coupling membrane impermeable for solutes and particularly for hydrogen ions and hydroxyl ions.

These four postulates can be summarized in more modern biochemical language as follows: The coupling membrane has a low permeability for ions in general, including protons and hydroxyl anions. The respiratory or photoredox chain builds a proton electrochemical gradient across the membrane. The energy stored in the proton electrochemical gradient can be used by the F_oF_1-ATP-synthase for the production of ATP from ADP and P_i. In this case, the protons flow from the P-side (positive side) to the N-side (negative side). The F_oF_1-ATP-synthase can hydrolyze ATP to ADP and P_i, thus building the proton electrochemical gradient. The proton electrochemical gradient can be used for transport of other ions and nutrients across the membrane. The driving force of the proton electrochemical gradient was described by Peter Mitchell as the Proton Motive Force (pmf), as an analogue to the Electron Motive Force (emf) in an electrochemical cell.

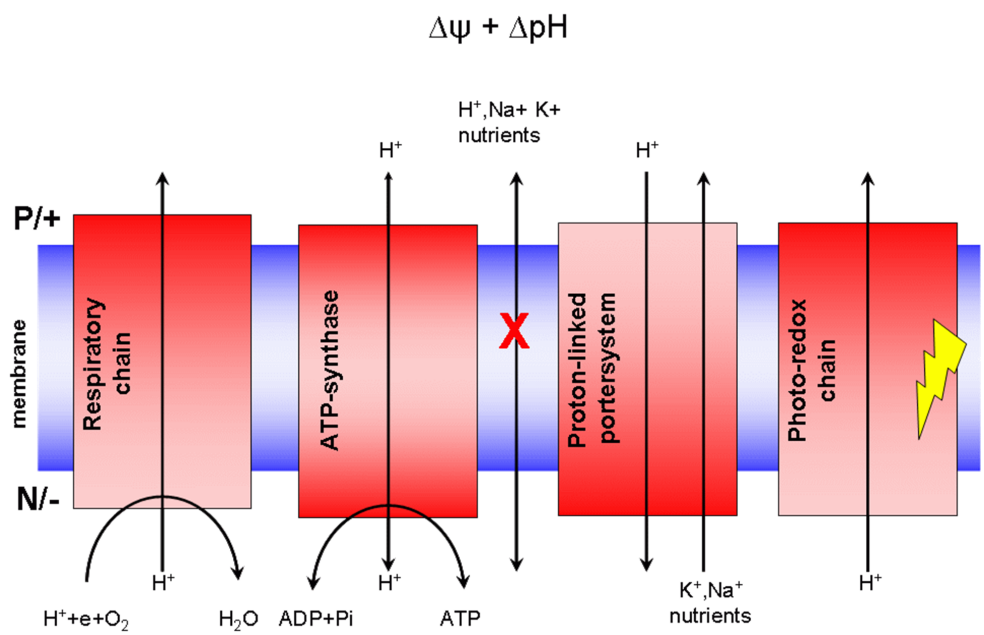

Figure 2 Schematic overview of the coupling membrane according to the chemiosmotic hypothesis. The red blocks represent the systems plugged through an osmotic membrane; this membrane is impermeable to ions and nutrients. The proton electrochemical gradient built up by the respiratory chain or photo-redox chain can either be used for transport of other ions or nutrients across the membrane or for the production of ATP by the ATP-synthase. The latter enzyme is reversible and can use ATP to build up the proton electrochemical gradient. The + sign represents the positive side and the – sign the negative side of the membrane. In bacteria the cytoplasm is negatively charged with respect to the periplasm, in mitochondria the matrix is negatively charged with respect to the intermembrane space. In thylakoïds the stroma is negatively charged with respect to the lumen.

The proton electrochemical gradient ($\Delta\mu_{H+}$) refers to the difference in concentration of the protons across the membrane (ΔpH) **and** the resulting difference in the electrical potential ($\Delta\psi$), a direct consequence of the charge separation (when the protons move without a counter-ion) according to the following formula:

For the **proton** electrochemical gradient:

$$\Delta\mu_{H+} = -F\Delta\psi + 2.3RT\Delta pH \text{ (in kJ/mol)}$$

The **proton** electrochemical gradient can be expressed in voltage units instead of kJ/mol as follows:

$$\Delta p = -(\Delta\mu_{H+})/F = \Delta\psi - 59\Delta pH \text{ (in mV/mol at 25°C)}$$

In mitochondria the pH difference is rather small (~0.5) owing to the buffering capacities of the matrix and the intermembrane space and cytosol. The main driving force is given by the membrane potential. In the chloroplasts of plants, however, the main component of the pmf is the difference in pH across the thylakoïd membrane because in concert with protons, chloride ions move across the membrane [12-14].

Several years subsequent to Mitchell's publication of the chemiosmotic hypothesis, the 'acid-bath experiments' by Jagendorf and the finding of the F_oF_1-ATPsynthase by Racker separately provided the first experimental proof for the theory [15-17]. In 1978 Peter Mitchell was awarded the Nobel Prize in Chemistry **"for his contribution to the understanding of biological energy transfer through the formulation of the chemiosmotic theory"**

Nowadays the chemiosmotic hypothesis by Mitchell is widely accepted. Research over the years has pointed out that the proton electrochemical gradient is not only used for ATP production but also for example for motion (flagella), production of heat (by uncoupling) and ion and metabolite transport [17-19]. The reversibility of the ATP-synthase complex has profound physiological consequences. ATP as a chemical energy carrier can be converted into the proton electrochemical gradient when needed for processes, which require the input of energy but which do not or cannot use ATP directly.

Energy production

A well studied example for the production of ATP is the oxidation of glucose. Glucose is broken down via the glycolytic pathway (or Embden-Meyerhof pathway) according to:

$$\text{Glucose} + 2NAD^+ + 2\ ADP + 2\ P_i \rightarrow \text{pyruvate} + 2\ NADH + 2\ H^+ + 2\ ATP$$

In the absence of final electron acceptors such as oxygen, nitrate or sulfate, respiratory chain complexes are not expressed and NADH cannot be

further oxidized. However, the produced NADH needs to be reoxidized to replenish the NAD^+ pool. In many fermentation processes the reducing equivalents of NADH are transferred to pyruvate, which acts as the final electron acceptor. Lactic acid bacteria which can grow both aerobically and anaerobically replenish NAD^+ in the absence of oxygen by producing lactic acid according to the following reaction:

$$\text{Pyruvate} + \text{NADH} + H^+ \rightarrow \text{lactate} + NAD^+$$

Yeast cells produce ethanol when grown under anaerobic conditions according to:

$$\text{Pyruvic acid} + \text{NADH} + H^+ \rightarrow \text{ethanol} + NAD^+ + CO_2$$

The yield of ATP is in both cases very low, namely 2 ATP per glucose molecule. The energy stored in glucose cannot be used to its full extent under fermentation conditions since glucose is not completely converted to CO_2. If a respiratory chain is present with oxygen as a final electron acceptor the complete breakdown of glucose occurs via glycolysis, pyruvate decarboxylation and the citric-acid cycle (TCA or Krebs-cycle) according to the overall reaction in mitochondria:

$$\text{Glucose} + 10\ NAD^+ + 2\ Q + 2\ ADP + 2\ GDP + 4\ P_i \rightarrow 10\ \text{NADH} + 10\ H^+ + 2\ QH_2 + 2\ \mathbf{ATP} + 2\ \mathbf{GTP} + 6\ CO_2 + 6\ H_2O$$

In these three metabolic pathways two molecules of ATP and two of GTP (an energy carrier similar to ATP) are produced. GTP can be directly converted into ATP by the family of nucleoside diphosphate kinases. The ATP and GTP produced in this way are formed via substrate phosphorylation. Bacteria solely produce four molecules of ATP and no GTP in the TCA. The reduction equivalents formed in the TCA-cycle come in the form of NADH and QH_2 (a membrane dissolved electron carrier, capable of diffusing within and across the membrane). These reduction equivalents need to be oxidized to maintain the cellular redox balance exactly as in the case of fermentation. Eukarya (in their mitochondria) and aerobic Bacteria and Archaea couple the oxidation of NADH and QH_2 via the respiratory chain to the reduction of molecular oxygen (Figure 3, complex I to IV). The total ATP yield is 36, which is far more efficient then

the two ATP produced during fermentation process as described above per glucose molecule.

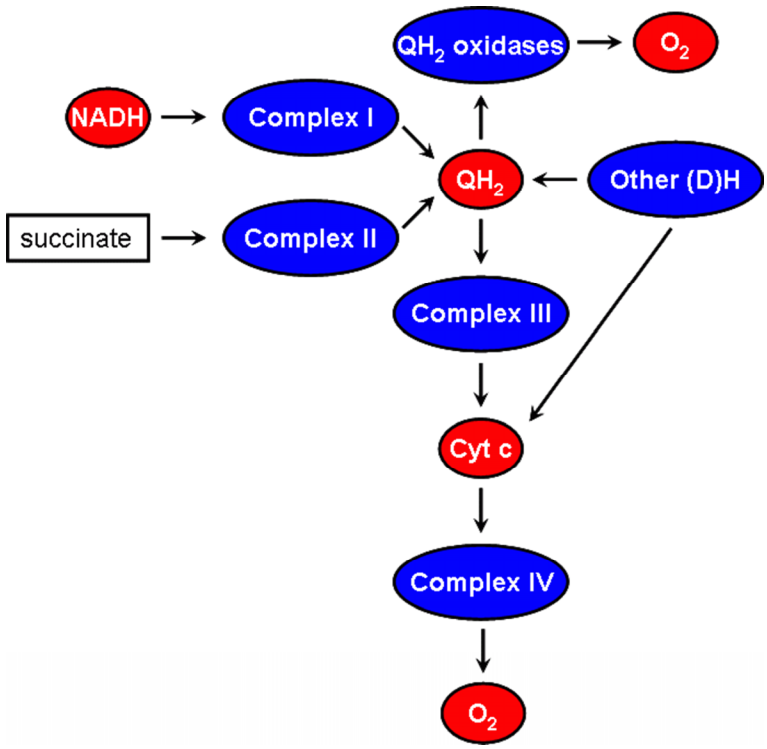

Figure 3 Schematic overview of a branched respiratory chain with alternative entry and exit routes of reduction equivalents. In red, the mobile electron carriers and 'H-atom' carriers - in case of QH_2 and NADH- in aerobic respiration. In blue the enzyme complexes some of which (Complex I, Complex III and Complex IV) use the redox potential energy difference between their electron donors and acceptors to build up the proton electrochemical gradient. Succinate is the substrate for Complex II, which is also part of the TCA cycle. Complex I, Complex III and Complex IV are characteristic for mitochondria but are also found in several bacteria. Other routes –indicated by other (de)hydrogenases ((D)H) or QH_2 oxidases- are characteristic for bacteria and archaea and their expression depends on the presence of a particular final electron acceptor in the growth medium. Examples of 'Other (de)hydrogenases ((D)H)' are formate dehydrogenase, hydrogenases, which reduce Q, while methylamine dehydrogenase and quino-hemoprotein-aminedehydrogenase reduce cyt.*c*.

In contrast to the Eukarya, Archaea and Bacteria have a very broad respiratory repertoire and respiratory flexibility enabling them to adapt to

changing environmental conditions. They can use for example NO_3^-, SO_4^{2-} and Fe_2O_3 as final electron acceptors (anaerobic respiration) besides oxygen and directly couple the electrons from the quinone pool to the reduction or oxygen (QH_2-oxidases) or directly reduce cytochrome c ('other (de)hydrogenases') [20-25].

The Aerobic Respiratory Chain

The respiratory chain consists of four respiratory complexes, which are responsible for generating the proton electrochemical gradient. Higher organisms, Eukaryotes and several Bacteria use this system as their main energy production pathway. Electrons enter the respiratory chain via NADH and succinate. The four respiratory complexes which are connected via the electron carriers Q and cytochrome *c* each contain a series of electron carriers such as iron-sulphur centers, flavins, hemes and copper centers. The redox potential energy of the electrons decreases in the direction form Complex I to Complex IV because the reduction potential of the electron carriers in the complexes increases. The redox potential difference between the various electron carriers is used by the complexes to transport protons across the membrane thus building an electrochemical gradient. The final step in aerobic respiration is the formation of water from oxygen, which is the terminal electron acceptor in aerobic organisms. The electrochemical gradient built up by Complex I to IV is used by Complex V (the F_oF_1-ATPsynthase) for ATP production. In the following a short description is provided on the respiratory chain complexes with references to recent reviews.

Complex I also known as NADH-quinone oxidoreductase (or NADH dehydrogenase) uses the NADH produced in glycolysis, pyruvate oxidation and the TCA cycle for the reduction of quinone. When quinone is reduced by 2 electrons it binds 2 protons forming quinol. During the reduction of quinone 4 protons are pumped across the membrane. Complex I is considered a true proton pump which means that protons are physically translocated from the negative side to the positive side[24, 26]. The proton pumping mechanism of Complex I remains to be unraveled. The overall reaction of Complex I is as follows:

$$NADH + Q + 6H^+_{in} \rightarrow NAD^+ + QH_2 + 4H^+_{out}$$

Complex I is by far the most complex respiratory complex consisting in mitochondria of 42-46 subunits, in bacteria of 14 subunits. It contains FMN, and 8 different iron-sulphurs centers, two of which are binuclear and six tetranuclear iron-sulfur clusters [27-31].

Complex II or succinate-quinone oxidoreductase is the only membrane bound enzyme from the TCA cycle. This is the reason why it is seen as part of the respiratory chain. The electrons freed during the oxidation of succinate to fumarate are donated to quinone. The overall reaction of complex II is as follows:

$$\text{Succinate} + Q + 2H^{+}_{in} \rightarrow \text{fumarate} + QH_2$$

Complex II consists of 4 subunits the two smallest anchoring the enzyme to the membrane. The largest hydrophilic subunit contains FAD and the succinate binding site. The smaller hydrophilic subunit contains three iron-sulphur centers which translocate the electrons between the FAD and the quinone. Quinone is bound to one of the small membrane subunits, which in the case of mitochondria, also contains a low-potential heme *b* of unknown function [32-34].

Complex III or quinol-cytochrome *c* oxidoreductase, better known as the bc_1 complex, catalyses the oxidation of quinol and reduction of cytochrome *c*. Although the bc_1 complex does not pump protons across the membrane as Complex I, which acts as a proton pump, the enzyme generates a proton motive force via a Q-cycle mechanism [35]. When QH_2 is oxidized at the P-side of the membrane by the Rieske iron-sulphur center one cytochrome *c* is reduced via cytochrome c_1 and one electron is transferred via two transmembrane oriented heme's *b* to a bound Q at the N-side of the membrane. When a second QH_2 is oxidized the Q at the N-side becomes two-electron reduced and accepts 2 protons from the N-side. Since QH_2 (like Q) can cross the membrane it can be used in the same manner on the P-side to reduce cytochrome *c* and another Q on the N-side of the membrane. In this manner the bc_1 complex generates a proton electrochemical gradient [36, 37]. The overall reaction is as follows:

$$QH_2 + 2\ \text{cyt}\ c^{3+} + 2H^{+}_{N} \rightarrow Q + 2\ \text{cyt}\ c^{2+} + 4H^{+}_{P}$$

The mitochondrial Complex III consists of 9-11 subunits, the bacterial Complex III of only three subunits [38-40].

Complex IV, also known as cytochrome *c* oxidase is the final electron acceptor in the respiratory chain. It is part of the family of heme-copper oxidases, a sub-class of the terminal oxidases. It catalyses the oxidation of cytochrome *c* while reducing oxygen to water. Four so-called "chemical" protons are used for the formation of water and four protons are translocated across the membrane which results in the following reaction equation:

$$4 \text{ cyt } c^{2+} + O_2 + 8\ H^+_C \rightarrow 4 \text{ cyt } c^{3+} + 2\ H_2O + 4\ H^+_P$$

The mitochondrial Complex IV consists of 11-13 subunits, the bacterial Complex IV of only four subunits. The mitochrondrial enzyme contains two heme *a* groups, and two copper centers, Cu_A and Cu_B.

In the following paragraph the family of the terminal oxidases is discussed in more detail.

Terminal oxidases

The family of terminal oxidases, can be divided into two sub-classes which represent independent evolutionary developments: the cytochrome *bd* quinol oxidases and the heme-copper oxidases.

Cytochrome *bd* quinol oxidase

Cytochrome *bd* quinol oxidase catalyses the oxidation of quinol to quinone by reducing oxygen to water:

$$2\ QH_2 + O_2 + 4\ H^+_C \rightarrow 2\ Q + 2\ H_2O + 4\ H^+_P$$

It is a high affinity oxidase expressed in bacteria under micro-aerophilic conditions. In contrast to the heme-copper oxidases their catalytic mechanism is less well understood. The cytochrome *bd* oxidase consists of two subunits that harbour three different hemes. A low spin heme b_{558} located in subunit I, which is believed to play an important role in the oxidation of quinol, and a high spin heme b_{595} and a heme *d* located in

subunit II, which form the bi-nuclear reaction center. In contrast to the heme-copper terminal oxidases, cytochrome *bd* does not pump protons across the membrane. The proton electrochemical gradient is build up by the protons participating in the formation of water from oxygen which are withdrawn from the N-side of the membrane [41].

Heme-copper oxidases

The second family of terminal oxidases is comprised by the heme-copper oxidases.

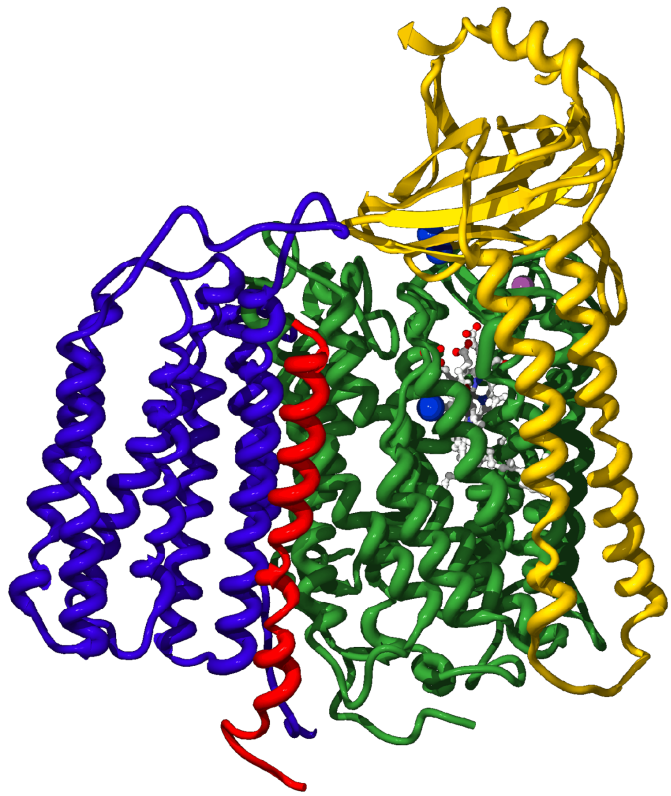

Figure.4 The 3D-structure of cytochrome *c* oxidase from *Paracoccus denitrificans*. Subunit I is shown in green with heme *a* and the binuclear reaction centre consisting of heme a_3 and Cu_B. In yellow, subunit II with Cu_A, the electron accepter for cytochrome *c* and in blue and red subunit III and IV, respectively. Structure from PDB file 1qle [51]

All the oxidases in this super family have in common that the active site where oxygen binds consists of a binuclear center made up of a heme group and copper ion, hence the super family's name. The heme-copper oxidases build up a proton electrochemical gradient across the membrane by physically pumping four protons across the membrane and translocating four (the 'chemical' protons) in the same way as cytochrome *bd*.

The NO-reductases also belong to the family of heme-copper oxidases although they do not contain a copper but instead an iron molecule in the active site [22, 42-46]. They catalyze the reduction of NO according to the following reaction scheme:

$$2\ NO + 2\ H^+ + 2\ e \rightarrow N_2O + H_2O$$

The NO reductases are distant members of the heme-copper oxidases because they contain the conserved histidines which are the ligands to the heme's and copper/iron and also can perform the reduction of O_2 to H_2O [47-49]. However, NO-reductases do not translocate protons across the membrane in contrast to the heme-copper oxidases [50].

The electron donors for the family of heme-copper oxidases are very divers, as well as the heme types in subunit I and the subunit II. The mitochondrial oxidases contain 11-13 subunits in contrast to the bacteria which contain in general 4 subunits [51-56]. In spite of the great diversity in all these factors subunit I and some parts of subunit II contain several highly conserved regions. In the following paragraphs a more detailed description of the subunits will be given.

Subunit I

Subunit I has a minimum of 12 transmembrane α-helices forming three pores A, B and C. The binuclear center is embedded in the center of pore B, the low spin heme in pore C. The binuclear reaction center is approximately 13 Å away from the N-side of the membrane and 30 Å from the P-side [51-57]. Because the binuclear center is far away from either aqueous phase, the risk that potentially reactive oxygen species such as superoxide or hydrogen peroxide come in contact with cellular components is greatly reduced. Subunit I harbours a six-coordinated low-spin heme and the binuclear reaction center consisting of a high-spin heme and a three

histidine coordinated $Cu^{1+/2+}$ centre (Cu_B), which is common to all heme-copper oxidases. The low-spin heme functions as the direct electron donor to the binuclear reaction center. The six histidine ligands coordinating the hemes and Cu_B are strictly conserved in all heme-copper oxidases. The low-spin heme is coordinated by HisI-413 and HisI-94, the high-spin heme by HisI-411 and the Cu_B by HisI-276, HisI-325 and HisI-326 (*P.denitrificans* numbering). Besides the six histidines only three other amino-acid residues are strictly conserved in all oxidases: a valine (ValI-279) in helix VI which is part of the oxygen transport channel to the active site[58], a tryptophan (TrpI-272) in helix VI which is π-stacked with HisI-326, one of the Cu_B ligands [59] in the active site and an arginine (ArgI-474) which is located between helix XI and XII in the P-side of the membrane and hydrogen-bonded to the δ-propionate of the low-spin heme.

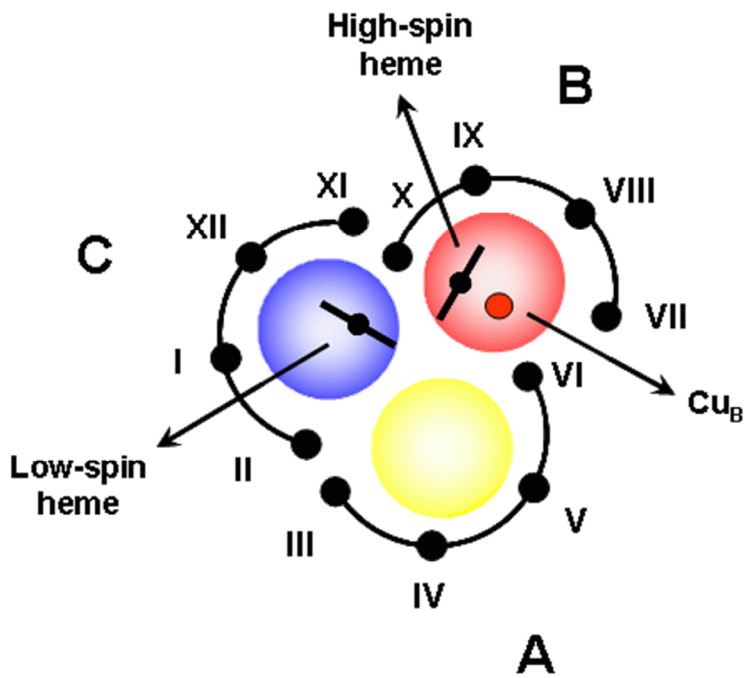

Figure 5 Schematic drawing of subunit I from heme-copper oxidases seen from the P-side of the membrane. The 12 transmembrane α-helices numbered I-XII form a three-pore structure with pore C harbouring the low-spin heme and pore B the binuclear reaction centre consisting of a high-spin heme and Cu_B.

It is proposed that this propionate plays an important role in proton transport to the P-side of the membrane [60, 61].

The structure of the heme groups varies within the super family. Both the high-spin and the low-spin heme may accommodate heme *o*, *a* or *b*. There is no functional relation between the electron donor and the particular structure of the heme groups, e.g. cytochrome ba_3 from *Thermus termophilus* uses cytochrome *c* as electron donor while the *P. denitrificans* ba_3 type uses quinol.

Two proton pathways have been identified in subunit I, the K- and D-proton pathway [62-65]. Mutation of specific residues indicated reduced or absence of proton pumping [63, 64, 66, 67]. A third possible pathway, the H-pathway, has been indicated but its role in proton pumping is presently unclear [68, 69].

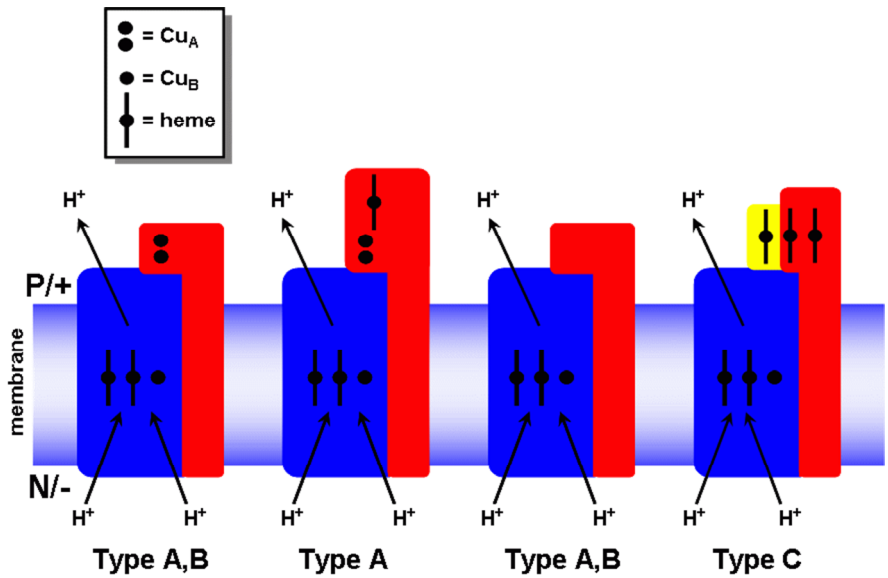

Figure. 6 Schematic overview of the different types of heme-copper oxidases of Subunit I (blue) and II (red). The type C oxidases have an extra peripheral subunit represented in yellow.

The D-proton pathway is composed of AspI-124 (giving the D-pathway its name), AsnI-199, AsnI-113, AsnI-131, TyrI-35, SerI134, SerI-193 and GluI-278. The D-pathway runs from the lower part of pore A (N-side) to the upper part of pore B [51, 53-55]. The K-proton pathway is comprised

of LysI-354 (hence K-proton pathway), ThrI-351, SerI-291 and TyrI-280 and is located in the B-pore. A remarkable fact about the TyrI-280 of the K-pathway is that it is cross-linked to the HisI-276. The TyrI-280 is located in helix VI. The *cbb*$_3$ type oxidases do not have this tyrosine located in helix VI, although an important role is ascribed in proton pumping and the catalytic mechanism of O-O bond breaking [70-72]. Because the crystal structure has not been resolved for the *cbb*$_3$ type oxidases it is unknown how e.g. O-O bond breaking would occur without this tyrosine. Recent research pointed out that a conserved tyrosine within the *cbb*$_3$ type oxidases is located in helix VII. This tyrosine residue is indeed cross-linked to the histidine ligand of the Cu_B [73]. Despite the fact that the amino acid sequence of the *cbb*$_3$ types differ here from the other oxidases, all heme-copper oxidases contain this Tyr-His crosslink motive.

The heme-copper oxidases can be divided into 3 different sub-families according to their proton pathway architecture. The type A heme-copper oxidases (mitochondrial like oxidases) show all great similarities in the structure of the D- and K-pathways. They can be divided in a type A1 and A2 based on the GluI-278. The type A1 oxidases have this characteristic residue in the D-pathway but the type A2 oxidases have a conserved tyrosine and serine residue resulting in a YS motif instead of the Glu [74-76].

The type B oxidases do not have the characteristic proton pathway structure as the type A oxidases and seem to lack conserved residues potentially forming a similar proton pathway. Type B oxidases occur among the bacteria and archaea and show a much larger diversity with respect to the amino-acid residues which form the proton pathways. Nevertheless K-proton pathway homologous sequences are present for which a threonine, serine and tyrosine substitute for LysI-354, ThrI-351 and SerI-291 respectively. Two putative proton pathways could be identified in the crystal structure of *T. thermophilus* cytochrome *ba*$_3$. One similar to the D-proton pathway formed by the residues GluI-17, TyrI-91, ThrI-21, SerI-109, GluI-86, SerI-155, ThrI-156 and GlnI-82 (*T. thermophilus* numbering). The second proton pathway, the so-called Q-pathway, is composed of GlnI-254, ThrI-396, LeuI-392, SerI-391, ThrI-394, ThrI81, GlnI-388 and LeuI-387 (*T. thermophilus* numbering). The Q-pathway ends between the low-spin heme and high-spin heme and not at the binuclear reaction center as in Type A oxidases. The precise role of both proton pathways is still under investigation.

The last type of oxidases, the type C, comprises solely the family of cytochrome *cbb*$_3$ oxidases and occurs only in bacteria. Sequence comparison

indicates that part of the K-proton pathway is preserved in this family with ThrI-35 and SerI-291 apparently replaced by a serine and a tyrosine residue, respectively. No D-proton pathway residues are identified in the type C oxidases and amino acid sequence comparisons have so far not yielded an indication for other proton pathways. The absence of a Type C oxidase crystal structure hampers the identification of other proton pathways in this family.

Although there is a great diversity in the type heme groups and proton pathways the heme copper oxidases all are true proton pumps. For all three different families proton pumping experiments showed that the characteristic H^+/e equals 2 [75, 77-80] with the *T. thermophilus* cytochrome ba_3 as a possible exception[81].

Subunit II

The subunit II of the type A and type B oxidases is composed of a transmembrane α-helical domain and a peripheral domain at the P-side of the membrane. The only exception, based on sequence comparison, is the putative subunit II (named B2) from the *Aq.aeolicus* oxidase which only has the peripheral domain [82]. The membrane part contains one (type B oxidases) or two (type A oxidases) transmembrane α-helices. However, one extra small subunit consisting of a single transmembrane α-helix was detected in the crystal structure of *T. thermophilus* cytochrome ba_3 (type B oxidase) at the same position as of one of the two transmembrane α-helices of subunit II of Type A oxidases, showing that Type A and Type B oxidases have highly similar structures [56]. Other Type B oxidases like those from *N. pharaonis* cytochrome ba_3, *A. ambivalens* cytochrome aa_3 and *S. acidocaldarius* SoxABCD may contain a similar extra subunit of approximately 50 amino-acids forming a transmembrane α-helix , but it is unknown if this is common to all type B oxidases.

All subunits II have a glutamate residue in common (EII-78, *P.denitrificans* numbering) which is proposed to be the entry of the K-pathway if this channel is present [83]. *T. thermophilus* ba_3 oxidase is the only known exception with GluII-218 substituted by a glutamine residue [84]. The glutamate residue is located either in the single helix of the type B oxidases or in the second transmembrane α-helix of the type A oxidases. The peripheral domain is comprised by a 10-stranded β-barrel and has a central cupredoxin fold. This domain serves as the electron entry site. The

peripheral domain can contain a binuclear copper site, Cu_A, which is the electron acceptor for cytochrome *c*. For the quinol oxidases the peripheral domain doesn't contain any metal center to accept the electrons [57, 85]. Several type A oxidases contain besides the Cu_A centre also a heme *c* site in the peripheral domain, the cytochrome caa_3 oxidases. The ligands of the Cu_A, namely HisII-181, CysII-216, GluII-218, CysII-220, HisII-224 and MetII-227, are strictly conserved.

The subunit II of the type C oxidases is very divers in comparison with the type A and B oxidases regarding the amino acid sequence. Even within the group of type C oxidases the similarity appears to be low. The cbb_3 family has actually two subunits for electron entry. The subunit similar to subunit II of the type A and B oxidases with respect to the transmembrane α-helices and peripheral domain harbours a di-heme cytochrome *c* site. The other 'extra' subunit in the peripheral domain contains a mono-heme cytochrome *c* [76, 86]. It is unknown which subunit acts as the initial electron acceptor, but research pointed out that a cbb_3 oxidase lacking the di-heme subunit is fully capable of oxygen reduction. The exact function of the di-heme subunit is unknown[87-89].

Subunit III and IV

The function of subunits III and IV is unknown, particularly so because a cytochrome oxidase preparation of only Subunits I and II is similarly active in O_2 reduction and proton pumping as the four-subunit enzyme. Subunits III and IV do not contain any metal centers, but Subunit III contains several strongly bound phospholipid residues [53, 54, 90-92]. Subunit III is apparently essential to extend the lifetime of the oxidase since in its absence the enzyme can perform only a limited number of turnovers (~10000 turnovers) in comparison with the four-subunit enzyme (>500000) [93-95]. Studies in which the level of Subunit IV was suppressed, showed a loss of assembly of the cytochrome *c* oxidase complex [96].

Catalytic cycle of the heme copper oxidases

The reduction of oxygen obeys the following overall equation:

$$4 \text{ cyt } c^{2+} + O_2 + 8\ H^+_C \rightarrow 4 \text{ cyt } c^{3+} + 2\ H_2O + 4\ H^+_P$$

The catalytic cycle of the oxidases has been studied extensively by many different groups with a vast amount of different techniques [97-100] and has led to a general understanding of the reaction mechanism (Figure 7) (for reviews see [100-108]). The reduction of oxygen to water consumes four protons itself which come from the N-side, the so called chemical protons. However, during the reduction of oxygen four more protons are translocated across the membrane, the so-called pumped protons. Both the chemical and pumped protons contribute to the formation of the proton electrochemical gradient by withdrawing protons from the N-side of the membrane. One of the main goals of research in the past was to identify intermediates formed during oxygen reduction, determine their structures and to determine how these intermediates play a role in proton translocation and coupling electron transfer to proton transfer. The main question to be answered is how the redox free energy is converted into $\Delta\mu_{H+}$. In the following section a short introduction will be given to the catalytic cycle of oxygen reduction by the heme copper oxidases.

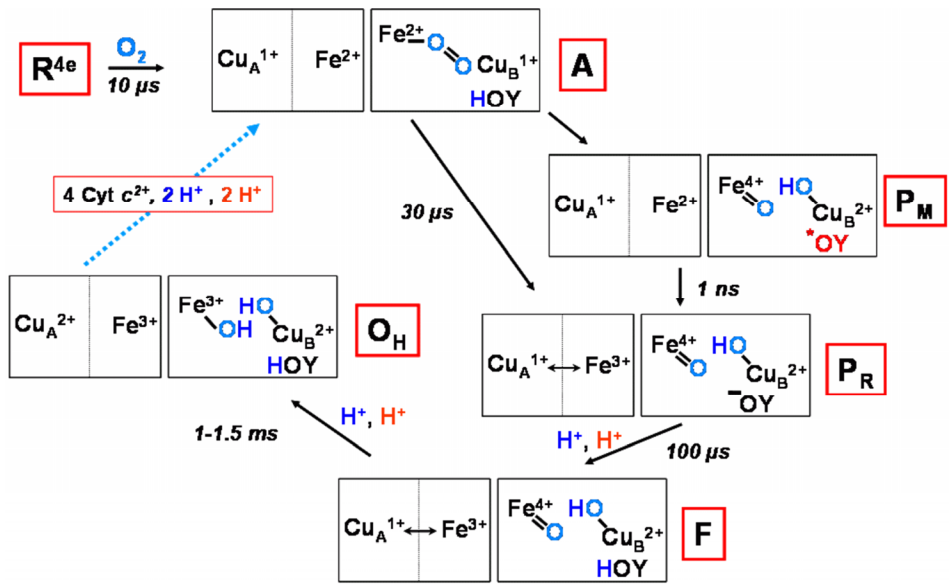

Figure 7 General scheme of the catalytic cycle of CcO. The protons in red depicture the pumped protons, the protons in blue the chemical protons and, HOY represents the TyrI-280 (*P.denitrificans* numbering). For further explanation see text.

The flow-flash method is the major technique used in studies on cytochrome oxidases. To monitor the reaction of cytochrome oxidase with oxygen the enzyme is first fully reduced (**R^{4e}** in which both hemes, Cu_A and Cu_B are reduced) in the presence of CO. The CO-bound enzyme is subsequently rapidly mixed with an oxygen-saturated solution and the CO is flashed off with a laser. Immediately after CO has left the enzyme, oxygen binds and the enzyme goes through the catalytic cycle. With this method the catalytic cycle can be studied with a time resolution of approximately 1μs determined by the off-rate of CO. One can also prepare a so-called mixed-valence or half-reduced enzyme. The mixed-valence enzyme (**MV** or **R^{2e}** in which only heme a_3 and Cu_B are reduced) is obtained by incubation of the oxidized enzyme with CO for several hours. In this time CO is oxidized to CO_2 by an unknown mechanism and the two electrons reduce heme a_3 and Cu_B; the excess CO binds to heme a_3 and can be flashed by a laser. The flow-flash set-up is usually combined with UV-Vis spectroscopy and resonance Raman spectroscopy but not with other techniques like EPR. The intermediates shown in Figure 7 have been determined with the flow-flash technique.

When the fully reduced or mixed valence enzyme reacts with oxygen the first detectable intermediate is **A** (see figure. 7). The oxygen is bound to heme a_3 and forms the oxy-ferrous complex (Fe^{2+}-O_2) in which the O-O bond is still intact [109, 110]. When starting from the mixed valence enzyme the following intermediate is **P_M**. In the **P_M**-state the O-O bond is broken and an oxo-ferryl (Fe^{4+}=O) is formed at the heme a_3 while Cu_B is oxidized to Cu_B^{2+}-OH. For O-O bond breaking four electrons and a proton are needed. In the **MV** state only three electrons are present for O-O bond breaking (heme a_3 going from Fe^{2+} to Fe^{4+} and Cu_B from 1+ to 2+). It is believed that the fourth electron is donated by the TyrI-280 under formation of a tyrosine radical [111]. After the **P_M** state the reaction cycle stops unless electrons are added to the active site. If one electron is added the cycle continues further to the **P_R** state [112]; when an additional electron is added –as if the reaction was started from **R^{4e-}** -the enzyme oxidizes completely to **O_H**.

When starting the reaction from the **R^{4e-}** state, the next intermediate succeeding the **A** state detected so far is **P_R**. The O-O bond is broken, an oxo-ferryl formed and an electron from the heme *a* /Cu_A site is withdrawn. It is speculated by Cherepanov and de Vries [100] that a '**P_M**-like' state precedes **P_R** with a radical as the electron donor for the fourth electron, but this intermediate could not be detected up till now. So far it is unclear which group acts as the primary electron donor for the fourth electron for O-O

bond breaking in fully reduced CcO. Recently it was shown that electron transfer between heme *a* and the binuclear reaction centre occurs within ns, making it difficult to trap an intermediate between the **A** and $\mathbf{P_R}$ state if any exists [113-117]. The $\mathbf{P_R}$ state is followed by the **F** state. During the transition from $\mathbf{P_R}$ to **F** one proton is pumped across the membrane and the TyrI-280 is (proposed to be) re-protonated [113-117]. The **F** state is succeeded by the $\mathbf{O_H}$ state. During this transition again one proton is pumped and the oxo-ferryl is reduced to a Fe^{3+}-OH^- intermediate by the second electron in heme *a*/Cu_A. In the following steps from $\mathbf{O_H}$ to **R**, the so-called reductive phase, two more protons are pumped across the membrane and the redox groups are reduced again.

Aim of this research

Figure 7 indicates that intermediates in enzyme reaction cycles may be formed on the microsecond time-scale necessitating fast kinetic techniques to observe them. The flow-flash technique described above is such a technique, but has its limitations. First it is used in combination with UV-Vis [101, 115, 116, 118-123]or resonance Raman spectroscopy [104-107, 124, 125], and can be used in combination with EPR at low temperatures [126, 127], but not with other spectroscopic techniques such as FTIR, Mössbauer or EXAFS spectroscopy. Second, and more importantly, it relies on the rapid photolysis of the Fe^{2+}-CO bond. Only for the mitochondrial-like heme-copper oxidases the CO dissociation is fast enough (and association slow) in combination with fast oxygen association to perform fast kinetic experiments. For the cytochrome bo_3 oxidases the dissociation of CO is rather slow (500 s^{-1}) and even slower for the cytochrome cbb_3 for which the technique cannot be applied. Hence the reaction mechanism of cytochrome cbb_3 is largely unknown.

To study enzyme reactions on the microsecond time scale, we have developed in our laboratory a new microsecond freeze-hyperquenching/sampling technique (MHQ) [100]. MHQ can be generally applied to the study of enzyme and chemical reactions (for an excellent review on freeze-quench kinetics see reference [128]). The technique relies on a micro-mixer, which mixes solutions within a microsecond. The mixed components leave the mixer as a high-speed jet and the reaction is quenched by rapid freezing on a cold plate or in cold liquid isopentane. The cold film thus obtained is removed from the cold plate and used for low-temperature UV-Vis, resonance Raman or EPR spectroscopic analyses, enabling the determination of the electronic structure of reaction intermediates. The instrumental dead time of the MHQ is approximately 60-80 μs, 100-fold faster than the classical Rapid Freeze Quench technique and competitive with the flow-flash technique.

To test the scope and limitations of the MHQ we have undertaken a detailed mechanistic study of the cytochrome aa_3 from *P. denitrificans*. In a broader sense, detailed information on the mechanism of enzyme catalyzed reactions may lead to the rational design of (mutant) enzymes or biomimetic complexes, which could be used in industrial applications. With respect to the cytochrome aa_3, in spite of the great amount of publications in the field of the heme-copper oxidases, relatively little is known about the mechanism of proton pumping and its mechanistic and thermodynamic relation to the

various electron transfer events. Application of MHQ, in particular the use of EPR to identify transient intermediates, might enable the detection of the postulated Y280 radical.

In Chapter 2 the adaptation of the MHQ set up to quench the reaction on a cold plate –yielding a frozen protein film- instead of in liquid isopentane is described. The instrumental dead time is reduced from 130-140 μs to 60-80 μs. The frozen protein film is amenable to resonance Raman spectroscopy (Chapter 3) and to low temperature kinetic studies (Chapter 4).

Chapters 5 and 6 provide detailed kinetic studies of the cytochrome oxidase in which the formation and breakdown of various intermediates could be determined by EPR and UV-Vis spectroscopy. A new tryptophan neutral radical located on the strictly conserved W272 was detected. Chapter 6 provides a hypothesis how this tryptophan residue drives and directs proton pumping in the cytochrome oxidases.

In the final chapter (Chapter 7) an electrochemical method is described to measure nitrite reductase, nitric oxide reductase and cytochrome oxidase activity by means of cyclic voltammetry with an electrode covered with a monolayer of cytochrome *c*. Since the enzymes employed in this study have high affinities for their substrates, such an electrode system can potentially be used as a biosensor for the detection of small amounts -potentially below 1 ppm at ambient conditions- of nitrite, nitric oxide or oxygen.

References

1. Stryer, L., *Biochemistry 4th edition*. 1999.
2. Slater, E. C., Mechanism of Phosphorylation in the Respiratory Chain. *Nature* **1953,** 172, (4387), 975-978.
3. Lehninger, A. L., Esterification of Inorganic Phosphate Coupled to Electron Transport between Dihydrodiphosphopyridine Nucleotide and Oxygen.2. *Journal of Biological Chemistry* **1949,** 178, (2), 625-644.
4. Lehninger, A. L.; Friedkin, M. E., Esterification of Phosphate Coupled to Electron Transport between Dihydrodiphosphopyridine Nucleotide and Oxygen. *Federation Proceedings* **1949,** 8, (1), 218-218.
5. Lehninger, A. L.; Smith, S. W., Efficiency of Phosphorylation Coupled to Electron Transport between Dihydrodiphosphopyridine Nucleotide and Oxygen. *Journal of Biological Chemistry* **1949,** 181, (1), 415-429.
6. Belitzer, W. A.; Golovskaya, K. S., Phosphate Acceptors In "Respiratory Phosphorylation" In Muscle Tissue. *Science* **1940,** 92, (2397), 536-537.

7. Friedkin, M.; Lehninger, A. L., Oxidation-Coupled Incorporation of Inorganic Radiophosphate into Phospholipide and Nucleic Acid in a Cell-Free System. *Journal of Biological Chemistry* **1949,** 177, (2), 775-788.
8. Mitchell, P., Chemiosmotic Coupling in Oxidative and Photosynthetic Phosphorylation. *Biochemical Journal* **1961,** 79, (3), P23.
9. Mitchell, P., Aspects of Chemiosmotic Hypothesis. *Biochemical Journal* **1970,** 116, (4), P5.
10. Mitchell, P., Chemiosmotic Molecular Mechanism for Proton-Translocating Adenosine Triphosphatases. *Febs Letters* **1974,** 43, (2), 189-194.
11. Mitchell, P., Vectorial Chemistry and Molecular Mechanics of Chemiosmotic Coupling - Power Transmission by Proticity. *Biochemical Society Transactions* **1976,** 4, (3), 399-430.
12. Deamer, D. W.; Crofts, A. R.; Prince, R. C., Response of Fluorescent Amines to Ph Gradients across Liposome Membranes. *Biochimica Et Biophysica Acta* **1972,** 274, (2), 323-335.
13. Rumberg, B.; Siggel, U., Ph Changes in Inner Phase of Thylakoids during Photosynthesis. *Naturwissenschaften* **1969,** 56, (3), 130-132.
14. Nicholls, D. G.; Ferguson, S. J., *Bioenergetics 3*. 2002.
15. Jagendorf,.A.T, Acid-Base Transitions and Phosphorylation by Chloroplasts. *Federation Proceedings* **1967,** 26, (5), 1361-1369.
16. Racker, E., Resolution and Reconstitution of Inner Mitochondrial Membrane. *Federation Proceedings* **1967,** 26, (5), 1335-1340.
17. Lanoue, K. F.; Schoolwerth, A. C., Metabolite Transport in Mitochondria. *Annual Review of Biochemistry* **1979,** 48, 871-922.
18. Kadenbach, B., Intrinsic and extrinsic uncoupling of oxidative phosphorylation. *Biochim Biophys Acta* **2003,** 1604, (2), 77-94.
19. Berg, H. C., The rotary motor of bacterial flagella. *Annual Review of Biochemistry* **2003,** 72, 19-54.
20. Berks, B. C.; Ferguson, S. J.; Moir, J. W.; Richardson, D. J., Enzymes and associated electron transport systems that catalyse the respiratory reduction of nitrogen oxides and oxyanions. *Biochim Biophys Acta* **1995,** 1232, (3), 97-173.
21. Schroder, I.; Johnson, E.; de Vries, S., Microbial ferric iron reductases. *FEMS Microbiol Rev* **2003,** 27, (2-3), 427-47.
22. Wasser, I. M.; de Vries, S.; Moenne-Loccoz, P.; Schroder, I.; Karlin, K. D., Nitric oxide in biological denitrification: Fe/Cu metalloenzyme and metal complex NO(x) redox chemistry. *Chem Rev* **2002,** 102, (4), 1201-34.
23. Nealson, K. H.; Saffarini, D., Iron and Manganese in Anaerobic Respiration - Environmental Significance, Physiology, and Regulation. *Annual Review of Microbiology* **1994,** 48, 311-343.
24. Brandt, U., Energy converting NADH: Quinone oxidoreductase (Complex I). *Annual Review of Biochemistry* **2006,** 75, 69-92.
25. Hosler, J. P.; Ferguson-Miller, S.; Mills, D. A., Energy transduction: Proton transfer through the respiratory complexes. *Annual Review of Biochemistry* **2006,** 75, 165-187.
26. Walker, J. E., The Nadh - Ubiquinone Oxidoreductase (Complex-I) of Respiratory Chains. *Quarterly Reviews of Biophysics* **1992,** 25, (3), 253-324.

27. Hinchliffe, P.; Carroll, J.; Sazanov, L. A., Purification, characterisation and crystallisation of the hydrophilic domain of respiratory complex I from Thermus thermophilus. *Biochimica Et Biophysica Acta-Bioenergetics* **2006**, 175-175.
28. Hinchliffe, P.; Carroll, J.; Sazanov, L. A., Identification of a novel subunit of respiratory complex I from Thermus thermophilus. *Biochemistry* **2006,** 45, (14), 4413-4420.
29. Hinchliffe, P.; Sazanov, L. A., Organization of iron-sulfur clusters in respiratory complex I. *Science* **2005,** 309, (5735), 771-774.
30. Sazanov, L. A.; Hinchliffe, P., Structure of the hydrophilic domain of respiratory complex I from Thermus thermophilus. *Science* **2006,** 311, (5766), 1430-1436.
31. Walker, J. E., The NADH:ubiquinone oxidoreductase (complex I) of respiratory chains. *Q Rev Biophys* **1992,** 25, (3), 253-324.
32. Cecchini, G.; Maklashina, E.; Yankovskaya, V.; Iverson, T. M.; Iwata, S., Variation in proton donor/acceptor pathways in succinate:quinone oxidoreductases. *FEBS Lett* **2003,** 545, (1), 31-8.
33. Yankovskaya, V.; Horsefield, R.; Tornroth, S.; Luna-Chavez, C.; Miyoshi, H.; Leger, C.; Byrne, B.; Cecchini, G.; Iwata, S., Architecture of succinate dehydrogenase and reactive oxygen species generation. *Science* **2003,** 299, (5607), 700-4.
34. Cecchini, G.; Schroder, I.; Gunsalus, R. P.; Maklashina, E., Succinate dehydrogenase and fumarate reductase from Escherichia coli. *Biochimica Et Biophysica Acta-Bioenergetics* **2002,** 1553, (1-2), 140-157.
35. Mitchell, P., The protonmotive Q cycle: a general formulation. *FEBS Lett* **1975,** 59, (2), 137-9.
36. Trumpower, B. L., The Protonmotive Q-Cycle - Energy Transduction by Coupling of Proton Translocation to Electron-Transfer by the Cytochrome-Bc1 Complex. *Journal of Biological Chemistry* **1990,** 265, (20), 11409-11412.
37. Trumpower, B. L., Cytochrome-Bc1 Complexes of Microorganisms. *Microbiological Reviews* **1990,** 54, (2), 101-129.
38. Iwata, S.; Lee, J. W.; Okada, K.; Lee, J. K.; Iwata, M.; Rasmussen, B.; Link, T. A.; Ramaswamy, S.; Jap, B. K., Complete structure of the 11-subunit bovine mitochondrial cytochrome bc1 complex. *Science* **1998,** 281, (5373), 64-71.
39. Hunte, C.; Koepke, J.; Lange, C.; Rossmanith, T.; Michel, H., Structure at 2.3 A resolution of the cytochrome bc(1) complex from the yeast Saccharomyces cerevisiae co-crystallized with an antibody Fv fragment. *Structure* **2000,** 8, (6), 669-84.
40. Berry, E. A.; Huang, L. S.; Saechao, L. K.; Pon, N. G.; Valkova-Valchanova, M.; Daldal, F., X-ray structure of Rhodobacter capsulatus cytochrome bc(1): comparison with its mitochondrial and chloroplast counterparts. *Photosynthesis Research* **2004,** 81, (3), 251-275.
41. Junemann, S., Cytochrome bd terminal oxidase. *Biochimica Et Biophysica Acta-Bioenergetics* **1997,** 1321, (2), 107-127.
42. de Vries, S.; Schroder, I., Comparison between the nitric oxide reductase family and its aerobic relatives, the cytochrome oxidases. *Biochemical Society Transactions* **2002,** 30, 662-667.

43. Moenne-Loccoz, P.; Richter, O. M. H.; Huang, H. W.; Wasser, I. M.; Ghiladi, R. A.; Karlin, K. D.; de Vries, S., Nitric oxide reductase from Paracoccus denitrificans contains an oxo-bridged heme/non-heme diiron center. *Journal of the American Chemical Society* **2000,** 122, (38), 9344-9345.
44. de Vries, S.; Mulder, T. C.; Strampraad, M. J. F.; Richter, O. M. H.; Moenne-Loccoz, P., Structural and functional characterization of the active site of NO reductase and comparison to bc-type oxidases. *Journal of Inorganic Biochemistry* **1999,** 74, (1-4), 20-20.
45. Moenne-Loccoz, P.; de Vries, S., Structural characterization of the catalytic high-spin heme b of nitric oxide reductase: A resonance Raman study. *Journal of the American Chemical Society* **1998,** 120, (21), 5147-5152.
46. Hendriks, J.; Warne, A.; Gohlke, U.; Haltia, T.; Ludovici, C.; Lubben, M.; Saraste, M., The active site of the bacterial nitric oxide reductase is a dinuclear iron center. *Biochemistry* **1998,** 37, (38), 13102-13109.
47. Hendriks, J.; Gohlke, U.; Saraste, M., From NO to OO: Nitric oxide and dioxygen in bacterial respiration. *Journal of Bioenergetics and Biomembranes* **1998,** 30, (1), 15-24.
48. Castresana, J.; Lubben, M.; Saraste, M.; Higgins, D. G., Evolution of Cytochrome-Oxidase, an Enzyme Older Than Atmospheric Oxygen. *Embo Journal* **1994,** 13, (11), 2516-2525.
49. Saraste, M.; Castresana, J., Cytochrome-Oxidase Evolved by Tinkering with Denitrification Enzymes. *Febs Letters* **1994,** 341, (1), 1-4.
50. Hendriks, J. H. M.; Jasaitis, A.; Saraste, M.; Verkhovsky, M. I., Proton and electron pathways in the bacterial nitric oxide reductase. *Biochemistry* **2002,** 41, (7), 2331-2340.
51. Iwata, S.; Ostermeier, C.; Ludwig, B.; Michel, H., Structure at 2.8-Angstrom Resolution of Cytochrome-C-Oxidase from Paracoccus-Denitrificans. *Nature* **1995,** 376, (6542), 660-669.
52. Ostermeier, C.; Iwata, S.; Ludwig, B.; Michel, H., F-V Fragment Mediated Crystallization of the Membrane-Protein Bacterial Cytochrome-C-Oxidase. *Nature Structural Biology* **1995,** 2, (10), 842-846.
53. Tsukihara, T.; Aoyama, H.; Yamashita, E.; Tomizaki, T.; Yamaguchi, H.; ShinzawaItoh, K.; Nakashima, R.; Yaono, R.; Yoshikawa, S., The whole structure of the 13-subunit oxidized cytochrome c oxidase at 2.8 angstrom. *Science* **1996,** 272, (5265), 1136-1144.
54. Tsukihara, T.; Aoyama, H.; Yamashita, E.; Tomizaki, T.; Yamaguchi, H.; Shinzawaitoh, K.; Nakashima, R.; Yaono, R.; Yoshikawa, S., Structures of Metal Sites of Oxidized Bovine Heart Cytochrome-C-Oxidase at 2.8 Angstrom. *Science* **1995,** 269, (5227), 1069-1074.
55. Ostermeier, C.; Harrenga, A.; Ermler, U.; Michel, H., Structure at 2.7 angstrom resolution of the Paracoccus denitrificans two-subunit cytochrome c oxidase complexed with an antibody F-V fragment. *Proceedings of the National Academy of Sciences of the United States of America* **1997,** 94, (20), 10547-10553.
56. Soulimane, T.; Gohlke, U.; Huber, R.; Buse, G., 3-Dimensional Crystals of Cytochrome-C-Oxidase from Thermus-Thermophilus Diffracting to 3.8 Angstrom Resolution. *Febs Letters* **1995,** 368, (1), 132-134.

57. Abramson, J.; Riistama, S.; Larsson, G.; Jasaitis, A.; Svensson-Ek, M.; Laakkonen, L.; Puustinen, A.; Iwata, S.; Wikstrom, M., The structure of the ubiquinol oxidase from Escherichia coli and its ubiquinone binding site. *Nature Structural Biology* **2000,** 7, (10), 910-917.
58. Riistama, S.; Puustinen, A.; Verkhovsky, M. I.; Morgan, J. E.; Wikstrom, M., Binding of O-2 and its reduction are both retarded by replacement of valine 279 by isoleucine in cytochrome c oxidase from Paracoccus denitrificans. *Biochemistry* **2000,** 39, (21), 6365-6372.
59. Wikstrom, M., Mechanism of proton translocation by cytochrome c oxidase: a new four-stroke histidine cycle. *Biochimica Et Biophysica Acta-Bioenergetics* **2000,** 1458, (1), 188-198.
60. Puustinen, A.; Finel, M.; Virkki, M.; Wikstrom, M., Cytochrome-O (Bo) Is a Proton Pump in Paracoccus-Denitrificans and Escherichia-Coli. *Febs Letters* **1989,** 249, (2), 163-167.
61. Behr, J.; Michel, H.; Mantele, W.; Hellwig, P., Functional properties of the heme propionates in cytochrome c oxidase from Paracoccus denitrificans. Evidence from FTIR difference spectroscopy and site-directed mutagenesis. *Biochemistry* **2000,** 39, (6), 1356-1363.
62. Gennis, R. B., How does cytochrome oxidase pump protons? *Proceedings of the National Academy of Sciences of the United States of America* **1998,** 95, (22), 12747-12749.
63. Karpefors, M.; Adelroth, P.; Aagaard, A.; Sigurdson, H.; Ek, M. S.; Brzezinski, P., Electron-proton interactions in terminal oxidases. *Biochimica Et Biophysica Acta-Bioenergetics* **1998,** 1365, (1-2), 159-169.
64. Wikstrom, M., Proton translocation by the respiratory haem-copper oxidases. *Biochimica Et Biophysica Acta-Bioenergetics* **1998,** 1365, (1-2), 185-192.
65. Mills, D. A.; Ferguson-Miller, S., Proton uptake and release in cytochrome c oxidase: separate pathways in time and space? *Biochim Biophys Acta* **1998,** 1365, (1-2), 46-52.
66. Gennis, R. B., Multiple proton-conducting pathways in cytochrome oxidase and a proposed role for the active-site tyrosine. *Biochimica Et Biophysica Acta-Bioenergetics* **1998,** 1365, (1-2), 241-248.
67. Mills, D. A.; Ferguson-Miller, S., Proton uptake and release in cytochrome c oxidase: separate pathways in time and space? *Biochimica Et Biophysica Acta-Bioenergetics* **1998,** 1365, (1-2), 46-52.
68. Pfitzner, U.; Odenwald, A.; Ostermann, T.; Weingard, L.; Ludwig, B.; Richter, O. M. H., Cytochrome c oxidase (Heme aa(3)) from Paracoccus denitrificans: Analysis of mutations in putative proton channels of subunit I. *Journal of Bioenergetics and Biomembranes* **1998,** 30, (1), 89-97.
69. Lee, H. M.; Das, T. K.; Rousseau, D. L.; Mills, D.; Ferguson-Miller, S.; Gennis, R. B., Mutations in the putative H-channel in the cytochrome c oxidase from Rhodobacter sphaeroides show that this channel is not important for proton conduction but reveal modulation of the properties of heme a. *Biochemistry* **2000,** 39, (11), 2989-96.

70. Buse, G.; Soulimane, T.; Dewor, M.; Meyer, H. E.; Bluggel, M., Evidence for a copper-coordinated histidine-tyrosine cross-link in the active site of cytochrome oxidase. *Protein Sci* **1999,** 8, (5), 985-90.
71. Michel, H., The mechanism of proton pumping by cytochrome c oxidasex127e comments]. *Proc Natl Acad Sci U S A* **1998,** 95, (22), 12819-24.
72. Blomberg, M. R.; Siegbahn, P. E.; Babcock, G. T.; Wikstrom, M., O-O bond splitting mechanism in cytochrome oxidase. *J Inorg Biochem* **2000,** 80, (3-4), 261-9.
73. Rauhamaki, V.; Baumann, M.; Soliymani, R.; Puustinen, A.; Wikstrom, M., Identification of a histidine-tyrosine cross-link in the active site of the cbb(3)-type cytochrome c oxidase from Rhodobacter sphaeroides. *Proceedings of the National Academy of Sciences of the United States of America* **2006,** 103, (44), 16135-16140.
74. Pereira, M. M.; Santana, M.; Soares, C. M.; Mendes, J.; Carita, J. N.; Fernandes, A. S.; Saraste, M.; Carrondo, M. A.; Teixeira, M., The caa(3) terminal oxidase of the thermohalophilic bacterium Rhodothermus marinus: a HiPIP: oxygen oxidoreductase lacking the key glutamate of the D-channel. *Biochimica Et Biophysica Acta-Bioenergetics* **1999,** 1413, (1), 1-13.
75. Pereira, M. M.; Verkhovskaya, M. L.; Teixeira, M.; Verkhovsky, M. I., The caa(3) terminal oxidase of Rhodothermus marinus lacking the key glutamate of the D-channel is a proton pump. *Biochemistry* **2000,** 39, (21), 6336-6340.
76. Santana, M.; Pereira, M. M.; Elias, N. P.; Soares, C. M.; Teixeira, M., Gene cluster of Rhodothermus marinus high-potential iron-sulfur protein: oxygen oxidoreductase, a caa(3)-type oxidase belonging to the superfamily of heme-copper oxidases. *Journal of Bacteriology* **2001,** 183, (2), 687-699.
77. Antonini, G.; Malatesta, F.; Sarti, P.; Brunori, M., Proton-Pumping by Cytochrome-Oxidase as Studied by Time-Resolved Stopped-Flow Spectrophotometry. *Proceedings of the National Academy of Sciences of the United States of America* **1993,** 90, (13), 5949-5953.
78. Capitanio, N.; Capitanio, G.; DeNitto, E.; Papa, S., Vectorial nature of redox Bohr effects in bovine heart cytochrome c oxidase. *Febs Letters* **1997,** 414, (2), 414-418.
79. Verkhovskaya, M. L.; GarciaHorsman, A.; Puustinen, A.; Rigaud, J. L.; Morgan, J. E.; Verkhovsky, M. I.; Wikstrom, M., Glutamic acid 286 in subunit I of cytochrome bo(3) is involved in proton translocation. *Proceedings of the National Academy of Sciences of the United States of America* **1997,** 94, (19), 10128-10131.
80. Honnami, K.; Oshima, T., Purification and Characterization of Cytochrome-C Oxidase from Thermus-Thermophilus Hb8. *Biochemistry* **1984,** 23, (3), 454-460.
81. Kannt, A.; Soulimane, T.; Buse, G.; Becker, A.; Bamberg, E.; Michel, H., Electrical current generation and proton pumping catalyzed by the ba3-type cytochrome c oxidase from Thermus thermophilus. *FEBS Lett* **1998,** 434, (1-2), 17-22.
82. Deckert, G.; Warren, P. V.; Gaasterland, T.; Young, W. G.; Lenox, A. L.; Graham, D. E.; Overbeek, R.; Snead, M. A.; Keller, M.; Aujay, M.; Huber, R.; Feldman, R. A.; Short, J. M.; Olsen, G. J.; Swanson, R. V., The complete genome of the hyperthermophilic bacterium Aquifex aeolicus. *Nature* **1998,** 392, (6674), 353-8.

83. Ma, J. X.; Tsatsos, P. H.; Zaslavsky, D.; Barquera, B.; Thomas, J. W.; Katsonouri, A.; Puustinen, A.; Wikstrom, M.; Brzezinski, P.; Alben, J. O.; Gennis, R. B., Glutamate-89 in subunit II of cytochrome bo(3) from Escherichia coli is required for the function of the heme-copper oxidase. *Biochemistry* **1999,** 38, (46), 15150-15156.
84. Larsson, S.; Kallebring, B.; Wittung, P.; Malmstrom, B. G., The CuA center of cytochrome-c oxidase: electronic structure and spectra of models compared to the properties of CuA domains. *Proc Natl Acad Sci U S A* **1995,** 92, (16), 7167-71.
85. Wilmanns, M.; Lappalainen, P.; Kelly, M.; Sauer-Eriksson, E.; Saraste, M., Crystal structure of the membrane-exposed domain from a respiratory quinol oxidase complex with an engineered dinuclear copper center. *Proc Natl Acad Sci U S A* **1995,** 92, (26), 11955-9.
86. Pereira, M. M.; Santana, M.; Teixeira, M., A novel scenario for the evolution of haem-copper oxygen reductases. *Biochim Biophys Acta* **2001,** 1505, (2-3), 185-208.
87. Pitcher, R. S.; Brittain, T.; Watmough, N. J., Cytochrome cbb(3) oxidase and bacterial microaerobic metabolism. *Biochemical Society Transactions* **2002,** 30, 653-658.
88. Zufferey, R.; Preisig, O.; Hennecke, H.; ThonyMeyer, L., Assembly and function of the cytochrome cbb(3) oxidase subunits in Bradyrhizobium japonicum. *Journal of Biological Chemistry* **1996,** 271, (15), 9114-9119.
89. Preisig, O.; Zufferey, R.; ThonyMeyer, L.; Appleby, C. A.; Hennecke, H., A high-affinity cbb(3)-type cytochrome oxidase terminates the symbiosis-specific respiratory chain of Bradyrhizobium japonicum. *Journal of Bacteriology* **1996,** 178, (6), 1532-1538.
90. Ostermeier, C.; Harrenga, A.; Ermler, U.; Michel, H., Structure at 2.7 A resolution of the Paracoccus denitrificans two-subunit cytochrome c oxidase complexed with an antibody FV fragment. *Proc Natl Acad Sci U S A* **1997,** 94, (20), 10547-53.
91. Iwata, S.; Ostermeier, C.; Ludwig, B.; Michel, H., Structure at 2.8 A resolution of cytochrome c oxidase from Paracoccus denitrificans. *Nature* **1995,** 376, (6542), 660-9.
92. Svensson-Ek, M.; Abramson, J.; Larsson, G.; Tornroth, S.; Brzezinski, P.; Iwata, S., The X-ray crystal structures of wild-type and EQ(I-286) mutant cytochrome c oxidases from Rhodobacter sphaeroides. *Journal of Molecular Biology* **2002,** 321, (2), 329-339.
93. Steverding, D.; Kohnke, D.; Ludwig, B.; Kadenbach, B., Proton Slippage in Cytochrome-C-Oxidase of Paracoccus-Denitrificans - Membrane-Potential Measurements with the 2-Subunit and 3-Subunit Enzyme. *European Journal of Biochemistry* **1993,** 212, (3), 827-831.
94. Bratton, M. R.; Pressler, M. A.; Hosler, J. P., Suicide inactivation of cytochrome c oxidase: catalytic turnover in the absence of subunit III alters the active site. *Biochemistry* **1999,** 38, (49), 16236-45.
95. Haltia, T.; Semo, N.; Arrondo, J. L. R.; Goni, F. M.; Freire, E., Thermodynamic and Structural Stability of Cytochrome-C-Oxidase from Paracoccus-Denitrificans. *Biochemistry* **1994,** 33, (32), 9731-9740.

96. Li, Y.; Park, J. S.; Deng, J. H.; Bai, Y., Cytochrome c oxidase subunit IV is essential for assembly and respiratory function of the enzyme complex. *J Bioenerg Biomembr* **2006,** 38, (5-6), 283-91.
97. Babcock, G. T.; Wikstrom, M., Oxygen Activation and the Conservation of Energy in Cell Respiration. *Nature* **1992,** 356, (6367), 301-309.
98. Richter, O. M.; Ludwig, B., Cytochrome c oxidase--structure, function, and physiology of a redox-driven molecular machine. *Rev Physiol Biochem Pharmacol* **2003,** 147, 47-74.
99. Michel, H.; Behr, J.; Harrenga, A.; Kannt, A., Cytochrome c oxidase: structure and spectroscopy. *Annu Rev Biophys Biomol Struct* **1998,** 27, 329-56.
100. Cherepanov, A. V.; de Vries, S., Microsecond freeze-hyperquenching: development of a new ultrafast micro-mixing and sampling technology and application to enzyme catalysis. *Biochimica Et Biophysica Acta-Bioenergetics* **2004,** 1656, (1), 1-31.
101. Sucheta, A.; Szundi, I.; Einarsdottir, O., Intermediates in the reaction of fully reduced cytochrome c oxidase with dioxygen. *Biochemistry* **1998,** 37, (51), 17905-17914.
102. Sucheta, A.; Georgiadis, K. E.; Einarsdottir, O., Mechanism of cytochrome c oxidase-catalyzed reduction of dioxygen to water: Evidence for peroxy and ferryl intermediates at room temperature. *Biochemistry* **1997,** 36, (3), 554-565.
103. Einarsdottir, O.; Szundi, I., Time-resolved optical absorption studies of cytochrome oxidase dynamics. *Biochimica Et Biophysica Acta-Bioenergetics* **2004,** 1655, (1-3), 263-273.
104. Proshlyakov, D. A.; Ogura, T.; Shinzawa-Itoh, K.; Yoshikawa, S.; Appelman, E. H.; Kitagawa, T., Selective resonance Raman observation of the "607 nm" form generated in the reaction of oxidized cytochrome c oxidase with hydrogen peroxide. *J Biol Chem* **1994,** 269, (47), 29385-8.
105. Ogura, T.; Kitagawa, T., Resonance Raman characterization of the P intermediate in the reaction of bovine cytochrome c oxidase. *Biochim Biophys Acta* **2004,** 1655, (1-3), 290-7.
106. Kitagawa, T., Structures of reaction intermediates of bovine cytochrome c oxidase probed by time-resolved vibrational spectroscopy. *J Inorg Biochem* **2000,** 82, (1-4), 9-18.
107. Han, S. H.; Ching, Y. C.; Rousseau, D. L., Cytochrome c oxidase: decay of the primary oxygen intermediate involves direct electron transfer from cytochrome a. *Proc Natl Acad Sci U S A* **1990,** 87, (21), 8408-12.
108. Han, S.; Takahashi, S.; Rousseau, D. L., Time dependence of the catalytic intermediates in cytochrome c oxidase. *J Biol Chem* **2000,** 275, (3), 1910-9.
109. Proshlyakov, D. A.; Pressler, M. A.; Babcock, G. T., Dioxygen activation and bond cleavage by mixed-valence cytochrome c oxidase. *Proc Natl Acad Sci U S A* **1998,** 95, (14), 8020-5.
110. Proshlyakov, D. A.; Pressler, M. A.; DeMaso, C.; Leykam, J. F.; DeWitt, D. L.; Babcock, G. T., Oxygen activation and reduction in respiration: involvement of redox-active tyrosine 244. *Science* **2000,** 290, (5496), 1588-91.
111. Siletsky, S. A.; Han, D.; Brand, S.; Morgan, J. E.; Fabian, M.; Geren, L.; Millett, F.; Durham, B.; Konstantinov, A. A.; Gennis, R. B., Single-electron

photoreduction of the P-M intermediate of cytochrome c oxidase. *Biochimica Et Biophysica Acta-Bioenergetics* **2006,** 1757, (9-10), 1122-1132.

112. Pilet, E.; Jasaitis, A.; Liebl, U.; Vos, M. H., Electron transfer between hemes in mammalian cytochrome c oxidase. *Proceedings of the National Academy of Sciences of the United States of America* **2004,** 101, (46), 16198-16203.
113. Wikstrom, M., Cytochrome c oxidase: 25 years of the elusive proton pump. *Biochimica Et Biophysica Acta-Bioenergetics* **2004,** 1655, (1-3), 241-247.
114. Wikstrom, M.; Verkhovsky, M. I., Towards the mechanism of proton pumping by the haem-copper oxidases. *Biochim Biophys Acta* **2006,** 1757, (8), 1047-51.
115. Ruitenberg, M.; Kannt, A.; Bamberg, E.; Fendler, K.; Michel, H., Reduction of cytochrome c oxidase by a second electron leads to proton translocation. *Nature* **2002,** 417, (6884), 99-102.
116. Faxen, K.; Gilderson, G.; Adelroth, P.; Brzezinski, P., A mechanistic principle for proton pumping by cytochrome c oxidase. *Nature* **2005,** 437, (7056), 286-289.
117. Belevich, I.; Verkhovsky, M. I.; Wikstrom, M., Proton-coupled electron transfer drives the proton pump of cytochrome c oxidase. *Nature* **2006,** 440, (7085), 829-832.
118. Verkhovsky, M. I.; Belevich, I.; Bloch, D. A.; Wikstrom, M., Elementary steps of proton translocation in the catalytic cycle of cytochrome oxidase. *Biochimica Et Biophysica Acta-Bioenergetics* **2006,** 1757, (5-6), 401-407.
119. Belevich, I.; Verkhovsky, M. I.; Wikstrom, M., Proton-coupled electron transfer drives the proton pump of cytochrome c oxidase. *Nature* **2006,** 440, (7085), 829-32.
120. Adelroth, P.; Ek, M. S.; Mitchell, D. M.; Gennis, R. B.; Brzezinski, P., Glutamate 286 in cytochrome aa(3) from Rhodobacter sphaeroides is involved in proton uptake during the reaction of the fully-reduced enzyme with dioxygen. *Biochemistry* **1997,** 36, (45), 13824-13829.
121. Szundi, I.; Cappuccio, J.; Einarsdottir, O., Amplitude analysis of single-wavelength time-dependent absorption data does not support the conventional sequential mechanism for the reduction of dioxygen to water catalyzed by bovine heart cytochrome c oxidase. *Biochemistry* **2004,** 43, (50), 15746-58.
122. Sucheta, A.; Einarsdottir, O., The mechanism of the reduction of dioxygen to water catalyzed by cytochrome c oxidase. *Biophysical Journal* **1997,** 72, (2), Wp393-Wp393.
123. Einarsdottir, O.; Szundi, I., Time-resolved optical absorption studies of cytochrome oxidase dynamics. *Biochim Biophys Acta* **2004,** 1655, (1-3), 263-73.
124. Varotsis, C.; Zhang, Y.; Appelman, E. H.; Babcock, G. T., Resolution of the reaction sequence during the reduction of O2 by cytochrome oxidase. *Proc Natl Acad Sci U S A* **1993,** 90, (1), 237-41.
125. Han, S.; Ching, Y. C.; Rousseau, D. L., Ferryl and hydroxy intermediates in the reaction of oxygen with reduced cytochrome c oxidase. *Nature* **1990,** 348, (6296), 89-90.
126. Chance, B.; Saronio, C.; Leigh, J. S., Functional Intermediates in Reaction of Membrane-Bound Cytochrome-Oxidase with Oxygen. *Journal of Biological Chemistry* **1975,** 250, (24), 9226-9237.

127. Morgan, J. E.; Verkhovsky, M. I.; Palmer, G.; Wikstrom, M., Role of the PR intermediate in the reaction of cytochrome c oxidase with O2. *Biochemistry* **2001,** 40, (23), 6882-92.
128. De Vries, S., Freeze-Quench Kinetics. *Application of Physical Methods to Inorganic and Bioinorganic Chemistry* **2007**, 125-142.

Chapter 2

A microsecond freeze-hyperquenching/sampling setup equipped with a rotating cylindrical cold plate

Frank G.M. Wiertz, Alexei C. Cherepanov, Marc Strampraad, Angela Paulus, Nanning de Jong and Simon de Vries

manuscript in preperation

Summary

A microsecond freeze-hyperquenching/sampling device is described to quench (bio)chemical reactions with a characteristic dead-time of 75-85 microseconds. The reactants are mixed in a recently developed stainless steel micro-mixer with a mixing time below 2 µs operating at high pressures (up to 400 bar) and high linear flow-rates (up to 200 m/s) (Cherepanov, A.V. and de Vries, S. (2004) Biochimica et Biophysica Acta, 1656, 1-31 [1]). The mixed reactants exit the mixer body as a free high-speed jet, which is rapidly frozen (50-60µs) on a rotating cylindrical cold plate cooled to 77K. The thin (90 µm) vitrified film produced in this way is subsequently collected and sampled. The mixer and cold plate are mounted in a vacuum chamber at 30 mbar preventing jet break up. Procedures are described to handle the cold powder enabling analysis by low-temperature UV-Vis spectroscopy, resonance Raman spectroscopy and X- and Q-band EPR spectroscopy.

Introduction

The relation between the active site structure of an enzyme and its function is of great interest in biochemistry. Single turnover or pre-steady state kinetic studies provide information on the catalytic mechanism through the analysis of transient intermediates. Today many different pre-steady state kinetic techniques exist e.g. photoflash caged compound release, flow-flash, temperature jump, pressure jump, stopped-flow and rapid freeze-quenching, [1-16].

In the caged compound technique one of the substrates is an inactive photo-labile analogue that is activated by a short intense laser flash producing the substrate ready to react without the need for mixing [2]. The flow-flash technique is a variation on the caged compound method. The enzyme is inactivated by binding an inhibitor (e.g. CO, NO) to the active site which can be released by a laser flash. By mixing the enzyme with substrate (e.g. O_2) prior to the laser flash, substrate will bind and the reaction proceeds. Reaction progress is monitored e.g. by UV-Vis spectroscopy. In the flow-flash technique it is of great importance that the inhibitor is quickly released from the active site and that the second substrate binds much faster to the active site than rebinding of the inhibitor [3].

In the temperature jump method the reactants are already mixed and in equilibrium. With a laser flash the temperature is increased rapidly by 5 to 10 °C. The increase in temperature shifts the equilibrium due to the $T\Delta S$ term and the reaction mixture adapts to the new equilibrium. Besides the optical artifacts caused by the laser flash the small deviation from equilibrium by the temperature jump is a major drawback. The pressure jump uses a quick rise of the pressure up to 100 bar and release of the pressure; the technique suffers similar drawbacks as the temperature jump technique. For a more extensive overview of pre-steady state kinetic techniques a recently published review is recommended [4].

The continuous flow technique originally designed by Roughton and Millikan [5] allowed fast mixing of two fluids (then ~ 1-2 ms, currently ~ 60 μs) while monitoring the mixture with a spectrophotometer at different time intervals by measuring perpendicular to the flow direction at different points along the stream. Based on this device and to save sample, the stopped-flow technique was developed [6]. The stopped-flow method is a technique in which enzyme and substrate are rapidly mixed (~ 1 ms) and the reaction progress is followed by UV-Vis spectroscopy in an observation chamber.

When the observation chamber is filled, the flow stops abruptly, hence the name. Both the stopped-flow and continuous-flow method are not very suitable for monitoring by EPR spectroscopy since the techniques are rather sample consuming (~0.5 mM and ~1 ml). Though radicals can in general be detected at room temperatures by EPR, transition metals need low temperatures. Freeze-quenching is an alternative to the continuous-flow and stopped-flow techniques, in which enzyme and substrate are rapidly mixed (5-7 ms) and subsequently frozen. By freezing the sample quickly the catalytic cycle is brought to a standstill and the frozen powder can be used for low temperature UV-Vis, EPR and resonance Raman spectroscopy. In this way transient intermediates that were trapped can be studied and if samples are frozen at different time intervals a full kinetic profile of a single turnover can be made. Although freeze-quenching doesn't have the time resolution of other pre-steady state kinetic methods it is broadly applicable and has been used successfully in the study of redox enzymes, but also in many other enzymes. Rapid freeze-quenching was developed in the nineteen sixties and seventies initially for studying redox-enzyme kinetics with EPR spectroscopy since the continuous- and stopped-flow methods were not very suitable for EPR spectroscopy. One of the first practical rapid freeze-quench devices (RFQ) had a total dead-time of approximately 5 to 7 ms and was developed by Graham, Ballou and Palmer from various other rapid quenching methods [7-13]. The standard instrument has a four-jet tangential mixer, which had been developed in 1923 and further improved to a mixer with a dead-time of approximately 40µs [5, 14-16].

In spite of the high time resolution (< 1ns) of the various photoflash-activation kinetic techniques, they are obviously not as generally applicable as the mixing techniques, which, however, suffer from a relatively long dead time (~ 1ms). Since peptide movements in enzymes may occur at the µs time scale, enzyme catalytic intermediates may be formed within microseconds. To deepen our understanding of enzyme catalysis we set out to design methods for trapping and characterizing such transient intermediates. Our mixing/sampling method MHQ (Microsecond freeze-HyperQuenching) is an extension of the RFQ technique operating in the microsecond time domain.

The RFQ is basically a continuous flow instrument (like Roughton et al. [5]). The flow is generated by a drive-ram pushing two syringes, one loaded with enzyme and the other with substrate, to the mixer after which the sample is delivered through a nozzle to a cryo-bath where the reaction is rapidly quenched (Figure 1).

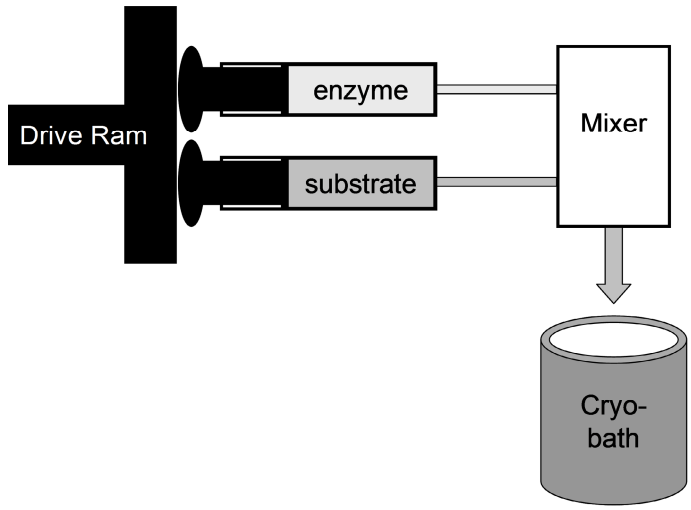

Figure 1 Schematics of a freeze-quench setup. As a cryo-medium cold iso-pentane (T = ~135 K) or liquid ethane (T = ~ 90 to 120 K) might be employed. By varying the length of nozzle tubing attached to the mixer body (indicated by the arrow) the sample aging time is varied.

The sample aging time is varied by changing the length of the nozzle tubing rather then varying the drive-ram speed, because this could lead to too low Reynolds number resulting in incomplete mixing due to laminar flow. Mixing efficiency depends on the flow rate and is determined by the Reynolds number, a dimensionless number. The Reynolds number (*Re*) is defined as the ratio of inertial forces to viscous forces and is a measure for turbulence:

Equation 1 $\boldsymbol{Re = \rho \bullet \langle \upsilon \rangle \bullet d/\eta}$

in which *Re* is the Reynolds number, ρ the density of the solvent (in kg/m^3), $\langle \upsilon \rangle$ the average flow velocity (m/s) of the liquid, d the diameter of the channel and η the dynamic viscosity (in $kg/(m^3 \bullet s)$). For fluid flows in pipes, a Reynolds number > 2000-2500 results in turbulent flow enhancing the mixing efficiency. If the flow rate is too low the Reynolds number drops below 2000 and the fluid comes in the regime where laminar flow occurs. Mixing between the two streams would still occur, but slowly and may take milliseconds up to seconds, depending on the contact area between the two streams.

To quench the reaction either cold isopentane (~135K) or liquid ethane (~90 to 120 K) was used. Ethane has the advantage that it can be pumped off under vacuum making the samples suitable for resonance Raman spectroscopy [17].

The dead-time or minimal total sample aging time (τ_a) can be formulated as follows:

Equation 2 $\boldsymbol{\tau_a = \tau_m + \tau_t + \tau_q}$

in which τ_a is the total aging time of the sample, τ_m the mixing time, τ_t the transport or sample delivery time and τ_q the quenching (or freezing) time. The total dead-time of the RFQ is composed of ~40 µs mixing time, ~ 1 to 2 ms sample delivery time and 4 to 6 ms for the quenching time yielding a total dead-time of 5 to 7 ms.

The properties of the mixer of the freeze-quenching device are important to obtain a short sample ageing time. It should be a fast mixer with a τ_m as low as possible. It should withstand high pressures for fast flow rates and be able to mix viscous samples and produce a small jet to decrease the freezing time [18].

Tanaka et al.[19] and Lin et al.[20] developed a freeze-quenching device with a micro mixer based on silicon developed with micro chip technologies. As a freezing medium they used either copper or silver rollers partially emerged in liquid nitrogen. The sample is sprayed on the rollers and is grinded to a fine powder eventually. They claim a dead time of 50 µs (Tanaka et al.) and 200 µs (Lin et al.). The deadtime of these devices was critically evaluated by Cherepanov et al. [1] and De Vries [4] and estimated to be rather 0.5 ms then the reported 50 and 200 µs. Tanaka's dead time is calculated from the conversion of metmyoglobin to its azide complex, but they used wrong reaction rate constants (an order of magnitude too low). Furthermore, the setup with the rollers works at ambient pressure –leading to jet break up. The rollers are placed above a container of cold liquid nitrogen creating turbulent cold nitrogen vapours causing the jet temperature to decrease drastically, leading to underreaction of the sample and to smaller calculated dead times.

In 2004 a stainless steel mixer based on the four-jet tangential mixing principle was built with micro-channels (50µm) by Cherepanov and de Vries [1]. It can handle high pressures and therefore high flow rates. The mixing time was determined at < 2 µs and the mixer was used in combination with cold isopentane as a quenching medium. The total dead-

time of the system developed was 130 µs. The major time limitation of the setup was the spraying distance, which was minimally 2 cm; at smaller distances the jet would freeze by the cold isopentane vapors. To improve on the dead time and avoid the use of isopentane, the MQH set up was modified employing a rotating cold plate cooled to 77 K to quench the reaction. The whole setup is built in a vacuum chamber at 30 mbar preventing jet-breakup and warming of the cold plate. The minimal spray distance was decreased to 4 mm and the dead-time of the setup was determined to be 75-85 µs. The advantage of the setup is not only the lower dead-time, but the sample – a cold powder devoid of cryo-medium - is also suitable for many different techniques (e.g. (thermal slope) UV-Vis, resonance Raman spectroscopy, EPR etc.) without the interference of the isopentane. For EPR and resonance Raman spectroscopy we developed an easy to use and reproducible packing method for freeze-quenched samples dispersed in liquid nitrogen.

Materials and methods

The microsecond freeze-hyperquenching setup (MHQ)

The microsecond freeze-hyperquenching device is a modified version of the one described by Cherepanov and de Vries [1] (Figure 2). The stainless-steel mixer **(7)** is the same as used before with a platinum inlay of 20 µm (µs time regime) or 100 µm (ms time regime) purchased from Provac GmbH. The rotating cylindrical cold plate plus mixer is built within a vacuum chamber **(10)** (Polymethylmethacrylate (PMMA), height 42 cm, lid 2cm, inner diameter 32 cm outer diameter 36 cm). Instead of a swing-arm for horizontal motion of the mixer, the mixer is mounted on a robot arm **(6)** (Applied Motion Products, with a programmable stepper motor driver 1240i with sliding arm) to move the mixer up and down within the rotating cold plate **(8)** at a constant speed. The rotating cylindrical cold plate (built in house from ST51 grade aluminum), has a total height of 11 cm, an inner depth of 7 cm, an inner diameter of 13 cm and an outer diameter of 16 cm). Using manual timing the sample is being sprayed on the inner side of the cylindrical cold plate producing a frozen film with a thickness of 90 µm (enzyme volume of 250 µl mixed 1:1 with substrate resulting in a total sample volume of 500 µl).

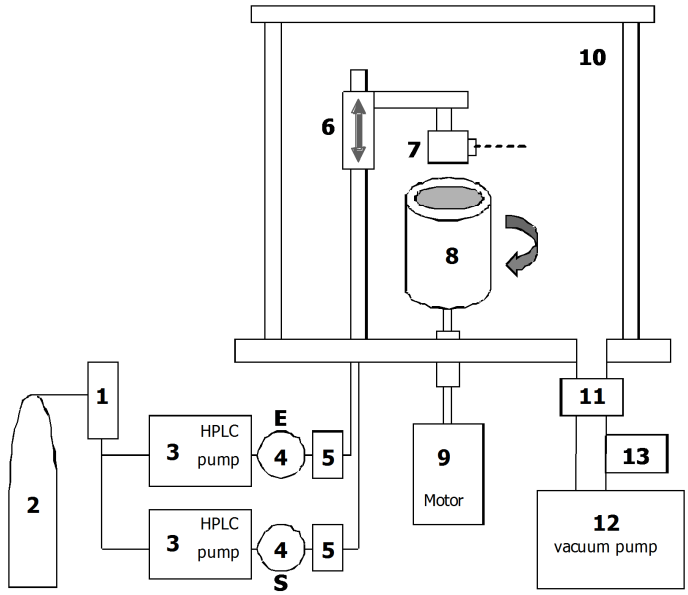

Figure 2 Schematic drawing of the microsecond freeze-hyperquenching setup. 1) buffer bottle for continuously flowing the system when not in operation, flushed with argon (2). 3) 2 HPLC pumps for the enzyme and substrate lines, 4) Rheodyne injectors for injecting the enzyme and substrate, 5) low dead-volume 0.2 micrometer filters, 6) robot arm controlling the mixer motion during the sample spraying, 7) four-jet tangential mixer, 8) rotating cylindrical cold plate with a tungsten coating on the inside driven by a centrifugal motor (9), 10) vacuum chamber , 11+12) valve and vacuum pump to evacuate the chamber, 13) control valve for maintaining a constant low pressure within the chamber by shortcutting the pump line.

The cold plate in the vacuum chamber is connected with the motor outside the chamber by a special ferromagnetic-fluid axis feedthrough (from Ferrotech, model SS-500-SLAEW). The axis was kept at 40 °C with a heating circulator to prevent freezing of the ferromagnetic fluid when cooling down the cold plate. The motor **(9)** was taken from a Sorval centrifuge. The system was evacuated with a Varian (Tri scroll^{tm} 300) vacuum pump **(12)** connected to the chamber via an electronic valve **(11)** (Edwards C41752000). Sample delivery and injection were performed with HPLC pumps from Waters (Type 515) **(3)** and Rheodyne injectors (type 7725i), respectively **(4)**. Filters **(5)** (ultra-low dead volume filters (0.5µm, 0.61µl dead volume from Upchurch), were placed in the substrate and enzyme lines to prevent clogging of the orifice. All fluid lines are from Peek

tubing (blue, maximum pressure 7000psi, Upchurch) and fittings used are carbon enhanced Graph-Tite fittings (Upchurch). The pressure in the vacuum chamber was controlled with an Edwards active gauge controller (APG-M-NW-16 pressure meter and AGC-single disp., NORS232, 3 head controller) by a controllable electronic Air Admit N/C valve (Edwards C41731000) **(13)**. The vacuum release valve (Varian, L9480-301) was a simple manual valve to gently let the vacuum off from the spray chamber at the end of a spray session.

Sample preparation, and packing device

Horse heart met-myoglobin (Mb) and sodiumazide (Az) were purchased from Sigma. A stock solution of Mb was prepared by dissolving the Mb in Millipore grade water to a concentration of 0.7 mM. Prior to use the Mb solution was diluted 1:1 with citrate buffer 125 mM pH 5.2. Sodiumazide stock solutions were made by dissolving the sodiumazide in 125 mM citrate buffer pH 5.2 at a concentration of 2 M and dilution in the same buffer for lower azide concentrations. After spraying the cold powder was stored in Greiner tubes in liquid nitrogen until further use. The Greiner tubes were cut off at the bottom and sealed with cheese cloth to assure that LN_2 can freely enter and leave the tube.

EPR and resonance Raman tube packing is a simplified version of the one earlier described by Tsai et al.[21]. EPR tubes were cut at the end and a 20 to 60 μm hydrophobic poly-ethylene filter was mounted (a kind gift from Porex, Germany). An aluminum funnel was connected to the tube by silicon tubing. The funnel and tube were cooled in liquid nitrogen. The sample dispensed in liquid nitrogen was poured into the funnel. The funnel was gently closed with a rubber stopper to build up some pressure enabling flow of the cold powder into the EPR tube. When the tube was filled with the powdery sample, the sample was packed with a pre-cooled packing rod. The packed EPR tubes were stored under liquid nitrogen until further use.

Low-temperature UV-Vis spectroscopy

For UV-Vis spectroscopy a small amount of powdery sample was transferred to cold isopentane into a sample-reference two-window cuvet equipped with special UV transparent PMMA [22]. Isopentane served as a reference. The spectra were recorded with a SLM-Aminco DW2000

spectrophotometer equipped with a quartz dewar connected to a LN_2 vessel providing a continuous flow of cold N_2 gas to keep the temperature at 90K.

Millisecond nozzle extensions

For spraying in the millisecond time frame a special nozzle was designed. With the standard mixer set up with a jet of 20 µm maximum reaction times of ~ 600-800 µs can be obtained since the distance of the mixer to the cold plate could not be extended further than 7 cm owing the dimensions of the cylinder; lower flow rates than ~ 100 m/s would result in incomplete mixing. To prepare samples aged for milliseconds an extension tubing of stainless steel with a diameter of 125 µm was welded on the brass screw which acts as a delay loop. To obtain proper jet speeds a platinum inlay of 100 µm was used instead of 20 µm further preventing too high backpressures. By making nozzles with different lengths of stainless steel the reaction time can be varied from ms up to hundreds of milliseconds as in the RFQ method [23]. Although a 100 µm nozzle is used complete mixing within 2 µs is assured because the flow rates used are much higher, up to 12 ml/min, which produce turbulent flow.

Coating of the rotating cylindrical cold plate and other metals used as a cold plate

Ultra pure tungsten (99.999 %, International materials), silver (99.95% purity, Goodfellow), palladium (99.95%, Goodfellow) were applied by physical vapor deposition on the inside of the cylindrical cold plate. To assure sticking of the sample to the inside of the cold plate, the cold plate was powder blasted with glass pearls (grain size 50 to 100 µm, pressure 2 bar, Normfinish) and washed thoroughly with Milli-Q water and chloroform prior to sputtering. Approximately 50 cycles sputtering yielded a solid layer of approximately 50µm. Chromium coating was by electrolytical deposition. Other metallic surfaces that were tested included titanium (purity unknown) and commercial brass.

Temperature measurements

A copper constantan thermocouple was used to determine the jet temperature. The temperature during a spray session was monitored on a recorder.

Results and discussion

Operating the MHQ

The cold plate was cooled with liquid nitrogen until the plate reached 77 K. The enzyme and substrate injectors were loaded (enzyme line 250 µl and substrate line with 1 ml) a few minutes before the cold plate was at 77 K. The excess liquid nitrogen was removed from the cylinder and the vacuum chamber mounted. After the vacuum reached 30 mbar the rotor was started and when 7000 rpm was reached first the substrate line was injected (to assure optimal substrate concentration in the mixer) and a few seconds later the enzyme line was injected. The robot arm was activated and the mixture of enzyme and substrate was sprayed as a film on the inner surface of the cold cylinder. After spraying the vacuum was released by letting cold nitrogen gas into the chamber (withdrawn from a dewar with liquid nitrogen), the chamber was removed and quickly 1 l of liquid nitrogen was poured into the cold plate. This whole procedure takes approximately two minutes in which the temperature of the rotating cold plate never exceeded 90 K. The film was scraped off from the inside of the cold plate while great care was taken that liquid nitrogen was in contact with the cold powder.

Jet temperature measurements

The jet temperature is an important parameter since it corresponds to the reaction temperature. To determine the temperature of the jet during deposition of the frozen film a copper constantan thermocouple was mounted 3 mm away from the orifice (20 µm) in the jet. The temperature was measured at this position with the mixer placed at 6, 10 or 40 mm total distance from the cold plate. The cold plate was cooled down and the temperature was measured while a total sample size of 1 ml water was sprayed at a flow rate of 2 ml/min at 30, 50, 100 and 500 mbar pressure in the vacuum chamber. The results are shown in table 1.

During evacuation a temperature drop was observed which was highest at the lowest pressure (30 mbar). On average the temperature drops by 10 °C at 30 mbar. The temperature drop is probably caused by degassing of the jet and some evaporation of water.

The temperature drop is smaller at longer distances from the cold plate as might be expected, but surprisingly, at 30 mbar the temperature gradient in the jet is negligible.

Table 1 Jet temperatures measured with a thermocouple in the jet at 3 mm from the orifice. The mixer was placed 6, 10 and 40 mm away from the cold plate at a pressure of 30, 50, 100 and 500 mbar. The measurements were done with 1 ml sprayed at a flow rate of 2 ml/min giving a total spray time of 30 seconds.

Distance from plate in mm	T in °C at Start*	T in °C at vacuum	T in °C End of spraying	T in °C average during spraying	ΔT during spraying
		500 mbar			
6	21	16	3.5	10	12.5
10	22.5	19	13	16	6
40	22.5	19	12	15.5	7
		100 mbar			
6	18.5	12.5	3	7.5	9
10	22	16.5	10.5	13.5	6
40	23	18.5	13.5	16	6
		50 mbar			
6	18	10	0.5	5.25	9.5
10	22	15	9.5	12.25	5.5
40	22	17.5	10.5	14	7
		30 mbar			
6	23	11.5	6.5	9	5
10	21	12	6.5	9.25	5.5
40	20	13.5	6.5	10	7

* at ambient pressure

The best working pressure of the MHQ set up is 30 mbar. At this pressure the temperature drops to 6.5 °C at the end of the film deposition while during spraying the temperature changes by 5 to 7 °C. This yields a spray temperature of 9 ±3 °C under the standard operating conditions. At higher pressures the temperature drops are apparently higher close to the cold plate and decrease at positions further away from the cold plate. During spraying the rotating cold plate creates a cold vortex within the vacuum chamber. At lower pressures is the jet cools more than at higher pressures

due to faster out gassing and evaporation. It can be concluded that operating the set up at 30 mbar does not only prevent jet-breakup but also leads to a more constant jet temperature. The main temperature drop at 30 mbar is caused during evacuation and not during deposition of the film. The temperature drop is found to be proportionally smaller for shorter operation times yielding an average temperature of 10 ± 2°C when operating for 15 seconds and a total sample of 0.5 ml at 2 ml/min flow rate.

Determination of the freezing time

Millisecond nozzle (125 µm) freezing time determination

To determine the freezing time and minimal dead time of the MHQ setup, equipped with a nozzle of 125 µm, samples at various Az concentrations (5 to 20 mM end concentrations) were sprayed with Mb (0.35mM end concentration). The reaction constants at various Az concentrations and temperatures have been determined by Cherepanov and de Vries [1]and were used in the experiments described in Figures 3-5. The reaction of met-myoglobin with azide is a two-step reaction with an initial high-spin Azide complex as intermediate, which decays to the stable low-spin complex in ~ 100 µs [9]:

$$\mathbf{MbFe^{3+} + N_3^{1-} \leftrightarrow MbFe^{3+}{\bullet}N_3^{1-}\ (high\ spin) \leftrightarrow MbFe^{3+}{\bullet}N_3^{1-}\ (low\ spin)}$$

By determining the amount of Az bound to Mb by deconvolution of the low temperature UV-Vis spectrum the reaction progress and thus the total sample ageing time can be determined. The time-of-flights used were 1, 2 and 5 ms, which are achieved by using different nozzle lengths. The flow rate was 12 ml/min resulting in a jet speed of 25 m/s to assure fast mixing within µs with an orifice diameter or jet diameter of 100 µm. The results are shown in figure 3. The y-axis cutoff through the points with different reaction times represents a freezing time of 1.08 ± 0.1 ms.

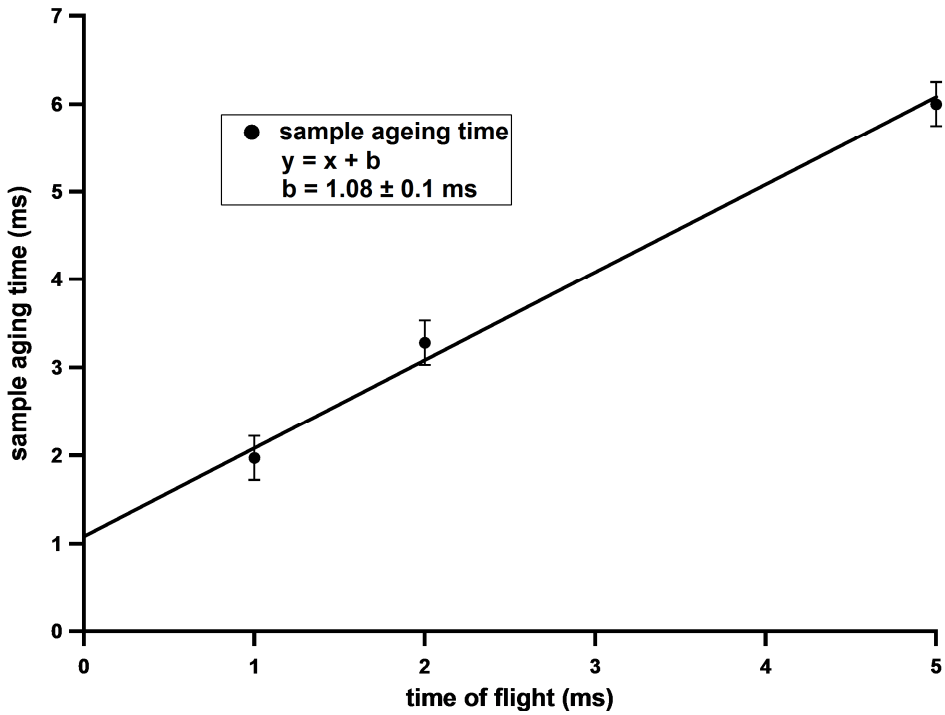

Figure 3 Determination of the freezing time of the MHQ setup for the ms extension nozzles with a jet diameter of 125µm.. By extrapolation of the fitted line to t=0 the actual freezing time can be determined.

Microsecond setup freezing time determination

To determine the freezing time of the 20 µm jet 0.7 mM of Mb was reacted with 2M Azide to ensure sufficient conversion for analysis to $MbFe^{3+}\bullet N_3^{1-}$ at the shortest reaction times. The reaction time was varied by placing the mixer at different distances from the cold plate. The flow rate was kept at 2 ml/min yielding a calculated jet speed of 106m/s. However, Cherepanov et al.[1] determined the jet speed with laser-doppler measurements and found that it was 10% higher (116 m/s) then the value calculated from the orifice diameter and flow rate, in accordance with fluid dynamics theory.

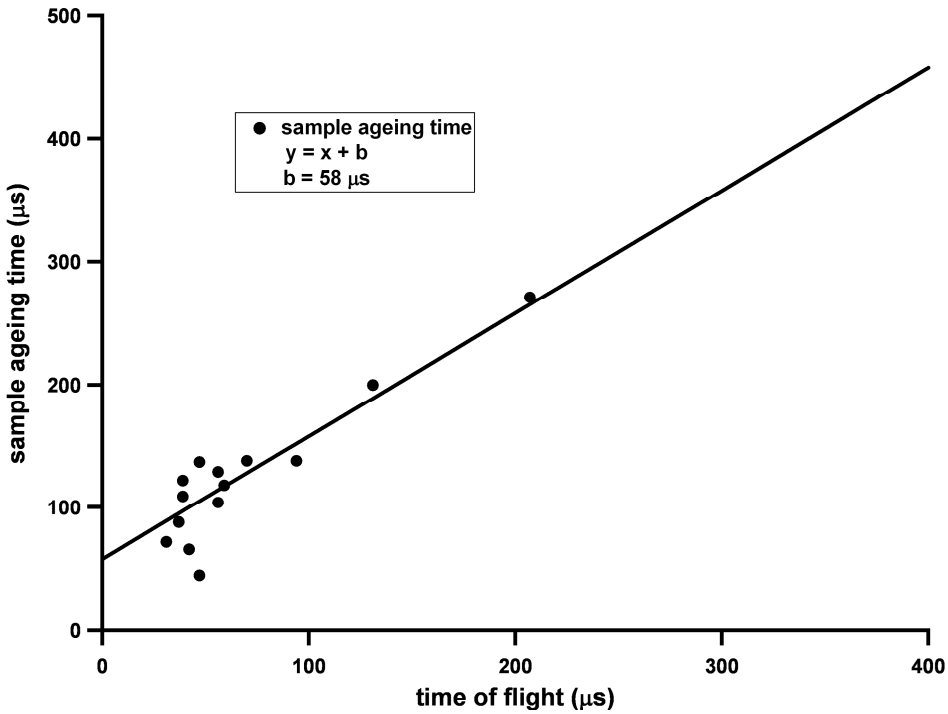

Figure 4 Determination of the freezing time of the μs setup with an orifice of 20 μm. Samples of 1 M azide and 0,35 mM Mb (end concentrations) were sprayed at different reaction times by varying the distance from the mixer to the cold plate. The flow speed was 2ml/min. The Y axis cutoff represents the freezing time which is determined at 54 μs.

Figure 4 indicates quite a large spread in the data at reaction times below 100 μs. The spread is observed when the mixer is closer than 6 mm to the cold plate in which case the true temperature may be lower than 10 °C leading to 'underreaction'; 'overreaction' may also occur due to jet break up caused by the turbulence caused by the rotation of the cold plate. By fitting a straight line through the data points with a slope of 1 the freezing time was determined from the Y-axis intersection at 54 ± 7 μs. This is somewhat larger than the 30-40 μs determined for freeze-quenching in isopentane [1].

In Figure 5 the cross sectional area of the jet is plotted versus the freezing time. The point at 49.10^3 μm^2 is adapted from Ballou and Palmer[23]. In their rapid freezing/rapid quenching setup a jet was used of 250 μm diameter and they determined a freezing time of 4-6 ms. The data show a linear relationship between the jet cross sectional area and the freezing time,

which is in agreement with theory since cooling of the jet occurs through its surface area [5, 18, 24, 25].

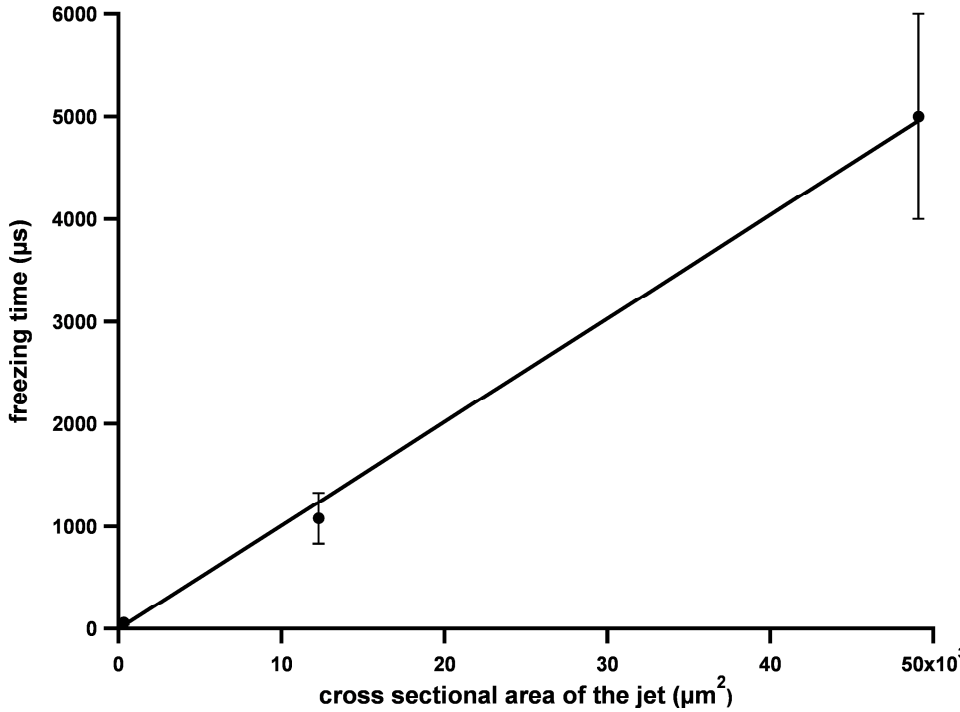

Figure 5 Relation between the jet cross sectional area and the freezing time. The point at 49.10^3 μm^2 is adapted from Ballou and Palmer [23]. The error bars represent the deviation in the freezing times.

Cold plate surface

Samples prepared with an aluminum rotating cold plate yielded intense and broad EPR signals covering the region between g= 2-4 (Figure 6, spectrum H). The presence of this signal prevents detection of e.g. low-spin heme centers and yields e.g. radical signals on a sloping baseline in particular because radical signals of interest were usually measured at approximately 10-fold higher receiver gains than shown in Figure 6. The origin of the signal at g= 2.5-2.6 is unknown, but is likely due to transition metal impurities (ferric iron?) in the aluminum, which combine with the sample when the frozen film is scraped off from the cold plate. In an attempt to get rid of the g= 2.5-2.6 signal several different metal coatings were

tested. Tungsten, silver and palladium were applied by physical vapor deposition (PVD) on the aluminum plate, while chromium was applied by electroplating. In addition, new rotors were constructed from brass and titanium. To test these surfaces, a sample of 0.5 ml of Milli-Q grade water was sprayed and worked up further as a normal sample. The results are shown in Figure 6. In all cases broad contaminating EPR signals were observed, but the coating with tungsten yielded a very small background. Titanium yielded the largest contaminating signal. As in the case of pure aluminum, the origin of the signals cannot be assigned, except perhaps in the case of the chromium coating; this (heterogeneous) signal might originate from low-symmetry Cr^{3+}.

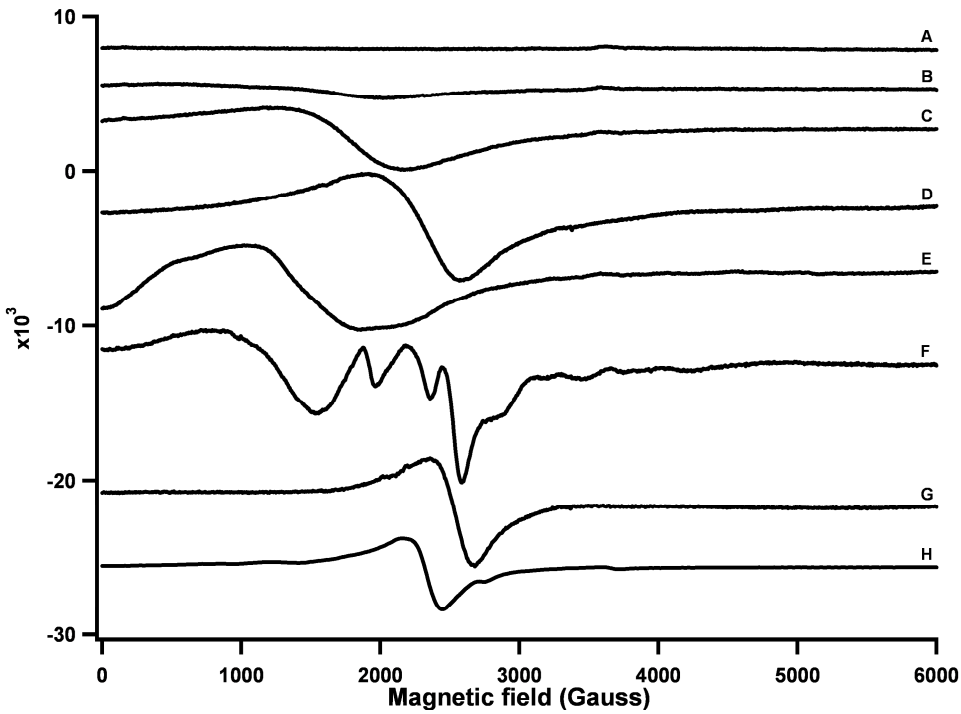

Figure 6 EPR spectra of milli-Q water samples sprayed on a cold-plate with different metal coatings. A) EPR spectrum of the empty cavity, B) Tungsten coating (99.999%), C) Silver coating 99.95+%, D) Chromium electroplated coating, E) Palladium coating (99.9+%), F) Brass plate, G) Aluminum plate, H) Titanium plate. EPR conditions: Frequency 9.44 GHz; modulation amplitude 10 G; Gain: 32000 except H, which was 8000); microwave power (20 mW), temperature 20 K.

Conclusions

We have constructed and tested a microsecond freeze-hyperquenching device equipped with a rotating aluminum cold plate. The freezing time of the 20µm jet is 50-60 µs, that of the 125µm jet approximately 1 ms. The minimal reaction time or dead time of the instrument operating at flow rates of 200 m/s and the mixer placed at 4 mm from the cold plate is 75-85 µs. Samples can be prepared which have reacted up to 200 ms by using simple extension stainless steel tubing with 125 µm inner diameter. By coating the aluminum plate with pure tungsten the surface is not only hardened but also yields samples in which background EPR signals were strongly diminished.

The MHQ device is relatively easy to use. The packing method described for EPR samples is simple and yields reproducible samples dispersed in liquid nitrogen, which can also be analyzed by resonance Raman spectroscopy. The absence of a cryo-medium yields packed samples approximately four-fold higher in concentration than obtained by freeze-quenching in isopentane widening its application to other spectroscopic methods like FTIR, Mössbauer and Solid State NMR spectroscopy. Results obtained with the set up described in this chapter are found in Chapters 3-6 of this thesis.

References

1. Cherepanov, A. V.; De Vries, S., Microsecond freeze-hyperquenching: development of a new ultrafast micro-mixing and sampling technology and application to enzyme catalysis. *Biochim Biophys Acta* **2004,** 1656, (1), 1-31.
2. Chance, B.; Saronio, C.; Leigh, J. S., Jr., Functional intermediates in the reaction of membrane-bound cytochrome oxidase with oxygen. *J Biol Chem* **1975,** 250, (24), 9226-37.
3. Adelroth, P.; Karpefors, M.; Gilderson, G.; Tomson, F. L.; Gennis, R. B.; Brzezinski, P., Proton transfer from glutamate 286 determines the transition rates between oxygen intermediates in cytochrome c oxidase. *Biochim Biophys Acta* **2000,** 1459, (2-3), 533-9.
4. De Vries, S., Freeze-Quench Kinetics. *Application of Physical Methods to Inorganic and Bioinorganic Chemistry* **2007**, 125-142.
5. Roughton, F. J. W., *Proc. Roy. Soc. (London)* **1930,** 126A, 470.
6. Chance, B., The Stopped-flow Method and Chemical Intermediates in Enzyme Reactions - A Personal Essay. *Photosynth Res* **2004,** 80, (1-3), 387-400.

7. Bray, R. C., Sudden Freezing as a Technique for the Study of Rapid Reactions. *Biochem J* **1961,** 81, 189-195.
8. Bray, R. C., Quenching by squirting into cold immiscible liquids. In *Rapid mixing and sampling techniques in biochemistry*, Chance, B.; Eisenhardt, R. H.; Gibson, Q. H.; Longberg-Holm, K. K., Eds. Academic Press: New York, 1964; pp 195-203.
9. Bray, R. C.; Pettersson, R., Addendum. Electron-Spin-Resonance measurements. *Biochem J* **1961,** 81, 194-195.
10. Hansen, R. E.; Beinert, H., Syringe Ram for a Rapid-Freeze Sampling Instrument. *Analytical Chemistry* **1966,** 38, (3), 484-&.
11. Hansen, R. E.; Van Gelder, B. F.; Beinert, H., Attachment to split-beam spectrophotometer for absorbance recording in round tubes of small diameter. *Anal Biochem* **1970,** 35, (1), 287-92.
12. Lymn, R. W.; Gibson, G. H.; Hanacek, J., A Chemical-Stop Rapid Flwo Apparatus. *Review of Scientific Instruments* **1971,** 42, (3), 356-&.
13. Walinder, O.; Zetterqv.O; Engstrom, L., Intermediary Phosphorylation of Bovine Liver Nucleoside Diphosphate Kinase - Studies with a Rapid Mixing Technique. *Journal of Biological Chemistry* **1969,** 244, (4), 1060-1064.
14. Hartridge, H.; Roughton, F. J. W., A method of measuring the velocity of very rapid chemical reactions. *Proc Royal Soc London, series A Math Phys Sci* **1923,** 104, 376-394.
15. Hartridge, H.; Roughton, F. J. W., Improvements in the apparatus for measuring the velocity of very rapid chemical reactions. *Proc Cambridge Phil Soc* **1925,** XXII, 426-431.
16. Hartridge, H.; Roughton, F. J. W., Improvements in the apparatus for measuring the velocity of very rapid chemical reactions. II. *Proc Cambridge Phil Soc* **1927,** XXIII, 450-460.
17. Moenne-Loccoz, P.; Krebs, C.; Herlihy, K.; Edmondson, D. E.; Theil, E. C.; Huynh, B. H.; Loehr, T. M., The ferroxidase reaction of ferritin reveals a diferric mu-1,2 bridging peroxide intermediate in common with other O2-activating non-heme diiron proteins. *Biochemistry* **1999,** 38, (17), 5290-5.
18. Mayer, E.; Bruggeller, P., Vitrification of pure liquid water by high pressure jet freezing. *Nature* **1982,** 298, 715-8.
19. Tanaka, M.; Matsuura, K.; Yoshioka, S.; Takahashi, S.; Ishimori, K.; Hori, H.; Morishima, I., Activation of Hydrogen Peroxide in Horseradish Peroxidase Occurs within approximately 200 micro s Observed by a New Freeze-Quench Device. *Biophys J* **2003,** 84, (3), 1998-2004.
20. Lin, Y.; Gerfen, G. J.; Rousseau, D. L.; Yeh, S. R., Ultrafast microfluidic mixer and freeze-quenching device. *Anal Chem* **2003,** 75, (20), 5381-6.
21. Tsai, A. L.; Berka, V.; Kulmacz, R. J.; Wu, G.; Palmer, G., An improved sample packing device for rapid freeze-trap electron paramagnetic resonance spectroscopy kinetic measurements. *Anal Biochem* **1998,** 264, (2), 165-71.
22. Wiertz, F. G. M.; de Vries, S., Low-temperature kinetic measurements of microsecond freeze-hyperquench (MHQ) cytochrome oxidase monitored by UV-visible spectroscopy with a newly designed cuvette. *Biochem Soc Trans* **2006,** 34, (Pt 1), 136-8.

23. Ballou, D. P.; Palmer, G. A., Practical rapid quenching instrument for the study of reaction mechanisms by electron paramagnetic resonance spectroscopy. *Anal Chem* **1974,** 46, (9), 1248-53.
24. Mayer, E., Vitrification of pure liquid water. *Journal of Microscopy* **1985,** 140, 3-15.
25. Bald, W. B., On crystal size and cooling rate. *Journal of Microscopy* **1986,** 143, 89-102.

Chapter 3

Low-temperature kinetic measurements of Microsecond freeze-Hyper Quenched (MHQ) cytochrome oxidase monitored by UV-Vis spectroscopy with a newly designed cuvet.

Frank G.M. Wiertz and Simon de Vries

Addapted from: biochemical society transactions, 2006, 34, 136-138

Summary

A special cuvet was designed to measure optical changes of Microsecond freeze-Hyper Quench (MHQ) powder samples [Wiertz et.al. 2004,FEBS Lett 575, 127-130] [1] at temperatures below ~250K. Reduced cytochrome c oxidase from Paracoccus denitrificans was reacted with O_2 for 100 μs, frozen as a powder and transferred to the cuvet. Subsequently, cytochrome oxidase was allowed to react further following stepwise increments of the temperature from 100K up to 250K while recording spectra between 300-700nm. The temperature was raised only when no further changes in the spectra could be detected. The experiment yielded spectra of the A, P, F and O intermediate states.

Introduction

Cytochrome oxidases are the final electron acceptor enzymes in aerobic Archaea, Bacteria and Eucaryotes [2-4]. During the process of dioxygen reduction to water, protons are pumped across the membrane yielding a transmembrane proton electrochemical gradient, according to the following reaction equation [5]:

$$4 \text{ cyt } c^{2+} + O_2 + 8\ H^+\text{In} \rightarrow 4 \text{ cyt } c^{3+} + 2\ H_2O + 4\ H^+\text{Out}$$

The catalytic mechanism of this reaction has been studied by a vast array of biophysical techniques, which led to a detailed understanding of the reaction mechanism [6-8].

Recently we have designed a Microsecond freeze-Hyper Quenching (MHQ) device equipped with a rotating cold plate [1, 9] to rapidly mix e.g. enzyme and substrate and stop the reaction by freeze quenching. The dead time of the set up is ~60 µs. The frozen sample thus obtained is a powder without cryo-medium and can be stored in e.g. liquid nitrogen without reacting further. The powder can be used for low-temperature UV-Vis spectroscopy, resonance Raman spectroscopy and EPR to determine the electronic structure of intermediates obtained after various times[1, 10].

To study low-temperature kinetics (100-250K) by UV-Vis a special cuvet was designed suitable for analysis of MHQ-powder samples. In this study fully reduced cytochrome aa_3 was first reacted for 100µs with O_2 yielding a frozen powder, which reacted further in the cuvet after raising the temperature. The UV-Vis spectral changes observed, indicated that the oxidase went through its regular catalytic cycle.

Materials and methods

Cytochrome aa_3 from *P.denitrificans* was purified as described [11]. The MHQ sample was prepared as in [1]. Cytochrome aa_3 (140 µM in 50 mM HEPES, pH 7.2) was reacted with O_2 saturated buffer for 100 µs. The sample compartment of a home built cuvet (see Figure 1) with UV-transparent PMMA windows was filled on the sample side with the reacted cytochrome aa_3 powder sample. Introduction into the cuvet was facilitated by an aluminum funnel pre-cooled with LN_2.The sample immersed in LN_2

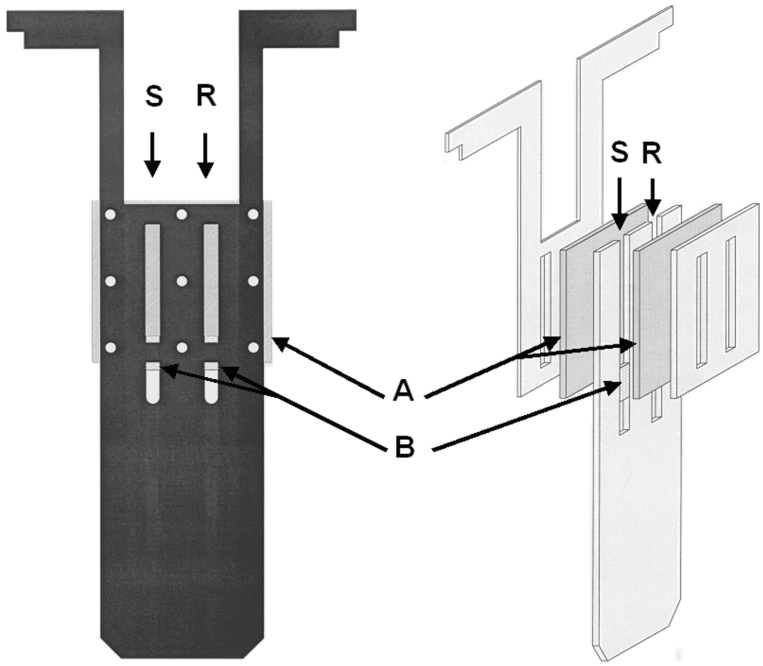

Figure 1 Cuvet holder for frozen powder samples. The left drawing shows a front view of the assembled cuvet; S and R indicate the sample and reference compartments, respectively. The picture on the right shows the disassembled cuvet. A denotes the two UV transparent PMMA windows and B the filters at the bottom of the cuvet.

flows down into the cuvet and the sample settles loosely on top of a filter, which forms the bottom of the cuvet. As a reference powdered ice was used. The cuvet was mounted in a quartz dewar cooled by a flow of cold nitrogen gas. To stabilize or vary the temperature a heater was placed in the gas flow; the heater was powered by a DC voltage (35V, 15A) supply. UV-Vis measurements were performed with an Olis Upgraded Aminco DW-2000 spectrophotometer equipped with a custom built 150W lamp. Spectra were recorded between 300 and 800 nm in steps of 0.5 nm with a bandwidth of 3 nm.

Results and Discussion

Figure 2 shows the intermediates formed at low-temperature after fully reduced cytochrome aa3 had reacted initially for 100 μs with O_2. The spectrum of this sample (Figure 2 Start) was recorded at 120K.

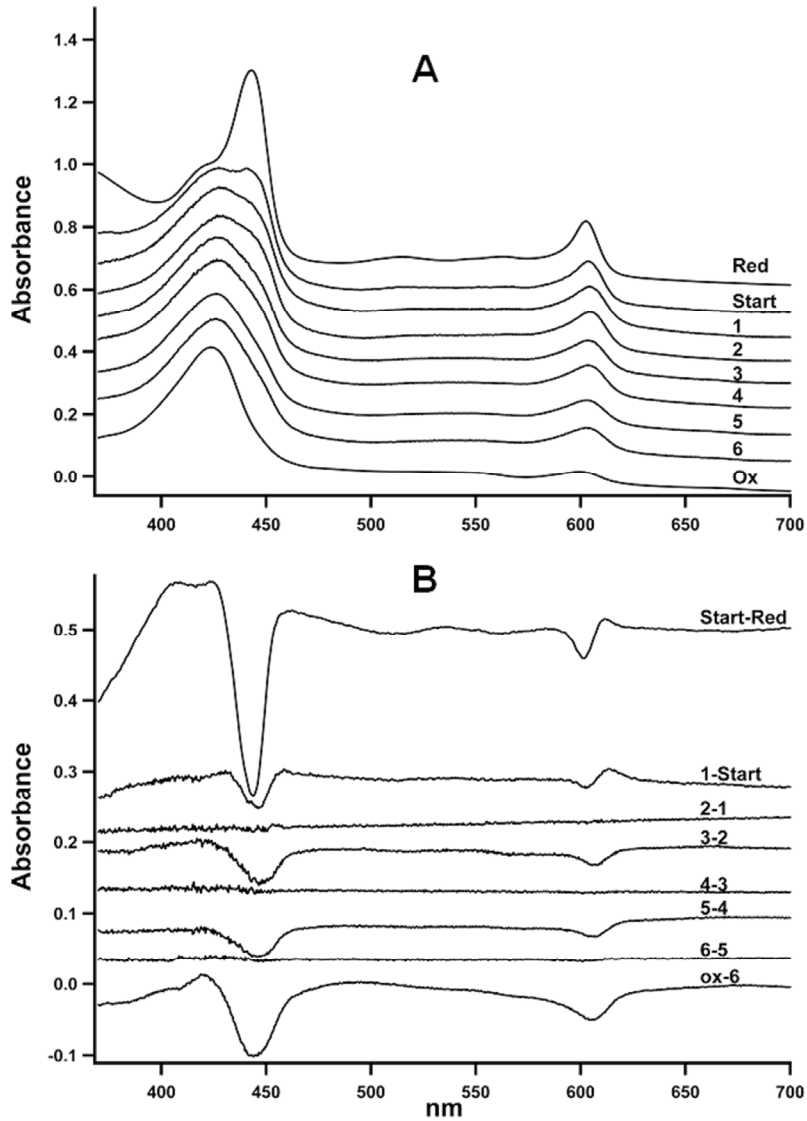

Figure 2 Absolute and difference UV-Vis spectra of cytochrome oxidase frozen after reacting for 100 µs with O_2 and subsequently annealed between 120-240K. Panel A, absolute spectra: Red: fully reduced cytochrome aa_3 recorded at (120K), start: 100 µs sample (120K), 1: sample reacting for 78 minutes at 180K, 2: sample reacted for 33 minutes at 190K, 3: sample reacting for 77 minutes at 200K , 4: sample reacting for 33 minutes at 210K, 5: sample reacting for 83 minutes at 220K , 6: sample reacting for 26 minutes at 240K, Ox: oxidized cytochrome aa_3. Panel B: Difference spectra of those shown in panel A.

We concluded previously [1] that after 200 μs the P_M state was fully formed, therefore after 100 μs a mixture of A and P_M was expected [8, 12, 13]. The maxima and minima of the difference spectrum 'Start-Red' in Figure 2 (and Table 1) are consistent with this assignment. Further reaction of the sample was initiated by slowly raising the temperature while recording spectra (6.5 min per spectrum). When an optical change was detected the temperature was kept constant. The first change was detected at 180 K. The enzyme reacted for 78 minutes until no further changes could be detected (Fig2. spectrum 1 and start-1). This latter spectrum is identical to that of the 200μs sample of reference 1 and corresponds to the P_M state (heme a_3 oxo-ferryl, Cu_B oxidized, heme *a* and Cu_A (nearly fully) reduced). The temperature was further raised to 190K but no change was detected (Figure 2. spectra 2 and 2-1). At 200K the oxidase reacted further (Fig2. spectrum 3 and 3-2). A decrease is seen in the Soret region due to oxidation of heme *a*. According to the reaction scheme 1, [8-13], the next intermediate would be F in which the radical produced in the P_M state is reduced by electron transfer from heme *a* (446 nm decrease) and/or Cu_A Therefore this spectrum is assigned to the F state. Next the temperature was raised to 210K but no further reaction took place (Figure 2 spectrum 4 and 4-3).

After warming the sample to 220K a further change was detected (Fig2. spectrum 5 and 5-4); this latter difference spectrum is very similar to '4-3'. When the sample was heated to 240K no change was detected (Fig.2 spectrum 6 and 6-5). Increasing the temperature further led to slow re-reduction of the hemes due to the presence of reductant

The difference between spectrum 6 and the oxidized sample (Fig2. spectrum ox and ox-6) shows that part of heme a did not react to the fully oxidized state. We conclude that spectrum 5 and 6 are a mixture of F and O states.

Previously the relative spectral contribution of heme a_3 and heme *a* in the Soret region was estimated at 3:2 [12]. In our experiments we found a similar ratio of 3:2 for heme a_3 and heme *a* in the Soret region, assuming that the spectral change in the first 2 kinetic steps, of A and P_M, are solely due to heme a_3. The same authors stated that after 1 catalytic cycle the cytochrome oxidase remains in a mixture of F and O, which is confirmed by our experimental results.

.

Table 1: Peak positions in low temperature UV-Vis spectra of cytochrome oxidase in different states. + or – indicates positive or negative absorbance changes in difference spectra; sh: shoulder; red, ox: fully reduced or oxidized, respectively.

Absolute spectra				
Sample	**Peak position (nm)**			**State**
Red	444	515, 563	603	R
Start	428, 441	515, 563	604	$A+P_M$
1	428, sh441		605	P_M
2	428, sh441		605	P_M
3	427, sh442		604	F
4	427, sh442		604	F
5	426, sh441		603	F+O
6	426, sh441		603	Mix F/O
Ox	424		600	Ox
Difference spectra				
Start-Red	+424, -444	-513, -564	-602, +612	R to A/P_M
Red-1	+424, -444		-602, +612	A to P_M
2-1	no change			-
3-2	+420, -446		-607	P_M to F
4-3	no change			-
5-4	+420, -446		-607	F to O
6-5	no change			-
Ox-6	+420, -446		-606	Mix F/O

Conclusions

Our results show that the catalytic cycle of cytochrome oxidase at low temperature is comparable to the room temperature cycle. Our method, preparing shortly reacted MHQ-powder samples and completing the catalytic cycle by controlled increase of the temperature, is a valuable tool for the study of enzymes with high turnover numbers. In addition, multi-

wavelength spectra are recorded instead of single-wavelength measurements as in most fast kinetic studies. Low temperature kinetics allows the isolation and spectroscopic characterization of single intermediate states, in particular of those involving protein conformational changes, which, apparently cannot occur at too low temperatures. The approach outlined here serves as an excellent tool for research in the field of fast kinetics to detect and characterize transient catalytic intermediate.

Acknowledgements

The authors would like to thank Drs. O. -M. Richter and B. Ludwig (J.W. Goethe Universität, Frankfurt) for generously providing the cytochrome oxidase.

We are also grateful to Mr. J.N. Rijnders for designing and machining the cuvet used in this study. This research was financed by the Foundation for Fundamental Research on Matter (FOM Grant 700-50-025).

References

1. Wiertz, F. G. M.; Richter, O. M.; Cherepanov, A. V.; MacMillan, F.; Ludwig, B.; de Vries, S., An oxo-ferryl tryptophan radical catalytic intermediate in cytochrome c and quinol oxidases trapped by microsecond freeze-hyperquenching (MHQ). *FEBS Lett* **2004,** 575, (1-3), 127-30.
2. Richter, O. M.; Ludwig, B., Cytochrome c oxidase--structure, function, and physiology of a redox-driven molecular machine. *Rev Physiol Biochem Pharmacol* **2003,** 147, 47-74.
3. Ferguson-Miller, S.; Babcock, G. T., Heme/Copper Terminal Oxidases. *Chem Rev* **1996,** 96, (7), 2889-2908.
4. Schäfer, G.; Engelhard, M.; Muller, V., Bioenergetics of the Archaea. *Microbiol Mol Biol Rev* **1999,** 63, (3), 570-620.
5. Wikstrom, M. K., Proton pump coupled to cytochrome c oxidase in mitochondria. *Nature* **1977,** 266, (5599), 271-3.
6. Michel, H., Proton pumping by cytochrome c oxidase. *Nature* **1999,** 402, (6762), 602-3.
7. Babcock, G. T.; Wikstrom, M., Oxygen Activation and the Conservation of Energy in Cell Respiration. *Nature* **1992,** 356, (6367), 301-309.
8. Ogura, T.; Kitagawa, T., Resonance Raman characterization of the P intermediate in the reaction of bovine cytochrome c oxidase. *Biochim Biophys Acta* **2004,** 1655, (1-3), 290-7.
9. Cherepanov, A. V.; De Vries, S., Microsecond freeze-hyperquenching: development of a new ultrafast micro-mixing and sampling technology and application to enzyme catalysis. *Biochim Biophys Acta* **2004,** 1656, (1), 1-31.

10. Lu, S.; Wiertz, F. G. M.; de Vries, S.; Moenne-Loccoz, P., Resonance Raman characterization of a high-spin six-coordinate iron(III) intermediate in metmyoglobin-azido complex formation trapped by microsecond freeze-hyperquenching (MHQ). *J Raman Spectrosc* **2005,** 36, (4), 359-362.
11. Hendler, R. W.; Pardhasaradhi, K.; Reynafarje, B.; Ludwig, B., Comparison of energy-transducing capabilities of the two- and three-subunit cytochromes aa3 from Paracoccus denitrificans and the 13-subunit beef heart enzyme. *Biophys J* **1991,** 60, (2), 415-23.
12. Szundi, I.; Cappuccio, J.; Einarsdottir, O., Amplitude analysis of single-wavelength time-dependent absorption data does not support the conventional sequential mechanism for the reduction of dioxygen to water catalyzed by bovine heart cytochrome c oxidase. *Biochemistry* **2004,** 43, (50), 15746-58.
13. Babcock, G. T.; Varotsis, C., Discrete steps in dioxygen activation--the cytochrome oxidase/O2 reaction. *J Bioenerg Biomembr* **1993,** 25, (2), 71-80.

Chapter 4

Resonance Raman characterization of a high-spin six-coordinate iron(III) intermediate in metmyoglobin - azido complex formation trapped by microsecond freeze-hyperquenching (MHQ)

Shen Lu, Frank G. M. Wiertz,
Simon de Vries and Pierre Moënne-Loccoz

Addapted from: Journal of Raman spectroscopy, 2005, 36, 4, 359-362

Summary

The reaction of metmyoglobin with azide was used to characterize a novel freeze-quench instrument with a mixing and freezing time resolution in the microsecond time range. Samples quenched within 95 and 245 μs after mixing of metmyoglobin with 1 M azide were characterized by low-temperature UV-visible and resonance Raman spectroscopy with excitation into the Soret band. Comparison of these data with control samples where azide is absent or metmyoglobin is preincubated with azide demonstrates the formation of an intermediate complex in the first 95 μs after mixing that has fully decayed after 245 μs. Porphyrin skeletal modes displayed by this transient species identify it as a six-coordinate high-spin species. Minor low-spin components are also observed and suggest that the hexacoordinated intermediate exists as a spin equilibrium. This preliminary study demonstrates the feasibility of this approach to detect new intermediates and to characterize early reaction intermediates in other metalloproteins.

Introduction

Resonance Raman (RR) spectroscopy represents a unique tool to investigate the structure of reaction intermediates in metalloproteins. Compared with other spectroscopic methods, it presents the advantage of selectively detecting chromophoric intermediates via resonance enhancement in charge-transfer or $\pi \rightarrow \pi^*$ electronic transitions, and it provides direct information on speciation and chemical bonding properties.[1] Intermediates in the catalytic turnover of cytochrome *c* oxidase have been successfully identified using RR spectroscopy and sample continuous flow techniques.[2-7] Recently, Proshlyakov *et al.*[8] applied this method to detect a ferryl-oxo species in the mononuclear non-heme iron protein α-ketoglutarate-dependent dioxygenase (α-KT-TauD) from *Escherichia coli*. The latter study represents a major breakthrough in the investigation of reductive activation of O_2 in iron proteins, but it required vast amounts of protein samples since 3 h of data averaging were necessary per isotope to reach convincing $^{16}O_2/^{18}O_2$ isotope difference spectra. Thus, rapid freeze quench (RFQ) techniques represent an attractive alternative, where a reaction mixture is quenched at low temperature to permit extensive data accumulation to extract the vibrational signatures of trapped intermediates.

In 1998, the combination of RFQ techniques and RR spectroscopy allowed, for the first time, the characterization of a peroxo diiron(III) reaction intermediate in a non-heme diiron enzyme.[9] This transient intermediate, identified as a bridging μ-1,2 peroxo diiron(III) species, was produced in an R2-W48F/D84E variant protein of ribonucleotide reductase from *E.coli* and an intermediate in a phenylalanine monooxygenase reaction.[10] The characterization of this peroxo intermediate was quickly followed by analogous vibrational studies of intermediates in two other non-heme diiron-containing proteins, stearoyl-acyl carrier protein Δ^9-desaturase and ferritin.[11,12] The μ-1,2 peroxo species of wild-type frog ferritin, which participates in the physiological ferroxidase activity of the protein, is significantly short-lived and requires rapid freeze-quenching within ~25 ms after mixing. In this work, liquid ethane was used as a cryosolvent in the preparation of RFQ samples, and eliminated previous problems of isopentane interference.[12] In a case study that used the azide binding reaction to metmyoglobin (metMb), Oellerich *et al.*[13] showed that ms-RFQ and RR spectroscopy could provide kinetic information.

In 2004, a major improvement in RFQ methodology was reported by Cherepanov and de Vries.[14] The new technique is referred to as microsecond

freeze-hyperquenching (MHQ) because it allows the trapping of transient species under 100 µs after sample mixing. Specifically, a mixing time of ~20 µs is achieved using a tangential mixing chamber with a volume of ~1 nl and high operating pressures and linear flow-rates (up to 400 bar and 200 $m.s^{-1}$). Originally a cryo-solvent was used for rapid freezing,[14] but the prototype now operates with a rotating cold plate.[15] This recent improvement permits a shorter distance between the exit nozzle and the freezing medium and alleviates problems of sample dilution and Raman contributions from cryosolvent. Indeed, the MHQ 'snow' is subsequently scraped from the cold plate and collected under liquid nitrogen. This material can be packed in EPR tubes for RR investigation and can be resuspended in isopentane for UV-visible spectroscopic analysis.

In their initial study, Cherepanov and de Vries[14] used the reaction of horse heart metMb with azide as a model system to validate MHQ, and determine the minimal sample aging time of their prototype. Not only did these experiments confirm the decreased freezing time achieved by this instrument, but the UV-visible analysis also suggested that an intermediate species might be trapped during these experiments. Here, we present the first RR characterization of these samples to confirm the feasibility of this approach and to bring further evidence in support of the accumulation of an intermediate species in the course of azide binding to metMb. In particular, RR spectra from early samples trapped within 95 µs after exposure to azide display porphyrin modes indicative of a six-coordinate high-spin species distinct from that of metMb, or of metMb azido complex observed in MHQ samples with longer delay times.

Expreimental

Preparation of MHQ samples

Myoglobin from horse heart was purchased from Sigma-Aldrich (>90% purity) and stock solutions were prepared in doubly distilled water at a concentration of 1.4 mM. Prior to use, the myoglobin stock solution was diluted with a 125 mM citrate buffer (pH 5.2) in a 1:1 ratio. Sodium azide was purchased from Fluka (>99% purity) and a 2 M stock solution was prepared in 125 mM citrate buffer (pH 5.2). The
final concentrations after rapid mixing were 1 M azide and 0.35 mM total myoglobin.

The metMb -azide reaction was performed at 10 °C as described previously,[14] except that the samples were sprayed on the inner surface of an aluminum cylinder precooled to 77 K and rotating at 7000 rpm as described by Wiertz et al.[15] After spraying the reaction mixture on the rotating cold-plate, liquid nitrogen was carefully poured into the cylinder. The samples were scraped off the wall of the cylinder and collected in Greiner tubes with liquid nitrogen. The samples were packed in EPR tubes fitted with a polypropylene filter at the end. An aluminum funnel was mounted on the top of the EPR tube. After cooling the funnel, the samples in liquid nitrogen were poured into the funnel and a cork was set on the top of the funnel to raise the pressure and facilitate the sample flow into the EPR tube. The samples were packed in the EPR tubes with a precooled rod and the samples were stored in liquid nitrogen until used. Portions of the samples were resuspended in isopentane and transferred in precooled UV-visible cells to obtain low-temperature UV-visible absorption spectra with an SLM-Aminco DW2000 spectrometer.[15]

Calculation of reaction times and control experiments were performed as previously.[14] Briefly, the kinetic rate constants for the reaction between metMb and azide were determined by stopped-flow analyses with varying azide concentrations (micromolar to molar range) at temperatures ranging from 4 to 20 °C. In the MHQ setup, the reaction temperature (set at 10 °C), the jet speed and time of flight are known and used to calculate the amount of azido complex expected to form. The calculated values are compared with those determined experimentally (UV -visible analysis), and they provide freezing time values with ~10% accuracy. Occasionally, a few samples were found to deviate from calculated values; overreacted samples were attributed to warming up during sample handling, while under-reacted samples were ascribed to poor mixing.

Resonance Raman spectroscopy

RR spectra were obtained in a backscattering geometry on samples kept at -180 °C with a liquid nitrogen coldfinger.[16] Excitation radiation of 413 nm from a krypton ion laser (Coherent, Innova 302) was kept at <20 mW and data accumulation of a few minutes was sufficient to reach high signal-to-noise ratio. A Kaiser supernotch filter was used to attenuate the Rayleigh scattering, and the backscattered light was analyzed with a McPherson 207 spectrograph equipped with a Princeton Instruments liquid nitrogen-cooled (LN-1100PB) charge-coupled device (CCD) detector.

Results and discussion

Previously, Cherepanov and de Vries[14] reported that the UV-visible absorption spectra of MHQ samples following the course of azide binding to metMb revealed the presence of an intermediate species. Figure 1 displays the 500–700 nm region of the UV–visible spectra of several representative MHQ samples that were analyzed by RR spectroscopy. Distinctive porphyrin α/β bands and porphyrin-to-iron(III) charge-transfer transitions in metMb and the azido complex permitted estimation of the percentage conversion in different MHQ samples.

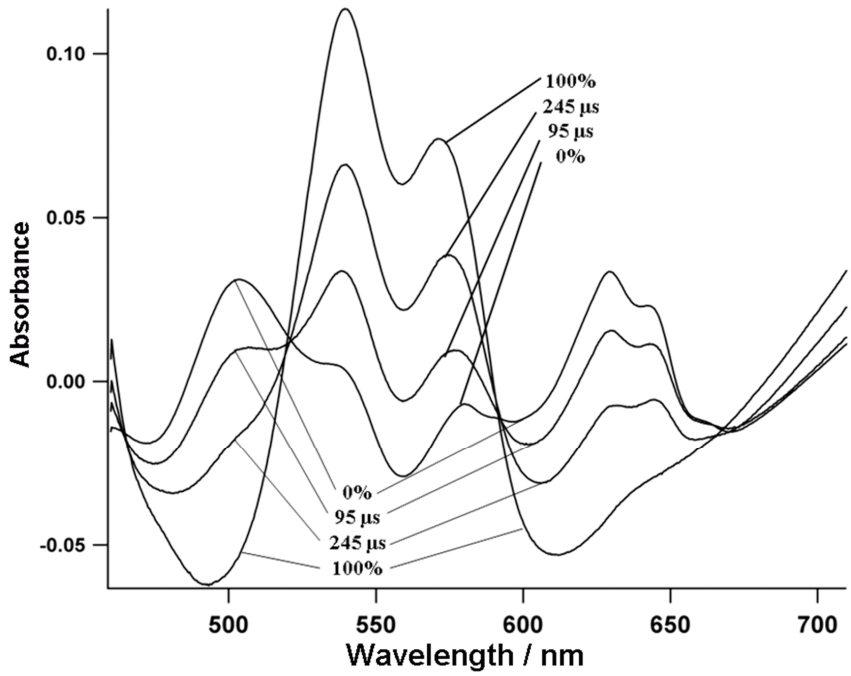

Figure 1. UV–visible absorption spectra of MHQ samples recorded at 77 K. The 95 and 245 µs MHQ samples produced after mixing of 1 M azide and 0.35 mM metMb were obtained by varying the distance from the nozzle and the pre-cooled cylinder. An azide-free metMb samples and a pre-incubated metMb–azido complex were used as reference samples.[14].

Analysis of these UV–visible absorption spectra suggests that MHQ samples trapped within 95 and 245 µs of mixing metMb with azide (1 M, final concentration) at pH 5.2 and 10 °C contain ~30% and ~60% of metMb

azido complex, respectively. A careful analysis of these spectra also revealed a lack of isosbestic points and the presence in early time points of UV–visible features distinct from those of the metMb (starting material) and the metMb azido complex (end product).[14]

The RR data obtained on these MHQ samples corroborate the existence of a trapped intermediate. Figure 2 shows RR spectra of MHQ samples containing 100% metMb [Figure 2(A)], trapped with 95 and 245 µs reaction times [Figure 2(B) and (C), respectively], and containing 100% of metMb azido complex [Figure 2(D)]. The two controls (i.e. starting material and end product) were sprayed and frozen under conditions identical with those used for the reaction mixtures.

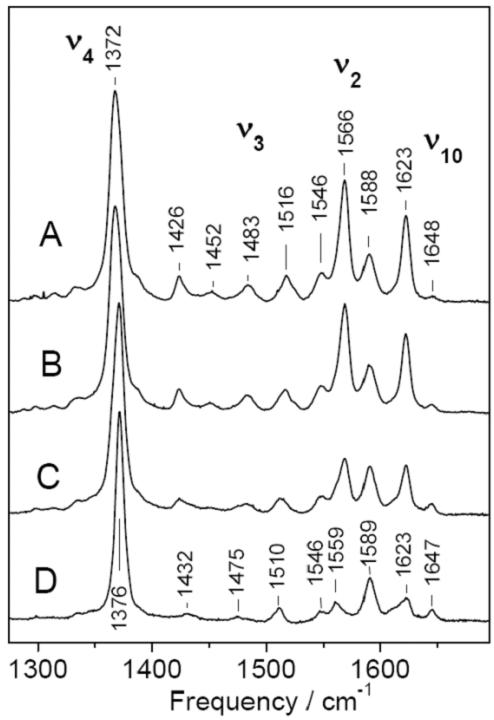

Figure 2. High-wavenumber resonance Raman spectra of (A) metMb, (B) 95 µs MHQ and (C) 245 µs MHQ samples after mixing of metMb with azide, and (D) of metMb preincubated with azide.

As reported previously,[13] RR spectrum of metMb collected at 90 K displays skeletal porphyrin modes indicative of a six-coordinate high-spin–six-coordinate low-spin mixture. Analogousmodes in the azido complex spectrum correspond to a pure six-coordinate low-spin species (Table 1).[17] For instance, the υ_4 band is observed at 1372 cm^{-1} in metMb and is composed of a high-spin component at 1370 and a low-spin component at 1375 cm^{-1}, whereas the metMb azido complex presents a single υ_4 component at 1376 cm^{-1}. Similarly, the υ_3 band is observed at 1483 cm^{-1} in metMb and at 1510 cm^{-1} in the metMb azido complex. Using the same experimental conditions to record RR spectra of a diluted solution of metMb and its azido complex with an internal intensity standard (200 mM cacodylic acid),[18] we determined that the same peak intensities were observed in the υ_4 region for both samples and, therefore, RR spectra of the MHQ samples were normalized with the υ_4 peak intensity.

Table 1. Resonane Raman wavenumbers (cm^{-1}) and assignments for metMb, Mb-N3 and the 95 μs intermediate formed during the reaction of azide with metMb

Met-Mb/cm^{-1}	Intermediatespecies/cm^{-1}	Mb-N3/cm^{-1}	Assignment
1372	1370	1376	υ_4
1426	1426	1432	υ_{28}
1452	1449	1475	$\delta(=C_bH_2)$
1483	1481	1510	υ_3
1516	1514	-	υ_{38}
1566	1566	1589	υ_2
1648	1647	1647	υ_{10}(low-spin)
1623	1622	1623	$\upsilon(C_a\text{-}C_b)$

The RR spectrum of the 245 μs MHQ sample [Figure 2(C)] can be recomposed as ~40% metMb and ~60% azido complex, leaving a residual RR trace that represents <3% of the raw data [Figure 3(C')].

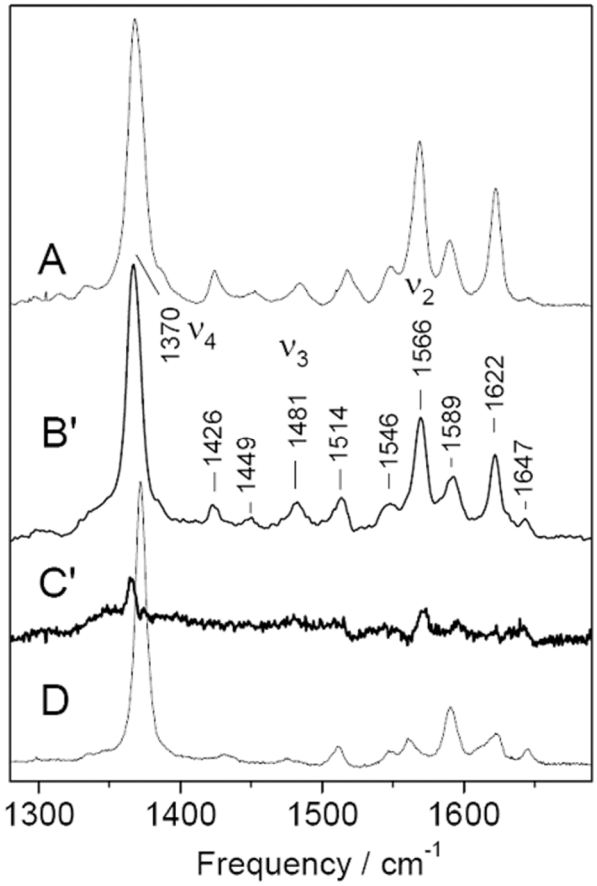

Figure 3. Traces B' and C' represent the residual spectra of the 95 µs MHQ (B') and 245 µs MHQ samples (C') after maximal subtraction of contribution from the starting material (A) and the end-product (D). Traces B' and C' were multiplied by 4 to allow easy comparison with those of (A) metMb and (D) metMb pre-incubated with azide.

In contrast, the spectrum of the MHQ sample at 95 µs [Figure 2(B)] cannot be recomposed as a combination of the two control spectra. Indeed, subtracting more than ~60% metMb or more than ~20% of the azido complex of metMb starts to generate negative features inconsistent with RR spectroscopy. Hence, the spectrum of the µs-RFQ sample at 95 µs reveals the presence of an intermediate species that accumulates to at least 20% [Figure 3(B')]. The difference spectra are dominated by spectral features consistent with a six-coordinate high-spin heme species with υ_4, υ_3 and υ_2 modes at 1370, 1481 and 1566 cm^{-1}, respectively (Table 1). As for metMb and the azido complex, a distinct low-spin υ_{10} contribution at 1647 cm^{-1}

reveals a low-spin component at this temperature and suggests that the hexacoordinated intermediate may exist as a spin equilibrium. Because RR contributions from metMb and/or the azido complex could be over-subtracted from the raw data, it can be argued that trace C' may not be an exact representation of the RR spectrum of the trapped transient species. However, since the analysis of the UV–visible data led to an equivalent population distribution and ~20% of a transient species, spectrum C' and the wavenumbers listed in Table 1 can be assumed to represent those of the transient species with a ±1 cm^{-1} experimental margin of error. The high-wavenumber RR spectra reveal a nascent azido complex [metMb–N3]* that is distinct from the resting azido complex. However, it remains to be determined whether the azido group is already coordinating the iron(III) but the ligand field splitting is smaller than that of the resting azido complex, or if azide is not coordinating the iron but perturbs interactions between the iron–aqua ligand and its distal-pocket environment. Investigating the spectral windows where iron–azide stretches, υ(Fe–N3), and asymmetric intra-azide stretches, υ_{as}(NNN),may distinguish between these alternative interpretations. Regardless of the outcome of these future experiments, the work carried out so far demonstrates the feasibility and potential of this new methodology. This approach will be applied to the characterization of early reaction intermediates in other metalloproteins under investigation in our laboratories.

Acknowledgments

This work was supported by the National Institutes of Health (P.M.-L., GM 18865) and by the Foundation for Fundamental Research on Matter (FOM grant D-26) of TheNetherlands Research Organization (NWO).

References

1. Nakamoto K. *Infrared and Raman Spectroscopy of Inorganic and Coordination Compounds* (5th ed). Wiley: New York,**1997**.
2. Ogura, T.; Takahashi, S.; Hirota, S.; Shinzawaitoh, K.; Yoshikawa, S.; Appelman, E. H.; Kitagawa, T., Time-Resolved Resonance Raman Elucidation of the Pathway for Dioxygen Reduction by Cytochrome-C-Oxidase. *Journal of the American Chemical Society* **1993,** 115, (19), 8527-8536.
3. Proshlyakov, D. A.; Ogura, T.; ShinzawaItoh, K.; Yoshikawa, S.; Kitagawa, T., Resonance Raman/absorption characterization of the oxo intermediates of

cytochrome c oxidase generated in its reaction with hydrogen peroxide: pH and H2O2 concentration dependence. *Biochemistry* **1996,** 35, (26), 8580-8586.

4. Han, S. W.; Ching, Y. C.; Rousseau, D. L., Ferryl and Hydroxy Intermediates in the Reaction of Oxygen with Reduced Cytochrome-C-Oxidase. *Nature* **1990,** 348, (6296), 89-90.
5. Han, S. H.; Ching, Y. C.; Rousseau, D. L., Primary Intermediate in the Reaction of Mixed-Valence Cytochrome-C Oxidase with Oxygen. *Biochemistry* **1990,** 29, (6), 1380-1384.
6. Han, S.; Ching, Y. C.; Rousseau, D. L., Primary Intermediate in the Reaction of Oxygen with Fully Reduced Cytochrome-C Oxidase. *Proceedings of the National Academy of Sciences of the United States of America* **1990,** 87, (7), 2491-2495.
7. Han, S.; Ching, Y. C.; Rousseau, D. L., Cytochrome-C-Oxidase - Decay of the Primary Oxygen Intermediate Involves Direct Electron-Transfer from Cytochrome-A. *Proceedings of the National Academy of Sciences of the United States of America* **1990,** 87, (21), 8408-8412.
8. Proshlyakov, D. A.; Henshaw, T. F.; Monterosso, G. R.; Ryle, M. J.; Hausinger, R. P., Direct detection of oxygen intermediates in the non-heme Fe enzyme taurine/alpha-ketoglutarate dioxygenase. *Journal of the American Chemical Society* **2004,** 126, (4), 1022-1023.
9. Moenne-Loccoz, P.; Baldwin, J.; Ley, B. A.; Loehr, T. M.; Bollinger, J. M., O-2 activation by non-heme diiron proteins: Identification of a symmetric mu-1,2-peroxide in a mutant of ribonucleotide reductase. *Biochemistry* **1998,** 37, (42), 14659-14663.
10. Baldwin, J.; Voegtli, W. C.; Khidekel, N.; Moenne-Loccoz, P.; Krebs, C.; Pereira, A. S.; Ley, B. A.; Huynh, B. H.; Loehr, T. M.; Riggs-Gelasco, P. J.; Rosenzweig, A. C.; Bollinger, J. M., Rational reprogramming of the R2 subunit of Escherichia coli ribonucleotide reductase into a self-hydroxylating monooxygenase. *Journal of the American Chemical Society* **2001,** 123, (29), 7017-7030.
11. Broadwater, J. A.; Ai, J. Y.; Loehr, T. M.; Sanders-Loehr, J.; Fox, B. G., Peroxodiferric intermediate of stearoyl-acyl carrier protein Delta(9) desaturase: Oxidase reactivity during single turnover and implications for the mechanism of desaturation. *Biochemistry* **1998,** 37, (42), 14664-14671.
12. Moenne-Loccoz, P.; Krebs, C.; Herlihy, K.; Edmondson, D. E.; Theil, E. C.; Huynh, B. H.; Loehr, T. M., The ferroxidase reaction of ferritin reveals a diferric mu-1,2 bridging peroxide intermediate in common with other O-2-activating non-heme diiron proteins. *Biochemistry* **1999,** 38, (17), 5290-5295.
13. Oellerich, S.; Bill, E.; Hildebrandt, P., Freeze-quench resonance raman and electron paramagnetic resonance spectroscopy for studying enzyme kinetics: Application to azide binding to myoglobin. *Applied Spectroscopy* **2000,** 54, (10), 1480-1484.
14. Cherepanov, A. V.; de Vries, S., Microsecond freeze-hyperquenching: development of a new ultrafast micro-mixing and sampling technology and application to enzyme catalysis. *Biochimica Et Biophysica Acta-Bioenergetics* **2004,** 1656, (1), 1-31.
15. Wiertz, F. G. M.; Richter, O. M. H.; Cherepanov, A. V.; MacMillan, F.; Ludwig, B.; de Vries, S., An oxo-ferryl tryptophan radical catalytic intermediate in

cytochrome c and quinol oxidases trapped by microsecond freeze-hyperquenching (MHQ). *Febs Letters* **2004,** 575, (1-3), 127-130.

16. Loehr, T. M.; Sanders-Loehr, J., Techniques for obtaining resonance Raman spectra of metalloproteins. *Methods Enzymol* **1993,** 226, 431-70.
17. Spiro TG, Li X-Y. In *Biological Applications of Raman Spectroscopy.Vol. 3. Resonance Raman Spectra of Hemes and Metalloproteins*, Spiro TG (ed). Wiley: New York, **1988**; 1.
18. Song, S. H.; Asher, S. A., Internal intensity standards for heme protein UV resonance Raman studies: excitation profiles of cacodylic acid and sodium selenate. *Biochemistry* **1991,** 30, (5), 1199-205.

Chapter 5

An Oxo-ferryl Tryptophan Radical Catalytic Intermediate in Cytochrome *c* and Quinol Oxidases trapped by Microsecond freeze-HyperQuenching (MHQ)

Frank G.M. Wiertz, Oliver-Matthias H. Richter,
Alexey V. Cherepanov, Fraser MacMillan,
Bernd Ludwig and Simon de Vries

Addapted from: FEBS Letters, 2004, 575,1-3,127-130

Summary

The pre-steady state reaction kinetics of the reduction of molecular oxygen catalyzed by fully reduced cytochrome oxidase from *Escherichia coli* and *Paracoccus denitrificans* were studied using the newly developed microsecond freeze-hyperquenching (MHQ) mixing-and-sampling technique. Reaction samples are prepared 60 μs and 200 μs after direct mixing of dioxygen with enzyme. Analysis of the reaction samples by low temperature UV-Vis spectroscopy indicates that both enzymes are trapped in the P_M state. EPR spectroscopy revealed the formation of a mixture of two radicals in both enzymes. Based on its apparent g-value and lineshape, one of these radicals is assigned to a weakly magnetically coupled oxo-ferryl tryptophan cation radical. Implications for the catalytic mechanism of cytochrome oxidases are discussed.

Introduction

Cytochrome oxidases couple dioxygen reduction to proton translocation to generate a proton electrochemical gradient for e.g. ATP production. Physiologically these enzymes act as terminal electron acceptors and are found in Archaea, Bacteria and Eucarya [1-3]. The overall reaction for cytochrome oxidases from the haem-copper oxidase superfamily such as cytochrome *c* oxidases (i.c. cytochrome aa_3 from *P.denitrificans*) or quinol oxidases (i.c. cytochrome bo_3 from *E.coli*) proceeds according to [4]:

$$4 \text{ cyt } c^{2+}/2QH_2 + O_2 + 8\ H^+_C \rightarrow 4 \text{ cyt } c^{3+}/(2Q + 4H^+_P) + 2\ H_2O + 4\ H^+_P$$

where "c" and "p" denote the cytoplasmic and the periplasmic space of the bacterial cell.

The catalytic mechanism of oxidases has been studied extensively over a long period of time with a great number of different techniques [5-12], which has led to a detailed understanding of the catalytic mechanism [13-16]. Accordingly, cleavage of the O-O bond had been proposed to involve Trp or Tyr residues from the enzyme [5]; later, H-atom donation by Y280 (*P. denitrificans* numbering system) was postulated, a residue covalently linked to a histidine (H276) ligating Cu_B. Indeed a neutral tyrosine radical has been detected using the iodine labeling technique in bovine cytochrome aa_3 oxidase prepared in the P_M state [10]. In *P. denitrificans* cytochrome aa_3 oxidase treated with stoichiometric amounts of H_2O_2 a tyrosine radical was also detected by EPR [17, 18], which has recently been identified as Y167, a residue close to the active site [18,19].

Other studies on the bovine cytochrome *c* oxidase employing excess H_2O_2 [20,21] suggest formation of a porphyrin cation radical and/or a tryptophan cation radical. In all these aforementioned studies the radicals were formed under quasi-equilibrium conditions hampering conclusions on their role in the catalytic mechanism. To overcome this problem, a novel pre-steady state kinetic method to analyse chemical reactions has recently been developed in our laboratory. The microsecond freeze-hyperquenching device (MHQ) enables chemical reaction intermediates to be trapped within 140 µs [12]. Studies on the reduction of molecular oxygen catalyzed by cytochrome bo_3 oxidase from *E. coli* showed the formation of a transient radical; unfortunately, the low enzyme concentration used in EPR studies necessitated saturating power for measurements preventing determination of

its nature [12]. The MHQ setup has now been modified employing a rotating cold plate instead of cold iso-pentane to quench the reaction, yielding quench times of 60 μs and more concentrated EPR samples. Using the cold plate MHQ setup we have studied the direct oxidation by O_2 of cytochrome *aa*$_3$ oxidase from *P. denitrificans* and cytochrome *bo*$_3$ oxidase from *E. coli*. The kinetic studies reported here indicate the formation of two radical species in the P_M state. One of these is assigned to an oxo-ferryl coupled tryptophan cation radical.

Materials and Methods

E. coli cytochrome *bo*$_3$ oxidase was purified as in [12] and *P. denitrificans* cytochrome *aa*$_3$ oxidase as previously described [22]**.** The MHQ setup is identical to the one described before [12] with the following modifications. Instead of quenching in iso-pentane at 140 K, the sample was sprayed on the inner surface of an aluminum cylinder (height 70 mm, diameter 130 mm, thickness 15 mm), pre-cooled to 77 K and rotating at 7000 rpm. In this way the surface of the cylinder is covered with a thin layer of sample, optimizing the quenching process. The enzyme reaction temperature is 10 ˚C.

Samples of 0.5 ml were prepared in anaerobic HPLC vials containing 140 μM cytochrome *aa*$_3$ oxidase in 50 mM HEPES buffer pH 7.2 with 0.05% Lauryl-maltoside (LM) or 150 μM of cytochrome *bo*$_3$ oxidase in 50 mM K-phosphate buffer pH 7.5 with 0.05% LM and were reduced with 10 mM ascorbate and 1 μM phenazine ethosulfate (PES). The degree of reduction was followed in situ with a HP 8453 UV-Vis spectrophotometer. The samples were loaded in the injector by means of an O_2-free gastight Hamilton syringe and mixed versus buffer flushed for 30 min with 100% O_2. After the freeze quenching the Al cylinder was filled with liquid nitrogen and the sample was scraped from the cylinder wall. The frozen powder was collected in a 50 ml Greiner tube first and then used for preparing UV-Vis and EPR samples.

Absorbance spectra were recorded with a SLM-Aminco DW2000 scanning spectrophotometer equipped with a low temperature setup. Part of the quenched sample was transferred into 2 ml cold 140 K iso-pentane and mixed well. Subsequently, a 1-ml aliquot of the sample suspension in iso-pentane was quickly transferred into a pre-cooled sample compartment (light path 2 mm) and frozen in liquid nitrogen. The reference compartment

contained iso-pentane. The sample was measured in split-beam mode at a scan-rate of 0.5 nm/s. The spectra shown in Fig.1 are averages of at least 20 spectra. The averaged spectra were baseline corrected and normalized for the total area of the γ-band to correct for differences in sample amounts. The areas between 400 and 467 nm for the oxidised sample and between 375 and 464 nm for the reduced sample were used for normalisation. For samples in different redox states the same area was assumed, which was obtained by small adjustments of the boundaries. EPR spectra were recorded as in [23].

Results and Discussion

Figure 1 shows low temperature UV-Vis spectra of cytochrome aa_3 and bo_3 oxidase samples freeze-quenched on the microsecond timescale after direct reaction with molecular oxygen.

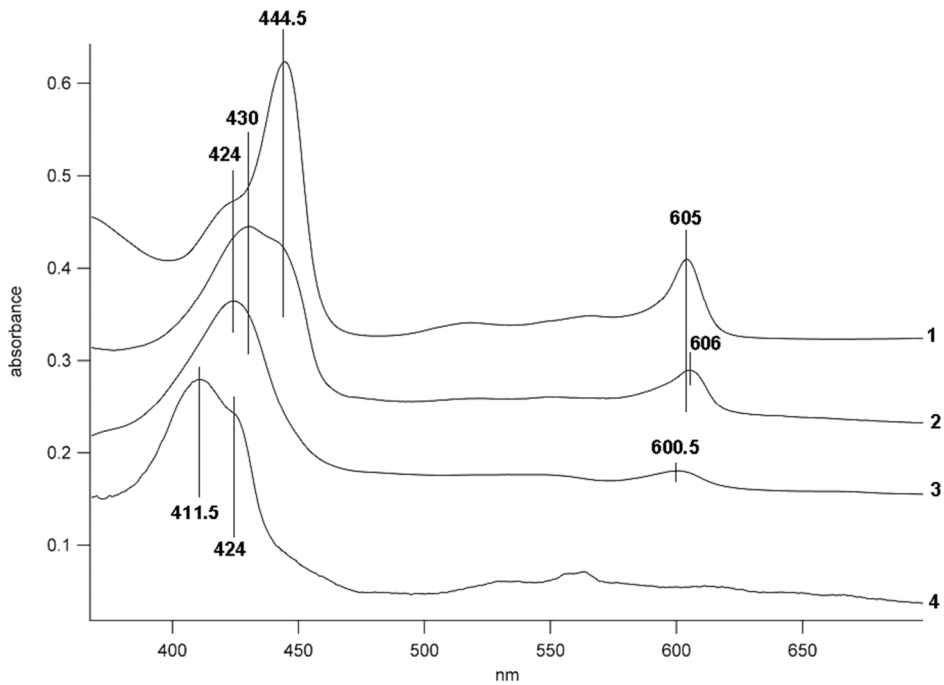

Figure 1 Low temperature UV-Vis spectra of cytochrome aa_3 and bo_3 oxidase. Spectrum 1: Cytochrome aa_3 oxidase fully reduced with ascorbate and PES. Spectrum 2: cytochrome aa_3 oxidase reacted with O_2 for 200 µs. Spectrum 3: Fully oxidized cytochrome aa_3 oxidase. Spectrum 4: Cytochrome bo_3 oxidase reacted with O_2 for 60 µs. Reference samples for cytochrome bo_3 oxidase are shown in Figure 18 of reference 12.

The absorbance of the 200-µs sample of cytochrome aa_3 oxidase at 444.5 nm and 605 nm (spectrum 2) is lower by approximately 40% and 20%, respectively, with respect to the fully reduced enzyme (spectrum 1). The new peak at 430 nm, which emerges concomitantly with the disappearance of the absorbance at 444.5 nm, represents the oxo-ferryl form of haem a_3 [10,15,24,25]. Since haem *a* remains largely reduced in the first 200 µs the enzyme is in the P_M state as is also seen from the small shift to 606 nm in the α-band.

The oxidation kinetics of cytochrome bo_3 oxidase employing MHQ have been reported recently, where the earliest data point was taken after 137 µs (see trace 2, figure 18 in reference 12). The low temperature UV-Vis spectrum of cytochrome bo_3 oxidase freeze-quenched after 60 µs is shown in figure. 1. Comparing the two spectra reveals very little differences: similar to the 137-µs sample, haem *b* remains fully reduced in the 60-µs sample, whereas haem o_3 is fully converted to the oxo-ferryl state, Fe^{IV}=O, absorbing at 411.5 nm. From this one can conclude that the enzyme has been converted to the P_M state after reacting for 60 µs with oxygen.

In figure 2 EPR spectra in the g=2 region of cytochrome bo_3 (60 µs) and aa_3 (200 µs) oxidase are compared. The spectra show in both cases similar resonances at g_{eff}= 2.005 (derivative-like), 2.018 and 2.038 (both absorption-like). The pair of resonances which yield an axial signal with g_{eff}= 2.038 and 2.005 is very similar to that detected e.g. in Compound I of cytochrome *c* peroxidase CcPO [26-29] and in Compound I of a Phe-Trp-221 mutant of horseradish peroxidase (HRP) [30]. Whereas an isolated radical in X-band EPR yields an isotropic signal at g~2.005, we propose that in analogy to Compound I, the axial signal in the oxidases with $g_{x,y}$= 2.038 and g_z=2.005 derives from a weakly exchanged-coupled oxo-ferryl tryptophan cation radical pair. The strength of the exchange coupling between the tryptophan radical (S=1/2) and the haem Fe^{IV}=O system (S=1) can be calculated directly from the observed g-values and from the spin Hamiltonian parameters of the oxo-ferryl system [27-29]. In general, the stronger the interaction, the larger the difference between $g_{x,y}$ and g_z. For the haem a_3 oxo-ferryl tryptophan cation radical with $g_{x,y}$= 2.038 the axial exchange interaction equals, $J_{x,y}$= -4.9 GHz.

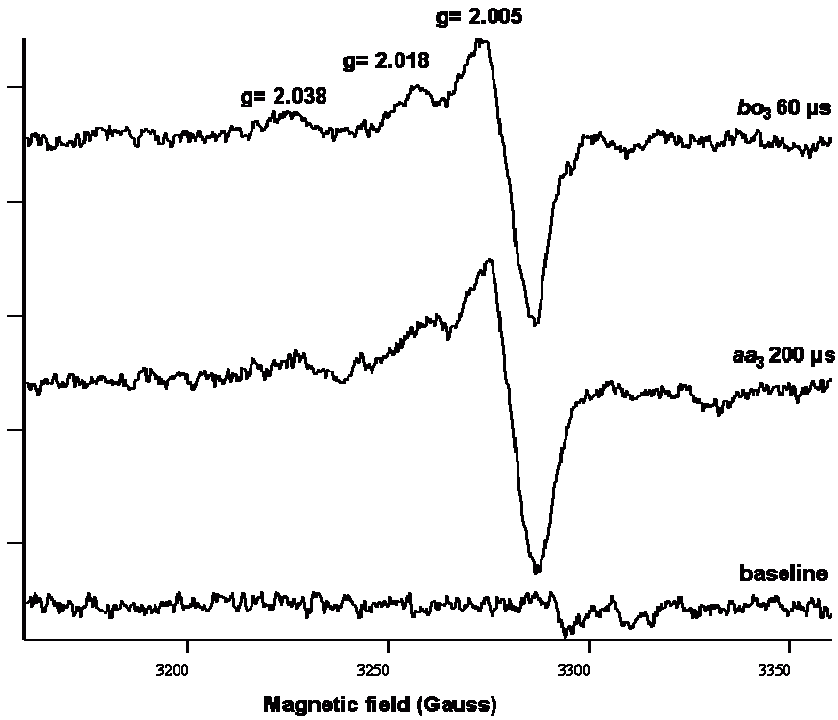

Figure 2 EPR spectra of transient radicals formed after reaction of cytochrome bo_3 and aa_3 oxidase with oxygen for 60 µs and 200 µs, respectively. The species with g= 2.038, 2.005 is assigned to an oxo-ferryl tryptophan cation radical. The nature of the species contributing to the g= 2.018 signal remains to be established. The small negative peaks between 3300 and 3350 Gauss, which do not coincide with those from the baseline, might represent the high field part of a tyrosine radical signal (see text for further explanations). The cytochrome aa_3 spectrum has been corrected for the Mn(II)-signal by subtracting the signal of the fully reduced enzyme. EPR conditions: Frequency: 9.25 GHz; microwave power: 200 µW; modulation amplitude: 0.63 mT; temperature: 45K.

The origin of the absorption-like resonance at g=2.018 is less clear. It could also be ascribed to a tryptophan radical in interaction with the Fe^{IV}=O state of haem a_3. In that case the radical with $g_{x,y}$= 2.018 and g_z=2.005, is calculated to have a smaller exchange coupling, $J_{x,y}$= -2.1 GHz. Alternatively, the resonance at g=2.018 might represent the high field part of a tyrosine radical, the central, derivative-like part of such a signal being obscured by the g= 2.005 peak; the negative absorption-like peaks to the right of the g=2.005 peak might represent the low field part of a tyrosine radical spectrum (Figure 2). It should be noted that such an overall spectral

width, while quite large for a tyrosine radical (ca. 50 Gauss), is similar to that observed in [17]. Given the uncertainties regarding the g= 2.018 signal and the magnetic interaction between the tryptophan radical and the haem a_3 Fe^{IV}=O state the current best estimate of the total radical concentration amounts to 10-40% of the oxidase concentration in samples yielding the highest EPR radical intensity.

In terms of EPR lineshape and temperature behaviour the signal with $g_{x,y}$= 2.038 and g_z=2.005 in the two oxidases is very similar to that of the oxo-ferryl tryptophan cation radical observed in Compound I of the HRP Phe-Trp-221 mutant [30]. The EPR spectrum of the oxidases recorded at 7K (data not shown) is the same as that shown in Figure 2, provided the spectrum is recorded at non-saturating microwave power. Although at saturating power the lineshape is distorted, no evidence for the presence of a porphyrin radical was found as e.g. in Compound I of CcPO [27-29].

The EPR spectra of the oxo-ferryl tryptophan cation radical and the g=2.018 species formed in the first steps of the catalytic cycle (Figure 2) are very different from the spectra assigned to tryptophan/porphyrin radicals obtained under pseudo-equilibrium conditions [21]. The role of the latter in catalysis is therefore unclear, in particular regarding the porphyrin radical, which according to resonance Raman spectroscopy is not formed [15].

Haem-copper oxidases contain two conserved tryptophan residues close to haem a_3, W164 and W272 (*P. denitrificans* numbering) [31,32]. It is interesting to note that W164 is located between haem *a* and haem a_3. Although the data presented here might suggest a direct role for W164 in mediating electron transfer between the two haem centers, the observed radicals are formed under conditions where haem *a* has remained reduced while haem a_3 is in the oxo-ferryl form. Therefore, it is more likely that at least one of the observed radicals acts as electron donor providing one of the four electrons needed to cleave the O-O bond as shown in Figure 3.

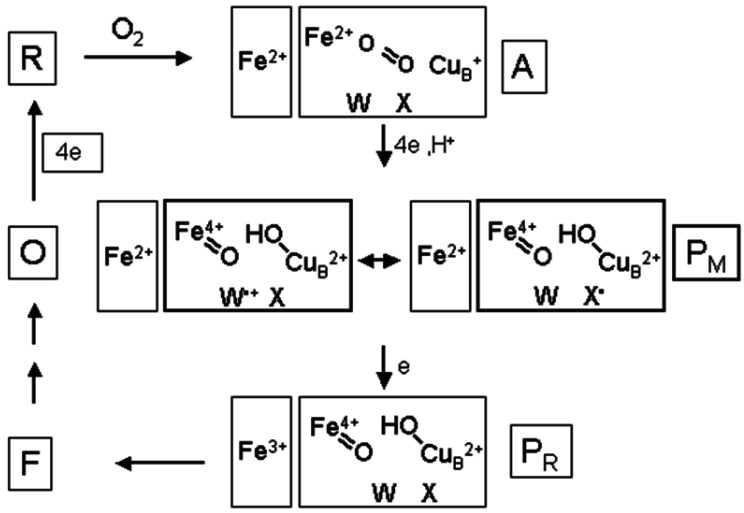

Figure 3 Proposed reaction scheme for cytochrome oxidase. Modified from ref. [12] and shortened indicating only the intermediates relevant to this study. The Cu_A site (of cytochrome aa_3) which is in rapid electronic equilibrium with haem *a*, is not depicted; the small rectangle to the left denotes haem *a* and the large rectangle the binuclear center consisting of haem a_3 and Cu_B. Four electrons and a proton are transferred internally in the transition from A to P_M. Two configurations of the P_M state are shown, which are in rapid electronic equilibrium. One of the four electrons necessary for O-O bond cleavage is delivered either by W272 (shown as W or as $W^{\bullet+}$, the tryptophan cation radical magnetically coupled to the heme a_3 oxo-ferryl) or by the g= 2.018 species depicted as X (Trp or Tyr) or in its radical form $X^{\bullet}$; see also text. In the transition from P_M to P_R an electron is transferred internally from haem *a* to $W^{\cdot+}$ or $X^{\bullet}$. External electrons delivered from cytochrome *c* via Cu_A to the haem centers are shown as boxed.

We propose that the radical with g= 2.038/2.005 is the active site Trp residue W272. The g= 2.018 species is due to Trp or Tyr. Although the Y280 radical/Cu_B^{2+} couple has been supposed to be EPR silent [21], we cannot rule it out as the species yielding the signal at g= 2.018. Our data suggest the formation of radicals on the microsecond timescale in the active site of cytochrome oxidases that are apparently capable of a very fast migration (cf. figure. 3). Studies are in progress to identify the tryptophan/tyrosine residues involved, to determine the transient kinetics and the protonation state of the radicals and to delineate the redox state of Cu_B in the first steps of the catalytic cycle.

Acknowledgements:

This research was financed by the Foundation for Fundamental Research on Matter (FOM grant D-26), The Netherlands Research Organization (NWO grant 700-50-025) and the Deutsche Forschungsgemeinschaft (SFB 472). We acknowledge Werner Müller (Frankfurt) for his excellent technical support. We further thank A. van den Berg, R. Suijkerbuijk, J. Langeveld and R. Bode (Delft) for their advice in designing and machining the cold plate set up.

References

1. Richter, O. M.; Ludwig, B., Cytochrome c oxidase--structure, function, and physiology of a redox-driven molecular machine. *Rev Physiol Biochem Pharmacol* **2003,** 147, 47-74.
2. Ferguson-Miller, S.; Babcock, G. T., Heme/Copper Terminal Oxidases. *Chem Rev* **1996,** 96, (7), 2889-2908.
3. Schäfer, G.; Engelhard, M.; Muller, V., Bioenergetics of the Archaea. *Microbiol Mol Biol Rev* **1999,** 63, (3), 570-620.
4. Wikstrom, M. K., Proton pump coupled to cytochrome c oxidase in mitochondria. *Nature* **1977,** 266, (5599), 271-3.
5. Wang, J.; Rumbley, J.; Ching, Y. C.; Takahashi, S.; Gennis, R. B.; Rousseau, D. L., Reaction of cytochrome bo3 with oxygen: extra redox center(s) are present in the protein. *Biochemistry* **1995,** 34, (47), 15504-11.
6. Babcock, G. T.; Jean, J. M.; Johnston, L. N.; Woodruff, W. H.; Palmer, G., Flow-Flash, Time-Resolved Resonance Raman-Spectroscopy of the Oxidation of Reduced and of Mixed-Valence Cytochrome-Oxidase by Dioxygen. *Journal of Inorganic Biochemistry* **1985,** 23, (3-4), 243-251.
7. Pardhasaradhi, K.; Ludwig, B.; Hendler, R. W., Potentiometric and spectral studies with the two-subunit cytochrome aa3 from Paracoccus denitrificans. Comparison with the 13-subunit beef heart enzyme. *Biophys J* **1991,** 60, (2), 408-14.
8. Verkhovsky, M. I.; Morgan, J. E.; Wikstrom, M., Oxygen binding and activation: early steps in the reaction of oxygen with cytochrome c oxidase. *Biochemistry* **1994,** 33, (10), 3079-86.
9. Hellwig, P.; Grzybek, S.; Behr, J.; Ludwig, B.; Michel, H.; Mantele, W., Electrochemical and ultraviolet/visible/infrared spectroscopic analysis of heme a and a3 redox reactions in the cytochrome c oxidase from Paracoccus denitrificans: separation of heme a and a3 contributions and assignment of vibrational modes. *Biochemistry* **1999,** 38, (6), 1685-94.
10. Proshlyakov, D. A.; Pressler, M. A.; DeMaso, C.; Leykam, J. F.; DeWitt, D. L.; Babcock, G. T., Oxygen activation and reduction in respiration: involvement of redox-active tyrosine 244. *Science* **2000,** 290, (5496), 1588-91.
11. Einarsdottir, O.; Szundi, I., Time-resolved optical absorption studies of cytochrome oxidase dynamics. *Biochim Biophys Acta* **2004,** 1655, (1-3), 263-73.

12. Cherepanov, A. V.; De Vries, S., Microsecond freeze-hyperquenching: development of a new ultrafast micro-mixing and sampling technology and application to enzyme catalysis. *Biochim Biophys Acta* **2004,** 1656, (1), 1-31.
13. Michel, H., Proton pumping by cytochrome c oxidase. *Nature* **1999,** 402, (6762), 602-3.
14. Babcock, G. T.; Wikstrom, M., Oxygen Activation and the Conservation of Energy in Cell Respiration. *Nature* **1992,** 356, (6367), 301-309.
15. Ogura, T.; Kitagawa, T., Resonance Raman characterization of the P intermediate in the reaction of bovine cytochrome c oxidase. *Biochim Biophys Acta* **2004,** 1655, (1-3), 290-7.
16. Popovic, D. M.; Stuchebrukhov, A. A., Proton pumping mechanism and catalytic cycle of cytochrome c oxidase: Coulomb pump model with kinetic gating. *FEBS Lett* **2004,** 566, (1-3), 126-30.
17. MacMillan, F.; Kannt, A.; Behr, J.; Prisner, T.; Michel, H., Direct evidence for a tyrosine radical in the reaction of cytochrome c oxidase with hydrogen peroxide. *Biochemistry* **1999,** 38, (29), 9179-84.
18. Budiman, K.; Kannt, A.; Lyubenova, S.; Richter, O. M. H.; Ludwig, B.; Michel, H.; MacMillan, F., Tyrosine 167: The origin of the radical species observed in the reaction of cytochrome c oxidase with hydrogen peroxide in Paracoccus denitrificans. *Biochemistry* **2004,** 43, (37), 11709-11716.
19. Svistunenko, D. A.; Wilson, M. T.; Cooper, C. E., Tryptophan or tyrosine? On the nature of the amino acid radical formed following hydrogen peroxide treatment of cytochrome c oxidase. *Biochim Biophys Acta* **2004,** 1655, (1-3), 372-80.
20. Fabian, M.; Palmer, G., The interaction of cytochrome oxidase with hydrogen peroxide: the relationship of compounds P and F. *Biochemistry* **1995,** 34, (42), 13802-10.
21. Rigby, S. E.; Junemann, S.; Rich, P. R.; Heathcote, P., Reaction of bovine cytochrome c oxidase with hydrogen peroxide produces a tryptophan cation radical and a porphyrin cation radical. *Biochemistry* **2000,** 39, (20), 5921-8.
22. Hendler, R. W.; Pardhasaradhi, K.; Reynafarje, B.; Ludwig, B., Comparison of energy-transducing capabilities of the two- and three-subunit cytochromes aa3 from Paracoccus denitrificans and the 13-subunit beef heart enzyme. *Biophys J* **1991,** 60, (2), 415-23.
23. von Wachenfeldt, C.; de Vries, S.; van der Oost, J., The CuAsite of the caa3-type oxidase of Bacillus subtilis is a mixed-valence binuclear copper centre. *FEBS Lett* **1994,** 340, (1-2), 109-13.
24. Pinakoulaki, E.; Pfitzner, U.; Ludwig, B.; Varotsis, C., Direct detection of Fe(IV)[double bond]O intermediates in the cytochrome aa3 oxidase from Paracoccus denitrificans/H2O2 reaction. *J Biol Chem* **2003,** 278, (21), 18761-6.
25. Kitagawa, T., Structures of reaction intermediates of bovine cytochrome c oxidase probed by time-resolved vibrational spectroscopy. *J Inorg Biochem* **2000,** 82, (1-4), 9-18.
26. Hori, H.; Yonetani, T., Powder and single-crystal electron paramagnetic resonance studies of yeast cytochrome c peroxidase and its peroxide and its peroxide compound, Compound ES. *J Biol Chem* **1985,** 260, (1), 349-55.

27. Houseman, A. L.; Doan, P. E.; Goodin, D. B.; Hoffman, B. M., Comprehensive explanation of the anomalous EPR spectra of wild-type and mutant cytochrome c peroxidase compound ES. *Biochemistry* **1993,** 32, (16), 4430-43.
28. Huyett, J. E.; Doan, P. E.; Gurbiel, R.; Houseman, A. L. P.; Sivaraja, M.; Goodin, D. B.; Hoffman, B. M., Compound Es of Cytochrome-C Peroxidase Contains a Trp Pi-Cation Radical - Characterization by Cw and Pulsed Q-Band Endor Spectroscopy. *Journal of the American Chemical Society* **1995,** 117, (35), 9033-9041.
29. Ivancich, A.; Dorlet, P.; Goodin, D. B.; Un, S., Multifrequency high-field EPR study of the tryptophanyl and tyrosyl radical intermediates in wild-type and the W191G mutant of cytochrome c peroxidase. *J Am Chem Soc* **2001,** 123, (21), 5050-8.
30. Morimoto, A.; Tanaka, M.; Takahashi, S.; Ishimori, K.; Hori, H.; Morishima, I., Detection of a tryptophan radical as an intermediate species in the reaction of horseradish peroxidase mutant (Phe-221 -> Trp) and hydrogen peroxide. *Journal of Biological Chemistry* **1998,** 273, (24), 14753-14760.
31. Ostermeier, C.; Harrenga, A.; Ermler, U.; Michel, H., Structure at 2.7 A resolution of the Paracoccus denitrificans two-subunit cytochrome c oxidase complexed with an antibody FV fragment. *Proc Natl Acad Sci U S A* **1997,** 94, (20), 10547-53.
32. Rich, P. R.; Rigby, S. E.; Heathcote, P., Radicals associated with the catalytic intermediates of bovine cytochrome c oxidase. *Biochim Biophys Acta* **2002,** 1554, (3), 137-46.

Chapter 6

Kinetic Resolution of a tryptophan-radical intermediate in the reaction cyle of *Paracoccus dentrificans* cytochrome *c* oxidase

Frank G.M. Wiertz, Oliver-Matthias H. Richter,
Bernd Ludwig and Simon de Vries

Addapted from: JBC, 2007, 282, 43, 31580-31591

Summary

The catalytic mechanism – electron transfer coupled to proton pumping – of heme-copper oxidases is not yet fully understood. Microsecond freeze-hyperquenching single turnover experiments were carried out with fully reduced cytochrome aa_3 reacting with O_2 between 83 µs and 6 ms. Trapped intermediates were analyzed by low temperature UV-Visible, X-band and Q-band EPR spectroscopy, enabling determination of the oxidation-reduction kinetics of Cu_A, heme *a*, heme a_3 and of a recently detected tryptophan radical (Wiertz et al. (2004) FEBS Lett. 575, 127-130). Cu_B and heme a_3 were EPR silent during all stages of the reaction.

Cu_A and heme *a* are in electronic equilibrium acting as a redox pair. The reduction potential of Cu_A is 4.5 mV lower than that of heme *a*. Both redox groups are oxidized in two phases with apparent half-lives of 57 µs and 1.2 ms together donating a *single* electron to the binuclear centre in each phase. The formation of the heme a_3 oxo-ferryl species P_R (maxima at 430 nm and 606 nm) was completed in ~130 µs, similar to the first oxidation phase of Cu_A and heme *a*. The intermediate F (absorbance maximum at 571 nm) is formed from P_R and decays to a hitherto undetected intermediate named F_{W*}. F_{W*} harbors a tryptophan radical, identified by Q-band EPR spectroscopy as the tryptophan neutral radical of the strictly conserved Trp-272 (Trp-272*). The Trp-272* populates to 4-5% due to its relatively low rate of formation ($t_{1/2}$= 1.2 ms) and rapid rate of breakdown ($t_{1/2}$ = 60 µs), which represents electron transfer from Cu_A/heme *a* to Trp-272*. The formation of the Trp-272* constitutes the major rate determining step of the catalytic cycle.

Our findings show that Trp-272 is a redox active residue and is in this respect on an equal par to the metallo-centers of the cytochrome *c* oxidase. Trp-272 is the direct reductant either to the heme a_3 oxo-ferryl species or to Cu_B^{2+}. The potential role of Trp-272 in proton pumping is discussed.

Introduction

The superfamily of heme-copper oxidases comprises the cytochrome oxidases, which catalyze the reduction of molecular oxygen to water and the NO reductases that catalyze the reduction of NO to N_2O [1-6]. Cytochrome oxidases (CcO)[1)] are the final electron acceptors in the respiratory chains of bacteria, archaea and mitochondria. Cytochrome aa_3 from *Paracoccus denitrificans*, is a Type A oxidase based on the structure of its D- and K-proton pathways [7, 8]. The reduction of oxygen (Reaction 1) generates a proton electrochemical gradient across the cytoplasmic membrane. Four protons are used for the formation of water, and four are pumped across the membrane according to,

$$4 \text{ cyt } c^{2+} + O_2 + 8\ H^+_C \rightarrow 4 \text{ cyt } c^{3+} + 2\ H_2O + 4\ H^+_P \qquad (1)$$

where H^+_C are protons taken up from the cytoplasm and H^+_P protons ejected to the periplasm [9-13].

The crystal structures of cytochrome aa_3 from bovine heart mitochondria, *P. denitrificans* and *Rhodobacter sphaeroides* have been solved [8, 14-18]. *P. denitrificans* cytochrome aa_3 is a four-subunit membrane complex. Subunit one harbors heme *a* and the heme a_3-Cu_B binuclear reaction center where reduction of oxygen takes place. Subunit two contains the docking site for cytochrome *c* [19, 20] and the Cu_A mixed-valence binuclear center with two Cu atoms separated by 2.5 Å [21]. Electrons from cytochrome *c* enter CcO at the Cu_A site and are further transferred via heme *a* to heme a_3 and Cu_B. Protons from the cytoplasm enter the enzyme via the D- or K-proton pathways [10-13, 22, 23]. These pathways connect the aqueous cytoplasmic phase with the conserved Glu-278 in the interior of the enzyme (D-pathway) or with the binuclear centre (K-pathway). The proton exit route to the periplasm is less well defined. Water is expelled to the periplasm via the Mg^{2+} or Mn^{2+} bound at the interface of subunit I and II [24-27].

The oxygen reduction cycle of CcO has been studied by a great variety of kinetic techniques such as the flow-flash method monitored by UV-visible spectroscopy [10-13, 23, 28-31] or resonance Raman scattering [32-38]. Collectively these studies have led to a general understanding of the catalytic mechanism in terms of oxygen chemistry, electron transfer and proton translocation. The catalytic cycle can be initiated from the fully reduced enzyme (**R**), from the mixed-valence form (**MV**) in which only heme a_3 and Cu_B are reduced or by single electron injection [39].

When the reaction is started with the fully reduced CcO, the enzyme cycles through a series of intermediates designated as **R** → **A** → $\mathbf{P_M}$ → $\mathbf{P_R}$ → **F** → $\mathbf{O_H}$ (see Figure 7). The first detectable intermediate after mixing **R** with O_2, **A**, is formed within ~10 µs. **A** is the oxy-ferrous complex (Fe^{2+}-O_2) of heme a_3 [29-31, 34-38]. Subsequently the O=O bond is broken yielding $\mathbf{P_M}$. $\mathbf{P_M}$ accumulates (~150 µs) when the reaction is started with **MV**. However, when the reaction is initiated from **R**, $\mathbf{P_R}$ accumulates (completed in ~100 µs). Direct evidence for O=O bond splitting in both $\mathbf{P_M}$ and $\mathbf{P_R}$ was provided by resonance Raman spectroscopy, which identified the specific vibrations of the oxo-ferryl (Fe^{4+}=O) state of heme a_3 [34-38]. In $\mathbf{P_M}$ and $\mathbf{P_R}$, the Cu_B^{1+} has been oxidized to Cu_B^{2+}-OH^-. The oxygen atom in Cu_B^{2+}-OH^- is derived from molecular oxygen [40]. The breaking of the O=O bond requires donation of four electrons and a proton. Since this also occurs when the reaction is started with **MV**, while heme a_3 and Cu_B provide only three electrons, an amino acid, Tyr-280 (*P. denitrificans* numbering) was proposed to act as the donor of the fourth electron (plus the proton) [33]. Tyr-280 is covalently linked to His-276, a ligand to Cu_B, and sufficiently close to the binuclear centre to act as a rapid reductant [8, 14, 16-18]. Indeed, some Tyr-280 had been converted to the radical Tyr-280* in $\mathbf{P_M}$ [41]. In $\mathbf{P_R}$, in contrast to $\mathbf{P_M}$, the Tyr-280* is absent [42] presumably because it has been reduced by heme *a* to the anion (Tyr-280$^-$) or to the protonated Tyr-280. Even though heme *a* oxidation in the sequence **R** → **A** → $\mathbf{P_M}$ → $\mathbf{P_R}$ is completed within ~100 µs, the true rate of electron transfer from heme *a* to heme a_3 (and to Tyr-280*?) is ~1 ns [43], which would explain why $\mathbf{P_M}$ (and Tyr-280*) does not accumulate to a measurable extent when the reaction is started from **R**. Instead of Tyr-280, the conserved Trp-272 has been proposed recently as the amino-acid residue involved in O=O bond breaking [44].

The $\mathbf{P_R}$ → **F** transition is not associated with electron transfer but with proton binding and proton translocation [9-13]. The slowest step of the oxidative part of the catalytic cycle (1-1.5 ms) is the **F** → $\mathbf{O_H}$ transition, which is linked to proton translocation as well [9-13]. In this step an electron is transferred from Cu_A/heme *a* to Fe^{4+}=O yielding Fe^{3+}-OH^- [38]. At this stage, the enzyme is completely oxidized, but in a metastable 'high energy state', $\mathbf{O_H}$. Reduction of $\mathbf{O_H}$, but not of the resting enzyme (**O**), leads to two successive proton-pumping events in the reaction sequence $\mathbf{O_H}$ → **E** → **MV** [11, 45].

To resolve enzyme catalytic mechanisms on the microsecond time scale, we have developed a microsecond freeze-hyperquenching

mixing/sampling device (MHQ) [5, 46-48]. MHQ is an extension of the rapid-freeze quench (RFQ) technique [49] in which the instrument dead time has been reduced from 5-7 ms to 60-80 µs [46, 47]. The great advantage of MHQ and RFQ is that the resulting frozen powder containing trapped intermediates can be analyzed by a variety of spectroscopic techniques including EPR spectroscopy, an invaluable tool in the study of metallo-redox enzymes. MHQ experiments with cytochrome bo_3 from *E. coli* and cytochrome aa_3 from *P. denitrificans* showed the formation of a tryptophan radical (Trp*) after ~ 200 µs, which was weakly magnetically coupled to the Fe^{4+}=O state of the heme a_3 [46]. The EPR properties of this transient radical differ from the Tyr-167* and the proposed porphyrin cation and/or tryptophan radicals obtained by incubation with H_2O_2 [50-52].

In the work presented in this paper we used MHQ to determine the kinetics of the Trp* found previously and assign its role in the catalytic cycle. Q-band EPR spectroscopy identifies the radical as the neutral radical form of Trp-272. The kinetics of Trp-272*, Cu_A, heme *a* and heme a_3 were determined and simulated with a single set of rate constants in a model including the new intermediate $\mathbf{F_W}$*, which harbors the Trp-272*. The Trp-272* is formed in the second part of the catalytic cycle and Trp-272 is proposed as the electron donor to heme a_3 or Cu_B. An additional role for Trp-272 in proton pumping is discussed.

Materials and Methods

Enzyme purification

P. denitrificans cytochrome aa_3 was purified as previously described [53, 54] and contained 0.2 mol Mn^{2+} per mol of enzyme as determined by EPR spectroscopy. Mn^{2+}-depleted enzyme was obtained by decreasing the Mn^{2+} concentration to 0.5 µM in the growth medium [55, 56].

Microsecond freeze-hyperquenching and sample handling

The MHQ setup (dead time of 60-80 µs and effective reaction temperature of 10 ± 1 °C.) and the sample handling procedures are identical to those described before [5, 46] except that the aluminum rotating cold plate was coated with a layer of approximately 5 µm of 99.999+ % tungsten. Tungsten was applied in 50 cycles of physical vapor deposition (PVD). The tungsten coating of the cold plate resulted in lower impurities (*e.g.* Fe^{3+}

trapped in corundum) in the samples analyzed by EPR spectroscopy. For each time point 0.25 ml of pulsed cytochrome aa_3 (100-280 μM) was used [5, 46]. The reduced enzyme (incubated with 10 mM ascorbate and 1 μM PES) was mixed 1:1 with an O_2-saturated (1.3 mM at 20 °C) buffer (50 mM HEPES, pH 7.2, 0.1% lauryl-maltoside). Sample preparation for the low temperature UV-visible spectroscopy and normalization and analysis of the spectra are described in [46]. Sample packing is described in [47].

UV-visible spectroscopy

UV-visible spectra were recorded with an Olis upgraded Aminco DW2000 scanning spectrophotometer equipped with a custom-made liquid N_2-flow system, to maintain the temperature during the measurement stable at 90 K [48]. The spectrophotometer was calibrated with a holmium oxide filter to an accuracy of 0.2 nm.

Data analysis

Data were processed and analyzed with the IGOR Pro software package (Wavemetrics). Q-band EPR spectra were simulated using a home-written simulation program in Pascal for the Macintosh computer. The program allows for non-linear g- and A-tensors. The kinetic data were fitted to a model of six consecutive irreversible reactions. The analytical solution of this set of homogeneous first-order differential equations has been added to the supplemental information.

EPR spectroscopy

X-band EPR spectroscopy was performed on a Bruker ER200D spectrometer, Q-band EPR spectra were recorded on a Varian E9 spectrometer. Both spectrometers were equipped with a home-built He-flow system [57]. EPR signals were quantitated with respect to a 10 mM $CuClO_4$ standard. Differences in sample packing were corrected using the Mn^{2+}-signal as internal standard in case Mn^{2+}-containing CcO was used (see Figure S2). For Mn^{2+}-free CcO no correction for sample packing was applied, only for differences in starting concentrations of the CcO. The overall dilution of the enzyme as present in the EPR tube is 6-10 fold with respect to the starting concentration. This dilution arises from the 1:1

mixing, condensation of water vapor during sample handling and the loose sample packing owing to the fine nature of the frozen powder. The uncertainty in sample packing was determined at 1 ± 0.20 (n = 25) and is indicated with error bars in the figures. However, the relative concentrations of Cu_A, heme *a* and the Trp* are accurate to 1 ± 0.05, since they are determined in the same sample. The g-values of the Trp* at Q-band frequency were determined with 2,2-diphenyl-1-picrylhydrazyl (DPPH) and the Mn^{2+} signal as an internal standard and are accurate to ± 0.0002.

Results

Low-temperature UV-visible spectroscopy of MHQ samples

MHQ samples were prepared by reacting fully reduced cytochrome aa_3 with O_2 for various times between 83 µs and 6 ms. Figure 1 shows the low-temperature absolute and difference UV-visible spectra of a selection of these samples. In the first 130 µs of the reaction the absorbance of the Soret band at 444 nm decreases and a new band appears at 430 nm (Figure 1A).

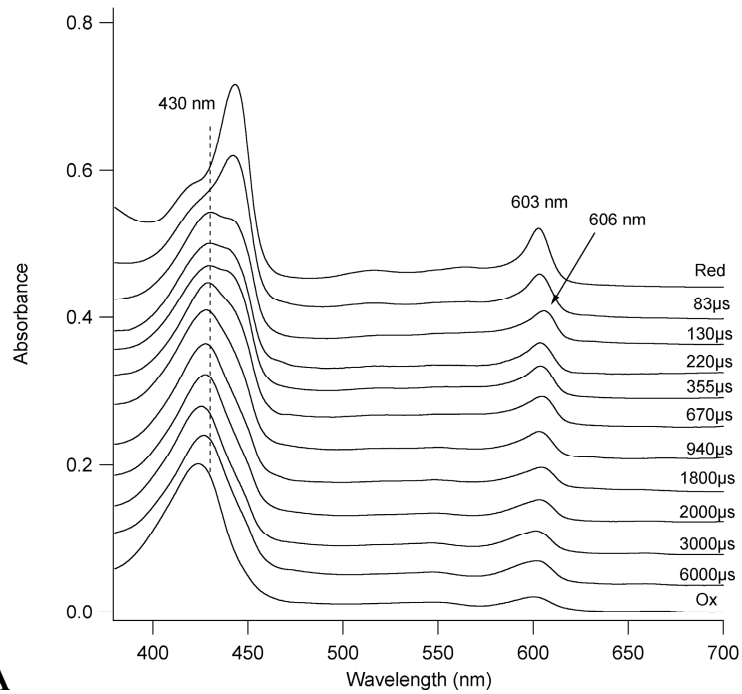

A

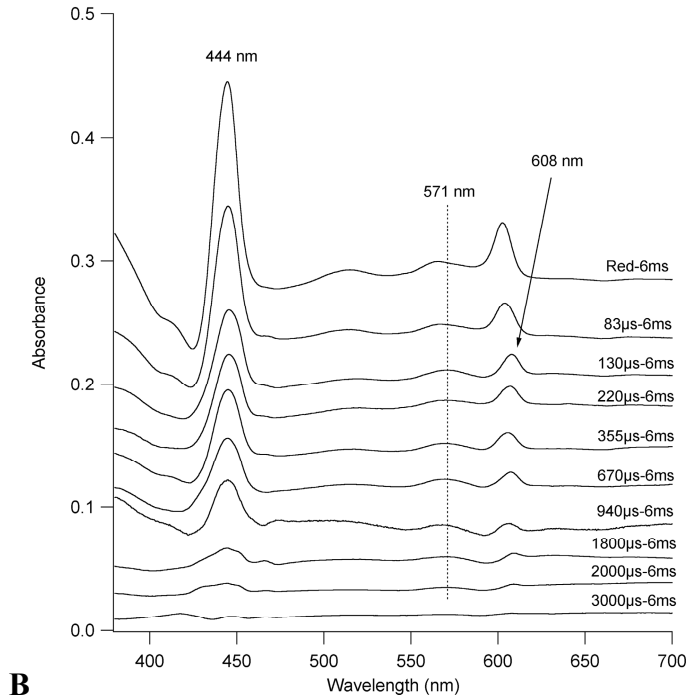

Figure 1 Low temperature absolute (*A*) and difference (*B*) visible spectra of cytochrome aa_3 from *P. denitrificans* recorded at 90 K. Fully reduced pulsed cytochrome aa_3 was rapidly mixed with an O_2 saturated buffer and reacted for various times (indicated in microseconds). *"Red"* refers to fully reduced cytochrome aa_3 with maxima at 444 nm in the Soret region and at 603 nm in the α-band region. *A*, the Soret maximum of the oxo-ferryl form of heme a_3 is at 430 nm. Formation of $\mathbf{P_R}$ (606 nm) after 130 µs is indicated by an arrow. The peak shifts to 603/604 nm after 220 µs and longer times. After 6 ms the enzyme is oxidized ($\mathbf{O_H}$); the Soret maximum is at 427 nm. *"Ox"* refers to the as-isolated oxidized form of cytochrome aa_3 displaying maxima at 424 nm and 600 nm in the Soret and α-band regions, respectively. *B*, the spectrum obtained after 6 ms was subtracted from those in *A*. The Soret maximum of reduced hemes ($a + a_3$) is at 444 nm. Formation of $\mathbf{P_R}$ (608 nm) after 130 µs is indicated by an arrow. The peak shifts to 603/604 nm after 220 µs and longer times. Formation of **F** is indicated by the shift of the α-band from 565 nm to 571 nm (0-130 µs). Decay of **F** is seen as a decrease in intensity of the 571 nm band (355 µs to 3000 µs).

The difference spectra (Figure 1B) indicate a loss of intensity of approximately ~50% at 444 nm. Concomitantly, the α-band shifts from 603 nm to 606 nm (Figure 1A) or, in the difference spectra (Figure 1B) to 608 nm while loosing some intensity. The peaks at 430 nm and 606 nm in the absolute spectra are characteristic for the oxo-ferryl state (Fe^{4+}=O) of heme

a_3, and the P-state, specifically $\mathbf{P_R}$ [32-38]. The spectra obtained after 220 µs and 355 µs indicate a small blue shift of the α-band from 608 nm to 603-604 nm without a change in the Soret region (Figure 1B). This blue shift is consistent with the $\mathbf{P_R} \rightarrow \mathbf{F}$ transition (10-13,23,28-31,33,35,38). More direct evidence for the formation of **F** came from control experiments using H_2O_2 (data not shown) to generate **F** at pH 6 and 7.2, the latter being the pH in our experiments. These experiments were performed exactly as in [44]. Samples were first monitored at room temperature to check for formation of **F** and subsequently frozen for analysis at 90 K by UV-visible spectroscopy. The low temperature UV-visible difference spectra (H_2O_2 minus oxidized enzyme) indicated the formation of a broad band with a maximum at 571 ± 1 nm instead of 580 nm at room temperature [42, 44, 58, 59]. The amplitude of the 571 nm band amounted to 7 and 11% (at pH 7.2 and 6, respectively) of the α-band intensity of the absolute spectrum of oxidized enzyme cf. [59]. Figure 1B shows a shift in the β-band position from 565 nm at t = 0 to 571 nm indicating formation of **F**. The 571 nm maximum persists up to 3 ms, which suggests rapid formation and relatively slow breakdown (1-1.5 ms) of **F**. The kinetics of formation and breakdown of **F** were calculated from Figure 1B (see Figure 8) and are in good agreement with the data in [28, 38].

After the formation of **F** the Soret maximum at 430 nm shifts to 427 nm (completed after 3-6 ms), corresponding to the absorbance maximum of the oxidized (pulsed) enzyme (Figure 1A). The disappearance of the Soret maximum at 444 nm also points to complete oxidation of hemes (a + a_3) after 3-6 ms (Figure 1B). The UV-Vis spectra do not resolve the concomitant reduction of heme a_3 (Fe^{4+}=O to Fe^{3+}-OH^-) and oxidation of heme a, neither in the Soret region nor in the α-band. The intensity of the α-band decreases (355 µs to 6 ms) due to oxidation of heme a. Control stopped-flow experiments indicated that after 4-6 ms no further optical changes occurred up to several minutes (data not shown).

When the oxidation of the hemes (a + a_3) is calculated as the optical absorbance difference at 444-462 nm (Figure S1) the characteristic apparent biphasic oxidation is observed, similar to that for the bovine heart mitochondrial cytochrome aa_3 oxidase [28].

EPR spectroscopy of MHQ samples

Representative EPR spectra of the Mn^{2+}-free CcO samples are shown in Figure 2.

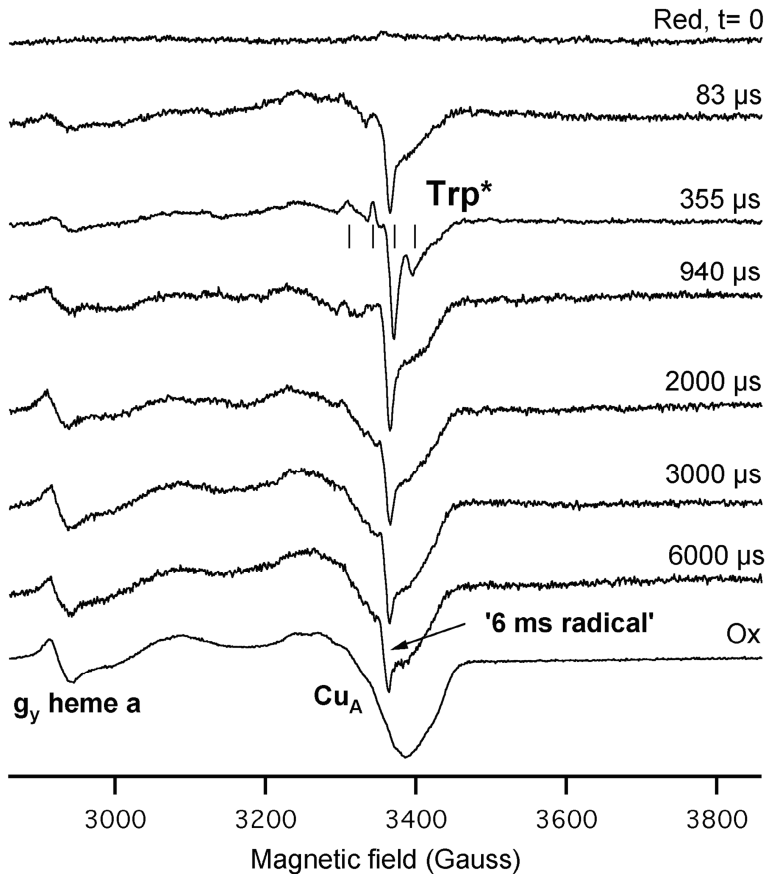

Figure 2
Representative X-band EPR spectra of cytochrome aa_3 from *P. denitrificans* rapidly mixed with O_2 and reacted for various times (indicated in microseconds). The four *vertical lines* indicate the peaks of the Trp* (spectrum after 355 µs). The g_y resonance of heme *a* and the $g_\perp$ of Cu_A were used to determine their redox states. EPR conditions: frequency, 9.42 GHz; modulation amplitude, 1.0 millitesla; microwave power, 2 milliwatts; temperature, 14 K. The spectra are normalized correcting for differences in gain and enzyme concentrations.

The magnetic field range displayed is suitable for the determination of the redox states of heme *a*, Cu_A, Cu_B, and for the detection of the radical described previously [5, 46]. The figure shows rapid oxidation of heme *a* and Cu_A to ~50% after 83 µs and 355 µs while the remainder is oxidized on the millisecond time scale. The Trp* is developed maximally after 355 µs and disappears within a few milliseconds concomitant with the second slow

heme *a*/Cu_A oxidation phase (Figure 2). After 6 ms another radical is observed, called the "6-ms radical" (Figure 3).

The X-band EPR spectrum of the Trp* (355 µs) in Mn^{2+}-depleted CcO (Figure 3) is slightly different form that reported previously; in that work the contribution from Mn^{2+} had to be subtracted (see Figure 2 in Ref. [46]). In particular, the low field line (g = 1.985) was poorly resolved, but present in both the cytochrome aa_3 and cytochrome bo_3 EPR spectra. The Trp* X-band EPR signal consists of four lines with apparent g values of g = 2.036, 2.018, 2.004 and 1.985.

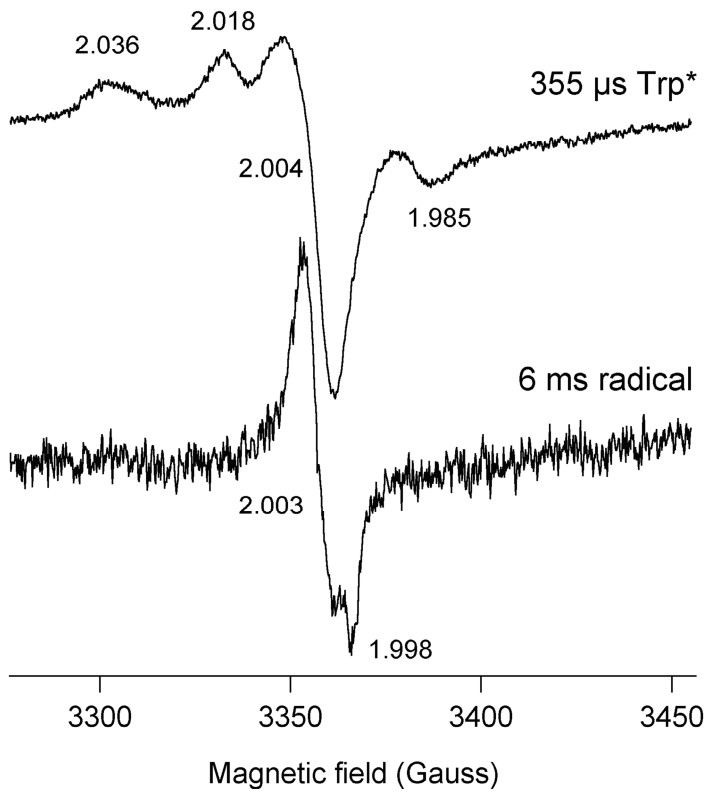

Figure 3 X-band EPR spectra showing two different radicals formed by cytochrome aa_3 from *P. denitrificans* during the reaction cycle. The enzyme has reacted for 355 µs (Trp*) or 6 ms (*lower spectrum*). The apparent g values are indicated. EPR conditions: frequency, 9.411 GHz; modulation amplitude, 0.5 millitesla; microwave power, 0.2 milliwatts; temperature, 14 K. Each spectrum is an average of four. The spectrum of the 6-ms radical was expanded vertically five times with respect to the 355-µs Trp* spectrum. The starting CcO concentrations were 280 µM (355 µs) and 120 µM.

We have previously attributed the lines at $g = 2.036$ and $g = 2.004$ to a Trp* weakly magnetically coupled ($J_{x,y}$ = -4.9 GHz) to the heme a_3 $Fe^{4=}$=O state [46]. The lines at $g = 2.018$ and $g = 2.005$ could originate from a second Trp* (with $J_{x,y}$ = -2.1 GHz) or from a Tyr* also including a low field feature now clearly resolved at $g = 1.985$. Q-band EPR spectroscopy (Figure 4) leads to a revision of this assignment regarding the Tyr*.

The EPR line shape of the four-line radical signal is fairly constant in the MHQ samples obtained up to 940 µs. However, after 2 ms and longer reaction times, a sharp and at X-band frequency axial signal with $g_{\perp} = 2.003$ and $g_{\|} = 1.998$ had clearly developed, which is the '6 ms radical' spectrally overlapping with the Trp* (Figures 2 and 3). In particular, part of the sharp feature at $g = 2.004$ of the Trp* is due to a contribution of the 6-ms radical (Figure 3).

EPR spectroscopy of the 355 µs and 6 ms MHQ samples at Q-band frequency allows a more solid assignment of the radical (Figure 4).

The four-line spectrum of the Trp* at X-band from $g = 2.04$ to $g = 1.98$ is apparently confined to a narrow magnetic field region around $g = 2$. The Zeeman interaction at Q-band frequency (35 GHz) is now much larger than the weak magnetic dipolar/exchange coupling (-4.9 GHz) leading to a simplification of the four-line spectrum seen at X-band frequencies. The Q-band spectrum of the 6-ms radical (Figure 4) is better resolved than the X-band spectrum (Figure 3) displaying a three-line rhombic signal. The rhombic signal represents approximately ~0.5% of the CcO concentration. The 6- ms radical is not an ascorbate or PES radical. The absence of resolved hyperfine structure in its spectrum and the g values ($g_{x,y,z}$ = 2.0022, 1.9965, 1.9994) close to the free electron g value suggest an organic radical, perhaps a main-chain radical. The structural characterization and the possible function of this radical have to await further experimentation.

The Q-band EPR spectrum of the radical obtained after 355 µs can be simulated as a $S = ½$ system with simulation parameters (Table 1) characteristic for Trp* radicals [60-62], in agreement with our previous assignment [46].

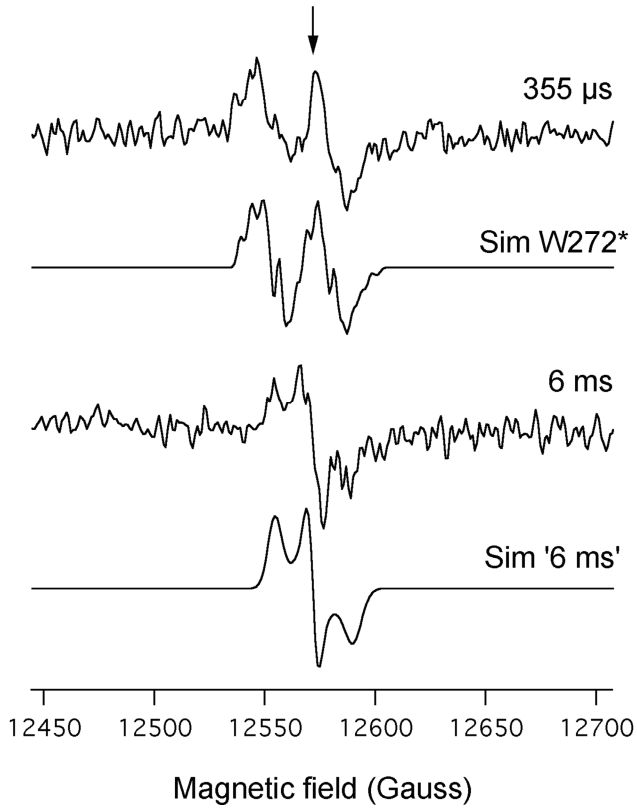

Figure 4 Q-band EPR spectra of the Trp* (355 µs), the 6-ms radical and their simulations. Part of the MHQ frozen powder used for the samples of Figure 4 were transferred to Q-band EPR tubes. The 6-ms radical contributes slightly to the Trp* in the spectrum of the 355 µs sample. This is seen most clearly in the *positive part* of the *right line*, which is relatively sharp. In this region (indicated by an *arrow*) the fit to the experimental spectrum is somewhat less. The simulation parameters for the Trp* are listed in Table 1. Those for the 6-ms radical are: $g_{x,y,z}$ = 2.0022, 1.9965, 1.9994. EPR conditions: frequency, 34.972 GHz; modulation amplitude, 1.0 millitesla; microwave power, 2.5 and 5 milliwatts (6-ms sample); temperature, 16 K. Each spectrum is an average of 85 scans.

The hyperfine constants determined by the simulation can be used to calculate the dihedral angles of the β-methylene protons with respect to the indole ring [60-62]. Because the dihedral angles are known from crystal structure [8, 14, 16-18] the radical was assigned as residing at Trp-272 (see Table 1 and "Discussion"). Tyrosine radicals have much larger *g*-anisotropy [56, 62, 65-67] and are absent from the spectrum. The Trp-272* EPR spectrum contains a small contribution from the 6-ms radical (indicated by the arrow in Figure 4), which is not reproduced in the simulation of Trp-272*.

Table 1 Orientation of the β-methylene protons of Trp residues of *P. denitrifcans* CcO, conserved in Type A1 oxidases, their predicted hyperfine ratios ($H\beta_2/H\beta_1$) and the simulation parameters for the Trp*.

Residue	Dihedral angle		$H\beta_2/H\beta_1$	Distance (Å) [1]			Comment
	θ_1	θ_2		δa_3-C_3	δCu_B-C_3	δa-C_3	
Trp-164	-13.6°	-133.6°	0.503	8.5	5.3	11.9	Trp* in W164T
Trp-272	3.8°	123.8°	0.31	9.8	7.1	13.4	Ok
Trp-323	30.9°	150.9°	1.04	10.7	7.5	18.0	wrong $H\beta_2/H\beta_1$
Trp-358	-81.5°	158.5°	0.025	16.1	21.9	22.2	F in *A. pernix*,
Trp-375[2]	-3.8°	116.2°	0.196	18.6	25.4	15.6	Too far[4]
Trp-431[3]	-78.5°	161.5°	0.044	23.5	29.5	22.2	Too far[4]
Trp-532	-2.8°	118.2°	0.22	28.8	34.6	29.2	Too far[4]
Trp-136	-10.7°	109.3°	0.113	29.2	31.3	24.7	Too far[4]
Trp-22	4.9°	124.9°	0.33	34.1	37.1	27.5	Too far[4]
Experimental	θ_1,3.1°	θ_2,123.1°	$H\beta_2/H\beta_1$ 0.30				
SD[4]			0-0.4				
Simulation parameters	g	$H\beta_1$ (Gauss)	$H\beta_2$ (Gauss)	H5 (Gauss)	H7 (Gauss)	N (Gauss)	
xx	2.0035	25	7.5	7	0	0	
yy	2.0026	25	7.5	0	5	0	
zz	2.0023	25	7.5	5	5	9	

The dihedral angles θ_1 and θ_2 are calculated from the crystal structure of *P. denitrifcans* CcO (PDB entry 1QLE*4*).

[1] δa_3-C_3, δCu_B-C_3, δCa-C_3: shortest distance from the C3 atom of the respective tryptophan residue to heme a_3, Cu_B *and heme a*, respectively. About 50% of the spin density is located at the C3 atom.

[2] Not conserved in other oxidases.

[3] *Y* in *Sulfolobus acidocaldarius*.

[4] "Standard deviation", the value for the ratio $H\beta_2/H\beta_1$ yielding EPR spectra quite similar to the experimental spectrum. See Figure S3 and text for further explanation. [4] The dipolar/exchange coupling of the oxoferryl-Trp-119 radical in cytochrome *c* peroxidase (-4.9 GHz) is the same as that observed for the Trp-272*. The coupling of -4.9 GHz yields for both radicals a peak at $g_z \sim 2.04$. The Trp* and Tyr* described in ([28,38,63,64] with similar couplings/g_z-values are all located within 9 Å from the oxoferryl. The dipolar contribution to the magnetic coupling is dominant over the exchange coupling at distances > 3-4 Å and falls off with the third power of the distance. Trp-358, at 16.1 Å is expected to yield a coupling < 1 GHz or $g_z \sim 2.009$, which is not seen in the X-band EPR spectrum. Both Trp164 and Trp-272 are at distances from the oxoferryl consistent with the $g_z \sim 2.04$.

The kinetics of the Trp-272* calculated from the X-band EPR spectra are displayed in Figure 5.

The relatively slow formation of the Trp-272* (1200 µs) and its rapid breakdown (60 µs) are consistent with the total accumulation to 4-5% as determined by EPR.

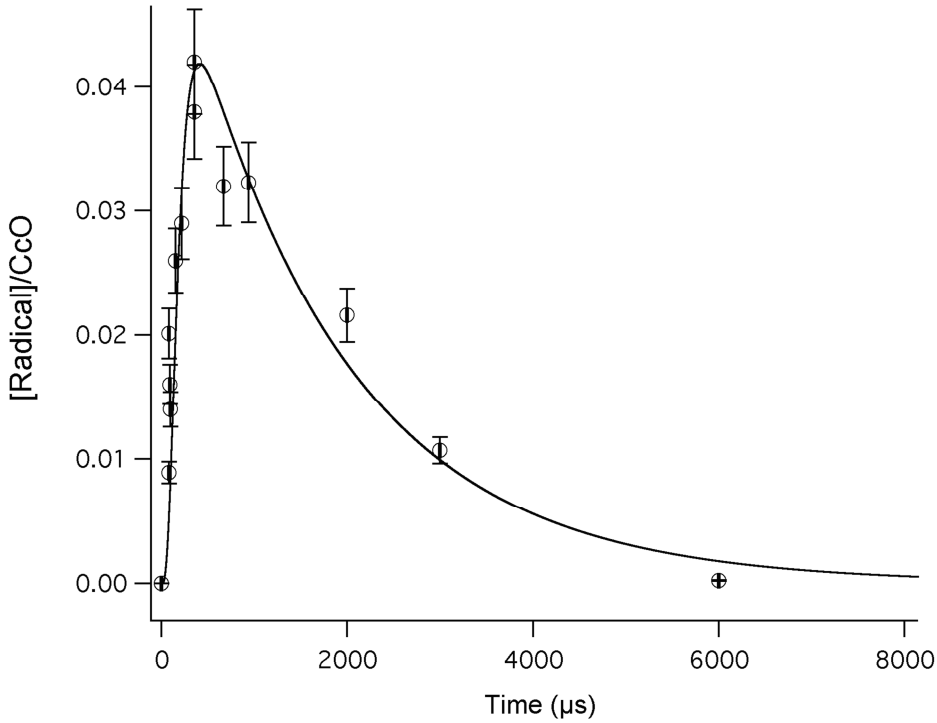

Figure 5 Time course of the tryptophan radical. The amount of radical (*open circles*) was determined from the X-band EPR spectra taken from freeze-quenched samples. The *line* through the data points is a simulation using the rate constants of Figure 7 and represents the kinetics of F_W* (Figure 8), indicating an *apparent* half-life of formation of 157 µs, maximal Trp* level after 414 µs and an *apparent* half-life of breakdown of 1.71 ms, yielding 0.042 Trp*/CcO as the maximal amount of radical formed. Note that, when species accumulate to low amounts like the Trp*, the apparent rate of formation is actually closer to the rate of decay and *vice versa* [68].

The maximum amount of the Trp-272* is formed after 300-500 µs and amounts to 4-5% of the CcO. The transient is fitted with the same rate constants as the Cu_A and heme *a* traces (see below Figure 6) and apply to the model shown in Figure 7.

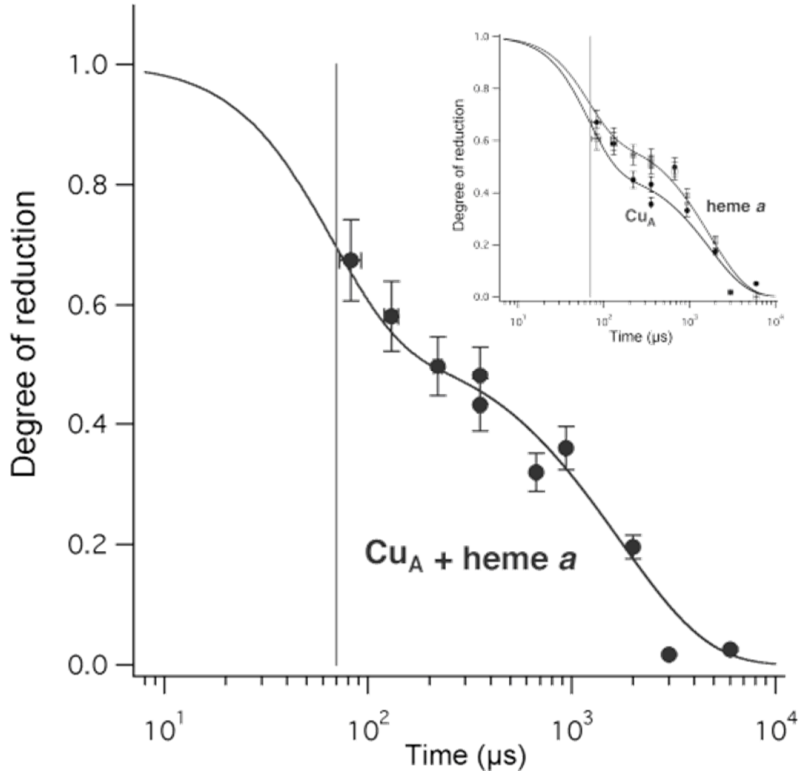

Figure 6 Oxidation kinetics of (Cu_A + heme *a*) (*filled circles*) and in the inset of Cu_A (*filled circles*) and heme *a* (*open circles*) plotted separately. Redox states of heme *a* and Cu_A were calculated from EPR spectra as shown in Figure 2. The *lines* through the data are simulations using the six rate constants shown in the model of Figure 7 and further applying the $K_{eq} = 1.2$ for the Cu_A/heme *a* equilibrium to calculate the traces of the inset. A single electron is donated by (Cu_A + heme *a*) in each oxidation phase. The *vertical line* represents the MHQ dead time (60-80 μs), positioned at 70 μs.

The oxidation kinetics of Cu_A and heme *a* determined by EPR are presented in Figure 6. Cu_A and heme *a* are oxidized in two kinetic phases. The kinetics of Cu_A and heme *a* suggest very similar reduction potentials for the two cofactors. The calculated equilibrium constant, $K_{eq} = 1.20 \pm 0.23$, corresponds to a 4.5 mV ± 5.4 mV ($n = 9$) lower midpoint potential for Cu_A relative to heme *a* (Figure 6, *inset*), a value in good agreement with pulse radiolysis experiments monitored optically [69]. Assuming redox equilibrium, the slightly lower midpoint potential of Cu_A leads to the slightly higher *apparent* rate of oxidation of Cu_A (apparent $t_{1/2} = 50$ μs for 25% oxidation) relative to heme *a* (apparent $t_{1/2} = 65$ μs for 25% oxidation) (Figure 6, *inset*).

The apparent half-lives for the second phase (each component oxidized for 75%) are 1.22 ms and 1.62 ms for Cu_A and heme *a*, respectively. Figure 6 further shows that (Cu_A + heme *a*) act as a redox pair donating a *single* electron to the binuclear center in each oxidation phase.

The typical four-line EPR signal of Cu_B [40, 42] was not detected in any of the MHQ samples, even though the temperature was varied between 6 and 100 K and the microwave power between 20 microwatts and 200 milliwatts. All samples including the time-zero sample, showed the $g = 6$ a signal of Fe^{3+} high-spin heme a_3, but its intensity was low (<3% of the CcO) and hardly changed (though slightly increased) between $t = 0$ and 6 ms (data not shown). These $g = 6$ data were not further analyzed.

The EPR spectra of MHQ samples obtained with Mn^{2+}-containing enzyme are shown in Figure S2. For these samples quantitation of the radical intensity and Cu_A was more difficult due to overlap of the Mn^{2+} EPR spectrum. However, the Mn^{2+} signal served as a good internal standard to determine sample reproducibility even though the Mn^{2+} spectrum is dependent on the redox state of Cu_A [27]. The sample preparation reproducibility ($n = 25$) was determined at 1 ± 0.20. The kinetic behavior of Mn^{2+}-containing or Mn^{2+}-depleted cytochrome aa_3 was found to be indistinguishable, consistent with similar turnover numbers (180-190 O_2 s^{-1}) for both types of oxidase preparations. Therefore, Figures 1, 5, 6, 8 and S1 display data obtained on both types of enzymes.

Discussion

In the oxidative part of the catalytic cycle of *P. denitrificans* cytochrome aa_3 two radicals are formed as determined by MHQ in conjunction with X-band and Q-band EPR spectroscopy. Simulation of the Q-band EPR spectrum identifies one of the radicals as the catalytically competent tryptophan neutral radical of the strictly conserved Trp-272 (Trp-272*). Formation of Trp-272* constitutes the rate-limiting step of the catalytic cycle. The current finding that the Trp-272 radical is neutral demonstrates that this residue couples electron transfer to proton movements. We will discuss below how oxidoreduction of Trp-272 can provide the driving force for the transmembrane movement of protons ("proton pumping") through its participation in a proton-relay network. Our findings underscore the general importance of amino-acid side chains in coupling electron transfer to proton transfer reactions, along side the well-known metallo-redox centres.

In this paper a full kinetic profile in a time window of 83 μs to 6 ms has been determined for the oxidation-reduction kinetics of Cu_A, heme *a*, heme a_3 and the Trp-272*. EPR spectroscopy has the great advantage over UV-visible and resonance Raman spectroscopy that the concentrations of these components can be determined without mutual spectral interference and without assumptions about (relative) extinction coefficients or about the resonance enhancement. The assignment of the Trp-272* and its possible function in catalysis are discussed within the framework of the model presented in Figure 7. This model describes the oxidation route of the fully reduced enzyme by the reaction sequence $\mathbf{R} \rightarrow \mathbf{A} \rightarrow \mathbf{P_M} \rightarrow \mathbf{P_R} \rightarrow \mathbf{F} \rightarrow \mathbf{F_W}^* \rightarrow \mathbf{O_H}$ in which the new intermediate F_W* contains the Trp-272*. Simulations of the kinetic traces (Figures 5, 6) were performed with a *single* set of rate constants (half-lives) shown in Figure 7. The appearance and accumulation of the various intermediates is depicted in Figure 8.

Scope and limitations of the MHQ set up

The formation of **A** ($t_{1/2}$ = 16 μs at 0.65 mM O_2 [29]) could not be resolved because the instrumental dead time of the MHQ set up is 60-80 μs. The oxygen-binding rate has been established with the flow-flash set up monitored by UV-visible spectroscopy (dead time ~1.5 μs determined by the CO dissociation rate [29]) and the structural assignment of **A** (Fe^{2+}-O_2) is based on resonance Raman spectroscopy (dead time ~25 μs [32-38]). We did observe the formation of $\mathbf{P_R}$ (Fe^{4+}=O) indicated by the α-band absorbance shift to 606 nm (608 nm in the difference spectra) concomitant with the formation of the Soret absorbance at 430 nm and the disappearance of ~50% of the Soret intensity at 444 nm (Figure 1, and Figure S1). The formation of **F** at 571 nm was also detected. In addition we could resolve and analyze by EPR spectroscopy rather than by UV-visible spectroscopy part of the initial oxidation phase of heme *a* and Cu_A. Transfer of the first electron to the binuclear center after O=O bond splitting is completed in ~130/200 μs (Figures 6, 7 and 8).

The heme (a + a_3) oxidation kinetics follow the characteristic biphasic pattern of the fully reduced enzyme (Figure S1, [28]). In our work the UV-visible spectral data are obtained from independently frozen samples, in contrast to the "continuous" flow-flash methods, and have to be normalized in order to compare the redox states of the hemes between different samples [5, 46, 48]. Because our data could be simulated with a similar set of kinetic and spectral parameters as for the bovine heart enzyme ([28] and Figure S1) we

conclude that the normalization procedure is adequate. A multi-component analysis of the UV-visible spectra to determine the spectra of the intermediates **A, P_R** or **F** proved too difficult at present and has not been pursued.

Formation of P_R, F and O_H

The major intermediate accumulating to 80-90% after 200-400 µs is **F** [28, 35, 36, 38], formed by rapid protonation of $\mathbf{P_R}$ (Figure 7 and Figure 8). While the optical spectra of $\mathbf{P_R}$ and **F** are indistinguishable in the Soret region (maximum at 430 nm due to Fe^{4+}=O of heme a_3), **F** absorbs at 571 nm in the low temperature UV-visible spectrum and $\mathbf{P_R}$ at 608 nm (606 nm in the absolute spectrum). We could monitor the shift in the α-band to 608 (606) nm (at 130 µs, Figures 1A and 1B) signifying $\mathbf{P_R}$ formation, and at slightly later times the formation of **F** at 571 nm. The decay of **F** was relatively slow (1-1.5 ms, Figure 1B) and was analyzed from the absorbance change at 571-580 nm (Figure 8). Except for the first 100-200 µs in which these wavelength pairs might contain significant contributions from **A** and $\mathbf{P_R}$ the time course of **F** is satisfactorily reproduced. The half-life for the $\mathbf{P_R}$ → **F** protonation is simulated as 27 µs, identical to the value in [38]. The value of 27 µs was, however, not determined directly from the time course of **F**, but was constrained to adequately fit the Cu_A/heme *a* and Trp* kinetics (Figures 5, 6, and 8). The decay rate of **F**, the **F** → $\mathbf{O_H}$ transition, can also be estimated from the oxidation of heme *a* in the α-band at 603 nm and in the Soret region at 444 nm (Figures 1A and 1B). Furthermore, the 430 nm maximum shifts with a similar rate ($t_{1/2}$ = 1.2 ms) yielding $\mathbf{O_H}$, characterized by the maximum at 427 nm after 3-6 ms (Figures 1A and 1B). Resonance Raman spectroscopy showed that in the **F** → $\mathbf{O_H}$ transition heme a_3 Fe^{4+}=O is reduced by heme *a*/Cu_A to Fe^{3+}-OH^- [36, 38]. The simultaneous oxidation of heme *a* and reduction of heme a_3 is very difficult to analyze by UV-visible spectroscopy. The rate of the **F** → $\mathbf{O_H}$ transition was calculated from the second oxidation phase ($t_{1/2}$ = 1.2 ms) of heme *a* and Cu_A and from the formation rate of the Trp-272* all three monitored by EPR spectroscopy (Figures 5, 6 and 8).

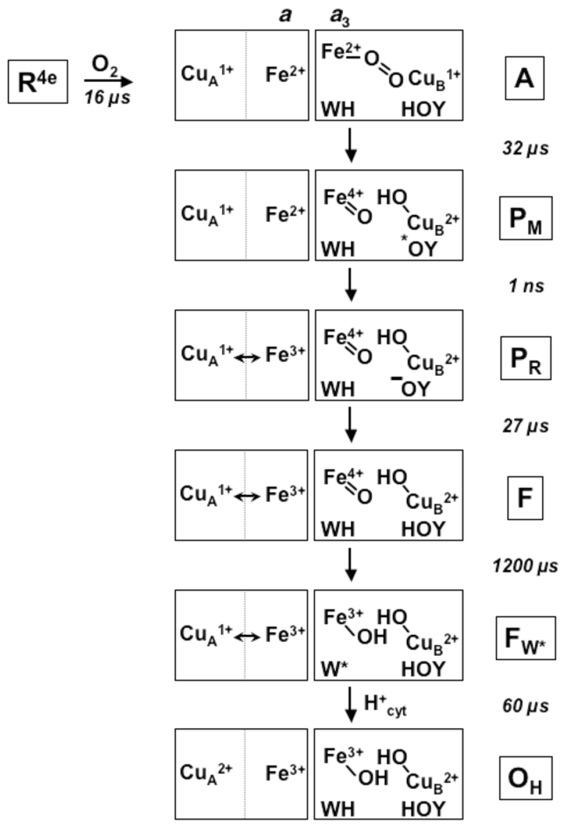

Figure 7 Reaction scheme of CcO showing the various intermediates with their half-lives. *WH*, denotes Trp-272; *W**, Trp-272*. Pumped and chemical protons are largely omitted from the scheme for reasons of clarity, except *"H^+_{cyt}"* for the $\mathbf{F_W}$* → $\mathbf{O_H}$ transition. Likewise, formation of the Trp-272$^-$ anion is not shown explicitly; the anion is formed in the $\mathbf{F_W}$* → $\mathbf{O_H}$ transition by electron transfer from Cu_A/heme *a* prior to protonation to Trp-272 by *"H^+_{cyt}"*. *"H^+_{cyt}"* signifies a proton originating from the cytoplasm that has traveled along one of the proton pathways. The direct proton donor to the Trp-272$^-$ anion might be *e.g.* Glu-278, a heme propionic acid residue, or an active site water molecule (see text for further details). *HOY*, **OY*, and *$^-$OY* refer to Tyr-280, its radical, and anion forms, respectively. Instead of Tyr-280, Trp-272 might be involved in the sequence $\mathbf{P_M}$ → **F** (see text). The half-lives shown in the scheme were derived as follows: **R** → **A**: calculated from Ref. [29] for 0.65 mM O_2. **A** → $\mathbf{P_M}$: imposed by simulation of the (initial phase of) Cu_A/heme *a* and Trp* radical kinetics and in agreement with previous studies [28, 38, 63, 64]. $\mathbf{P_M}$ → $\mathbf{P_R}$: taken from Ref. [43]. $\mathbf{P_R}$ → **F**: calculated from the simulation of the formation/decay of *F* (Figure 1B) and the Cu_A/heme *a* and Trp* radical kinetics. **F** → $\mathbf{F_W}$* and $\mathbf{F_W}$* → $\mathbf{O_H}$: calculated from the (second phase of) Cu_A/heme *a* oxidation and Trp-272* transient kinetics. The half-lives of 1200 µs and 60 µs model the Trp-272* transient kinetics and its accumulation to 4.2%. The half-life of 60 µs is due to electron transfer from Cu_A/heme *a* to the Trp-272*. See text for further explanation.

The majority of the high spin heme a_3 Fe^{3+}(-OH^-) was EPR silent under all conditions examined. Likewise the characteristic four-line EPR signal of Cu_B^{2+}-OH^- was not observed in any of the MHQ samples even though the experimental conditions were optimized for its detection. This specific Cu_B^{2+}-OH^- state has been observed in low-temperature kinetics ('triple-trapping experiments') of the bovine heart CcO and has been assigned to the $\mathbf{P_R}$ intermediate [42]. The Cu_B EPR signal is absent in **F** [70].

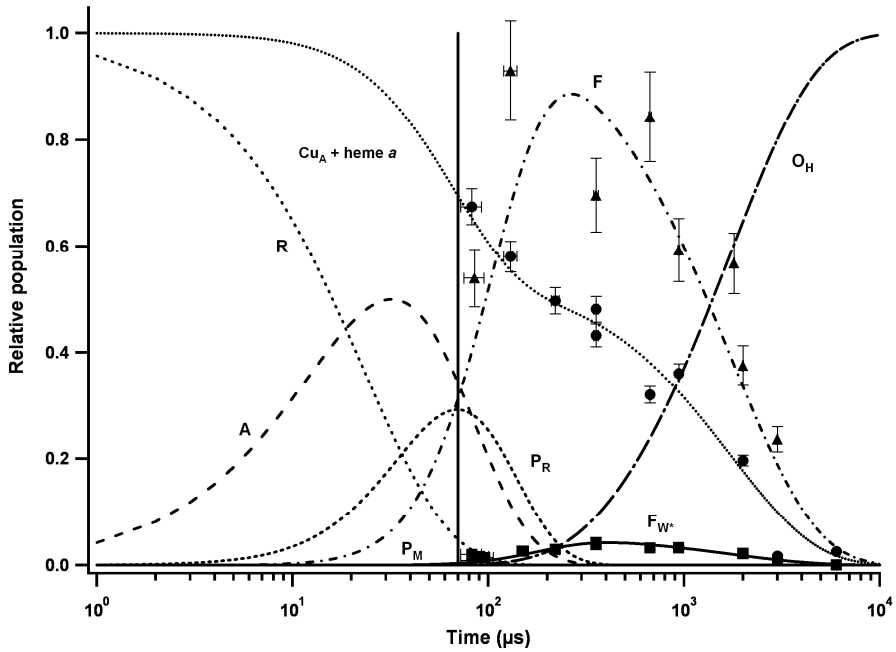

Figure 8 Simulated populations of the various intermediates formed in a single turnover of fully reduced cytochrome oxidase reacting with O_2. Simulations reflect a single set of half-lives based on the experimental data for the oxidation of Cu_A and heme *a*, **F** and the Trp-272* ($\mathbf{F_W}$*). Experimental data for formation of $\mathbf{O_H}$, which can be calculated directly from the relative populations of **F**, $\mathbf{F_W}$* and the redox state of Cu_A/heme *a* are omitted from the figure. The analytical solutions for the formation of the intermediates and the calculation of the redox state of Cu_A and heme *a* are given in the Supplemental Material. The calculated populations of **A**, which could not be resolved experimentally, and of $\mathbf{P_R}$, which was observed (Figure 1B), were calculated as indicated in the legend to Figure 7, and are in excellent agreement with [28, 38, 63, 64]. Note that the intermediate $\mathbf{P_M}$ does not accumulate, due to its rapid (1 ns) conversion to $\mathbf{P_R}$. The *vertical line* represents the MHQ dead time (60-80 µs), positioned at 70 µs. The *symbols* are experimentally determined values. *Squares*, Trp-272* (and $\mathbf{F_W}$*); c*ircles*, Cu_A plus heme *a; triangles*, **F**. **F** was measured at 571 nm (*cf.* Figure 1B).

The four-line EPR spectrum was suggested to disappear due to e.g. protonation of Cu_B^{2+}-OH^- or of another base close to the binuclear center, which would slightly change the magnetic interaction with Fe^{4+}=O to a value rendering Cu_B^{2+} EPR invisible [42]. Thus although our UV-visible spectra indicate formation of $\mathbf{P_R}$, our EPR data do not seem to support this. A possible explanation might be that the magnetic interaction in the *P. denitrificans* CcO differs from the bovine heart enzyme yielding an EPR silent Cu_B^{2+} in $\mathbf{P_R}$. We consider it, however, more likely that the protonation of Cu_B (and other) equilibria are somewhat different at the low temperatures employed in the triple-trapping method [40, 42, 70] compared to 10 °C in our experiments. This could lead to accumulation of different intermediates and rendering Cu_B^{2+} EPR silent. Such a shift in equilibria might also explain why the Trp-272* has not been observed in the triple-trapping experiments [40, 42, 70].

Heme a and Cu_A kinetics and equilibrium

The biphasic oxidation kinetics of heme *a* and Cu_A determined by EPR (Figure 6) display an initial phase completed within ~130/200 µs, (*apparent* $t_{1/2}$ = 55 µs) while the decay half-life of the second phase equals 1.2 ms. This biphasic time course and the half-lives are in perfect agreement with the kinetics of the two electrogenic events of the *P. denitrificans* CcO [63, 64]. In each oxidation phase a *single* electron from the heme *a*/Cu_A redox pair is donated to the binuclear centre (Figures 6 and 8).

Heme *a* oxidation proceeds on the nanosecond time scale [43] in the $\mathbf{P_M} \rightarrow \mathbf{P_R}$ transition (Figure 7), but the apparent $t_{1/2}$ for Cu_A and heme *a* are 50 µs and 65 µs, respectively (Figure 6, insert). These latter *apparent* half-lives are upper limits with respect to the true $Cu_A \Leftrightarrow$ heme *a* electron transfer rates because the preceding formation of $\mathbf{R} \rightarrow \mathbf{P_M}$ takes ~ 30-50 µs both for the bovine heart CcO [28, 35, 36, 38] and the *P. denitrificans* enzyme [63, 64]. The half-life for $Cu_A \rightarrow$ heme *a* electron transfer has been determined at $t_{1/2}$ = 24 and 35 µs for the *R. sphaeroides* and *P. denitrificans* CcO's, respectively [69, 71]. The actual freezing time of the MHQ is 30-40 µs and since the heme *a* → heme a_3 electron transfer rate is in the nanoseconds, the finding of similar degrees of reduction for Cu_A and heme *a* strongly suggests that they are in electronic equilibrium at all measured reaction times (Figure 3). The calculated equilibrium constant, indicates a 4.5 mV lower midpoint potential for Cu_A relative to heme *a* in good agreement with [69].

The lower reduction potential of Cu_A leads to a slightly faster apparent oxidation of Cu_A relative to heme *a*. In contrast, in the bovine heart CcO the oxidation of heme *a* is apparently faster than of Cu_A [38].

The second oxidation phase of Cu_A /heme *a* is slow ($t_{1/2}$ = 1.2 ms) and gated by the slow **F** → $\mathbf{F_W}$* reaction (Figure 7). The reduction of Trp-272* occurs with $t_{1/2}$ = 60 µs (Figures 5 and 7) by electron transfer from Cu_A/heme *a*. The value of 60 µs represents most likely electron transfer from Cu_A to heme *a*. So the rates of Cu_A ⇔ heme *a* electron transfer are actually very similar in the two oxidation phases, $t_{1/2}$ = ~ 30 µs in the first phase and 60 µs in the second. Both rates are similar to measured [69, 71] and calculated [72] electron transfer rates for Cu_A to heme *a*. The approximate twofold difference of $t_{1/2}$ in the two phases might reflect small differences in the effective reduction potentials and reorganization energies (totaling ~20 mV) for each oxidation phase.

The identification of the Trp* as Trp-272*

EPR spectroscopy reveals two different radicals (Figures 2-5). The origin of the 6-ms radical could not be established. Likewise, its functional assignment is difficult even though it is being formed on the time scale of turnover. The kinetics of the 6-ms radical, which accumulates to 0.5% of the CcO, could not be accurately established due to spectral overlap with the TRP-272*. However, the observation that two radicals are formed on the time scale of turnover indicates rapid radical migration within CcO [60, 62].

The Q-band spectrum of the radical formed maximally after 300-500 µs can be firmly assigned as a Trp*. The EPR and electron nuclear double resonance properties of Trp radicals are well understood. All Trp radicals have similar hyperfine constants for the indole ring protons (H5 and H7) and the indole nitrogen, and show similar small *g*-anisotropies [60, 62]. The major differences in Trp* EPR spectra are caused by variations in the angles of the two β-methylene protons ($H\beta_1$ and $H\beta_2$) with respect to the indole ring, which strongly affects their hyperfine values [62]. The relation between the ratio of the hyperfine values of the two β-methylene protons and the angles can be calculated with the McConnnel relation and thus permits assignment of the Trp* residue in case the crystal structure is known [62]. Furthermore, EPR can distinguish between a neutral Trp* and a protonated Trp*.

The hyperfine constants for the indole ring protons and nitrogen used for the Trp* simulation (Figure 4, Table 1) are very similar to those of other Trp* [62]. The best fitting values for the two β-methylene protons (25 and 7.5 Gauss) correspond to angles of 3.1° and 123.1° (calculated from the ratio $H\beta_1/H\beta_2$) characterizing the radical as that from Trp-272 (Table 1). However, given the signal to noise level in the Q-band spectrum (Figure 4), which required averaging of 85 spectra because the absolute Trp* concentration was only 1.4 μM, we need to discuss possible other Trp residues as the origin of the Trp*. In particular, simulated EPR spectra in which the ratio $H\beta_2/H\beta_1$ would be close to zero (Trp-358 and Trp-431, Table 1) are not entirely inconsistent with the experimental spectrum (see Figure S3). Our observation that the Trp* is also formed in the *E. coli* cytochrome bo_3 [5, 46], implies that it concerns a Trp residue conserved in the *P. denitrificans* and *E. coli* oxidases. There are 12 Trp residues in subunit I conserved between these two enzymes. Table 1 lists nine Trp residues conserved in the Type A1 oxidases, their distances to the metal sites and their predicted ratios of the β-methylene proton hyperfine constants. The highly conserved Trp-164 was ruled out because the radical was found to be present in W164F and W164T mutants (data not shown). Trp-323, although close enough to heme a_3 (and Cu_B) was ruled out on basis of its predicted EPR spectrum, which would show a strong central line (*cf.* Figure S3), in contrast to experimental observation. Residues Trp-22, Trp-136, Trp-431 and Trp-532 are judged too far from any of the metal centers to produce the magnetic coupling dominating the X-band EPR spectral features. In terms of its predicted EPR spectrum (Figure S3) and the 15- to 16-Å distance to heme a_3, which might lead to a weak magnetic coupling, Trp-358 is the only other serious candidate apart from Trp-272. However, Trp-358 is a phenylalanine residue in the *Aeropyrum pernix* oxidase and is not conserved in Type A2, Type B, and Type C oxidases [7]. We ascribe the observed radical to the Trp-272*, Because 1) the Q-band EPR spectrum is optimally simulated as a Trp-272*, 2) Trp-272 is close to all three metal centers in subunit I and 3) Trp-272 is strictly conserved in all cytochrome oxidases. The Q-band EPR spectrum could not be simulated as a protonated Trp-272* [73] and we therefore conclude that the species represents the neutral Trp-272*. A weak H-bond interaction of the indole-N with another residue can, however, not be ruled out. In fact the phenol-OH of Tyr-167 and the indole-N of Trp-272 are within H-bonding distance [3, 8].

In contrast to the Q-band spectrum, the four line X-band EPR spectrum of Trp-272* (Figure 4) cannot be simulated. With respect to our previous analysis [46] we know now, on basis of the Q-band spectrum, that this spectrum does not contain contributions from a Tyr* as suggested at the time, though it does contain a small contribution from the 6-ms radical (Figures 3 and 4). The rapid relaxation of the Trp* [46] and the increased resolution at Q-band indicate that the Trp-272* is weakly magnetically coupled as proposed earlier. Simulation of the X-band EPR spectrum would require a full diagonalization of the spin Hamiltonian matrix because the various magnetic interactions including the Zeeman interaction are in the same order of magnitude. This most complicated EPR-simulation scenario is outside the scope of this paper.

The function of the Trp-272* in the catalytic cycle.

Our current view on the catalytic cycle of cytochrome oxidases is depicted in Figure 7. The half-lives of the various intermediates indicated were used for simulation of Cu_A/heme *a* and Trp-272* kinetics (Figures 5, 6, 8) with values for $\mathbf{R} \rightarrow \mathbf{P_M}/\mathbf{P_R}$ taken from the literature.

Maximal Trp-272* formation occurs after 300-500 µs, to an extent of 4-5% of the oxidase. This low extent is due to an approximately 20-fold lower rate of formation ($t_{1/2}$ = 1.2 ms) than rate of breakdown (60 µs). The low formation rate may seem to preclude a direct role of Trp-272 as electron donor in the O=O bond splitting reaction ($\mathbf{A} \rightarrow \mathbf{P_M}$) as suggested recently [44]. However, any radical formed in this reaction (Tyr-280* or Trp-272*) would most likely accumulate to undetectable levels (like $\mathbf{P_M}$, Figure 8) given the ~1-ns rate of electron transfer from heme *a* to heme a_3. Thus while Trp-272 might nevertheless play a role in the O=O bond breaking (*cf.* [44]), our data suggest another role in the catalytic cycle.

The intermediate **F** accumulates to ~88% of the CcO concentration (Figure 8 and [38]) because it is formed with an apparent $t_{1/2}$ ~ 100 µs and decays in 1.2 ms, approximately the opposite of the kinetic parameters calculated for Trp-272*. Unless the quantitation of the X-band EPR spectrum of Trp-272* is off by a factor of 20, the accumulation of Trp-272* to 4-5% implies that Trp-272* is not present in **F** (Figure 8) and, in addition, that it is formed later than **F**. We therefore propose the new sequence $\mathbf{F} \rightarrow \mathbf{F_W}^* \rightarrow \mathbf{O_H}$ (Figure 7). The simulation of the kinetics allows for ~88% accumulation of **F** and ~4% of $\mathbf{F_W}^*$ (Figure 8). The low accumulation of $\mathbf{F_W}^*$ might explain why it has not been detected hitherto by UV-visible or

resonance Raman spectroscopy, even though several authors have proposed additional intermediates in the **F** → $\mathbf{O_H}$ reaction sequence [28, 51, 74, 75].

Formation of the neutral Trp-272* with $t_{1/2}$ = 1.2 ms represents the major rate determining step in the CcO catalytic cycle. The Trp-272* is obtained according to Reaction 2.

$$\text{Trp-272} \rightarrow \text{Trp-272*} + e + H^+ \qquad (2)$$

Which are the electron and proton acceptors for Trp-272? Potential electron acceptors are heme a_3 Fe^{4+}=O and Cu_B^{2+}-OH^-. Regarding Cu_B, its reduction to Cu_B^{1+}-OH_2 would explain its EPR silence. In the next step, Cu_B^{1+} would reduce Fe^{4+}=O while Trp-272* is re-reduced to Trp-272 by the electron residing in the Cu_A/heme *a* redox pair. This sequence of events would explain why heme a_3 and Cu_B are EPR silent in $\mathbf{F_W}$* and $\mathbf{O_H}$. In the alternative route (shown in Figure 7) Trp-272 is suggested as the direct reductant to heme a_3 Fe^{4+}=O yielding Fe^{3+}-OH^-. The Trp-272* is subsequently re-reduced to Trp-272 by electron transfer from Cu_A/heme *a*. In both scenarios, the metal ions can accept the proton (equation 2) upon their reduction. Our data and those availing in the literature do not appear to distinguish between these two alternatives in part due to the spectroscopic silence of Cu_B. However, resonance Raman spectroscopy indicates the formation of Fe^{3+}-OH^- prior to Fe^{3+}[38]. According to the literature, the electron donors Cu_A/heme *a* reduce heme a_3 Fe^{4+}=O to Fe^{3+}-OH^-. The source of the proton in this reaction remains unknown. In Figure 7, Trp-272 is indicated to act as the electroneutral reductant to Fe^{4+}=O. *However*, instead of Trp-272 the conserved Glu-278 might be the direct proton donor in the reduction (by Trp-272) of Fe^{4+}=O to Fe^{3+}-OH^- (in **F** → $\mathbf{F_W}$*), while the proton from Trp-272 (Reaction 2) is expelled to the periplasm, according to Reaction 3.

$$\text{Trp-272} + \text{Glu-278-COOH} + Fe^{4+}{=}O \rightarrow$$
$$\text{Trp-272*} + H^+_{peri} + \text{Glu-278-COO}^- + Fe^{3+}\text{-}OH^- \qquad (3)$$

Reprotonation of Glu-278$^-$ occurs via the D-pathway by proton uptake form the cytoplasm.The short distance of Trp-272 to Cu_B or heme a_3 (Table 1) would in any case ensure submillisecond to millisecond electron transfer rates even when the reduction potentials of the redox partners differ by 0.4 V [72]. The 1.2-ms rate of Reaction 2 thus suggests a reduction potential of 0.7-0.8 V for Trp-272, a value lower than the ~0.9 V and ~1.1 V

for free Trp in solution (pH 7) or buried, respectively [76], but adequate to play a role in O=O bond breaking and as reductant to heme a_3 or Cu_B.

In the reverse of Reaction 2 the strong base Trp-272$^-$ (pK_A> 15 cf. [76]) is formed initially by electron transfer from Cu_A/heme *a*. The Trp-272$^-$ anion might subsequently be rapidly protonated to Trp-272 by a proton *en route* from the cytoplasm to the periplasm, thus providing directionality to proton translocation (in **F** → $\mathbf{O_H}$). The conserved Glu-278 might serve as the direct proton donor to the Trp-272$^-$ anion according to Reaction 4.

$$\text{Trp-272}^- + \text{Glu-278-COOH} \rightarrow \text{Trp-272} + \text{Glu-278-COO} \qquad (4)$$

The Reactions 3 and 4, combined, describe (part of) a proton-relay network in which protons are translocated from the cytoplasm to the periplasm thermodynamically driven by the oxido-reduction of Trp-272 and the strong basicity of the Trp-272$^-$-anion.

Electrometric and proton translocation measurements have provided ample evidence for proton pumping in the **F** → $\mathbf{O_H}$ transition [9, 12, 39, 58, 63], which we here propose to occur actually in the $\mathbf{F_W}$* → $\mathbf{O_H}$ transition involving Trp-272. For the $\mathbf{P_R}$ → **F** transition a proton acceptor was suggested to be located close to or at the heme a_3 propionates, but not at the heme a_3-Cu_B binuclear center [9, 12, 39, 58, 63]. The Trp-272$^-$ anion fits both the proton acceptor properties and the proposed location.

In view of our findings, the concept of cytochrome oxidase as a redox-linked proton pump [9, 63] might thus be extended. While the various metal centers are engaged in oxidation-reduction linked deprotonation-protonation reactions, specific aromatic residues like the strictly conserved Trp-272 (and possibly Tyr-280) also change their redox- and protonation states during the catalytic cycle and are likewise involved in proton binding, proton release and proton translocation. In contrast to the metal ions of the binuclear center, the aromatic residues are not directly involved in the binding (and activation) of O_2. According to the model presented here, formation of the Trp-272$^-$ anion provides the driving force for proton binding and even translocation in the $\mathbf{F_W}$* → $\mathbf{O_H}$ transition, and thus constitutes an integral part of a proton-relay network in the cytochrome oxidases. Whether a similar mechanism applies to the $\mathbf{P_R}$ → **F** transition and to the two proton pumping events in the reductive part of the catalytic cycle and whether it would involve Trp-272 as well, is subject to future experimentation.

Acknowledgements

The authors wish to thank Werner Müller (Frankfurt) for enzyme preparation, Ing. Marc J.F. Strampraad (Delft) and Bsc. A. Paulus (Delft) for help with the kinetic experiments. We further acknowledge the constructive comments of one of the reviewers. This research was financed by the Foundation for Fundamental Research on Matter (FOM grant D-26) and the Deutsche Forschungsgemeinschaft (SFB 472).

[1)]Abbreviations

MHQ: Microsecond freeze-hyperquenching. CcO: Cytochrome *c* oxidase. Trp*: Tryptophan radical. TRP-272*: the neutral radical of TRP-272. EPR: Electron Paramagnetic Resonance. ENDOR: Electron Nuclear Double Resonance. PES: Phenazine ethosulfate. Residue numbering refers to the *P. denitrificans* aa_3 cytochrome *c* oxidase sequence.

REFERENCES

1. Wasser, I. M.; de Vries, S.; Moënne-Loccoz, P.; Schröder, I.; Karlin, K. D., Nitric oxide in biological denitrification: Fe/Cu metalloenzyme and metal complex NO(x) redox chemistry. *Chem Rev* **2002,** 102, (4), 1201-34.
2. Richter, O. M.; Ludwig, B., Cytochrome c oxidase--structure, function, and physiology of a redox-driven molecular machine. *Rev Physiol Biochem Pharmacol* **2003,** 147, 47-74.
3. Michel, H.; Behr, J.; Harrenga, A.; Kannt, A., Cytochrome c oxidase: structure and spectroscopy. *Annu Rev Biophys Biomol Struct* **1998,** 27, 329-56.
4. Hendriks, J.; Oubrie, A.; Castresana, J.; Urbani, A.; Gemeinhardt, S.; Saraste, M., Nitric oxide reductases in bacteria. *Biochim Biophys Acta* **2000,** 1459, (2-3), 266-73.
5. Cherepanov, A. V.; De Vries, S., Microsecond freeze-hyperquenching: development of a new ultrafast micro-mixing and sampling technology and application to enzyme catalysis. *Biochim Biophys Acta* **2004,** 1656, (1), 1-31.
6. Babcock, G. T.; Wikstrom, M., Oxygen Activation and the Conservation of Energy in Cell Respiration. *Nature* **1992,** 356, (6367), 301-309.
7. Pereira, M. M.; Santana, M.; Teixeira, M., A novel scenario for the evolution of haem-copper oxygen reductases. *Biochim Biophys Acta* **2001,** 1505, (2-3), 185-208.
8. Ostermeier, C.; Harrenga, A.; Ermler, U.; Michel, H., Structure at 2.7 A resolution of the Paracoccus denitrificans two-subunit cytochrome c oxidase complexed with an antibody FV fragment. *Proc Natl Acad Sci U S A* **1997,** 94, (20), 10547-53.
9. Wikstrom, M., Cytochrome c oxidase: 25 years of the elusive proton pump. *Biochim Biophys Acta* **2004,** 1655, (1-3), 241-7.

10. Verkhovsky, M. I.; Belevich, I.; Bloch, D. A.; Wikstrom, M., Elementary steps of proton translocation in the catalytic cycle of cytochrome oxidase. *Biochim Biophys Acta* **2006,** 1757, (5-6), 401-7.
11. Ruitenberg, M.; Kannt, A.; Bamberg, E.; Fendler, K.; Michel, H., Reduction of cytochrome c oxidase by a second electron leads to proton translocation. *Nature* **2002,** 417, (6884), 99-102.
12. Faxen, K.; Gilderson, G.; Adelroth, P.; Brzezinski, P., A mechanistic principle for proton pumping by cytochrome c oxidase. *Nature* **2005,** 437, (7056), 286-289.
13. Belevich, I.; Verkhovsky, M. I.; Wikstrom, M., Proton-coupled electron transfer drives the proton pump of cytochrome c oxidase. *Nature* **2006,** 440, (7085), 829-32.
14. Iwata, S.; Ostermeier, C.; Ludwig, B.; Michel, H., Structure at 2.8 A resolution of cytochrome c oxidase from Paracoccus denitrificans. *Nature* **1995,** 376, (6542), 660-9.
15. Tsukihara, T.; Aoyama, H.; Yamashita, E.; Tomizaki, T.; Yamaguchi, H.; Shinzawa-Itoh, K.; Nakashima, R.; Yaono, R.; Yoshikawa, S., Structures of metal sites of oxidized bovine heart cytochrome c oxidase at 2.8 A. *Science* **1995,** 269, (5227), 1069-74.
16. Svensson-Ek, M.; Abramson, J.; Larsson, G.; Tornroth, S.; Brzezinski, P.; Iwata, S., The X-ray crystal structures of wild-type and EQ(I-286) mutant cytochrome c oxidases from Rhodobacter sphaeroides. *J Mol Biol* **2002,** 321, (2), 329-39.
17. Yoshikawa, S.; Muramoto, K.; Shinzawa-Itoh, K.; Aoyama, H.; Tsukihara, T.; Ogura, T.; Shimokata, K.; Katayama, Y.; Shimada, H., Reaction mechanism of bovine heart cytochrome c oxidase. *Biochim Biophys Acta* **2006,** 1757, (5-6), 395-400.
18. Yoshikawa, S.; Muramoto, K.; Shinzawa-Itoh, K.; Aoyama, H.; Tsukihara, T.; Shimokata, K.; Katayama, Y.; Shimada, H., Proton pumping mechanism of bovine heart cytochrome c oxidase. *Biochim Biophys Acta* **2006,** 1757, (9-10), 1110-6.
19. Witt, H.; Malatesta, F.; Nicoletti, F.; Brunori, M.; Ludwig, B., Tryptophan 121 of subunit II is the electron entry site to cytochrome-c oxidase in Paracoccus denitrificans. Involvement of a hydrophobic patch in the docking reaction. *J Biol Chem* **1998,** 273, (9), 5132-6.
20. Drosou, V.; Malatesta, F.; Ludwig, B., Mutations in the docking site for cytochrome c on the Paracoccus heme aa3 oxidase. Electron entry and kinetic phases of the reaction. *Eur J Biochem* **2002,** 269, (12), 2980-8.
21. Blackburn, N. J.; Barr, M. E.; Woodruff, W. H.; van der Oost, J.; de Vries, S., Metal-metal bonding in biology: EXAFS evidence for a 2.5 A copper-copper bond in the CuA center of cytochrome oxidase. *Biochemistry* **1994,** 33, (34), 10401-7.
22. Brzezinski, P., Redox-driven membrane-bound proton pumps. *Trends in Biochemical Sciences* **2004,** 29, (7), 380-387.
23. Adelroth, P.; Ek, M. S.; Mitchell, D. M.; Gennis, R. B.; Brzezinski, P., Glutamate 286 in cytochrome aa(3) from Rhodobacter sphaeroides is involved in proton uptake during the reaction of the fully-reduced enzyme with dioxygen. *Biochemistry* **1997,** 36, (45), 13824-13829.

24. Schmidt, B.; McCracken, J.; Ferguson-Miller, S., A discrete water exit pathway in the membrane protein cytochrome c oxidase. *Proc Natl Acad Sci U S A* **2003,** 100, (26), 15539-42.
25. Schmidt, B.; Hillier, W.; McCracken, J.; Ferguson-Miller, S., The use of stable isotopes and spectroscopy to investigate the energy transducing function of cytochrome c oxidase. *Biochim Biophys Acta* **2004,** 1655, (1-3), 248-55.
26. Florens, L.; Schmidt, B.; McCracken, J.; Ferguson-Miller, S., Fast deuterium access to the buried magnesium/manganese site in cytochrome c oxidase. *Biochemistry* **2001,** 40, (25), 7491-7.
27. Espe, M. P.; Hosler, J. P.; Ferguson-Miller, S.; Babcock, G. T.; McCracken, J., A continuous wave and pulsed EPR characterization of the Mn2+ binding site in Rhodobacter sphaeroides cytochrome c oxidase. *Biochemistry* **1995,** 34, (23), 7593-602.
28. Szundi, I.; Cappuccio, J.; Einarsdottir, O., Amplitude analysis of single-wavelength time-dependent absorption data does not support the conventional sequential mechanism for the reduction of dioxygen to water catalyzed by bovine heart cytochrome c oxidase. *Biochemistry* **2004,** 43, (50), 15746-58.
29. Sucheta, A.; Szundi, I.; Einarsdottir, O., Intermediates in the reaction of fully reduced cytochrome c oxidase with dioxygen. *Biochemistry* **1998,** 37, (51), 17905-17914.
30. Sucheta, A.; Georgiadis, K. E.; Einarsdottir, O., Mechanism of cytochrome c oxidase-catalyzed reduction of dioxygen to water: Evidence for peroxy and ferryl intermediates at room temperature. *Biochemistry* **1997,** 36, (3), 554-565.
31. Einarsdottir, O.; Szundi, I., Time-resolved optical absorption studies of cytochrome oxidase dynamics. *Biochim Biophys Acta* **2004,** 1655, (1-3), 263-73.
32. Varotsis, C.; Zhang, Y.; Appelman, E. H.; Babcock, G. T., Resolution of the reaction sequence during the reduction of O2 by cytochrome oxidase. *Proc Natl Acad Sci U S A* **1993,** 90, (1), 237-41.
33. Proshlyakov, D. A.; Pressler, M. A.; Babcock, G. T., Dioxygen activation and bond cleavage by mixed-valence cytochrome c oxidase. *Proc Natl Acad Sci U S A* **1998,** 95, (14), 8020-5.
34. Proshlyakov, D. A.; Ogura, T.; Shinzawa-Itoh, K.; Yoshikawa, S.; Appelman, E. H.; Kitagawa, T., Selective resonance Raman observation of the "607 nm" form generated in the reaction of oxidized cytochrome c oxidase with hydrogen peroxide. *J Biol Chem* **1994,** 269, (47), 29385-8.
35. Ogura, T.; Kitagawa, T., Resonance Raman characterization of the P intermediate in the reaction of bovine cytochrome c oxidase. *Biochim Biophys Acta* **2004,** 1655, (1-3), 290-7.
36. Kitagawa, T., Structures of reaction intermediates of bovine cytochrome c oxidase probed by time-resolved vibrational spectroscopy. *J Inorg Biochem* **2000,** 82, (1-4), 9-18.
37. Han, S. W.; Ching, Y. C.; Rousseau, D. L., Primary intermediate in the reaction of oxygen with fully reduced cytochrome c oxidase. *Proc Natl Acad Sci U S A* **1990,** 87, (7), 2491-5.
38. Han, S.; Takahashi, S.; Rousseau, D. L., Time dependence of the catalytic intermediates in cytochrome c oxidase. *J Biol Chem* **2000,** 275, (3), 1910-9.

39. Siletsky, S. A.; Han, D.; Brand, S.; Morgan, J. E.; Fabian, M.; Geren, L.; Millett, F.; Durham, B.; Konstantinov, A. A.; Gennis, R. B., Single-electron photoreduction of the P-M intermediate of cytochrome c oxidase. *Biochimica Et Biophysica Acta-Bioenergetics* **2006,** 1757, (9-10), 1122-1132.
40. Hansson, O.; Karlsson, B.; Aasa, R.; Vanngard, T.; Malmstrom, B. G., The structure of the paramagnetic oxygen intermediate in the cytochrome c oxidase reaction. *Embo J* **1982,** 1, (11), 1295-7.
41. Proshlyakov, D. A.; Pressler, M. A.; DeMaso, C.; Leykam, J. F.; DeWitt, D. L.; Babcock, G. T., Oxygen activation and reduction in respiration: involvement of redox-active tyrosine 244. *Science* **2000,** 290, (5496), 1588-91.
42. Morgan, J. E.; Verkhovsky, M. I.; Palmer, G.; Wikstrom, M., Role of the PR intermediate in the reaction of cytochrome c oxidase with O2. *Biochemistry* **2001,** 40, (23), 6882-92.
43. Pilet, E.; Jasaitis, A.; Liebl, U.; Vos, M. H., Electron transfer between hemes in mammalian cytochrome c oxidase. *Proceedings of the National Academy of Sciences of the United States of America* **2004,** 101, (46), 16198-16203.
44. MacMillan, F.; Budiman, K.; Angerer, H.; Michel, H., The role of tryptophan 272 in the Paracoccus denitrificans cytochrome c oxidase. *FEBS Lett* **2006,** 580, (5), 1345-9.
45. Bloch, D.; Belevich, I.; Jasaitis, A.; Ribacka, C.; Puustinen, A.; Verkhovsky, M. I.; Wikstrom, M., The catalytic cycle of cytochrome c oxidase is not the sum of its two halves. *Proc Natl Acad Sci U S A* **2004,** 101, (2), 529-33.
46. Wiertz, F. G. M.; Richter, O. M.; Cherepanov, A. V.; MacMillan, F.; Ludwig, B.; de Vries, S., An oxo-ferryl tryptophan radical catalytic intermediate in cytochrome c and quinol oxidases trapped by microsecond freeze-hyperquenching (MHQ). *FEBS Lett* **2004,** 575, (1-3), 127-30.
47. Lu, S.; Wiertz, F. G. M.; de Vries, S.; Moenne-Loccoz, P., Resonance Raman characterization of a high-spin six-coordinate iron(III) intermediate in metmyoglobin-azido complex formation trapped by microsecond freeze-hyperquenching (MHQ). *J Raman Spectrosc* **2005,** 36, (4), 359-362.
48. Wiertz, F. G. M.; de Vries, S., Low-temperature kinetic measurements of microsecond freeze-hyperquench (MHQ) cytochrome oxidase monitored by UV-visible spectroscopy with a newly designed cuvette. *Biochemical Society Transactions* **2006,** 34, 136-138.
49. Ballou, D. P., Freeze-quench and chemical-quench techniques. *Methods Enzymol* **1978,** 54, 85-93.
50. Rigby, S. E.; Junemann, S.; Rich, P. R.; Heathcote, P., Reaction of bovine cytochrome c oxidase with hydrogen peroxide produces a tryptophan cation radical and a porphyrin cation radical. *Biochemistry* **2000,** 39, (20), 5921-8.
51. Rich, P. R.; Rigby, S. E.; Heathcote, P., Radicals associated with the catalytic intermediates of bovine cytochrome c oxidase. *Biochim Biophys Acta* **2002,** 1554, (3), 137-46.
52. Fabian, M.; Palmer, G., The interaction of cytochrome oxidase with hydrogen peroxide: the relationship of compounds P and F. *Biochemistry* **1995,** 34, (42), 13802-10.

53. Ludwig, B., Cytochrome c oxidase from Paracoccus denitrificans. *Methods Enzymol* **1986,** 126, 153-9.
54. Hendler, R. W.; Pardhasaradhi, K.; Reynafarje, B.; Ludwig, B., Comparison of energy-transducing capabilities of the two- and three-subunit cytochromes aa3 from Paracoccus denitrificans and the 13-subunit beef heart enzyme. *Biophys J* **1991,** 60, (2), 415-23.
55. Küss, H.; MacMillan, F.; Ludwig, B.; Prisner, T. F., Investigation of the Mn Binding Site in Cytochrome c Oxidase from Paracoccus denitrificans by High-Frequency EPR. *J. Phys. Chem. B* **2000,** 104, 5362-5371.
56. Budiman, K.; Kannt, A.; Lyubenova, S.; Richter, O. M.; Ludwig, B.; Michel, H.; MacMillan, F., Tyrosine 167: the origin of the radical species observed in the reaction of cytochrome c oxidase with hydrogen peroxide in Paracoccus denitrificans. *Biochemistry* **2004,** 43, (37), 11709-16.
57. von Wachenfeldt, C.; de Vries, S.; van der Oost, J., The CuAsite of the caa3-type oxidase of Bacillus subtilis is a mixed- valence binuclear copper centre. *FEBS Lett* **1994,** 340, (1-2), 109-13.
58. Salomonsson, L.; Faxen, K.; Adelroth, P.; Brzezinski, P., The timing of proton migration in membrane constituted cytochrome c oxidase. *Proceedings of the National Academy of Sciences of the United States of America* **2005,** 102, (49), 17624-17629.
59. Nyquist, R. M.; Heitbrink, D.; Bolwien, C.; Gennis, R. B.; Heberle, J., Direct observation of protonation reactions during the catalytic cycle of cytochrome c oxidase. *Proc Natl Acad Sci U S A* **2003,** 100, (15), 8715-20.
60. Pogni, R.; Baratto, M. C.; Teutloff, C.; Giansanti, S.; Ruiz-Duenas, F. J.; Choinowski, T.; Piontek, K.; Martinez, A. T.; Lendzian, F.; Basosi, R., A tryptophan neutral radical in the oxidized state of versatile peroxidase from Pleurotus eryngii: a combined multifrequency EPR and density functional theory study. *J Biol Chem* **2006,** 281, (14), 9517-26.
61. Lendzian, F.; Sahlin, M.; MacMillan, F.; Bittl, R.; Fiege, R.; Potsch, S.; Sjoberg, B.-M.; Graslund, A.; Lubitz, W.; Lassmann, G., Electronic Structure of Neutral Tryptophan Radicals in Ribonucleotide Reductase Studied by EPR and ENDOR Spectroscopy. *J Am Chem Soc* **1996,** 118, 8111-8120.
62. Bleifuss, G.; Kolberg, M.; Potsch, S.; Hofbauer, W.; Bittl, R.; Lubitz, W.; Graslund, A.; Lassmann, G.; Lendzian, F., Tryptophan and tyrosine radicals in ribonucleotide reductase: a comparative high-field EPR study at 94 GHz. *Biochemistry* **2001,** 40, (50), 15362-8.
63. Wikstrom, M.; Verkhovsky, M. I., Towards the mechanism of proton pumping by the haem-copper oxidases. *Biochim Biophys Acta* **2006,** 1757, (8), 1047-51.
64. Ribacka, C.; Verkhovsky, M. I.; Belevich, I.; Bloch, D. A.; Puustinen, A.; Wikstrom, M., An elementary reaction step of the proton pump is revealed by mutation of tryptophan-164 to phenylalanine in cytochrome c oxidase from Paracoccus denitrificans. *Biochemistry* **2005,** 44, (50), 16502-12.
65. Svistunenko, D. A.; Wilson, M. T.; Cooper, C. E., Tryptophan or tyrosine? On the nature of the amino acid radical formed following hydrogen peroxide treatment of cytochrome c oxidase. *Biochim Biophys Acta* **2004,** 1655, (1-3), 372-80.

66. Ivancich, A.; Jakopitsch, C.; Auer, M.; Un, S.; Obinger, C., Protein-based radicals in the catalase-peroxidase of synechocystis PCC6803: a multifrequency EPR investigation of wild-type and variants on the environment of the heme active site. *J Am Chem Soc* **2003,** 125, (46), 14093-102.
67. Ivancich, A.; Dorlet, P.; Goodin, D. B.; Un, S., Multifrequency high-field EPR study of the tryptophanyl and tyrosyl radical intermediates in wild-type and the W191G mutant of cytochrome c peroxidase. *J Am Chem Soc* **2001,** 123, (21), 5050-8.
68. Fersht, A., *Structure and Mechanism in Protein Science. A Guide to Enzyme Catalysis and Protein Folding*. W.H. Freeman and Company: NY, 1999; p 631.
69. Farver, O.; Grell, E.; Ludwig, B.; Michel, H.; Pecht, I., Rates and Equilibrium of CuA to heme a electron transfer in Paracoccus denitrificans cytochrome c oxidase. *Biophys J* **2006,** 90, (6), 2131-7.
70. Blair, D. F.; Witt, S. N.; Chan, S. I., Mechanism of Cytochrome Oxidase-Catalyzed Dioxygen Reduction at Low Temperatures. Evidence for Two Intermdiates at the Three-Electron Level and Entropic Promotion of the Bond-Breaking Step. *J Am Chem Soc* **1985,** 107, 7389-7399.
71. Adelroth, P.; Brzezinski, P.; Malmstrom, B. G., Internal Electron-Transfer in Cytochrome-C-Oxidase from Rhodobacter-Sphaeroides. *Biochemistry* **1995,** 34, (9), 2844-2849.
72. Moser, C. C.; Page, C. C.; Dutton, P. L., Darwin at the molecular scale: selection and variance in electron tunnelling proteins including cytochrome c oxidase. *Philos Trans R Soc Lond B Biol Sci* **2006,** 361, (1472), 1295-305.
73. Baldwin, J.; Krebs, C.; Ley, B. A.; Edmondson, D. E.; Huynh, B. H.; Bollinger, J. M., Mechanism of Rapid Electon Transfer during Oxygen Activiation in the R2 Subunit of Escherichia coli Ribonucleotide Reductase. 1. Evidence for aTransient Tryptophan Radical. *J. Am. Chem. Soc.* **2000,** 122, 12195-12206.
74. Zaslavsky, D.; Smirnova, I. A.; Adelroth, P.; Brzezinski, P.; Gennis, R. B., Observation of a novel transient ferryl complex with reduced Cu-B in cytochrome c oxidase. *Biochemistry* **1999,** 38, (8), 2307-2311.
75. Pecoraro, C.; Gennis, R. B.; Vygodina, T. V.; Konstantinov, A. A., Role of the K-channel in the pH-dependence of the reaction of cytochrome c oxidase with hydrogen peroxide. *Biochemistry* **2001,** 40, (32), 9695-708.
76. Tommos, C.; Skalicky, J. J.; Pilloud, D. L.; Wand, A. J.; Dutton, P. L., De novo proteins as models of radical enzymes. *Biochemistry* **1999,** 38, (29), 9495-507.

SUPPLEMENTAL INFORMATION

Contains: Figure S1, Table S1, Figure S2, Figure S3, analytical solution to seven-component fit and references.

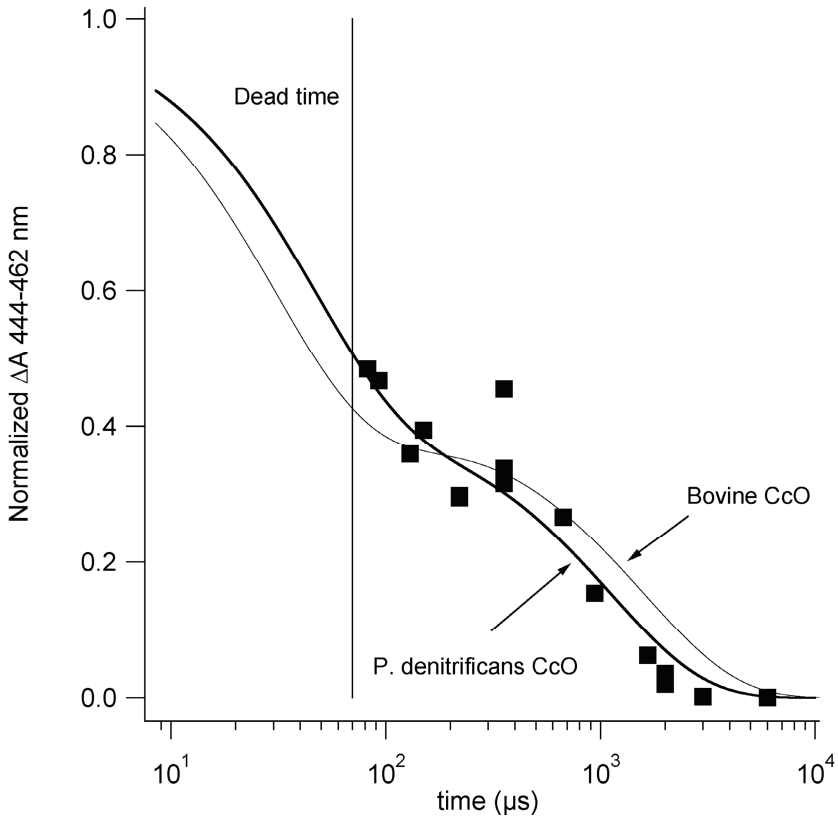

Figure S1. Normalized absorbance change at 444 - 462 nm (squares) representing the time course of oxidation of hemes (a+a_3) calculated from the low temperature UV-Vis spectra of Fig. 1. The simulations (thick line for the *P. denitrificans* CcO) are four-exponential fits exactly as in (S1), with the parameters summarized in Table S1. The relative spectral contributions determined for the bovine heart CcO (S1) were used for the *P. denitrifcans* CcO. The initial oxidation of the hemes is apparently faster in the bovine heart enzyme, while the second oxidation phase is faster in the *P. denitrificans* CcO (Table S1).

Table S1 Simulated half-lives for the oxidation of (heme a+a_3)

Transitions	**R → A**	**A → P_R**	**P_R → F**	**F → O_H**
Spectral contribution at 444-462 nm[1)]	b_1 0.363	b_2 0.327	b_3 -0.106	b_4 0.415
P. denitrificans CcO $t_{1/2}$	31.3 µs	34.3 µs	48.9 µs	776 µs
Bovine CcO[1)] $t_{1/2}$	15.9 µs	24.3 µs	65.9 µs	1109 µs

[1)] See ref (S1) for the meaning and values of the $b_{1\text{-}4}$ coefficients.

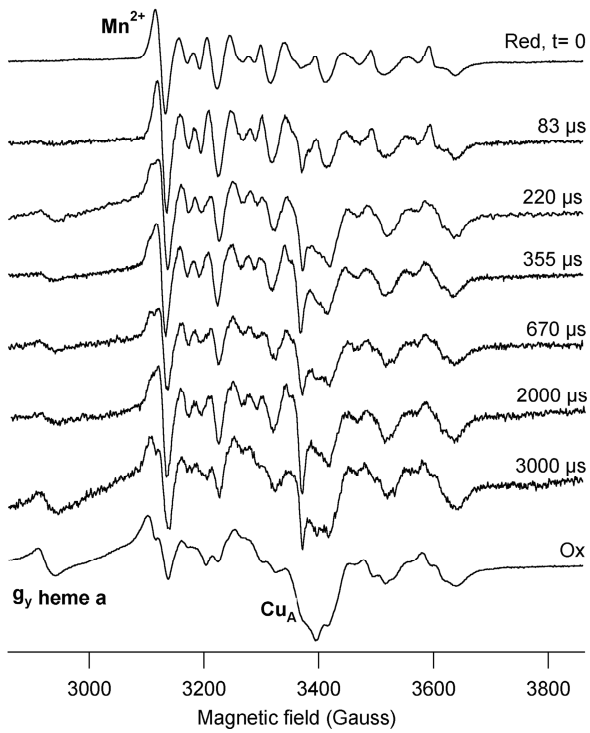

Figure S2. Representative X-band EPR spectra of Mn^{2+}-containing cytochrome aa_3 from *P. denitrificans* rapidly mixed with O_2 and reacted for various times (indicated in µs).
The g_y-resonance of heme *a* and the $g_\perp$ of Cu_A corrected for the Mn^{2+} contribution were used to determine their redox states. Expansion of the g=2 region (not shown) allowed estimation of the Trp* concentration though less accurate than in the Mn^{2+}-free samples. Some of these data are, however, also plotted in Figure 6. EPR conditions: Frequency: 9.42 GHz; modulation amplitude: 1.0 mT; microwave power: 2 mW; Temperature: 14 K. The spectra are normalized correcting for differences in gain and enzyme concentrations.

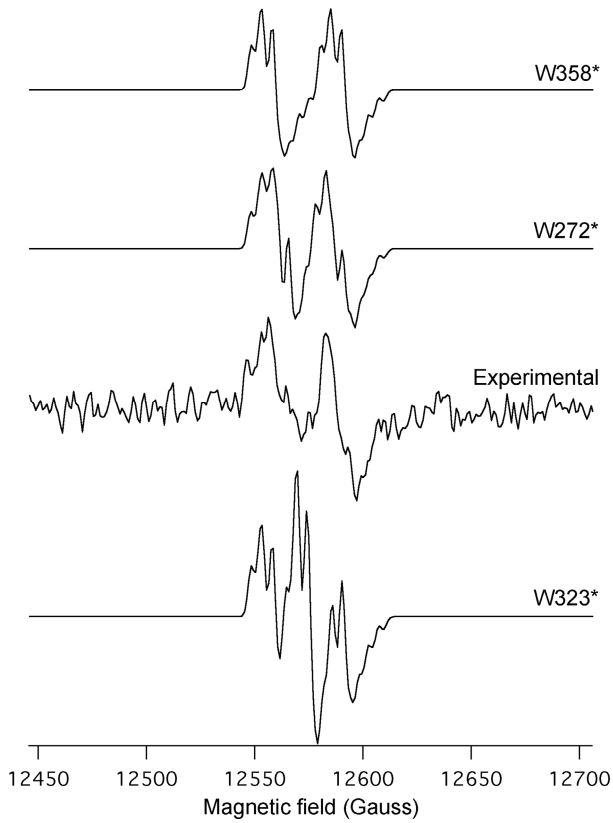

Figure S3. Experimental Q-band EPR spectrum (as in Figure 4) and simulations of specific Trp* radicals. For W328* and W358* all simulation parameters were the same as for TRP-272* (Table 1) except the values for the □-methylene protons. For W358*: $H\beta_1$= 16; $H\beta_2$=16. For W325*: $H\beta_2$= 32; $H\beta_1$=0.

Analytical solution for a series of six irreversible sequential reactions.

The formation and decay rates of the reaction sequence $\mathbf{R} \rightarrow \mathbf{A} \rightarrow \mathbf{P_M} \rightarrow \mathbf{P_R} \rightarrow \mathbf{F} \rightarrow \mathbf{F_{W*}} \rightarrow \mathbf{O_H}$ can be calculated by solving a set of seven differential equations. Analytical solutions for three or four components have appeared in textbooks (e.g. (S2)) and in the literature (e.g. (S1)), respectively. The basic calculation strategy described in these references was extended to seven components. The mathematical expressions below were used to simulate the traces in Figures 5, 6, and 8.

Define: A_0 = [R] at t=0 and $\alpha=1/((k_1-k_2)*(k_1-k_3)*(k_4-k_1))$; $\beta=1/((k_1-k_2)*(k_2-k_3)*(k_4-k_2))$; $\gamma=1/((k_1-k_3)*(k_2-k_3)*(k_4-k_3))$.

The expressions are written according to computer-programming language rather than to mathematical convention.

$\mathbf{R}=A_0*(\exp(-k_1*x))$

$\mathbf{A}=A_0*(((-k_1)/(k_1-k_2))*(\exp(-k_1*x)) + ((k_1)/(k_1-k_2))*(\exp(-k_2*x)))$

$\mathbf{P_M}=A_0*(((k_1*k_2)/((k_1-k_2)*(k_1-k_3)))*(\exp(-k_1*x))-((k_1*k_2)/((k_1-k_2)*(k_2-k_3)))*(\exp(-k_2*x))+((k_1*k_2)/((k_1-k_3)*(k_2-k_3)))*(\exp(-k_3*x)))$

$\mathbf{P_R}=A_0*(k_1*k_2*k_3)*\exp(-k_4*x)*((1/((k_1-k_2)*(k_1-k_3)*(k_4-k_1)))*(\exp((k_4-k_1)*x)-1)-(1/((k_1-k_2)*(k_2-k_3)*(k_4-k_2)))*(\exp((k_4-k_2)*x)-1)+(1/((k_1-k_3)*(k_2-k_3)*(k_4-k_3)))*(\exp((k_4-k_3)*x)-1))$

$\mathbf{F}=A_0*(k_1*k_2*k_3*k_4)*(\alpha*((\exp(-k_1*x)-\exp(-k_5*x))/(k_5-k_1)+(\exp(-k_5*x)-\exp(-k_4*x))/(k_5-k_4))-\beta*((\exp(-k_2*x)-\exp(-k_5*x))/(k_5-k_2)+(\exp(-k_5*x)-\exp(-k_4*x))/(k_5-k_4))+\gamma*((\exp(-k_3*x)-\exp(-k_5*x))/(k_5-k_3)+(\exp(-k_5*x)-\exp(-k_4*x))/(k_5-k_4)))$

$P\alpha=\alpha*((\exp(-k_1*x)-\exp(-k_6*x))/((k_6-k_1)*(k_5-k_1))+(\exp(-k_6*x)-\exp(-k_5*x))/((k_5-k_1)*(k_6-k_5))+(\exp(-k_5*x)-\exp(-k_6*x))/((k_5-k_4)*(k_6-k_5))+(\exp(-k_6*x)-\exp(-k_4*x))/((k_6-k_4)*(k_5-k_4)))$

$P\beta=-\beta*((\exp(-k_2*x)-\exp(-k_6*x))/((k_6-k_2)*(k_5-k_2))+(\exp(-k_6*x)-\exp(-k_5*x))/((k_5-k_2)*(k_6-k_5))+(\exp(-k_5*x)-\exp(-k_6*x))/((k_5-k_4)*(k_6-k_5))+(\exp(-k_6*x)-\exp(-k_4*x))/((k_6-k_4)*(k_5-k_4)))$

$P\gamma=\gamma*((\exp(-k_3*x)-\exp(-k_6*x))/((k_6-k_3)*(k_5-k_3))+(\exp(-k_6*x)-\exp(-k_5*x))/((k_5-k_3)*(k_6-k_5))+(\exp(-k_5*x)-\exp(-k_6*x))/((k_5-k_4)*(k_6-k_5))+(\exp(-k_6*x)-\exp(-k_4*x))/((k_6-k_4)*(k_5-k_4)))$

$\mathbf{F_{W*}}= A_0*(k_1*k_2*k_3*k_4*k_5)*(P\alpha+P\beta+P\gamma)$

$\mathbf{O_H} = A_0 - \mathbf{R} - \mathbf{A} - \mathbf{P_M} - \mathbf{P_R} - \mathbf{F} - \mathbf{F_{W*}}$

Or to check for the correctness of the expressions: $\mathbf{O_H} = k_6*\int\mathbf{F_{W*}}.dt$

Reduced (Cu_A + heme *a*)= $A_0*(1 - 0.5*(\mathbf{P_R}+\mathbf{F}+\mathbf{F_{W*}}) - \mathbf{O_H})$

Substitution of the half-lives ($t_{1/2}$= ln2/k) given below, reproduces the traces in Figure 8.

Transitions	$R \rightarrow A$	$A \rightarrow P_M$	$P_M \rightarrow P_R$	$P_R \rightarrow F$	$F \rightarrow F_{W*}$	$F_{W*} \rightarrow O_H$
P. denitrificans CcO $t_{1/2}$	16 µs	32 µs	.001 µs	27 µs	1200 µs	60 µs

References supplemental information

S1 Szundi, I., Cappuccio, J., and Einarsdottir, O. (2004) *Biochemistry* **43**(50), 15746-15758

S2 Fersht, A. (1999) *Structure and Mechanism in Protein Science. A Guide to Enzyme Catalysis and Protein Folding*, W.H. Freeman and Company, NY

Chapter 7

Direct immobilization of native yeast iso-1 cytochrome c on bare gold: fast electron relay to redox enzymes and zeptomole protein-film voltammetry

Hendrik A. Heering , Frank G. M. Wiertz , Cees Dekker and Simon de Vries

An extension of the paper published in JACS, 2004, 11103-11112

Summary

Cyclic voltammetry shows that yeast iso-1-cytochrome *c* (YCC), chemisorbed on a bare gold electrode via Cys102, exhibits fast, reversible interfacial electron transfer (k0=1.8·103 s-1) and retains its native functionality. Vectorially immobilized YCC relays electrons to yeast cytochrome *c* peroxidase, to cytochrome cd_1 nitrite reductase (NIR), nitric oxide reductase, and cytochrome *c* oxidase from *Paracoccus denitrificans*, thereby revealing mechanistic properties of these enzymes. On a micro-electrode, we measured nitrite turnover by ~80 zeptomole (49,000 molecules) of NIR, co-adsorbed on 0.65 attomole (390,000 molecules) of YCC.

Introduction

Protein electrochemistry has become a powerful tool, both to study redox enzymes and to make sensitive biosensor devices[1-6]. For optimal control of the oxidation state of the cofactors and efficient relay of electrons to the active site, fast interfacial electron transfer is a prerequisite. Often, however, the cofactors cannot make efficient contact with the electrode surface, or substrate access is blocked by the electrode. Since small redox proteins like azurin, ferredoxin and cytochromes are natural electron shuttles for redox enzymes and readily exchange electrons with solid electrodes, these can be used as mediators[7-9]. To reveal the properties of the enzyme under study, fast electron relay by the mediating protein is required. Diffusion limitations can be minimized by immobilizing the mediator, with the correct orientation for electron exchange with both the electrode and the enzyme. Although an orientation with the cofactor towards the electrode surface favors interfacial electron transfer, the same side is usually involved in docking of enzymes. Moreover, close proximity of the cofactor to the electrode can significantly modify its properties [10,11]. One solution is a flexible tether to confine the protein to the surface, allowing reorientation for fast electron exchange with both the electrode[12] and the enzyme[8]. However, such an arrangement will considerably attenuate the overall electron shuttling rate.

Iso-1-cytochrome *c* from bakers yeast (*Saccharomyces cerevisiae*),YCC, is of particular interest since it contains a unique surface cysteine residue. Notably, this Cys102 is located next to the surface-exposed C-terminal Glu, and approximately opposite the lysine-rich site with the exposed heme edge[13]. In the crystal structure of the reduced protein, the thiol is slightly buried, but YCC nonetheless forms disulfide dimers upon oxidation. Proton NMR studies revealed that although dimerization induces small changes at the heme site, this does not result in drastic structural disruption. The NMR spectrum of the dimer is similar to that of the monomer with a chemically modified Cys102[14]. The opposite, lysine-rich site has been shown to interact with the natural redox partners of cytochrome *c* to facilitate fast inter-protein electron transfer. Its role in docking to yeast cytochrome *c* peroxidase (CCP)[15,16], the bc_1 complex[17], and cytochrome *c* oxidase[18,19] has been demonstrated. Moreover, modification of Cys102 does not affect the binding and electron transfer to cytochrome *c* oxidase[20]

Specific tethering of Cys102 to the electrode surface thus ensures a unique and functional orientation of YCC[21]. In this arrangement, the distance between the thiol and the buried edge of the heme is approximately 1.6 nm[22]. Since this is already close to the maximum distance for physiologically relevant electron tunneling rates[23], an additional spacer between the electrode and Cys102 will render electron transfer severely rate limiting. Notably, Dutton and co-workers[9] found that YCC can be physisorbed on thiopropanol-modified gold, with the heme cleft facing solution. Upon coadsorption with cytochrome *c* oxidase, a stable complex was obtained that is active in oxygen reduction. However, even though the thiopropanol spacer is only 0.6 nm long, the authors found that electron relay through cytochrome *c* is rate limiting. This illustrates that *direct* binding of the cysteine thiol to the electrode surface is imperative. Ulstrup and co-workers achieved direct chemisorbtion of YCC on bare Au(111), and a low coverage of YCC was demonstrated by scanning tunneling microscopy[24]. However, only a very weak, transient voltammetric signal of native YCC was observed due to unfolding of the protein. Bonanni and co-workers reported similar scanning probe measurements[25]. Although their cyclic voltammogram shows mostly native, adsorbed YCC, the very broad, asymmetrical peaks indicate extremely slow electron transfer.

In the present report, we demonstrate for the first time that YCC, directly chemisorbed on bare gold via Cys102, retains its native electron transfer functionality. Vectorially immobilized YCC is highly stable, displays very fast interfacial electron transfer, and efficiently relays electrons to its natural partner cytochrome *c* peroxidase as well as to cd_1 nitrite reductase, NO-reductase, and cytochrome *c* oxidase from *Paraccocus denitrificans*. Moreover, the immobilization procedure can be scaled down to interrogate zeptomole protein samples at a micro-electrode.

Materials and methods

Materials

Iso-1-cytochrome *c* from the yeast *Saccharomyces cerevisiae* (YCC) was purchased from Sigma. Yeast cytochrome *c* peroxidase (CCP), expressed in *E. coli*, was a kind gift from Dr. M. Ubbink (Leiden University)[16]. Crystals of CCP were dissolved in 20 mM sodium phosphate buffer (pH 6.1) with 80 mM NaCl, and aliquots stored at -80ºC until use. Nitric oxide reductase (NOR) and cytochrome cd_1 nitrite reductase (NIR)

were purified from *Paracoccus denitrificans* Pd1222, grown anaerobically with nitrate as terminal electron acceptor, according to published methods[26,27]. Cytochrome *c* oxidase from *P.denitirifcans* was a kind gift of Prof. Dr. B. Ludwig (J.W. Goethe University, Frankfurt). Potassium nitrite (Fluka) solutions were freshly prepared, and hydrogen peroxide was diluted immediately before use from a new bottle (Sigma, 30%). Nitric oxide (NO) was added from a fresh stock solution of 100 μM, obtained by flushing anaerobic water with a 5% NO / 95% N_2 gas mixture[28]. Carbon monoxide was added from a saturated solution, prepared by flushing deinonized water with 100% CO for at least 15 min. Deionized water (18 MΩ.cm milli-Q, Millipore) was used to prepare all solutions and for rinsing the electrodes.

Electrochemistry

A 10-25 μl droplet of solution was placed between the working electrode, the reference electrode, and a platinum wire counter electrode as described by Hagen[29]. The cell was flushed with wetted Argon, and connected to either an EcoChemie Autolab 10 potentiostat or to a Bioanalytical systems (BAS) CV-50W potentiostat. The step size of only 0.1 mV used by the latter in combination with low-pass filtering enables accurate determination of the surface coverage from the area under the voltammetric peaks[30]. For sub-nA current measurements, the BAS potentiostat was used in combination with a PA-1 preamplifier and a C-3 cell stand with Faraday cage. The working electrodes were gold disk electrodes (BAS) with diameters of 1.6 mm (2.0 mm^2) and 5 μm (20 μm^2), or a piece of gold foil with a wetted area of ~15 mm^2. The reference electrode was either a saturated calomel electrode (SCE, Radiometer K-401), +244 mV versus the normal hydrogen electrode(NHE), or a Ag/AgCl/3M NaCl electrode (BAS RE-5B), +215 mV versus NHE.

Prior to immobilization of cytochrome *c*, the gold surface was polished with a water-based diamond suspension (Buehler, 1 μm particles for the macroscopic electrodes, and 50 nm for the micro-electrodes), rinsed, cleaned in 0.1 M H_2SO_4 by applying +1.6 V, -1.2 V, +1.6 V and -1.2 V versus NHE for 60s each, and rinsed with water. Because in the oxidized, dimeric yeast cytochrome *c*, the surface cysteine is not accessible, the protein was reduced with dithiotreitol (DTT, Sigma) or tris[2-carboxyethyl]phosphine (TCEP, Pierce). Excess reductant was removed using a Biorad P6 microspin column. In the presence of 50-100 μM reduced YCC, cyclic voltammograms were recorded between +0.5 and -0.1 V versus

NHE with a 10 mV/s scan rate until a stable response was obtained. The electrode was subsequently rinsed with water and a fresh droplet of buffer was applied. The buffer was 10 to 100 mM potassium phosphate (KH_2PO_4 and K_2HPO_4 from Baker) or N-(2-hydroxyethyl) piperazine-N-(2-ethanesulfonate) (HEPES, Merck) at pH 7. A low surface coverage could also be obtained by 20 min. incubation of the gold electrode at open circuit with reduced YCC in 50 mM Tris(hydroxymetryl)aminomethane (TRIS, ICN) buffer at pH 8.5, followed by thorough rinsing with water. Analysis of the non-catalytic peaks for adsorbed YCC was performed after subtracting a cubic splines background curve[31], estimated by interpolation from the flanks of the peak. Control experiments with a solution of oxidized YCC were performed in the presence of 4,4'-dipyridyl (Sigma) as facilitator[32]. For the experiments with cytochrome *c* oxidase and mercapto propianic acid (MPA, Sigma) was prepared with and without YCC. The standard chemisorbed YCC electrode was incubated for 15 min with a 1 mM MPA solution. The electrode was rinsed and left in buffer for at least 15 min to wash away the non-specific absorbed MPA molecules. As a blank the same procedure was repeated but without a YCC layer.

Atomic Force microscopy

Gold electrodes for AFM were made by evaporating approximately 250 nm gold on freshly cleaved mica (grade V-4, SPI supplies) that was degassed overnight at 400 ºC and 10^{-7} Bar prior to gold deposition. To obtain atomically flat gold(111) terraces, the gold was annealed in a hydrogen flame. A freshly annealed electrode was mounted in a custom-made 25 µl electrochemical cell with a flexible Ag/AgCl/saturated KCl reference electrode (FLEXREF from World Precision Instruments, +199 mV versus NHE) and a Pt wire as counter electrode. A rubber O-ring holding the mica/gold chip defines an electrode area of 7 mm^2. To preserve the Au(111) terraces, no further electrochemical cleaning was done on this type of electrode. Immobilization of cytochrome *c*, followed by rinsing the electrode and measuring the surface coverage in buffer were done as described above, using the BAS potentiostat After electrochemistry, the electrode was rinsed with filtered water, dried under a stream of nitrogen, and mounted in the AFM (Nanoscope IV, Digital Instruments). Images were recorded in tapping mode, using silica cantilevers with a typical tip size of 10 nm (Olympus).

NIR activity measurements

The activity of NIR was measured in an anaerobic solution of 50 mM potassium phosphate at pH 7 with 10 mM ascorbate, 0.1 mM phenazine ethosulphate (Sigma), 0.1 mM reduced horse heart cytochrome c (Sigma), 10 mM KNO_2, and 5.6 nM of NIR. The production of NO was measured using a Clark electrode[26]. The activity was determined from the maximum slope, before the onset of NO-inhibition.

Results

Cytochrome c on gold

As shown in Figure 1A, oxidized YCC does not give any response on a freshly cleaned, bare gold electrode. Only when a facilitator such as 4,4'-dipyridyl is added, a reversible, diffusion-controlled response is obtained (Figure 1B). The midpoint potential of 290 mV versus NHE at pH 7 is close to reported reduction potentials of YCC[33,34]. In contrast, a solution of *reduced* YCC without facilitator yields a reversible response with a midpoint potential of 268 mV (Figure 1C), reaching a maximum intensity after 2 to 5 scan cycles (4 to 10 min.). When this electrode is subsequently rinsed and brought into contact with buffer at pH 7 without protein, part of the YCC response is still present (Figure 1D), indicating that the protein is adsorbed on the surface (cf. Figure 2). Upon addition of 0.7 M KCl, the response does not change (Figure 1E), showing that the adsorption is not electrostatic in nature. The YCC layer is remarkably stable: in many cases some or all of the response is still observed after storing the electrode in pH 7 buffer for up to 48 hours at 4°C. The surface coverage, calculated from the area under the baseline-corrected peaks, ranges from 5 to 40% of a full monolayer (the crystallographic dimensions of 2.5 x 3.5 nm[13] yield 19 pmol/cm^2 for a densely packed monolayer) which is probably related to variations in surface cleanliness and roughness. The scan-rate dependence of the heights and potentials of the peaks of a typical sample are plotted in Figure 2. Analysis of the baseline-corrected voltammograms by peak fitting yields an average width correspond to n=0.99±0.08 and an average integral of 2.20±0.14 nC, which computes to 1.1 pmol/cm^2, or 6 % of a monolayer. The proportionality of the peak heights to the scan rate (Figure 2A) confirms the adsorbed nature of YCC.

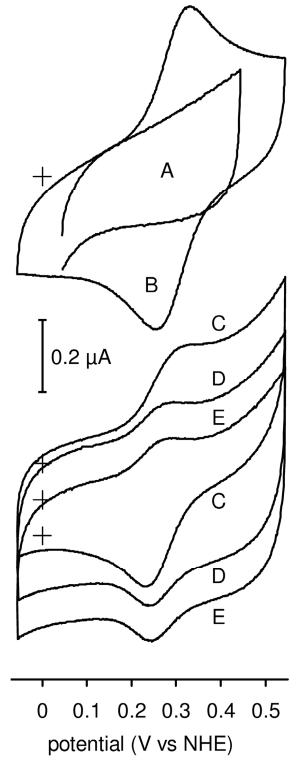

Figure 1. Cyclic voltammograms of YCC on a bare gold electrode (area ~15 mm^2). **A:** 100 µM oxidized YCC in 10 mM KPi, pH 7. **B:** 100 µM oxidized YCC in 100 mM HEPES, pH 7, and 5 mM 4,4'-dipyridyl. **C:** 50 µM reduced YCC in 10 mM KPi, pH 7 on bare gold. **D:** The same electrode after rinsing, in 10 mM KPi, pH 7, without YCC. **E:** 0.7 M KCl added. Traces C, D, and E are offset by -0.8, -0.9, and -1.0 µA, respectively, for clarity (the crosses indicate origins). The scan rate is 10 mV/s for all traces

Although a small peak separation is observed at low scan rates, additional broadening only occurs above 1 V/s (Figure 2B). A similar non-zero separation has also been observed for YCC, electrostatically adsorbed on indium/tin oxide[35]. Because this constant peak separation (termed "unusual quasi-reversibility", UQR, by Feldberg and Rubinstein[36]) is not due to interfacial electron transfer kinetics[36-38], the rate constant for electron transfer between the gold surface and the heme is determined from the additional peak separation at high scan rates.

The data is fitted to the peak potentials of simulated voltammograms[30], using the Butler-Volmer equations to calculate the interfacial electron transfer rate constants for reduction and oxidation:

$$k_{\text{red}} = k_0 \exp\left\{-\alpha nF\left(E - E^{0'}\right)/RT\right\} \quad (1)$$

$$k_{\text{ox}} = k_0 \exp\left\{(1-\alpha)nF\left(E - E^{0'}\right)/RT\right\} \quad (2)$$

where k_0 is the standard rate constant, E is the applied potential, $E^{0'}$ is the equilibrium (midpoint) potential, α is the transfer coefficient, n is the number of electrons, F is the Faraday constant, R is the gas constant, and T is the temperature[39]. With α=0.5, n=1, T=298 K this yields k_0=1774 s^{-1}, $E^{0'}$=270 mV, and a low scan rate separation $\Delta E_p(v \rightarrow 0)$=10 mV. The midpoint potential of adsorbed YCC is close to that of YCC in solution. Since the reduction potential is extremely sensitive to the protein conformation and interactions between the surface and the lysine residues near the exposed heme-edge[10,40], this indicates that the heme edge is facing solution.

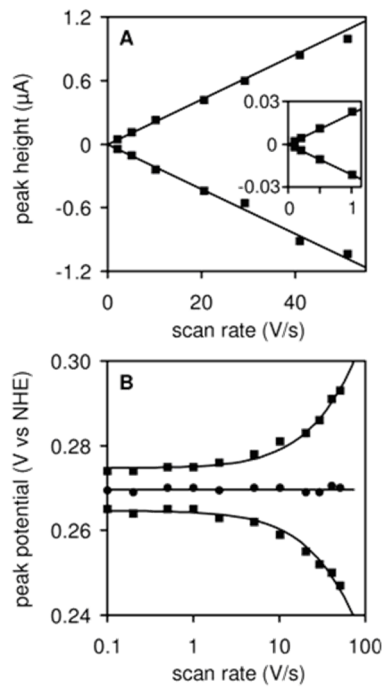

Figure 2. Scan rate dependence of YCC, chemisorbed on gold (2 mm^2), in 50 mM KPi, pH 7. **A:** peak heights versus scan rate. The inset shows the data at low scan rates. The slope of the lines correspond to the average peak height divided by scan rate of 21.2±1.2 nC/V. **B:** peak potentials E_p (squares) and midpoint potentials (circles) versus log scan rate. The solid lines are the peak potentials resulting from the Butler-Volmer equation with $\Delta E_p(0)$=10 mV, $E^{0'}$=270 mV, k_0=1774 s^{-1} (α=0.5, n=1, T=298 K).

Figure 3 shows a voltammogram and corresponding AFM image of the same sample of YCC, chemisorbed on flame-annealed gold on mica. Features with an average height of 2.1±0.5 nm and lateral dimensions (cross section widths) between 14 and 25 nm are observed on the Au(111) terraces. These features remain present after rinsing with water and are neither present on freshly annealed gold, nor on gold incubated with buffer only. The density of the features increases upon raising the applied YCC concentration. The observed heights are comparable to the height of 2.5 nm estimated from the crystal structure of YCC[13], but the lateral dimensions suggest that the features are composed of multiple YCC molecules (assuming a tip width ≤ 14 nm).

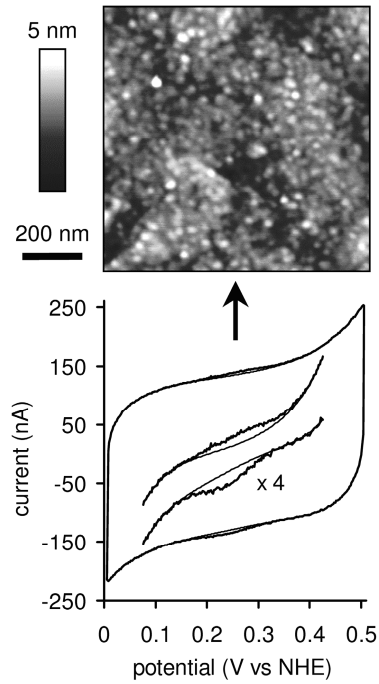

Figure 3. Tapping mode AFM (885 x 885 nm, 512 x 512 pixels, 5 nm z scale) of flame-annealed gold on mica with chemisorbed YCC (top) and cyclic voltammogram of the same sample (bottom) in 50 mM KPi, pH 7 (7 mm^2 exposed Au, 100 mV/s scan rate). The original data and four-fold expanded data (minus an arbitrary slope for clarity) are plotted together with the estimated background used to determine the peak area.

Approximately 650 features are counted per μm^2 in the AFM image, while the area under the voltammetric peaks is 5.9 nC. The peak area calculates to 61 femtomole on an exposed geometric area of 7 mm^2, or 5300

molecules per μm^2 (i.e., 0.9 pmol/cm^2 or 5% of a fully packed monolayer). This implies that the observed features in the AFM image represent clusters of YCC, containing an average of approximately eight native, electrochemically active molecules. The stability of the samples during repeated AFM imaging, the observed height of the features, and uniformly fast electron transfer show that the clusters are monolayer islands of chemisorbed YCC.

Catalytic electron transfer

To test the functionality that is expected for YCC, vectorially immobilized via Cys102, its capability to relay electrons to enzymes was investigated. Cytochrome *c* peroxidase (CCP) is one of the *in vivo* redox partners of YCC. When both CCP and hydrogen peroxide are added to the YCC-modified gold electrode, a clear reductive catalytic current is observed (Figure 4). The half-wave potential of the sigmoidal catalytic wave (267 mV at pH 7, 281 mV at pH 5.5) is close to the non-catalytic reduction potential of cytochrome *c*, and the slope of the wave corresponds to n=1.0 (determined from the derivative peak, see inset of Figure 4). The catalytic current increases with the CCP concentration, sharply decreases upon addition of the CCP inhibitor NaF[4,41], and is higher at pH 5.5 (> 16 s^{-1} per YCC) than at pH 7 (> 6 s^{-1} per YCC) as expected from the pH-dependence of the enzyme activity[42]. When either YCC or CCP are absent, only the low-potential background due to direct reduction of H_2O_2 on gold is observed. These results show that H_2O_2 reduction is catalyzed by CCP and that YCC is properly oriented on the electrode to allow docking and electron transfer to CCP. However, the catalytic current and YCC coverage decrease with a half-life of around 2 minutes. With H_2O_2 present but no CCP, the YCC peaks decrease on a similar time-scale. The rate is first order in H_2O_2 (k_1=0.54 $M^{-1}s^{-1}$) with a half-life of 2½ min. in the presence of 8 mM H_2O_2. Moreover, when 4.8 mM H_2O_2 is added to 0.2 mM oxidized YCC and 5 mM 4,4'-dipyridyl in 0.1 M HEPES pH 7, the voltammetric response decays with a half-life of 4 min., with concomitant bleaching of the cytochrome *c* solution. Villegas and co-workers[43] reported that yeast cytochrome *c* is sensitive to oxidative damage by H_2O_2, causing both bleaching of the heme and oxidation of the cysteine to cysteic acid.

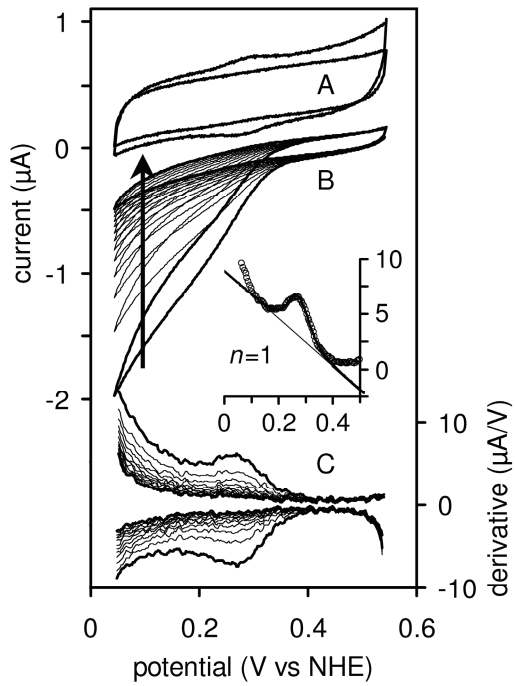

Figure 4. YCC-modified gold electrode (~15 mm^2) with CCP. **A:** in 100 mM HEPES pH 7 before and after catalysis (50 mV/s scan rate). Both voltammograms are offset by 0.4 μA for clarity. **B:** in 80 mM Hepes pH 7 with 20 μM CCP and 8 mM H_2O_2; the bold lines are scans 1 and 13, scan rate is 10 mV/s. **C:** derivatives of B (cathodic sweeps are plotted with negative peaks). The inset shows the average derivative of the first cathodic and anodic sweep (symbols), and the fit to an n=1.0 peak at 267 mV (bold line) with linear baseline (thin line).

The more general applicability of the YCC-modified gold electrode has been explored by testing its ability to relay electrons to two key enzymes in the denitrification pathway of *Paracoccus denitrificans*, involved in the formation and reduction of nitric oxide and with cytochrome *c* oxidase from *Paracoccus denitrificans*, complex IV of the respiratory chain. The soluble periplasmic cytochrome cd_1 nitrite reductase (NIR) catalyzed the one-electron reduction of NO_2^- to nitric oxide (NO). This enzyme has 97.1% homology to the cd_1 NIR from *Paracoccus pantotrophus*[44], which can use both cytochrome c_{550} and pseudoazurin as electron donor, and can also accept electrons from mitochondrial (horse heart) cytochrome *c*[45]. The next enzyme in the denitrification pathway is nitric oxide reductase (NOR), the membrane-bound cytochrome *bc* complex

that catalyzes the reduction of two NO to N_2O by cytochrome c_{550} or pseudoazurin. *In vitro*, horse heart cytochrome *c* can also be used as electron donor.[46,47] Cytochrome *c* oxidase is the electron acceptor of cytochrome *c* in the respiratory chain. It catalyses the reaction of cytochrome *c* oxidation by reducing oxygen to water. During this reaction 4 electrons are donated by cytochrome *c*, 4 protons used for the formation of water from oxygen and 4 protons are pumped across the membrane. Although the native electron donor for cytochrome *c* oxidase is cytochrome c_{552} other positively charged and homologous Type I cytochrome *c*'s can be used as well as efficient electron donors.

With a solution containing both NIR and nitrite, the YCC-modified gold electrode gives a reductive catalytic wave (Figure 5A). The maximum catalytic current increases with time until a stable maximum is reached (i_{lim}=-65 nA). When the electrode is rinsed and placed in a buffered nitrite solution without NIR (Figure 5B), the catalytic current is initially higher (-99 nA, Figure 5C) compared to the last scans with NIR in solution, and decreases to a value that is comparable to the latter (-59 nA). This shows that NIR is firmly adsorbed, presumably on top of the cytochrome *c* layer. The initially higher turnover is most likely due to absence of NO inhibition, and the decrease is due to accumulation of NO near the surface rather than desorption of NIR. Control experiments in which either YCC, NIR or nitrite is absent do not show catalytic activity, and addition of the inhibitor cyanide decreases the catalytic current (data not shown). The results clearly demonstrate that electrons are mediated to NIR by cytochrome *c*. As shown in Figure 5D, the half-wave potential is 260 mV, which is close to the YCC potential. However, the shape of the wave corresponds to a non-integer n_{app}=1.3, which suggests cooperativity of the cofactors (c.f. Discussion section). With the area under the cytochrome *c* peak in buffer after recording trace B (34 nC = 0.35 pmol, or 2.4 pmol/cm^2, data not shown), the maximum catalytic current of -99 nA corresponds to a turnover rate of 2.9 s^{-1} per adsorbed cytochrome *c* molecule.

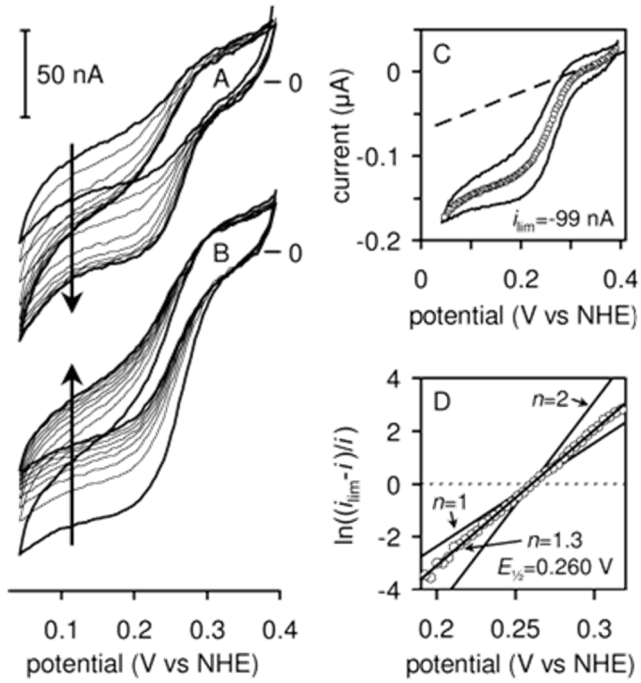

Figure 5. YCC-modified gold electrode (~15 mm^2) with NIR. **A:** 76 μM NIR and 4.4 mM KNO_2 in 50 mM KPi pH 7. **B:** same electrode after rinsing, in 50 mM KPi pH 7 with 4.4 mM KNO_2 without NIR. Arrows indicate development with time (scan rate 5 mV/s); scans 1 and 9 are in bold. **C:** Analysis of scan 1 from B. The symbols are the average of the cathodic and anodic sweep, the dashed line is the estimated baseline. **D:** logarithmic plot of the average from C minus the baseline, with i_{lim}=-99 nA. The fitted line is for n=1.3 and $E_{½}$=260 mV. The n=1 and n=2 slopes are also shown.

Upon addition of both NOR and nitric oxide to the YCC-modified gold electrode, a clear and very stable catalytic reduction current is observed (Figure 6A) with an n=1.0 steepness and a half-wave potential of +108 mV (determined from the peak fit, see inset of Figure 6A), which is well below the reduction potential of YCC. No catalytic response is observed when either YCC, NOR or NO are absent. Since the catalytic half-wave potentials with NIR and with NOR are well separated, it is possible to measure both enzymes simultaneously on the same electrode, and because the product of NIR is the substrate for NOR, it should be possible to observe NOR activity without adding NO. As shown in Figure 6B, with both NIR and NOR in solution but only nitrite as substrate, the two-step conversion of nitrite via nitric oxide to nitrous oxide is indeed observed. Interestingly, under these

conditions the NO reduction wave comprises two n~1 sub-waves, clearly visible in the derivative, which points at a turnover mechanism involving multiple catalytic states or electron relay pathways in NOR[2,3].

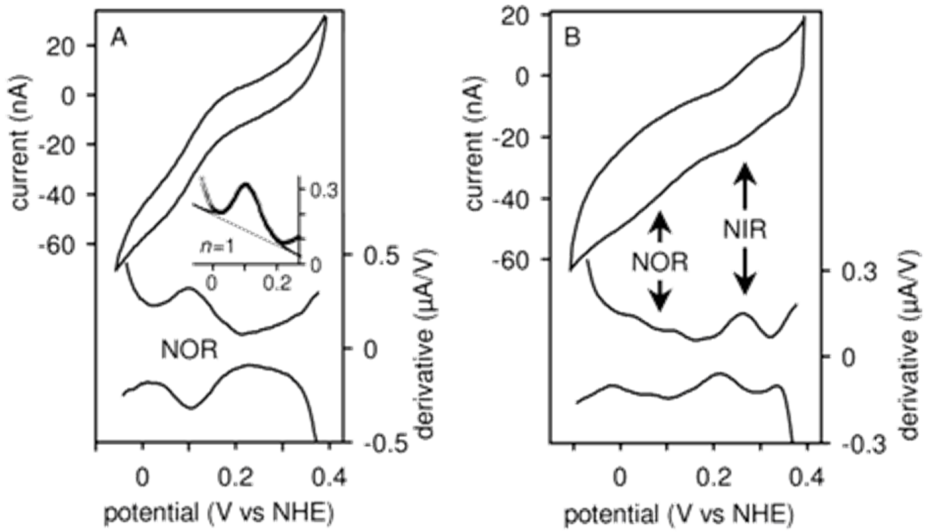

Figure 6. YCC-modified gold electrode (~15 mm^2) with NOR. **A:** in 17 mM KPi pH 6 with 15 μM NOR and ~5 μM NO; scan rate 1 mV/s. **B:** 17 mM KPi pH 6 with 7 μM NOR, 19 μM NIR and 34 mM KNO_2,; scan rate 5 mV/s. The derivatives of the cathodic sweeps have negative peaks. The inset shows the average derivative of the cathodic and anodic sweep, and the fit to an n=1.0 peak at 108 mV (bold line) with linear baseline (thin line).

Cytochrome *c* oxidase activity was measured on an YCC modified electrode with co-immobilized mercapto-propionic acid. The mercapto-propionic acid self-assembling monolayer was applied after YCC immobilization to cover the free gold surrounding the YCC molecules, to prevent sticking of cytochrome *c* oxidase directly onto the gold electrode. Furthermore, the SAM partially blocks non-enzymatic oxygen reduction. The SAM does not influence the signal of the chemisorbed YCC layer (Figure 7 scan A). After a stable signal was obtained the electrode was washed and cytochrome *c* oxidase was added to a fresh droplet of buffer at a final concentration of 2 μM. After 10-20 scans under aerobic conditions a stable catalytic current signal was attained. The electrode was rinsed with clean buffer and a fresh droplet of buffer was applied and measured again under aerobic conditions. The signal became stable after approximately 5 scans, which represented almost the same catalytic current obtained with cytochrome *c* oxidase in solution proving 1) that the cytochrome *c* oxidase

is absorbed on the YCC molecules in the mixed YCC/MPA monolayer and 2) that diffusion of cytochrome *c* oxidase to the electrode surface and back to the solution did not cause the catalytic current (Figure 7 scan B). It can be excluded that the cytochrome *c* oxidase was directly adsorbed on gold or mercapto-propionic acid because a mercapto-propionic acid SAM without YCC did not yield a catalytic response. To confirm that the activity is solely from the cytochrome *c* oxidase, CO was added, which is a specific inhibitor for cytochrome *c* oxidase and binds to the reduced form. When CO was added to the solution (90μM final concentration) the activity of the reduced enzyme was inhibited by 75% (Figure 7 scan C).

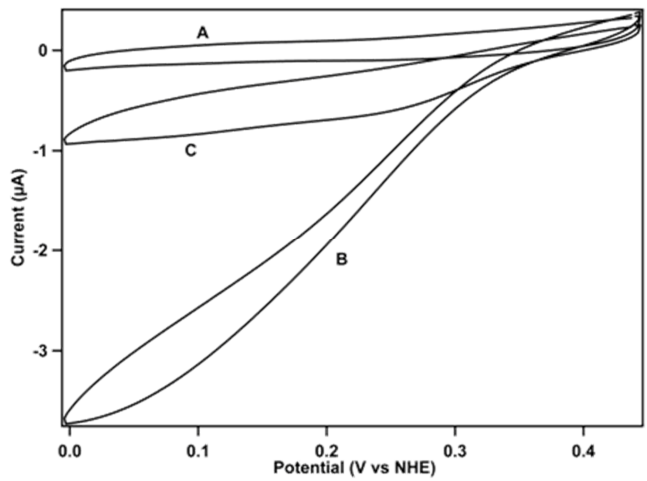

Figure 7 YCC-modified gold electrode (~8 mm^2) stabilized with a mercaptopropionic acid self-assembling monolayer. (A) In 10 mM KPi pH 7 and 1 mM EDTA under anaerobic conditions, scan rate 10mV/s. (B) same electrode with cytochrome *c* oxidase added (2 μM concentration), then washed after 10-20 scans (when a stable signal was obtained) to wash away the free cytochrome *c* oxidase in solution, and a fresh drop of buffer was applied to the electrode. The absorbed YCC-cytochrome *c* oxidase layer was measured under aerobic conditions with highest and stable activity reached after approximately 5 scans, scan rate 10mV/s. (C) same electrode as (B) with 90 μM CO (final concentration) added to the droplet, scan rate 10mV/s.

YCC and NIR on a microelectrode

Mass transport to a large planar electrode occurs by linear diffusion, which is characterized by a decreasing flux with time ($\propto 1/\sqrt{t}$) and depletion of substrate. The turnover rate of NIR at the electrode could therefore be limited by diffusion. For the same reason, the formed product nitric oxide

will accumulate near the surface and inhibit the enzyme (see Figure 5B). Contrarily, diffusion to a micro-electrode is radial, which results in a steady-state flux proportional to the electrode radius[39]. Because the mass-transport limited current density (per area) increases with *de*creasing radius, smaller micro-electrodes support higher enzymatic turnover rates. A 5 μm diameter disk electrode supports a diffusion-limited current of $i=4nFDCr \approx 1$ nA for a substrate concentration C=1 mM and a diffusion constant $D=10^{-9}$ m^2/s.

Considering the dimensions of YCC[13], a full monolayer on a 5 μm (20 μm^2) gold electrode consists of only ~$2.3 \cdot 10^6$ molecules (3.8 attomole). Following the same procedure to immobilize YCC as for macro-electrodes, and accumulating 100 scans at 20 mV/s scan rate, cytochrome *c* oxidation and reduction peaks can be detected with heights of 15 fA, on top of a capacitive electrode charging background current of ~1 pA (Figure 8A). No such peaks are observed on untreated gold electrodes. After subtracting the estimated background[48a], the peaks are fitted to the theoretical shape for a reversible surface-confined one-electron redox process with an area of 77 fC. This computes to as little as 0.8 attomole, which is less than 500,000 cytochrome *c* molecules and corresponds to a surface coverage of 4.0 $pmol/cm^2$ or 21% of a monolayer. Figure 8B shows that when NIR and nitrite are added to the solution, a catalytic current of 0.30 pA is observed[48b]. This corresponds to a nitrite turnover rate of 3.9 s^{-1} per adsorbed cytochrome *c* molecule in this experiment. The reproducibility of these experiments is demonstrated in Table 1. The average sample size is 0.65 attomole (3.2 $pmol/cm^2$), or ~390,000 YCC molecules. To our knowledge, these are by far the smallest samples detected by protein film voltammetry to date. In the presence of NIR and nitrite, the average turnover rate per YCC molecule is 3.2 s^{-1} and the slope of the wave yields n_{app}~1.4. These numbers are equal to those observed at macroscopic electrodes. However, both the non-catalytic midpoint potential and the catalytic half-wave potential are shifted compared to the results on macroscopic electrodes, without affecting their shapes. A ~40 mV downshift is reproduced with different batches of chemicals and different reference and 5 μm Au electrodes (experiments listed in Table 1). Test measurements with ferrocene derivatives in solution do not reproduce the shift, excluding impedance-related artifacts. Therefore, the lowered potentials most likely reflects a slightly altered environment.

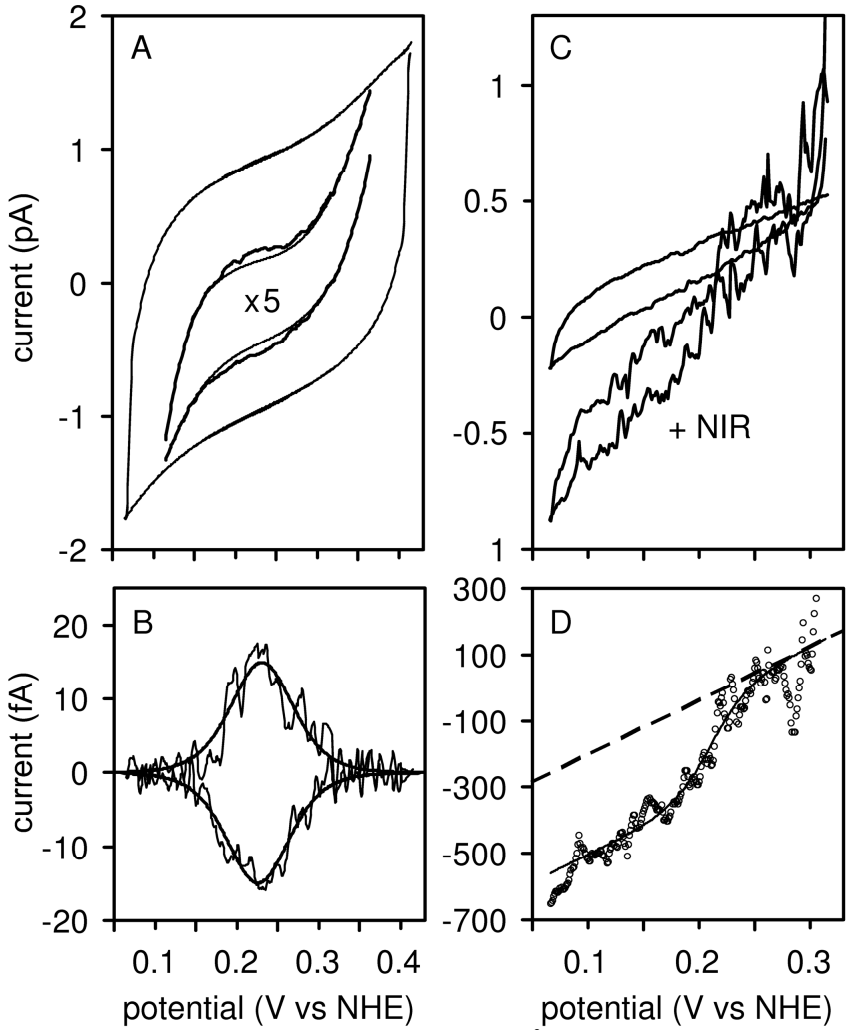

Figure 8. A: YCC on a gold micro-electrode (20 μm^2) in 50 mM KPi, pH 7; 20 mV/s scan rate; 1.5 Hz filter; average of 100 cycles. The original data and five-fold expanded data (minus an arbitrary slope for clarity) are plotted together with the estimated background. B: Baseline-corrected voltammogram, and fitted peaks: E_m=228 mV, ΔE_p=5 mV, width = 89 mV (n=1), height = 14.9 fA. C: Sample from A before and after adding 10 mM KNO_2 and 10 μM NIR; 2 mV/s scan rate; 0.15 Hz filter, averages of 10 (without NIR) and 3 (with NIR) cycles. D: Average of cathodic and anodic scans recorded with NIR minus those without NIR.The dashed line is the estimated residual slope. The solid line is the fitted sigmoidal ($E_{½}$=211 mV, n=1.5, i_{lim}=-301 fA) plus slope. The results are listed in Table 1 as experiment no. 1.

Table 1. Summary of the data with YCC adsorbed on 5 μm diameter gold electrodes. The experiments in which both non-catalytic and catalytic currents are measured have corresponding numbers. Experiment number 1 is plotted in Figure 8.

non-catalytic (in 50 mM KPi, pH 7):

experiment [a]	E_m **(mV)**	ΔE_p **(mV)**	n_{app} [b]	**height (fA)**	**area (fC)**	**coverage (attomole)**	**molecules (10^5)**
1 (A, I)	228	5	1.00	15	77	0.80	4.8
2 (A, I)	238	53	0.86	9	51	0.53	3.2
3 (A, I)	225	46	1.01	15	70	0.73	4.4
4 (A, I)	226	6	0.78	11	66	0.69	4.1
5 (B, I)	233	49	0.98	12	53	0.56	3.3
6 (B, I)	221	32	0.94	15	75	0.78	4.7
7 (B, II)	223	16	1.01	125 [c]	45	0.47	2.8
Average	228	30	0.94	12.4 [c]	62	0.65	3.9

catalytic (10 μM NIR and 10 mM KNO_2 in 50 mM KPi, pH 7):

experiment [a]	$E_{½}$ **(mV)**	n_{app}	i_{cat} **(fA)**	**turnover per YCC (s^{-1})**
1 (A, III)	211	1.5	301	3.9
4 (A, IV)	198	1.4	226	3.4
7 (B, V)	201	1.2	65	1.4
8 (C, V)	213	1.5	246	4.0 [d]
average	206	1.4	210	3.2

[a] Three different electrodes have been used, labeled A, B, and C. The roman numbers are the measurement conditions: I, average of 100 scans at 20 mV/s with a 1.5 Hz filter; II, average of 100 scans at 250 mV/s and 50 Hz; III, average of 3 scans at 2 mV/s and 0.15 Hz; IV, average of 6 scans at 2 mV/s and 0.15 Hz; V, average of 3 scans at 2 mV/s and 0.5 Hz. [b] Non-catalytic n_{app} = 89/(peak width at half-height, in mV). [c] The average includes experiment 7, normalized to 20 mV/s (10 fA). [d] Turnover calculated using the average coverage of experiments 1 to 7 (0.65 attomole).

Discussion

Cytochrome c electrochemistry and immobilization

Oxidized, dimeric YCC does not exchange electrons with a gold electrode unless the surface is modified with a facilitator like 4,4'-bipyridyl that promotes electron transfer to the positively charged heme edge. In contrast, when the bulk of YCC in solution is chemically reduced prior to voltammetry, a stable response rapidly develops without a facilitator. Because the exposed heme edge is equally accessible in both the oxidized (cystine) dimer and the reduced (cysteine) monomer, the response of reduced YCC is most likely due to the interaction between the exposed cysteine thiol and the gold electrode: reduced YCC is chemisorbed on the gold electrode, and this layer mediates electrons to cytochrome *c* in solution. When the excess cytochrome *c* is subsequently removed from solution, only the response of the adsorbed layer remains. The insensitivity of this response to high salt concentrations, the midpoint potential close to that of YCC in solution, and the ability to transfer electrons to YCC in solution, to CCP, NIR, and NOR all indicate that YCC is covalently bound to gold via Cys102, and oriented with the accessible heme cleft towards solution.

Adsorption from a solution of reduced YCC is not only important to expose the thiol, but probably also prevents denaturation on the gold surface. NMR data has revealed that reduced YCC is substantially more rigid compared to the oxidized species[49], and EPR studies of spin-labeled Cys102 demonstrated more rapid temperature-induced unfolding of the C-terminal region in the oxidized state[50]. Voltammetric cycling probably promotes chemisorption by creating a transient, local population of oxidized but monomeric YCC with a more flexible C-terminus. The stability of the chemisorbed YCC is almost certainly related to the observed tendency to form islands. The lateral confinement within such an island reduces its orientational freedom and thus prevents extensive direct contact between the protein and the gold surface.

Our results differ from those recently published by others. Ulstrup and co-workers[24] report that after 3 hours of incubation of flame-annealed Au(111) with YCC, their *in situ* STM and voltammetric data show a low density overage with individual molecules, that are mostly unfolded. Bonanni and co-workers[25] reported very similar SPM data of YCC on gold. Although their voltammetric data show mostly native, adsorbed YCC, the coverage is much too high compared to the SPM data and the peaks are

highly asymmetric and very broad (~140 mV peak separation at a scan rate of 50 mV/s). This is symptomatic for very slow interfacial electron transfer: allowing for a large non-kinetic hysteresis of 50 mV, the remaining 90 mV compute to a k_0 of only 0.6 s^{-1}. This is more than 3 orders of magnitude slower than our measurements, and suggests a separation between the heme and the gold of more than 2 nm (see below). This points at either multilayer adsorption or at least a very unfavorable orientation that does not involve a direct Cys102 to gold bond.

Interfacial electron-transfer kinetics

According to the semi-classical model of Marcus[51], the rate constant for non-adiabatic electron transfer between weakly coupled donor and acceptor sites at fixed distance depends on the driving force (difference between the reduction potentials of donor and acceptor, E_D and E_A) and the reorganization energy λ, which is the energy (in eV) required to change the nuclear coordinates of the donor to those of the acceptor without transferring the electron:

$$k_{DA} = k_{max} \exp\left\{ -\frac{RT}{4\lambda F}\left[\frac{F}{RT}\left(E_D - E_A + \lambda\right)\right]^2 \right\} \quad (3)$$

The electron-transfer rate constant increases with energy difference, reaching a maximum k_{max} when E_D-E_A=-λ, and decreases again at higher driving force (the inverted region). The pre-exponential factor k_{max} depends on the electronic coupling between the donor and acceptor. For long-range electron transfer from redox centers in proteins to a surface-bound acceptor, Gray and co-workers observed that k_{max} decreases exponentially with distance (r) between the donor and acceptor[52]. Extrapolated to van der Waals contact (0.36 nm), a common tunneling rate constant of ~10^{13} s^{-1} was found for all systems:

$$k_{max} \approx 10^{13} \exp\{-\beta(r - 0.36\,\text{nm})\}\ \text{s}^{-1} \quad (4)$$

The decay constant β falls in the range of 8 to 16 nm^{-1}, depending on the nature of the protein matrix[23,52,53].

For application of Equation 3 to electron transfer between an electrode at potential E and a redox center in the protein with reduction potential $E^{0'}$, all occupied (or vacant) states in the electrode must be considered as electron donor (or acceptor)[39,54-56]. The contribution of each state i at potential E_i can be estimated by multiplying the Marcus rate constant at driving force E_i-$E^{0'}$ by the probability that the state is occupied. For a metallic electrode, this probability is described by the Fermi-Dirac distribution 1/(1+exp(x)) for a dimensionless potential difference x=(E-E_i)F/RT from the applied potential E (i.e., the Fermi level). The total electron transfer rate constant at given E is obtained by summing the contributions of all states:

$$k_{\text{red/ox}} = \frac{k_{\text{lim}}}{\sqrt{4\pi \text{L}}} \int \frac{\exp\left\{-\left(\text{L} \pm \text{P} - \text{x}\right)^2 / 4L\right\}}{1 + \exp(\text{x})} d\text{x} \qquad (5)$$

where the dimensionless parameters L= $\lambda F/RT$ and P=(E-$E^{0'}$)F/RT, and L+P and L-P apply to k_{red} and k_{ox}, respectively. The integration yields a *sigmoidal* dependence of the rate constant on applied potential, reaching a plateau[57]

$$k_{\text{lim}} = k_{\text{max}} \rho \frac{RT}{F} \sqrt{4\pi \text{L}} \qquad (6)$$

at high overpotential (E-$E^{0'}$<<-λ for reduction), and k=½k_{lim} at E-$E^{0'}$=-λ. As in Equations 3 and 4, k_{max} is the driving-force optimized Marcus rate constant for any single, fully occupied state, and ρ (in eV^{-1}) is the effective density of electronic states near the Fermi level. At small overpotentials relative to λ, equation 5 is indistinguishable from the Butler-Volmer equations 1 and 2 with α=0.5 [55].

At the maximum scan rate of 51.2 V/s available with our equipment, the peak separation increases by as little as 37 mV (Figure 2B). This is much smaller than the reorganization energy of 0.61 eV, found for diffusion-controlled reduction and oxidation of YCC on ω-hydroxythiol-modified gold at pH 7.[33,58] We therefore used the Butler-Volmer equation with α=0.5 to fit the data, yielding k=1774 s^{-1} at E=$E^{0'}$. Substituting this and λ=0.61 eV in Equation 5 yields k_{lim}=4.0·10^6 s^{-1}, which is more than sufficient to drive even the fastest enzymes. With ρ =0.9/eV [59], Equation 6

yields $k_{max} = 1.0 \cdot 10^7$ s^{-1}, which for a tunneling distance of 1.6 nm calculates to decay constant β=11.1 nm^{-1} (Equation 4). This shows that the direct covalent bond between gold and Cys102 provides efficient coupling between the heme and the electrode surface, consistent with the many through-bond sections between the heme and the C-terminus as seen in the crystal structure. For YCC, physisorbed on a thiopropanol monolayer with the heme cleft facing solution, Dutton and co-workers measured a standard rate constant k_0 of just 20 s^{-1}, ascribed to the additional 0.6 nm distance between the gold surface and the heme.[9] When cytochrome *c* oxidase is co-adsorbed on this YCC layer, the catalytic oxygen reduction current is limited by electron relay through YCC. Since the rate of electron transfer from YCC to cytochrome *c* oxidase is $>10^4$ s^{-1} [20], the rate limiting step seems to be the interfacial electron transfer. Evidently, direct chemisorption will remove this limitation, and enable detailed mechanistic studies of intra- and inter-protein electron-transfer processes.

A finite peak separation at low scan rates is regularly observed in protein film voltammetry[37]. For both equine and yeast cytochrome *c*, electrostatically adsorbed on indium/tin oxide, Kasmi and co-workers report a limiting peak separation of around 10 mV, and propose that this is due to a reversible, electron-transfer induced conformational change[35]. However, a redox reaction coupled to a reversible chemical reaction will appear as a single, reversible net reaction at low scan rates, with peak separations approaching zero[37,38]. Instead, Feldberg and Rubinstein[36] propose an N-shaped free energy (potential versus charge) curve that results in a time-independent hysteresis equal to the free energy difference between the maximum and minimum of the curve. We postulate that such an N-shaped curve can be due to vibrational relaxation associated with the redox reaction. The observed minimum peak separations between 5 and 50 mV correspond to frequencies of 40-400 cm^{-1}, a range that is dominated by protein conformational (collective mode) vibrations that are very important for electron transfer[60]. Moreover, a large number of YCC heme vibrational modes are found in this region[61].

Electron relay to enzymes

The YCC-modified gold electrode mediates electrons to CCP from yeast, with a catalytic wave for the two-electron reduction of H_2O_2 to water centered close to the YCC redox potential. This differs markedly from CCP, directly adsorbed on a pyrolytic graphite edge electrode, for which the wave

is centered close to the compound I redox potential of ~750 mV.[4,5] Clearly, the shift is due to slow interfacial electron transfer to YCC at such an unfavorably high potential: the reported [6] electrocatalytic turnover of 407 H_2O_2/s^{-1} (814 *e*/s) at pH 5.4 is only matched by the interfacial electron transfer rate to YCC below 309 mV (Equation 5). But since this rate increases exponentially as the potential is lowered further, the shape and height of the catalytic wave will, although displaced, still reflect the properties of the YCC/CCP/H_2O_2 system. The observed n=1 slope, despite the two-electron reaction that is catalyzed, suggests that the turnover rate is proportional to the fraction of reduced YCC, and thus (at least in part) limited by the rate of electron transfer from YCC to CCP. In fact, for CCP on graphite, Heering et al have found that reduction of compound II to Fe(III) is rate limiting due to gating by a coupled chemical step.[3] The decay of the catalytic H_2O_2 reduction current with CCP is caused by the instability of cytochrome *c* in the presence of H_2O_2, as reported by Villegas and co-workers[43]. Nevertheless, the initial catalytic response of the gold/YCC/CCP system proves that YCC is adsorbed with retention of its native electron transfer activity.

The results demonstrate that chemisorbed YCC also mediates electrons to *Paracoccus denitrificans* nitrite reductase, and that NIR is co-adsorbed on the YCC layer. Comparison between the AFM and voltammetric data shows that YCC adsorbes in clusters of around eight molecules. Using the crystallographic dimensions of YCC[13], such monolayer islands have diameters of ~ 9 nm. Since the crystal dimensions of the *Paracoccus pantotrophus* NIR dimer are 5 nm x 10 nm (and 6 nm "high", from the perspective of the *c*-domains)[62], only one NIR dimer is likely to find a favorable docking position per YCC island. This implies that as little as 80 zeptomole (~49,000 molecules) of NIR is co-adsorbed on the average 0.65 attomole (~390,000 molecules) of YCC at the 5 µm electrodes. The average electrocatalytic activity of 3.2 s^{-1} per YCC thus yields an estimated turnover of 26 s^{-1} per NIR dimer, or 12.5 U/mg. This is comparable to the specific activity of 13.6 U/mg, measured at pH 7 in the presence of saturating concentrations of reduced cytochrome *c* and nitrite. The turnover per YCC is equal on macroscopic and micro-electrodes, although linear diffusion to the former should cause substrate depletion. The equality can be explained by the topography of the YCC layer: since NIR does not exchange electrons with bare gold, the ensemble of islands acts as an array of nano-electrodes, allowing more efficient mass transport.

The turnover rate of NIR is much lower than the interfacial electron transfer to YCC (k_0), but the half-wave potential of the catalytic wave is slightly lower than the midpoint potential of YCC. Although this might suggest that the turnover is limited by the fraction of reduced YCC and thus by inter-protein electron transfer, the n_{app}=1.4 slope of the wave is clearly at odds with this. Therefore, electron relay through YCC is not rate limiting, and both the wave shape and potential reflect the properties of the heme centers of NIR. For the one-electron reduction of nitrite to nitric oxide, catalyzed by a one-electron redox center (d_1 heme), an $n \leq 1$ Nernstian sigmoidal catalytic wave should be expected. Consequently, the $n>1$ catalytic wave is indicative of positive cooperativity between the heme groups, either within or between the NIR subunits, or between YCC and NIR. For the related *Paracoccus pantotrophus* NIR, positive cooperativity is observed between hemes *c* and d_1 within one subunit.[63] Titration curves with n_{app}=1.4 are found at 20ºC, increasing to fully n=2 at higher temperature with an equilibrium potential of 140 mV. The one-electron reduced intermediate state cannot be obtained unless NIR is depleted of the d_1 heme. The authors suggest that this cooperativity is due to coupling of the redox states of hemes *c* and d_1 via the connected ligands His17 and Tyr25 of oxidized *c* and d_1, respectively, that are exchanged for Met106 and released upon reduction of the respective hemes. *Pseudomonas aeruginosa* cd_1 NIR has more tightly intertwined subunits compared to *Paracoccus pantotrophus* NIR, and the heme sites within each subunit do not cooperate. Instead, a positive allosteric cooperativity of 30 mV has been observed between the two d_1 hemes and an equal negative cooperativity between the *c* hemes, resulting in a titration curve with a slope of n=1.6.[64] In contrast, the cd_1 NIR from *Pseudomonas stutzeri* exhibits negative allosteric cooperativity between the two d_1 sites[65]. With the YCC electrode, it may be possible to clarify whether the cooperativity in *P. denitrificans* NIR is allosteric or not.

Chemisorbed YCC is also able to relay electrons to *Paracoccus denitrificans* NOR. Notably, the half-wave potential for electrocatalytic NO reduction of +108 mV at pH 6 is much lower than the YCC equilibrium potential, and is in fact close to the reduction potential of the high-spin heme b_3 in the active site (+62 mV at pH 7, +20 mV at pH 8.5)[66]. Reduction of YCC by the electrode is not rate limiting: the interfacial electron transfer to YCC is $3 \cdot 10^4$ s^{-1} at E=108 mV (Equation 5), compared to the reported k_{cat} of 200 NO/s [46]. The catalytic wave is not centered at the

redox potential of YCC, which means that the turnover is not proportional to the fraction of reduced YCC and thus that inter-protein electron transfer is also not limiting. The fact that the applied potential must be close to the heme b_3 redox potential for turnover signifies the importance of the fully reduced heme b_3 Fe(II) / Fe_B(II) active site in the mechanism, as proposed by de Vries and co-workers[46,67]. The n=1 steepness of the catalytic wave reflects the rate-limiting reduction of heme b_3 via the high-potential centers in NOR ($E_{m(pH\ 7.6)}$ = +345 mV for LS heme *b*, +310 mV for LS heme *c*, and +320 mV for Fe_B [66]), which in turn are rapidly reduced by YCC (E_m = +270 mV). Interestingly, the lower catalytic half-wave potential of NOR compared to that of NIR makes it possible to measure the activities of both enzymes on the same electrode. This is advantageous, not only to study the interaction between the enzymes, but potentially also for simultaneous sensing of nitrite and nitric oxide.

Cytochrome *c* oxidase binds specifically to chemisorbed YCC. A mercapto-propionic acid SAM blocks the remaining gold surface, which implies that YCC is able to absorb cytochrome *c* oxidase and relay electrons to this enzyme. The MPA layer also prevents oxygen to react directly on the electrode. Catalytic current densities of 40-60 $\mu A/cm^2$ are measured under aerobic conditions. With CO, a specific inhibitor of cytochrome *c* oxidase, the activity dropped drastically at low potentials. CO is known to bind to the reduced form of cytochrome *c* oxidase. A fraction of the activity remains because CO and oxygen are in competition for binding to the active site. Since CO has no effect on the YCC monolayer it can be concluded that the catalytic wave is solely due to cytochrome *c* oxidase activity.

The down-shifted half-wave potential (derivative peak maximum at -24 mV) and broadened wave (derivative peak-width-at-half-height of 164 mV) are indicative of rate-limiting electron-transfer. Because the inter-protein ET rate is >10,000 s-1[20], this suggests that at least one of the (proton-coupled) CcO re-reduction steps is very fast, and is limited by ET from gold to YCC (~1800 s^{-1} at $E=E_0$; an overpotential is apparently required to match the demand of CcO).

Conclusions

We have demonstrated that cytochrome *c* from yeast, chemisorbed *directly* on a gold electrode, is stable and retains its native redox potential and electron transfer functionality. The bond between Cys102 and the gold surface allows for very fast interfacial electron transfer to the heme, and at

the same time ensures an orientation that is favorable for functional docking of redox enzymes. The ability to relay electrons to CCP, NIR, NOR and CcO clearly illustrates the versatility of the system. Although a detailed analysis of the catalytic properties of each of these systems is beyond the scope of this paper, some tentative conclusions can already be drawn: 1) The turnover of CCP is, at least partially, limited by electron transfer between YCC and CCP. 2) The catalytic wave shape with NIR shows positive cooperativity between the cofactors. 3) The catalytic activity of NOR depends on the redox state of the active site heme b_3. 4) The catalytic activity of cytochrome *c* oxidase absorbed on an YCC modified gold electrode depends on the electron transfer rate from the electrode to YCC. These examples demonstrate that, due to the very fast interfacial electron transfer and proper vectorial orientation, redox enzymes can be interrogated electrochemically via YCC, thus significantly extending the applicability of protein film voltammetry to enzymes that cannot directly communicate with an electrode. The feasibility to miniaturize the system to sub-attomole samples offers great potential for applications in microscopic biosensor devices and multi-enzyme arrays. Direct immobilization of native cytochrome *c* on gold(111) terraces, and co-adsorption of enzymes opens the way to detailed scanning probe microscopy studies of redox protein complexes.

Acknowledgements

HAH is financially supported by the Delft Interfacultary Research Center Life science and Technology (DIOC LifeTech) and by the Netherlands Organization for Scientific Research (NWO), and FGMW by the Netherlands Foundation for Fundamental Research on Matter (FOM). Recombinant cytochrome *c* peroxidase from yeast was kindly provided by Dr. M. Ubbink (Leiden University). Marc Strampraad is acknowledged for purification of *Paracoccus denitrificans* NIR and NOR. Cytochrome *c* oxidase from *P.denitirifcans* was kindly provided by Prof. Dr. B. Ludwig (J.W. Goethe University, Frankfurt)

References

1. a) Armstrong, F. A.; Wilson, G. S., Recent developments in faradaic bioelectrochemistry. *Electrochimica Acta* **2000,** 45, (15-16), 2623-2645. b) Fedurco, M., Redox reactions of heme-containing metalloproteins: dynamic effects

of self-assembled monolayers on thermodynamics and kinetics of cytochrome c electron-transfer reactions. *Coordination Chemistry Reviews* **2000,** 209, 263-331. c) Willner, I.; Katz, E., Integration of layered redox proteins and conductive supports for bioelectronic applications. *Angewandte Chemie-International Edition* **2000,** 39, (7), 1180-1218. d) Chaki, N. K.; Vijayamohanan, K., Self-assembled monolayers as a tunable platform for biosensor applications. *Biosensors & Bioelectronics* **2002,** 17, (1-2), 1-12. e) Zu, Y. B.; Shannon, R. J.; Hirst, J., Reversible, electrochemical interconversion of NADH and NAD(+) by the catalytic (I lambda) subcomplex of mitochondrial NADH : ubiquinone oxidoreductase (complex I). *Journal of the American Chemical Society* **2003,** 125, (20), 6020-6021.

2. a) Armstrong, F. A.; Heering, H. A.; Hirst, J., Reactions of complex metalloproteins studied by protein-film voltammetry. *Chemical Society Reviews* **1997,** 26, (3), 169-179. b) Anderson, L. J.; Richardson, D. J.; Butt, J. N., Using direct electrochemistry to probe rate limiting events during nitrate reductase turnover. *Faraday Discussions* **2000**, (116), 155-169. c) Angove, H. C.; Cole, J. A.; Richardson, D. J.; Butt, J. N., Protein film voltammetry reveals distinctive fingerprints of nitrite and hydroxylamine reduction by a cytochrome c nitrite reductase. *Journal of Biological Chemistry* **2002,** 277, (26), 23374-23381. d) Armstrong, F. A., Insights from protein film voltammetry into mechanisms of complex biological electron-transfer reactions. *Journal of the Chemical Society-Dalton Transactions* **2002**, (5), 661-671. e) Elliott, S. J.; Leger, C.; Pershad, H. R.; Hirst, J.; Heffron, K.; Ginet, N.; Blasco, F.; Rothery, R. A.; Weiner, J. H.; Armstrong, F. A., Detection and interpretation of redox potential optima in the catalytic activity of enzymes. *Biochimica Et Biophysica Acta-Bioenergetics* **2002,** 1555, (1-3), 54-59. f) Leger, C.; Elliott, S. J.; Hoke, K. R.; Jeuken, L. J. C.; Jones, A. K.; Armstrong, F. A., Enzyme electrokinetics: Using protein film voltammetry to investigate redox enzymes and their mechanisms. *Biochemistry* **2003,** 42, (29), 8653-8662. g) Liu, H. H.; Pang, D. W., Studies in electrochemistry of redox proteins. *Progress in Chemistry* **2002,** 14, (6), 425-432. h) Elliott, S. J.; Hoke, K. R.; Heffron, K.; Palak, M.; Rothery, R. A.; Weiner, J. H.; Armstrong, F. A., Voltammetric studies of the catalytic mechanism of the respiratory nitrate reductase from Escherichia coli: How nitrate reduction and inhibition depend on the oxidation state of the active site. *Biochemistry* **2004,** 43, (3), 799-807. i) Frangioni, B.; Arnoux, P.; Sabaty, M.; Pignol, D.; Bertrand, P.; Guigliarelli, B.; Leger, C., In Rhodobacter sphaeroides respiratory nitrate reductase, the kinetics of substrate binding favors intramolecular electron transfer. *Journal of the American Chemical Society* **2004,** 126, (5), 1328-1329.
3. Heering, H. A.; Hirst, J.; Armstrong, F. A., Interpreting the catalytic voltammetry of electroactive enzymes adsorbed on electrodes. *Journal of Physical Chemistry B* **1998,** 102, (35), 6889-6902.
4. Scott, D. L.; Paddock, R. M.; Bowden, E. F., The Electrocatalytic Enzyme Function of Adsorbed Cytochrome-C Peroxidase on Pyrolytic-Graphite. *Journal of Electroanalytical Chemistry* **1992,** 341, (1-2), 307-321.
5. Mondal, M. S.; Fuller, H. A.; Armstrong, F. A., Direct measurement of the reduction potential of catalytically active cytochrome c peroxidase compound I:

Voltammetric detection of a reversible, cooperative two-electron transfer reaction. *Journal of the American Chemical Society* **1996,** 118, (1), 263-264.

6. Mondal, M. S.; Goodin, D. B.; Armstrong, F. A., Simultaneous voltammetric comparisons of reduction potentials, reactivities, and stabilities of the high-potential catalytic states of wild-type and distal-pocket mutant (W51F) yeast cytochrome c peroxidase. *Journal of the American Chemical Society* **1998,** 120, (25), 6270-6276.

7. a) Moreno, C.; Franco, R.; Moura, I.; Legall, J.; Moura, J. J. G., Voltammetric Studies of the Catalytic Electron-Transfer Process between the Desulfovibrio-Gigas Hydrogenase and Small Proteins Isolated from the Same Genus. *European Journal of Biochemistry* **1993,** 217, (3), 981-989. b) Amine, A.; Deni, J.; Kauffmann, J. M., Amperometric Biosensor Based on Carbon-Paste Mixed with Enzyme, Lipid and Cytochrome-C. *Bioelectrochemistry and Bioenergetics* **1994,** 34, (2), 123-128. c) Verhagen, M. F. J. M.; Wolbert, R. B. G.; Hagen, W. R., Cytochrome C(553), from Desulfovibrio-Vulgaris (Hildenborough) - Electrochemical Properties and Electron-Transfer with Hydrogenase. *European Journal of Biochemistry* **1994,** 221, (2), 821-829. d) Willner, I.; Katz, E.; Willner, B.; Blonder, R.; HelegShabtai, V.; Buckmann, A. F., Assembly of functionalized monolayers of redox proteins on electrode surfaces: Novel bioelectronic and optobioelectronic systems. *Biosensors & Bioelectronics* **1997,** 12, (4), 337-356. e) Jin, W.; Wollenberger, U.; Kargel, E.; Schunck, W. H.; Scheller, F. W., Electrochemical investigations of the intermolecular electron transfer between cytochrome c and NADPH cytochrome P450 reductase. *Journal of Electroanalytical Chemistry* **1997,** 433, (1-2), 135-139. f) Abass, A. K.; Hart, J. P.; Cowell, D., Development of an amperometric sulfite biosensor based on sulfite oxidase with cytochrome c, as electron acceptor, and a screen-printed transducer. *Sensors and Actuators B-Chemical* **2000,** 62, (2), 148-153. g) Fridman, V.; Wollenberger, U.; Bogdanovskaya, V.; Lisdat, F.; Ruzgas, T.; Lindgren, A.; Gorton, L.; Scheller, F. W., Electrochemical investigation of cellobiose oxidation by cellobiose dehydrogenase in the presence of cytochrome c as mediator. *Biochemical Society Transactions* **2000,** 28, 63-70. h) Wirtz, M.; Klucik, J.; Rivera, M., Ferredoxin-mediated electrocatalytic dehalogenation of haloalkanes by cytochrome P450(cam). *Journal of the American Chemical Society* **2000,** 122, (6), 1047-1056. i) Liu, H. H.; Hill, H. A. O.; Chapman, S. K., Electrochemistry of the flavodehydrogenase domain of flavocytochrome b(2) engineered for L-mandelate dehydrogenase activity. *Journal of Electroanalytical Chemistry* **2001,** 500, (1-2), 598-603. j) Lopes, H.; Besson, S.; Moura, I.; Moura, J. J. G., Kinetics of inter- and intramolecular electron transfer of Pseudomonas nautica cytochrome cd(1) nitrite reductase: regulation of the NO-bound end product. *Journal of Biological Inorganic Chemistry* **2001,** 6, (1), 55-62. k) Takagi, K.; Yamamoto, K.; Kano, K.; Ikeda, T., New pathway of amine oxidation respiratory chain of Paracoccus denitrificans IFO 12442. *European Journal of Biochemistry* **2001,** 268, (2), 470-476. l) Lojou, E.; Cutruzzola, F.; Tegoni, M.; Bianco, P., Electrochemical study of the intermolecular electron transfer to Pseudomonas aeruginosa cytochrome cd(1) nitrite reductase. *Electrochimica Acta* **2003,** 48, (8), 1055-1064. m) Okuda, J.; Wakai, J.; Yuhashi, N.; Sode, K., Glucose enzyme electrode using cytochrome

b(562) as an electron mediator. *Biosensors & Bioelectronics* **2003,** 18, (5-6), 699-704.

8. Pardo-Yissar, V.; Katz, E.; Willner, I.; Kotlyar, A. B.; Sanders, C.; Lill, H., Biomaterial engineered electrodes for bioelectronics. *Faraday Discussions* **2000**, (116), 119-134.
9. Haas, A. S.; Pilloud, D. L.; Reddy, K. S.; Babcock, G. T.; Moser, C. C.; Blasie, J. K.; Dutton, P. L., Cytochrome c and cytochrome c oxidase: Monolayer assemblies and catalysis. *Journal of Physical Chemistry B* **2001,** 105, (45), 11351-11362.
10. a) Dopner, S.; Hildebrandt, P.; Rosell, F. I.; Mauk, A. G., Alkaline conformational transitions of ferricytochrome c studied by resonance Raman spectroscopy. *Journal of the American Chemical Society* **1998,** 120, (44), 11246-11255. b) Chen, X. X.; Ferrigno, R.; Yang, J.; Whitesides, G. A., Redox properties of cytochrome c adsorbed on self-assembled monolayers: A probe for protein conformation and orientation. *Langmuir* **2002,** 18, (18), 7009-7015. c) Wackerbarth, H.; Hildebrandt, P., Redox and conformational equilibria and dynamics of cytochrome c at high electric fields. *Chemphyschem* **2003,** 4, (7), 714-724.
11. a) Hirota, S.; Hayamizu, K.; Endo, M.; Hibino, T.; Takabe, T.; Kohzuma, T.; Yamauchi, O., Plastocyanin-peptide interactions. Effects of lysine peptides on protein structure and electron-transfer character. *Journal of the American Chemical Society* **1998,** 120, (32), 8177-8183. b) Rivera, M.; Seetharaman, R.; Girdhar, D.; Wirtz, M.; Zhang, X. J.; Wang, X. Q.; White, S., The reduction potential of cytochrome b(5) is modulated by its exposed heme edge. *Biochemistry* **1998,** 37, (6), 1485-1494. c) Johnson, D. L.; Maxwell, C. J.; Losic, D.; Shapter, J. G.; Martin, L. L., The influence of promoter and of electrode material on the cyclic voltammetry of Pisum sativum plastocyanin. *Bioelectrochemistry* **2002,** 58, (2), 137-147.
12. Baymann, F.; Barlow, N. L.; Aubert, C.; Schoepp-Cothenet, B.; Leroy, G.; Armstrong, F. A., Voltammetry of a 'protein on a rope'. *Febs Letters* **2003,** 539, (1-3), 91-94.
13. Louie, G. V.; Brayer, G. D., High-Resolution Refinement of Yeast Iso-1-Cytochrome-C and Comparisons with Other Eukaryotic Cytochromes-C. *Journal of Molecular Biology* **1990,** 214, (2), 527-555.
14. Moench, S. J.; Satterlee, J. D., Proton Nmr Comparison of the Saccharomyces-Cerevisiae Ferricytochrome-C Isozyme-1 Monomer and Covalent Disulfide Dimer. *Journal of Biological Chemistry* **1989,** 264, (17), 9923-9931.
15. Pelletier, H.; Kraut, J., Crystal-Structure of a Complex between Electron-Transfer Partners, Cytochrome-C Peroxidase and Cytochrome-C. *Science* **1992,** 258, (5089), 1748-1755.
16. Worrall, J. A. R.; Kolczak, U.; Canters, G. W.; Ubbink, M., Interaction of yeast iso-1-cytochrome c with cytochrome c peroxidase investigated by [N-15,H-1] heteronuclear NMR spectroscopy. *Biochemistry* **2001,** 40, (24), 7069-7076.
17 a) Hunte, C.; Solmaz, S.; Lange, C., Electron transfer between yeast cytochrome bc(1) complex and cytochrome c: a structural analysis. *Biochimica Et Biophysica Acta-Bioenergetics* **2002,** 1555, (1-3), 21-28. b) Lange, C.; Hunte, C., Crystal structure of the yeast cytochrome bc(1) complex with its bound substrate

cytochrome c. *Proceedings of the National Academy of Sciences of the United States of America* **2002,** 99, (5), 2800-2805.

18. Dopner, S.; Hildebrandt, P.; Rosell, F. I.; Mauk, A. G.; von Walter, M.; Buse, G.; Soulimane, T., The structural and functional role of lysine residues in the binding domain of cytochrome c in the electron transfer to cytochrome c oxidase. *European Journal of Biochemistry* **1999,** 261, (2), 379-391.
19. a) Roberts, V. A.; Pique, M. E., Definition of the Interaction Domain for Cytochrome c on Cytochrome c Oxidase. III prediction of the docked complex by a complete, systematic search, *J. Biol. Chem.*, **1999**, 274, 38051-38060 b) Flock, D.; Helms, V., Protein-protein docking of electron transfer complexes: Cytochrome c oxidase and cytochrome c. *Proteins-Structure Function and Genetics* **2002,** 47, (1), 75-85.
20. Kotlyar, A.; Borovok, N.; Hazani, M.; Szundi, I.; Einarsdottir, O., Photoinduced intracomplex electron transfer between cytochrome c oxidase and TUPS-modified cytochrome c. *European Journal of Biochemistry* **2000,** 267, (18), 5805-5809.
21. a) Wood, L. L.; Cheng, S. S.; Edmiston, P. L.; Saavedra, S. S., Molecular orientation distributions in protein films .2. Site-directed immobilization of yeast cytochrome c on thiol-capped, self-assembled monolayers. *Journal of the American Chemical Society* **1997,** 119, (3), 571-576. b) Edmiston, P. L.; Saavedra, S. S., Molecular orientation distributions in protein films: III. Yeast cytochrome c immobilized on pyridyl disulfide-capped phospholipid bilayers. *Biophysical Journal* **1998,** 74, (2), 999-1006. c) Edwards, A. M.; Zhang, K.; Nordgren, C. E.; Blasie, J. K., Heme structure and orientation in single monolayers of cytochrome c on polar and nonpolar soft surfaces. *Biophysical Journal* **2000,** 79, (6), 3105-3117. c) Tronin, A.; Edwards, A. M.; Wright, W. W.; Vanderkooi, J. M.; Blasie, J. K., Orientation distributions for cytochrome c on polar and nonpolar interfaces by total internal reflection fluorescence. *Biophysical Journal* **2002,** 82, (2), 996-1003.
22. Taking 1YCC.PDB (ref. 13) as starting point, reorientation of the three C-terminal amino acids Ala101, Cys102, and Glu103, avoiding overlapping van der Waals radii, results in a surface-exposed thiol at a distance of ~1.6 nm from the burried heme edge. Experimentally, a distance >1.5 nm between the heme and a spin label attached to Cys102 has been found: Qu, K. B.; Vaughn, J. L.; Sienkiewicz, A.; Scholes, C. P.; Fetrow, J. S., Kinetics and motional dynamics of spin-labeled yeast iso-1-cytochrome c .1. Stopped-flow electron paramagnetic resonance as a probe for protein folding/unfolding of the C-terminal helix spin-labeled at cysteine 102. *Biochemistry* **1997,** 36, (10), 2884-2897.
23. Page, C. C.; Moser, C. C.; Chen, X. X.; Dutton, P. L., Natural engineering principles of electron tunnelling in biological oxidation-reduction. *Nature* **1999,** 402, (6757), 47-52.
24. a) Hansen, A. G.; Boisen, A.; Nielsen, J. U.; Wackerbarth, H.; Chorkendorff, I.; Andersen, J. E. T.; Zhang, J. D.; Ulstrup, J., Adsorption and interfacial electron transfer of Saccharomyces cerevisiae yeast cytochrome c monolayers on Au(111) electrodes. *Langmuir* **2003,** 19, (8), 3419-3427. b) Zhang, J. D.; Grubb, M.; Hansen, A. G.; Kuznetsov, A. M.; Boisen, A.; Wackerbarth, H.; Ulstrup, J., Electron transfer behaviour of biological macromolecules towards the single-

molecule level. *Journal of Physics-Condensed Matter* **2003,** 15, (18), S1873-S1890.

25. Bonanni, B.; Alliata, D.; Bizzarri, A. R.; Cannistraro, S., Topological and electron-transfer properties of yeast cytochrome c adsorbed on bare gold electrodes. *Chemphyschem* **2003,** 4, (11), 1183-1188.
26. Girsch, P.; deVries, S., Purification and initial kinetic and spectroscopic characterization of NO reductase from Paracoccus denitrificans. *Biochimica Et Biophysica Acta-Bioenergetics* **1997,** 1318, (1-2), 202-216.
27. Moir, J. W. B.; Baratta, D.; Richardson, D. J.; Ferguson, S. J., The Purification of a Cd1-Type Nitrite Reductase from, and the Absence of a Copper-Type Nitrite Reductase from, the Aerobic Denitrifier Thiosphaera-Pantotropha - the Role of Pseudoazurin as an Electron-Donor. *European Journal of Biochemistry* **1993,** 212, (2), 377-385.
28. Lide, D.L. (Ed.) *Handbook of Chemistry and physics*, 81st ed.; CRC press LLC., 2000.
29. Hagen, W. R., Direct Electron-Transfer of Redox Proteins at the Bare Glassy-Carbon Electrode. *European Journal of Biochemistry* **1989,** 182, (3), 523-530.
30. Heering, H. A.; Mondal, M. S.; Armstrong, F. A., Using the pulsed nature of staircase cyclic voltammetry to determine interfacial electron-transfer rates of adsorbed species. *Analytical Chemistry* **1999,** 71, (1), 174-182.
31. Press, W.H.; Flannery, B.P.; Teukolsky, S.A.; Vetterling, W.T. *Numerical Recipes in Pascal*; Cambridge University Press, 1989.
32. Eddowes, M. J.; Hill, H. A. O., Novel Method for Investigation of Electrochemistry of Metalloproteins - Cytochrome-C. *Journal of the Chemical Society-Chemical Communications* **1977**, (21), 771-772.
33. Terrettaz, S.; Cheng, J.; Miller, C. J., Kinetic parameters for cytochrome c via insulated electrode voltammetry. *Journal of the American Chemical Society* **1996,** 118, (33), 7857-7858.
34. a)Rafferty, S. P.; Pearce, L. L.; Barker, P. D.; Guillemette, J. G.; Kay, C. M.; Smith, M.; Mauk, A. G., Electrochemical, Kinetic, and Circular Dichroic Consequences of Mutations at Position-82 of Yeast Iso-1-Cytochrome-C. *Biochemistry* **1990,** 29, (40), 9365-9369. b) Davies, A. M.; Guillemette, J. G.; Smith, M.; Greenwood, C.; Thurgood, A. G. P.; Mauk, A. G.; Moore, G. R., Redesign of the Interior Hydrophilic Region of Mitochondrial Cytochrome-C by Site-Directed Mutagenesis. *Biochemistry* **1993,** 32, (20), 5431-5435. c) Pollock, W. B. R.; Rosell, F. I.; Twitchett, M. B.; Dumont, M. E.; Mauk, A. G., Bacterial expression of a mitochondrial cytochrome c. Trimethylation of Lys72 in yeast iso-1-cytochrome c and the alkaline conformational transition. *Biochemistry* **1998,** 37, (17), 6124-6131. d) Lett, C. M.; Guillemette, J. G., Increasing the redox potential of isoform 1 of yeast cytochrome c through the modification of select haem interactions. *Biochemical Journal* **2002,** 362, 281-287.
35. El Kasmi, A.; Leopold, M. C.; Galligan, R.; Robertson, R. T.; Saavedra, S. S.; El Kacemi, K.; Bowden, E. F., Adsorptive immobilization of cytochrome c on indium/tin oxide (ITO): electrochemical evidence for electron transfer-induced conformational changes. *Electrochemistry Communications* **2002,** 4, (2), 177-181.

36. Feldberg, S. W.; Rubinstein, I., Unusual Quasi-Reversibility (Uqr) or Apparent Non-Kinetic Hysteresis in Cyclic Voltammetry - an Elaboration Upon the Implications of N-Shaped Free-Energy Relationships as Explanation. *Journal of Electroanalytical Chemistry* **1988,** 240, (1-2), 1-15.
37. Armstrong, F. A.; Camba, R.; Heering, H. A.; Hirst, J.; Jeuken, L. J. C.; Jones, A. K.; Leger, C.; McEvoy, J. P., Fast voltammetric studies of the kinetics and energetics of coupled electron-transfer reactions in proteins. *Faraday Discussions* **2000**, (116), 191-203.
38. Jeuken, L. J. C., Conformational reorganisation in interfacial protein electron transfer. *Biochimica Et Biophysica Acta-Bioenergetics* **2003,** 1604, (2), 67-76.
39. Bard, A. J.; Faulkner, L. R. *Electrochemical methods: fundamentals and applications*, 2nd ed.; John Wiley & Sons, 2001.
40. Battistuzzi, G.; Borsari, M.; Sola, M., Medium and temperature effects on the redox chemistry of cytochrome c. *European Journal of Inorganic Chemistry* **2001**, (12), 2989-3004.
41. Delauder, S. F.; Mauro, J. M.; Poulos, T. L.; Williams, J. C.; Schwarz, F. P., Thermodynamics of Hydrogen-Cyanide and Hydrogen-Fluoride Binding to Cytochrome-C Peroxidase and Its Asn-82-]Asp Mutant. *Biochemical Journal* **1994,** 302, 437-442.
42. Goodin, D. B.; Davidson, M. G.; Roe, J. A.; Mauk, A. G.; Smith, M., Amino-Acid Substitutions at Tryptophan-51 of Cytochrome-C Peroxidase - Effects on Coordination, Species Preference for Cytochrome-C, and Electron-Transfer. *Biochemistry* **1991,** 30, (20), 4953-4962.
43. Villegas, J. A.; Mauk, A. G.; Vazquez-Duhalt, R., A cytochrome c variant resistant to heme degradation by hydrogen peroxide. *Chemistry & Biology* **2000,** 7, (4), 237-244.
44. Baker, S. C.; Saunders, N. F. W.; Willis, A. C.; Ferguson, S. J.; Hajdu, J.; Fulop, V., Cytochrome cd(1) structure: Unusual haem environments in a nitrite reductase and analysis of factors contributing to beta-propeller folds. *Journal of Molecular Biology* **1997,** 269, (3), 440-455.
45. Richter, C. D.; Allen, J. W. A.; Higham, C. W.; Koppenhofer, A.; Zajicek, R. S.; Watmough, N. J.; Ferguson, S. J., Cytochrome cd(1), reductive activation and kinetic analysis of a multifunctional respiratory enzyme. *Journal of Biological Chemistry* **2002,** 277, (5), 3093-3100.
46. Wasser, I. M.; de Vries, S.; Moenne-Loccoz, P.; Schroder, I.; Karlin, K. D., Nitric oxide in biological denitrification: Fe/Cu metalloenzyme and metal complex NOx redox chemistry. *Chemical Reviews* **2002,** 102, (4), 1201-1234.
47. Zumft, W. G., Cell biology and molecular basis of denitrification. *Microbiology and Molecular Biology Reviews* **1997,** 61, (4), 533-+.
48. (a) Subtraction of a bare gold electrode blank is not sufficient for analysis because slight differences after polishing and cleaning yield differences in the background current that are relatively small, yet many times larger than the YCC peaks. (b) The voltammograms in the presence of enzyme and substrate are more noisy compared to the background. In part, this is expected because of the difference in the number of averaged traces (3 versus 10). Additional noise is probably

generated by small fluctuations in the diffusion profile due to the long time scale of the measurement.

49. Barker, P. D.; Bertini, I.; Del Conte, R.; Ferguson, S. J.; Hajieva, P.; Tomlinson, E.; Turano, P.; Viezzoli, M. S., A further clue to understanding the mobility of mitochondrial yeast cytochrome c - A N-15 T-1 rho investigation of the oxidized and reduced species. *European Journal of Biochemistry* **2001,** 268, (16), 4468-4476.
50. Pyka, J.; Osyczka, A.; Turyna, B.; Blicharski, W.; Froncisz, W., EPR studies of iso-1-cytochrome c: effect of temperature on two-component spectra of spin label attached to cysteine at positions 102 and 47. *European Biophysics Journal with Biophysics Letters* **2001,** 30, (5), 367-373.
51. Marcus, R. A.; Sutin, N., Electron Transfers in Chemistry and Biology. *Biochimica Et Biophysica Acta* **1985,** 811, (3), 265-322.
52. Gray, H. B.; Winkler, J. R., Electron tunneling in structurally engineered proteins. *Journal of Electroanalytical Chemistry* **1997,** 438, (1-2), 43-47.
53. a) Moser, C. C.; Keske, J. M.; Warncke, K.; Farid, R. S.; Dutton, P. L., Nature of Biological Electron-Transfer. *Nature* **1992,** 355, (6363), 796-802. b) Gray, H. B.; Winkler, J. R., Electron transfer in proteins. *Annual Review of Biochemistry* **1996,** 65, 537-561. c) Moser, C. C.; Page, C. C.; Chen, X.; Dutton, P. L., Biological electron tunneling through native protein media. *Journal of Biological Inorganic Chemistry* **1997,** 2, (3), 393-398. d) Winkler, J. R.; Gray, H. B., Electron tunneling in proteins: Role of the intervening medium. *Journal of Biological Inorganic Chemistry* **1997,** 2, (3), 399-404.
54. a) Chidsey, C. E. D., Free-Energy and Temperature-Dependence of Electron-Transfer at the Metal-Electrolyte Interface. *Science* **1991,** 251, (4996), 919-922. b) Chidsey, C. E. D., Correction. *Science* **1991,** 252, (5006), 631-631.
55. Honeychurch, M. J., Effect of electron-transfer rate and reorganization energy an the cyclic voltammetric response of redox adsorbates. *Langmuir* **1999,** 15, (15), 5158-5163.
56. Adams, D. M.; Brus, L.; Chidsey, C. E. D.; Creager, S.; Creutz, C.; Kagan, C. R.; Kamat, P. V.; Lieberman, M.; Lindsay, S.; Marcus, R. A.; Metzger, R. M.; Michel-Beyerle, M. E.; Miller, J. R.; Newton, M. D.; Rolison, D. R.; Sankey, O.; Schanze, K. S.; Yardley, J.; Zhu, X. Y., Charge transfer on the nanoscale: Current status. *Journal of Physical Chemistry B* **2003,** 107, (28), 6668-6697.
57. Two major differences with the single Donor-Acceptor model are noted: because all levels contribute, the inverted regions of the individual levels are compensated and do not appear in the total rate constant. Furthermore, the reorganization energy is associated with the half-reaction of the redox center only, because the electrode does not contribute to it.
58. For equine cytochrome *c*, electrostatically adsorbed with the heme cleft towards a carboxyl-terminated self-assembled monolayer on gold, Murgida and Hildebrandt reported that the reorganization energy is 0.22 eV, which is substantially lower compared to solution due to exclusion of water: a) Murgida, D. H.; Hildebrandt, P., Electrostatic-field dependent activation energies modulate electron transfer of cytochrome c. *Journal of Physical Chemistry B* **2002,** 106, (49), 12814-12819. b) Hildebrandt, P.; Murgida, D. H., Electron transfer dynamics of cytochrome c

bound to self-assembled monolayers on silver electrodes. *Bioelectrochemistry* **2002,** 55, (1-2), 139-143. However, since in our system the heme cleft is facing the solution, we assume that the reorganization energy is equal to that of YCC in solution.

59. For gold, the effective density of electronic states near the Fermi level is 0.3 eV^{-1} per atom (Papaconstantopoulos, D. A. *Handbook of the band structure of elemental solids*, Plenum Press: New York, **1986**). Since the thiol sulfur most likely binds to three surface gold atoms (Tachibana, M.; Tanaka, S.; Yamashita, Y.; Yoshizawa, K., Small band-gap polymers involving tricyclic nonclassical thiophene as a building block. *Journal of Physical Chemistry B* **2002,** 106, (14), 3549-3556.), we use ρ=0.9 eV^{-1}, which is similar to the estimated ρ=1 eV^{-1} for ferrocene-terminated alkanethiols studied by Chidsey (ref. 54).
60. a) Xie, A.; van der Meer, L.; Austin, R. H., Excited-state lifetimes of far-infrared collective modes in proteins. *Journal of Biological Physics* **2002,** 28, (2), 147-154. b) Morita, T.; Kimura, S., Long-range electron transfer over 4 nm governed by an inelastic hopping mechanism in self-assembled monolayers of helical peptides. *Journal of the American Chemical Society* **2003,** 125, (29), 8732-8733.
61. Zheng, J. W.; Ye, S. Y.; Lu, T. H.; Cotton, T. M.; Chumanov, G., Circular dichroism and resonance Raman comparative studies of wild type cytochrome c and F82H mutant. *Biopolymers* **2000,** 57, (2), 77-84.
62. Fulop, V.; Moir, J. W. B.; Ferguson, S. J.; Hajdu, J., The Anatomy of a Bifunctional Enzyme - Structural Basis for Reduction of Oxygen to Water and Synthesis of Nitric-Oxide by Cytochrome Cd(1). *Cell* **1995,** 81, (3), 369-377.
63. Koppenhofer, A.; Turner, K. L.; Allen, J. W. A.; Chapman, S. K.; J., Cytochrome cd(1) from Parococcus pantotrophus exhibits kinetically gated, conformationally dependent, highly cooperative two-electron redox behavior. *Biochemistry* **2000,** 39, (15), 4243-4249.
64. Blatt, Y.; Pecht, I., Allosteric Cooperative Interactions among Redox Sites of Pseudomonas Cytochrome-Oxidase. *Biochemistry* **1979,** 18, (13), 2917-2922.
65. Farver, O.; Kroneck, P. M. H.; Zumft, W. G.; Pecht, I., Allosteric control of internal electron transfer in cytochrome cd(1) nitrite reductase. *Proceedings of the National Academy of Sciences of the United States of America* **2003,** 100, (13), 7622-7625.
66. a) Gronberg, K. L. C.; Roldan, M. D.; Prior, L.; Butland, G.; Cheesman, M. R.; Richardson, D. J.; Spiro, S.; Thomson, A. J.; Watmough, N. J., A low-redox potential heme in the dinuclear center of bacterial nitric oxide reductase: Implications for the evolution of energy-conserving heme-copper oxidases. *Biochemistry* **1999,** 38, (42), 13780-13786. b) Field, S. J.; Prior, L.; Roldan, M. D.; Cheesman, M. R.; Thomson, A. J.; Spiro, S.; Butt, J. N.; Watmought, N. J.; Richardson, D. J., Spectral properties of bacterial nitric-oxide reductase - Resolution of pH-dependent forms of the active site heme b(3). *Journal of Biological Chemistry* **2002,** 277, (23), 20146-20150.
67. a) Moenne-Loccoz, P.; de Vries, S., Structural characterization of the catalytic high-spin heme b of nitric oxide reductase: A resonance Raman study. *Journal of the American Chemical Society* **1998,** 120, (21), 5147-5152. b) Moenne-Loccoz, P.; Richter, O. M. H.; Huang, H. W.; Wasser, I. M.; Ghiladi, R. A.; Karlin, K. D.;

de Vries, S., Nitric oxide reductase from Paracoccus denitrificans contains an oxo-bridged heme/non-heme diiron center. *Journal of the American Chemical Society* **2000,** 122, (38), 9344-9345.

Summary

Oxygen respiration is the most profitable way of energy production for living organisms. In oxygen respiration energy is conserved by means of a proton electrochemical gradient, which is used to drive a great number of cellular processes. The gradient is built up by the respiratory chain, which consists of four membrane bound enzyme complexes. The final enzyme of this chain, cytochrome *c* oxidase (complex IV) reacts with oxygen reducing it to water, a reaction that requires four electrons and four protons. To generate a proton electrochemical gradient, the cytochrome *c* oxidase takes up four protons from the N-side of the membrane to convert oxygen to water, the so-called chemical protons. In addition, four protons –the so-called pumped protons– are translocated from the N-side to P-side of the membrane during the catalytic cycle. The total uptake of eight protons yields a greater than 85% energy conversion efficiency. In the past decades the crystal structure of cytochrome *c* oxidase has been resolved highlighting its intricate transmembrane structure, the four redox cofactors and two proton pathways. Kinetic experiments have identified several key intermediates of the catalytic cycle. While these studies indicate how cytochrome *c* oxidase converts oxygen to water, the proton pumping mechanism and its key elements have remained elusive. In this thesis the relation between electron transfer and the structure of the proton pump has been investigated.

The reaction of cytochrome *c* oxidase with oxygen and the subsequent steps are very fast, from a few microseconds to several milliseconds. To resolve the various steps and to elucidate the proton pumping mechanism a microsecond freeze-hyperquenching mixing/sampling device (MHQ) was constructed in house previously. The MHQ set up was developed further and its performance tested in detail (Chapter 2). The MHQ setup enables one to quickly mix two reactants and quench the reaction after various times by rapid freezing of the reaction mixture on a rotating cold plate down to a temperature of 77K. The frozen sample can be analyzed by various techniques such as low-temperature UV-Vis, EPR and Resonance Raman spectroscopy. The improved MHQ device has a total dead-time of 75 - 85 μs. The dead-time is composed of the mixing time (< 2 μs), a minimal time of flight of 25 μs and a freezing time of 50 - 60 μs.

In Chapter 3 a specially designed cuvette is described enabling low temperature UV-Vis spectroscopy on frozen MHQ powder samples. By slowly increasing the temperature of a powder of freeze-quenched cytochrome *c* oxidase the enzyme went through its catalytic cycle displaying the characteristic spectra of the A, P, F and O intermediates.

Chapter 4 describes the trapping of a shortly lived intermediate (~ 100 μs) in the reaction between metmyoglobin and azide. Resonance Raman spectroscopy indicated that this intermediate was a high-spin ferric heme azide adduct.

In Chapters 5 and 6 an extensive kinetic study of cytochrome *c* oxidase is presented for the reaction of the fully reduced enzyme with oxygen. The kinetics of the four redox cofactors were analyzed by low temperature UV-Vis and EPR spectroscopy. During the reaction, a tryptophan radical is formed, which was shown by Q-band EPR spectroscopy to originate from the absolutely conserved tryptophan 272 (W272). The radical is formed between the F and O_H state in the new state F_{W*}. Kinetic analysis showed that the radical is formed relatively slowly - $t_{1/2}$=1200 μs, i.e. the rate limiting step- and broken down rapidly ($t_{1/2}$=60μs). During the transition from F to O_H a proton is pumped across the membrane. We propose that W272 is a key amino acid in this proton pumping step by acting as a redox-linked acid-base catalyst.

Electrochemical techniques are like kinetics capable of solving enzyme mechanisms. In the final Chapter 7, a monolayer of yeast iso-1 cytochrome *c* was applied on a gold electrode as an electron mediator to nitric oxide reductase and nitrite reductase allowing detection of zeptomole quantities of nitrite reductase. The activity of nitric oxide reductase was found to be determined by the redox state of the high-spin heme *b*. Cytochrome *c* oxidase was also shown to be reactive with the iso-1 cytochrome *c* monolayer as evidenced by the CO sensitive reduction of oxygen.

Samenvatting

Zuurstofverbranding is de meest efficiënte manier, waarop levende organismen energie produceren. Bij zuurstofverbranding wordt energie geconserveerd door middel van een proton electrochemische gradient, die weer gebruikt kan worden voor allerlei verschillende processen in de cel. De gradient wordt opgebouwd door de ademhalingsketen, die uit vier verschillende membraangebonden complexen bestaat. Het laatste enzym, cytochroom *c* oxidase (complex IV), reageert met zuurstof en reduceert dit tot water. Hierbij worden vier protonen en vier electronen gebruikt. Om een proton electrochemische gradient op te bouwen worden vier protonen opgenomen van de N-zijde van het membraan om water te vormen, de zogenoemde chemische protonen. Er worden tevens vier extra protonen – de zogenaamde gepompte protonen- van de N-zijde naar de P-zijde van het membraan getransporteerd tijdens de katalytische cyclus. De efficiëntie van energieconservering is daardoor groter dan 85%. In de afgelopen tientallen jaren is de kristalstructuur van cytochroom *c* oxidase opgehelderd waarin de complexe transmembraanstructuur zichtbaar is, alsmede de vier redox cofactoren en twee protonkanalen. Kinetische experimenten hebben een aantal belangrijke intermediairen aangetoond in de katalytische cyclus van cytochroom *c* oxidase. Ofschoon deze experimenten veel opheldering hebben verschaft met betrekking tot de reductie van zuurstof naar water, is er relatief weinig bekend over het protonpomp mechanisme en in het bijzonder welke aminozuren daarbij betrokken zouden zijn. In dit proefscrhift is de relatie tussen electronoverdracht en de structuur van de protonpomp onderzocht.

De reactie van cytochrome *c* oxidase met zuurstof en de vervolgstappen verlopen erg snel, varierend van een paar microseconde tot enkele milliseconden. Om de verschillende stappen en het protonpomp mechanisme op te helderen is eerder een microseconde vries/hyperquench apparaat (MHQ) ontworpen en gebouwd. Dit apparaat is verder ontwikkeld en uitvoerig getest (Hoofdstuk 2). De MHQ maakt het mogelijk om twee reactanten zeer snel te mengen en de reactie te stoppen op een roterende cilinder die gekoeld is tot 77 Kelvin, op verschillende tijdstippen van de reactie. Het ingevroren sample kan geanalyseerd worden met verschillende technieken zoals lage temperatuur UV-Vis, EPR of Resonantie Raman spectroscopie. De verbeterde versie van de MHQ heeft een totale dode tijd

van 75 tot 85 μs. De dode tijd is de som van de mengtijd (minder dan 2 μs), de minimale reactietijd van 25 μs en de vriestijd van 50 tot 60 μs.

In Hoofdstuk 3 wordt een speciaal ontworpen cuvet beschreven waarmee het mogelijk is om lage temperatuur UV-Vis spectroscopie te doen aan de ingevroren poedervormige MHQ monsters. Door langzaam de temperatuur van het ingevroren poeder met cytochrome *c* oxidase te verhogen, reageert het enzym langzaam en gecontroleerd verder en konden de karakteristieke spectra van de A, P, F en O toestanden opgenomen worden.

Hoofdstuk 4 beschrijft de detectie van een kort levend (~100 μs) intermediair in de reactie tussen metmyoglobine en azide. Met Resonantie Raman spectroscopie kon aangetoond worden dat dit intermediair een high-spin ferric heem azide complex is.

De Hoofdstukken 5 en 6 beschrijven een uitvoerige studie van volledig gereduceerd cytochroom *c* oxidase in reactie met zuurstof. De kinetiek van de vier redox cofactoren is bestudeerd met lage temperatuur UV-Vis en EPR spectroscopie. Met Q-band EPR spectroscopie is aangetoond dat tijdens de reactie een tryptofaan radicaal gevormd wordt dat afkomstig is van de strikt geconserveerde tryptofaan 272 (W272). Het radicaal wordt gevormd tussen de F en O_H toestanden, in de nieuwe toestand F_{W*}. Kinetische analyses hebben aangetoond dat het radicaal relatief langzaam gevormd wordt ($t_{1/2}$ = 1200 μs), hetgeen snelheidsbepalend is voor de reactie, en weer snel verdwijnt ($t_{1/2}$ = 60 μs). Tijdens de overgang van de F naar O_H toestand wordt een proton gepompt. Wij postuleren dat de W272 een sleutelrol speelt in deze protonpomp stap door als een redox gekoppelde zuur-base katalysator op te treden.

Met behulp van elektrochemische technieken is het, net als met kinetische studies, mogelijk om enzymmechanismen op te helderen. In het laatste hoofdstuk, Hoofdstuk 7, wordt een enkele laag van gist iso-1 cytochroom *c* aangebracht op een goudelektrode. Deze gemodificeerde elektrode wordt gebruikt als elektronenmediator voor nitriet reductase en NO reductase waarmee zeptomolen nitriet reductase gedetecteerd kunnen worden. De activiteit van NO reductase wordt bepaald door de redoxtoestand van de high-spin heem *b*. Cytochroom *c* oxidase blijkt ook electronen te accepteren van de gemodificeerde iso-1 cytochroom *c* electrode zoals blijkt uit de CO-gevoelige omzetting van zuurstof door cytochroom *c* oxidase.

Curriculum Vitae

Frank Gerard Marie Wiertz werd geboren op 31 oktober 1975 te Heerlen. Hij behaalde zijn gymnasium diploma (met klassiek Grieks) in 1994 aan de voormalige Scholengemeenschap Sint Michiel in Geleen (heden ten dagen het Graaf Huyn College). Aansluitend volgde een studie in de Bioprocestechnologie aan de Landbouw Universiteit Wageningen. Na een afstudeervak in de vakgroep Industriële Microbiologie onder begeleiding van dr. C.A.G.M. Weijers en prof. dr. J. De Bont en een stage bij TNO-Voeding in Zeist onder begeleiding van ing. N. Van Biezen en Dr. Z. Yang sloot hij zijn studie met succes af in 2000.
Hij begon in 2000 zijn promotie onderzoek bij prof. dr. G. Van Dedem en prof. dr. C. Dekker. Na 2 jaar heeft hij zijn onderzoek voortgezet in de Enzymologie groep bij Prof. Dr. S. de Vries waar hij zijn uiteindelijke promotieonderzoek voltooide getiteld 'electron transport and proton pumping pathways in cytochrome $aa_{3'}$. Het onderzoek aan cytochroom *c* oxidase gebeurde in een samenwerkings verband met de groep van prof. dr. B. Ludwig aan de J-W.G Universiteit te Frankfurt. De resultaten van het onderzoek in de verschillende groepen staan beschreven in dit proefschrift.
Frank is momenteel bezig als postdoc aan de Universiteit Leiden onder begeleiding van dr. ir. H. A. Heering. Hij onderzoekt het reactie mechanisme van cytochrome *c* oxidase met behulp van electrochemische technieken.

List of publications

1 **F.G.M. Wiertz**, O-M. H. Richter, B. Ludwig, S. de Vries, "Kinetic resolution of a tryptophan-radical intermediate in the reaction cycle of Paracoccus denitrificans cytochrome c oxidase" Journal of Biological chemistry,**2007**,282,43,31580-31591 2.

2 **F.G.M. Wiertz** and S. de Vries, "Low-temperature kinetic measurements of microsecond freeze-hyperquench (MHQ) cytochrome oxidase monitored by UV-visible spectroscopy with a newly designed cuvette", Biochemical society transactions,2006, 34, 136-138

3 S. Lu, **F.G.M. Wiertz**, S. de Vries, P. Moenne-Loccoz, "Resonance Raman characterization of a high-spin six-coordinate iron(III) intermediate in metmyoglobin-azido complex formation trapped by microsecond freeze-hyperquenching (MHQ)", Journal of Raman Spectroscopy,2005, 36, 4, 359-362

4 **F.G.M. Wiertz**, O-M. H. Richter ,A.V. Cherepanov, F. MacMillan, B. Ludwig, S. de Vries, "An oxo-ferryl tryptophan radical catalytic intermediate in cytochrome c and quinol oxidases trapped by microsecond freeze-hyperquenching (MHQ), **2004**, FEBS Letters, 575, 1-3, 127-130

5 H.A. Heering, **F.G.M. Wiertz**, C. Dekker, S. de Vries, "Direct immobilization of native yeast Iso-1 cytochrome c on bare gold: Fast electron relay to redox enzymes and zeptomole protein-film voltammetry", **2004**, Journal of the American Chemical Society, 126, 35, 11103-11112

6 J.O Lee, G. Lientschnig, **F.G.M Wiertz**, M. Struijk, R.A.J. Janssen, R. Egberink, D.N. Reinhoudt, A.C. Grimsdale, K. Mullen, P. Hadley, C. Dekker, "Electrical transport study of phenylene-based pi-conjugated molecules in a three-terminal geometry", **2003**, Molecular electronics III, 1006, 122-132

7 K. Besteman, J.O. Lee, **F.G.M. Wiertz**, H.A. Heering, C. Dekker, "Enzyme-coated carbon nanotubes as single-molecule biosensors",2003, Nano Letters, 3, 6, 727-730

8 J.O Lee, G. Lientschnig, **F.G.M Wiertz**, M. Struijk, R.A.J. Janssen, R. Egberink, D.N. Reinhoudt, P. Hadley, C. Dekker, "Absence of strong gate effects in electrical measurements on phenylene-based conjugated molecules", Nano Letters, 3, 2, 113-117

Dankwoord

Eindelijk ben ik dan beland bij het laatste stukje van mijn proefschrift. Ik mag terugblikken op een tijd waarin ik veel plezier beleefde in de verschillende groepen waar ik gewerkt heb tijdens mijn AIO-schap. Net zoals alle andere proefschriften is dit proefschrift niet door de auteur alleen tot stand gekomen. Ik durf zelfs te beweren dat het onmogelijk zou zijn geweest zonder een aantal mensen die in meerdere of mindere mate hebben bijgedragen aan het onderzoek en/of de zaken daaromheen. Ik wil me er daarom van verzekeren niemand te vergeten door nu alvast iedereen te bedanken die mij geholpen heeft.

Ten eerste bedank ik Gijs van Dedem en Cees Dekker onder wier leiding ik eerste twee jaar van mijn onderzoek gedaan heb in de groep van Cees Dekker. Gijs heel hartelijk bedankt voor het vertrouwen dat je in me stelde. Ondanks dat je weinig tijd had, was er altijd een plekje in je agenda voor goede raad en nuttige discussies. Cees, jij hartelijk bedankt dat ik voor de gastvrije ontvangst in je groep, hoewel ik een eend was in een voor mij vreemde bijt. Je altijd positieve houding ten opzichte van elke situatie waren erg verfrissend en ik mis de levendige discussies. De mensen in de toen kersverse biofysica groep, John, Arnold, Serge, Henk, Thijn, Koen, Jacob en Ralph, hartelijk dank voor de gezellige en leerzame tijd en voor het geduldig uitleggen van de fysica kant van de biofysica. Het heeft mij een heel andere kijk op onderzoek gegeven.

Zo ergens midden in het dankwoord kom ik bij mijn huidige promotor Simon. Jij nam de zware taak op je om in drie jaar tijd mij een volwaardige promotie te laten doen. Mijn respect en dank daarvoor dat je die uitdaging bent aangegaan. Niet alleen als begeleider heb ik je leren kennen maar ook als de persoon Simon. De road-trips, congressen en koffie/peuk pauzes die we samen hadden, hebben mooie herinneringen bij mij achtergelaten. Ik zal de zin en onzin discussies die we hadden missen! Hierdoor ben ik je als vriend en begeleider gaan zien.

Marc, als “partner in freeze-hyperquenching” hebben we menig uur met onze handen in het haar en in de vloeibare stikstof gezeten! Je praktische handigheden en je expertise in eiwitzuiveringene hebben mij veel geleerd en iedere keer als ik hulp nodig had was jij er! Bedankt dat je mijn paranimf wilt zijn.

Essengül, mijn roommate, ik vond het heel gezellig om al die tijd bij jou op de kamer te zitten! Ook jou bedank ik dat je mijn paranimf wil zijn.

Fred als de andere prof in de enzymologiegroep wil ik je bedanken voor de wijze raad die je me vaak gegeven hebt in allerlei situaties.
De andere mensen van de groep : Jaap J., Peter-Leon, Emile, Loesje, Nahid, Angela, Alexey, Sandra, Laurice, Marieke, Daan, Peter, Jana, Alidin, Barbara, Laura, Inga en Nanning. Bedankt voor de gezellige koffiepauzes en de fijne werksfeer in de labs.
Dirk, jij bedankt dat je eigenlijk de rode draad door mijn onderzoek bent geweest! Op alle plekken waar ik werkte kwam ik jou tegen, bij Cees, bij Simon en nu, in Leiden, waar ik je baas moet noemen! Je grote interesse voor wetenschap en enthousiasme hebben me door menig dip(je) geholpen en niet te vergeten je kunsten met plaatjes in Word-files....
Vervolgens bedank ik werkplaats in het kluyver lab, Arno, Sjaak, Ronald, Marcel, Herman, Jos, Jacques en Rob. Ik heb ontzettend veel van jullie geleerd over de technische kant van de apparatuur die jullie voor me gemaakt hebben en dat jullie altijd voor me klaarstonden als er gisteren iets gerepareerd moest worden. Zonder jullie was de MHQ niet zoals hij nu is!
Bernd and Olli and the other members of the molecular genetics group at the University of Frankfurt, I would like to thank you for the very nice collaboration we had during this project. The dinners in Der Esel were terrific and the time I have spent in your lab was great!
Armand, de cover design vind ik prachtig. Hartelijk dank voor de tijd en moeite die je erin gestoken hebt om dit voor elkaar te krijgen.
De yeastyboys: Johan, Jan, Roger, Michel, Dennis, Ton, Mickel, Alex en Victor. De dart avonden waren een welkome afleiding van het lab.
Daarnaast wil ik mijn vrienden bedanken voor de bemoedigende woorden als ik weer eens sacherijnig was of gewoon voor een ontspannend biertje.
Pa en ma, bedankt voor de onbezorgde jeugd die ik gehad heb. Jullie hebben me altijd de vrijheid gegeven om mijn eigen keuzes te maken. Pa, een extra bedankje voor de hulp bij de stellingen! Martijn jij ook bedankt als broer.
Als laatste bedank ik Heidi, het is onbeschrijfelijk hoe je me geholpen hebt in de afgelopen jaren. Jij wist me er altijd bovenop te helpen als het tegen zat en je onvoorwaardelijke liefde is mijn grootste steun geweest door alle makkelijk- en moeilijk-heden heen!

Frankie

Stellingen behorende bij het proefschrift
Electron transfer and proton pumping pathways in cytochrome aa_3
Frank G.M. Wiertz

1) Wolfraam geniet de voorkeur boven andere metalen als oppervlakte coating voor zeer snelle bevriezing, vanwege zijn goede warmtegeleiding, hardheid en beschikbaarheid in zuivere vorm.

2) Het protonpompmechanisme van cytochroom *c* oxidase is verschillend in het oxidatieve en reductieve deel van de catalytische cyclus.

3) Tryptofaan 272 is de vectorieel drijvende kracht voor energieconservering door cytochroom *c* oxidase.

4) De AFM en electrochemische resultaten van Bonanni et al. zijn inconsistent met hun conclusie dat gist cytochroom *c* een monolaag vormt op Au (111). *Bonanni et al., Topological and electrontransfer properties of yeast cytochrome c on bare gold electrodes, 2003, chem.phys.chem, 4, 1183-1188*

5) De aanname van Ferrari et al. dat cytochroom *c*551i de electron donor is voor cytochroom c oxidase mist elke kinetische basis. *Ferrari et al., Electron transfer in crystals of the binary and ternary complexes of methylamine dehydrogenase with amicyanin and cytochrome c 551i as detected by EPR spectroscopy. 2004, JBIC, 9, 2,231-237*

6) Communicamus ergo sumus.

7) In de discussie over de evolutietheorie en de intelligent design hypothese staat ieder aan de andere kant van het gelijk.

8) Het hóger onderwijs sluit niet slecht aan bij het míddelbaar onderwijs, maar juist andersom.

9) Single molecule experimenten zouden zo geoptimaliseerd moeten worden dat daadwerkelijk slechts één molecuul nodig is per experiment.

10) Wetenschappers zouden zich meer bewust moeten zijn van de uitspraak van Herman Finkers: ” De ene keer zit je uren te denken zonder dat je ook maar iets te binnen schiet en een andere keer bereik je precies hetzelfde in nog geen vijf minuten…”

Deze stellingen worden opponeerbaar en verdedigbaar geacht en zijn als zodanig goedgekeurd door de promotor, Prof. Dr. S. de Vries

Propositions with the thesis
'Electron transfer and proton pumping pathways in cytochrome aa_3'
Frank G.M. Wiertz

1) Tungsten is preferred over other metals as surface coating for ultrafast freezing, on account of its very good heat conductance, hardness and availability in pure form.

2) The proton pumping mechanism of cytochrome *c* oxidase is different in the oxidative and reductive parts of the overall catalytic cycle.

3) Tryptophan 272 is the vectorial driving force for energy conservation by cytochrome *c* oxidase

4) The AFM and electrochemistry results from Bonanni et al. are inconsistent with their conclusion that yeast cytochrome *c* forms a monolayer on Au (111). *Bonanni et al., Topological and electrontransfer properties of yeast cytochrome c on bare gold electrodes, 2003, Chem. Phys.Chem, 4, 1183-1188*

5) The assumption of Ferrari et al. that cytochrome *c*551i is the electron donor for cytochrome *c* oxidase, lacks any kinetic foundation. *Ferrari et al., Electron transfer in crystals of the binary and ternary complexes of methylamine dehydrogenase with amicyanin and cytochrome c 551i as detected by EPR spectroscopy. 2004, JBIC, 9, 2,231-237*

6) Communicamus ergo sumus.

7) In the discussion about the evolution theory and the intelligent design hypothesis each party stands on either side of the truth.

8) The híghe education program does not poorly match with the míddle (secondary) education program, but the other way around.

9) Single molecule experiments should be optimized in such a way that only a single molecule would be needed per experiment.

10) Scientists should be more aware of the statement by Herman Finkers:" At times you are thinking for hours without anything popping into your mind, while at other times you come to exactly the same conclusion within five minutes…"

These propositions are considered opposable and defendable and as such have been approved by the supervisor, Prof. Dr. S. de Vries